

University of Southampton Research Repository

Copyright © and Moral Rights for this thesis and, where applicable, any accompanying data are retained by the author and/or other copyright owners. A copy can be downloaded for personal non-commercial research or study, without prior permission or charge. This thesis and the accompanying data cannot be reproduced or quoted extensively from without first obtaining permission in writing from the copyright holder/s. The content of the thesis and accompanying research data (where applicable) must not be changed in any way or sold commercially in any format or medium without the formal permission of the copyright holder/s.

When referring to this thesis and any accompanying data, full bibliographic details must be given, e.g.

Thesis: Author (Year of Submission) "Full thesis title", University of Southampton, name of the University Faculty or School or Department, PhD Thesis, pagination.

Data: Author (Year) Title. URI [dataset]

UNIVERSITY OF SOUTHAMPTON

FACULTY OF MEDICINE

CANCER SCIENCES UNIT

**Generation and functional comparison of anti-CD20
chimeric antigen receptors.**

Volume 1 of 1

By

Ruth Hannah Britton

Thesis for the degree of Doctor of Philosophy

December 2019

UNIVERSITY OF SOUTHAMPTON

ABSTRACT

FACULTY OF MEDICINE

CANCER SCIENCES

Thesis for the degree of Doctor of Philosophy

**Generation and functional comparison of anti-CD20 chimeric antigen
receptors**

Ruth Hannah Britton

Chimeric antigen receptor (CAR) T-cell therapy has proven effective, particularly in targeting relapsed, refractory haematological malignancies. However, optimal CAR design is not fully understood. It is known that the antigen epitope position, affinity of interaction and the length of the CAR construct can all impact function, but these factors often depend on the individual antigen context. CD20 is a validated immunotherapy target for monoclonal antibody (mAb) and CAR therapies. This thesis investigated the impact of incorporating single chain variable fragments (scFv) with different properties into an anti-CD20 CAR. Anti-CD20 scFv were generated from a panel of 5 parental mAb; rituximab, BHH2, B1-WG, 2F2 and Leu16. These mAb each possess different affinities, targeted epitopes and binding angles to CD20. Using molecular biology techniques, the scFv were each combined into a CAR construct comprising spacer, transmembrane and intracellular T-cell signalling domains.

It was found that 3 of the 5 CARs, rituximab, BHH2 and Leu16, could successfully be expressed on the cell surface of mammalian cell lines and bound in a specific manner to CD20. Stable cell lines expressing each of these CARs were generated using BWZ.36 and CTLL-2 cells to assess *in vitro* functional activity. The BWZ.36 IL-2 reporter cell line revealed a hierarchy of activation with the BHH2 CAR eliciting the highest response, followed by the rituximab and Leu16 CARs. CTLL-2 cells were shown to be non-cytotoxic, but capable of producing IFN γ , with the BHH2 CAR inducing the highest level of the cytokine.

CAR expression could not be established on primary mouse T cells despite high expression on other primary murine cells. However, CAR expression was achieved on primary human T cells. The Leu16 and BHH2 CARs were compared in *in vitro* cytotoxicity assays using transduced human T cells. BHH2 CAR consistently demonstrated a superior level of target-specific cytotoxicity. Cytokine analysis revealed that BHH2 CAR also induced a higher level of IFN γ production in the human T cells, although both constructs elicited similar levels of IL-2. Together, the findings of this thesis demonstrate that the inclusion of anti-CD20 scFvs with different binding epitopes and properties can impact CAR function, with the BHH2 CAR proving to have higher overall T-cell activation and cytotoxic abilities.

Contents

List of Figures	10
List of Tables	14
List of Appendices	14
Declaration of Authorship	15
Acknowledgements	17
Abbreviations.....	19
1 Introduction	25
1.1 Cancer	25
1.2 B-cell malignancies	27
1.3 Traditional cancer therapy.....	28
1.4 Cancer and the immune system	29
1.5 Cancer immunotherapy.....	30
1.5.1 Active immunotherapy	30
1.5.2 Passive immunotherapy.....	34
1.6 CD20 and anti-CD20 mAb	45
1.7 T cells.....	49
1.7.1 T-cell development.....	49
1.7.2 T-cell receptor-mediated activation.....	52
1.7.3 T-cell co-stimulation and co-inhibition.....	56
1.7.4 T-cell subsets.....	61
1.8 Chimeric antigen receptors	66
1.8.1 The development of CAR design.....	67
1.8.2 CAR signalling	69
1.8.3 CAR Spacer domains	72
1.8.4 Target antigen selection and scFv properties	74
1.8.5 CAR targeting solid tumours and the microenvironment	78
1.8.6 T-cell subsets in CAR therapy	81

1.8.7	CAR Safety.....	83
1.8.8	Universal CAR.....	85
1.8.9	CARs in the clinic	86
1.9	Aims and Objectives.....	88
2	Materials and methods	89
2.1	Cell Culture.....	89
2.1.1	Cell culture conditions	89
2.1.2	Isolation of human peripheral blood mononuclear cells (PBMCs).....	90
2.1.3	Isolation of murine splenocytes	91
2.1.4	Isolation of murine bone marrow	91
2.1.5	Freezing and thawing cells.....	91
2.1.6	Harvesting adherent cells.....	92
2.1.7	Cell counting.....	92
2.2	Molecular biology techniques	92
2.2.1	Polymerase chain reaction (PCR)	92
2.2.2	Overlap PCR	93
2.2.3	Gel electrophoresis	93
2.2.4	DNA gel extraction	93
2.2.5	Restriction enzyme digestion	94
2.2.6	Ligation reaction	94
2.2.7	Site-directed mutagenesis.....	95
2.2.8	Recombination	95
2.2.9	Heat shock bacterial transformation.....	95
2.2.10	Bacterial culture.....	96
2.2.11	Plasmid DNA purification from bacterial cells.....	96
2.2.12	Short-chain termination DNA sequencing	97
2.3	Mammalian cell transfection	98
2.3.1	HEK 293F transient transfection	98
2.3.2	CHO-S transient transfection	98
2.3.3	Nucleofection of CTLL-2 cells	98

2.3.4	Sub-cloning and antibiotic selection.....	99
2.4	Retroviral transduction	99
2.4.1	Ecotropic retroviral transduction	99
2.4.2	Amphotropic retroviral transduction	100
2.5	Flow cytometry.....	101
2.5.1	Staining with fluorescent antibodies.....	101
2.5.2	Intracellular staining with fluorescent antibodies.....	102
2.5.3	Cell sorting.....	102
2.6	Microscopy.....	102
2.7	Soluble protein analysis	102
2.7.1	Protein purification	102
2.7.2	SDS-PAGE	103
2.7.3	Western blot.....	104
2.8	<i>In vitro</i> functional assays.....	104
2.8.1	Binding and blocking assay	104
2.8.2	CPRG assay	105
2.8.3	Calcein release cytotoxicity assay	105
2.8.4	Sandwich enzyme-linked immunosorbent assay (ELISA)	106
2.9	<i>In vivo</i> techniques	107
2.9.1	CTLL-2 cell tracking	107
2.9.2	Bone marrow chimeras	108
2.10	Statistical analysis.....	108
3	Molecular Generation and Expression of Chimeric Antigen Receptor Constructs	109
3.1	Introduction	109
3.2	Cloning and expression of anti-CD20 single chain variable fragments.....	111
3.2.1	Production and cloning of single chain variable fragments.....	111
3.2.2	Expression of scFv in mammalian cells	115
3.3	Cloning of chimeric antigen receptors.....	119
3.4	Expression of CARs by mammalian cells	124

3.4.1	Mutagenesis of B1-WG scFv.....	128
3.5	Discussion	130
4	Antigen-Specific Binding of CAR Constructs	133
4.1	Introduction.....	133
4.2	Confirmation of CAR-CD20 interactions.....	133
4.3	Confirmation of Antigen Binding Specificity.....	142
4.4	Discussion	144
5	Generation of CAR-Expressing Cell Lines and Evaluation of Functional Characteristics	145
5.1	Introduction.....	145
5.2	Investigation of CAR-specific T-cell activation.....	149
5.2.1	Generation of CAR+ve IL-2 reporter cell lines.....	149
5.2.2	Assessment of CAR-mediated BWZ.36 activation	153
5.2.3	Investigation of the relationship between CAR expression and T-cell activation level	162
5.3	Investigating the role of epitope distance from the membrane upon CAR function.....	165
5.4	Generation of CAR+ve cytotoxic T-cell lines	174
5.4.1	CTLL-2 Characterisation	174
5.4.2	Establishing CAR-expressing CTLL-2 cell lines	177
5.4.3	Functional assessment of CAR+ve CTLL-2 cell lines	179
5.5	Discussion	186
6	Assessment of CAR function in primary cells	191
6.1	Introduction.....	191
6.2	Retroviral transduction of murine splenocytes.....	192
6.3	Generation of bone marrow chimeras	198
6.4	Transduction of human peripheral blood mononuclear cells	203
6.4.1	Molecular cloning of CAR constructs into pSFG	203
6.4.2	Expression of CAR-SFG constructs	206
6.5	Functional comparisons of CAR-mediated cytotoxicity in primary human T cells	211

6.6	Discussion.....	222
7	Final discussion and future directions	229
8	References.....	251
9	Appendix	283

List of Figures

Figure	Page
1.1: The hallmarks of cancer	26
1.2: The structure of IgG	38
1.3: Epitopes bound by anti-CD20 mAb relevant to this project	47
1.4: The structure of the $\alpha\beta$ TCR and associated CD3 molecules	51
1.5: Control of Lck activation	53
1.6: A schematic of T-cell signalling pathways induced upon antigen recognition	54
1.7 Structure of CD28 showing intracellular motifs that are bound by signalling proteins	58
1.8: CD137 structure and intracellular TRAF-binding sites	60
1.9: The domains of a CAR	67
1.10: First, second, third and fourth generation CAR constructs.	68
3.1: An illustration of the CAR constructs generated.	110
3.2: An illustration of a single chain variable fragment structure.	111
3.3: scFv fragments were produced by PCR and products were ligated into pCR-Blunt-II-TOPO.	112
3.4: scFv sections were cloned together into the pcDNA4/HisMax B vector.	114
3.5: Western blot for His-tagged scFvs, expressed intracellularly by transfected HEK 293F cells.	116
3.6: Vector map of pFUSE-hlgG1-Fc2	117
3.7: Western Blot of secreted soluble HA-tagged BHH2 scFv expressed by transfected HEK 293F cells.	118
3.8: An illustration of the CAR molecule structure	119
3.9: PCR was used to generate the IgG1 hinge-CH2-CH3 spacer region	120
3.10: CAR constructs were generated by cloning DNA fragments together into pcDNA3.1(-).	121
3.11: An illustration of the overlap PCR used to generate fragments comprising the SP163 enhancer, leader sequence and each scFv	122
3.12: Additional CAR constructs were generated by cloning overlap PCR products into pcDNA3.1(-).	123
3.13: Mammalian cell surface expression of Leu16, BHH2 and Ritux CARs.	125
3.14: Surface and intracellular expression of B1-WG and 2F2 CARs on HEK 293F cells.	126
3.15: B1-WG scFv contains an additional cysteine residue in the VH domain.	127
3.16: Disulphide bond formation in the extracellular domains of CAR constructs	128
3.17 Site-directed mutagenesis was used to convert the additional cysteine in B1-WG to a serine residue.	129
4.1: Flow cytometry gating strategy employed to assess binding interactions between CAR+ve HEK 293F cells and CD20+ve target cells.	134
4.2: Binding assay to determine interactions between CAR-transfected HEK 293F cells and CD20+ve target cells.	136

4.3: Determination of size increase of effector-target conjugates from single non-bound cells.	138
4.4: Binding assay to determine interactions between CAR+ve HEK 293F cells and CD20+ve target cells.	140
4.5: Binding and blocking assay to assess specificity of CAR-CD20 interactions.	143
5.1: An illustration of β -galactosidase production and the catalysis reaction of the BWZ.36 CPRG assay	146
5.2: Vector map illustrating the retroviral vector pMIGR1	147
5.3: Illustration of the Rp3 epitope and CD137 fusion protein constructs	148
5.4: Molecular cloning to transfer CAR constructs into the retroviral vector pMIGR1	150
5.5: Retroviral transduction of BWZ.36 cells	152
5.6: Selection of a positive control for CPRG assays	153
5.7: CPRG assay with CAR+ve BWZ.36 cells and CD20+ve target cells to investigate CAR-induced T-cell stimulation.	155
5.8: Photographic image of a CPRG assay plate	156
5.9: CPRG assay to investigate the specificity of CAR-induced T-cell activation.	157
5.10: Combined data of CPRG assay repeats	159
5.11: Combined data of CPRG assay repeats shown as percentage maximal response	160
5.12: Combined data of CPRG assay repeats compared using one-way ANOVA tests	161
5.13: CPRG assays comparing CAR+ve BWZ.36 cells with equivalent CAR expression levels.	163
5.14: CPRG assays comparing the BWZ.36 activation responses of BHH2 CAR+ve and Leu16 CAR+ve cells at a range of expression levels.	164
5.15: CPRG assay comprising A20 cells expressing Rp3 epitope constructs as the target population.	166
5.16: CPRG assay incorporating HEK 293F cells transfected with Rp3 epitope constructs as target cell population.	168
5.17: CPRG assay incorporating CHO-S cells transfected with RP3 epitope constructs as targets.	169
5.18: CPRG assay incorporating CD20+ve and Rp3+ve CHO-S cells as the target populations.	170
5.19: Mutagenesis of the 4D Rp3 construct to generate the Rp15 cyclic epitope.	172
5.20: CPRG assay incorporating Rp3+ve and Rp15+ve CHO-S cells.	173
5.21: Granzyme B expression in CTLL-2 cells	174
5.22: Evaluation of short-term in vivo survival and tracking of CTLL-2 cells	175
5.23: Evaluation of in vivo survival and tracking of CTLL-2 cells at 72 h	176
5.24: Nucleofection of CTLL-2 cells to generate CAR+ve CTL cell lines	177
5.25: Calcein release cytotoxicity assay using transiently expressing Leu16 CAR and BHH2 CAR -transfected CTLL-2 cells	178
5.26: Subcloned and G418-selected Leu16 and BHH2 CAR+ve CTLL-2 populations	179

5.27: Calcein-release cytotoxicity assays incorporating stably-expressing CAR+ve CTLL-2 cell lines	181
5.28: Calcein-release cytotoxicity assay incorporating FBL-3 target cells	182
5.29: Calcein-release assay incorporating CTLL-2 cells deprived of T-stim IL-2 supplement for 12 h and re-stimulated prior to cytotoxic assessment	182
5.30: Calcein-release assay performed with pre-stimulated CTLL-2 cells	183
5.31: A calcein-release cytotoxicity assay incorporating 145-2C11 hybridoma cells	184
5.32: CTLL-2 cells stained for T-cell exhaustion markers	185
5.33: IFN γ ELISA performed on supernatants from CTLL-2 co-cultures with CD20+ve target cells	186
6.1: Phoenix-ECO cells transfected with BHH2 CAR in pMIGR1	193
6.2: NIH3T3 cells transduced with BHH2 CAR viral supernatant	193
6.3: Activated murine splenocytes showing clustering after incubation with anti-CD3 and anti-CD28	194
6.4: Murine splenocytes transduced with Leu16 CAR viral supernatant in the presence of polybrene	195
6.5: GFP expression in Phoenix-ECO cells at 48 and 72 h post-transfection	196
6.6: Murine splenocytes transduced with viral supernatant collected from Phoenix-ECO cells at 72 h post-transfection	197
6.7: Murine bone marrow transduced with CAR constructs	199
6.8: Assessment of GFP and CAR expression in the blood of reconstituted mice	201
6.9: CAR expression in the spleen of a Leu16 CAR bone marrow chimera	203
6.10: Molecular mutagenesis and cloning to transfer each CAR into pSFG	204
6.11: Expression of CAR constructs in the SFG vector in transiently transfected HEK 293F cells.	206
6.12: Expression of CAR constructs on transduced HEK 293T cells.	207
6.13: A comparison of HEK 293T transduction efficiency with filtered and unfiltered viral supernatant.	208
6.14: Human PBMCs treated with PHA-P and IL-2 to induce T-cell proliferation	209
6.15: Assessment of T cell populations present in Leu16 CAR-transduced human PBMCs	210
6.16: A calcein release assay to investigate CAR-mediated cytotoxicity of transduced primary human T cells	212
6.17: Calcein release assays to compare CAR-induced cytotoxicity in primary human T cells at 4 h and 24 h	214
6.18: Calcein assays performed using Leu16 and BHH2 CAR+ve T cells with total cell numbers adjusted to be equivalent	215
6.19: Calcein assays performed using total cell number-adjusted populations of Leu16 and BHH2 CAR-transduced T cells	217
6.20: Combined data of calcein assays comparing Leu16 and BHH2 CAR-mediated cytotoxicity at 4 h	218
6.21: Calcein assay performed using Leu16 and BHH2 CAR+ve T cells and CD20+ve and CD20-ve RPMI8226 target cells	219
6.22: CAR-mediated IFN γ production by human primary T cells	221

6.23: CAR-mediated IL-2 production by human primary T cells	221
7.1: An illustration of the CD20 binding epitopes of rituximab, Leu16 and BHH2 mAb	233
7.2: Proposed hypothesis for enhanced BHH2 CAR activity	235
7.3: The cyclic Rp3/15 CD20 mimotope constructs compared to the full rituximab epitope of CD20	237

List of Tables

Table	Page
1.1: anti-CD20 mAb	46
2.1: Growth conditions and media used for the culture of each cell type used in this thesis.	89
2.2: PCR protocol used to generate DNA constructs.	91
2.3: Protocol of site-directed mutagenesis.	95
2.4: Thermocycler sequencing reaction protocol	97
2.5: The buffers used in HA-scFv purification	103

List of Appendices

Appendix	Page
A1 Parental mAb	283
Table A1.1: Information on parental antibodies used as scFv in this thesis	283
A2: Primers	284
Table A2.1: PCR primers used in this project	284
Table A2.2: Mutagenesis primers used in this project	287
Table A2.3: Sequencing primers used in this project	289
A3: Antibodies	290
Table A3.1: Antibodies used in this thesis for fluorescent labelling of cells, assays and Western blots	290
A4: Bone marrow chimera analysis plots	292
Figure A4.1: Analysis plots of blood samples taken a 6 w post-reconstitution	292
Figure A4.2: Analysis plots of blood samples taken a 10 w post-reconstitution	294
A5: C57/BL6 lymphodepletion	296
Figure A5.1: Staining profiles for flow cytometric identification of murine lymphocyte compartments in tail blood samples	296
Figure A5.2: Tracking the return of peripheral lymphocyte populations in irradiated C57/BL6 mice	297
A6: Poster abstracts and publication details	298

Declaration of Authorship

I, **Ruth Hannah Britton**, declare that this thesis entitled '**Generation and functional comparison of anti-CD20 chimeric antigen receptors**' and the work presented in it is my own and has been generated by me as the result of my own original research.

I confirm that:

1. This work was done wholly or mainly while in candidature for a research degree at this University;
2. Where any part of this thesis has previously been submitted for a degree or any other qualification at this University or any other institution, this has been clearly stated;
3. Where I have consulted the published work of others, this is always clearly attributed;
4. Where I have quoted from the work of others, the source is always given. With the exception of such quotations, this thesis is entirely my own work;
5. I have acknowledged all main sources of help;
6. Where the thesis is based on work done by myself jointly with others, I have made clear exactly what was done by others and what I have contributed myself;
7. None of this work has been published before submission.

Signed:.....

Date:.....

Acknowledgements

I would first like to thank my supervisors Prof Martin Glennie and Dr Ruth French for initial project design and their supervision throughout. I also would like to thank Prof Mark Cragg for all his brilliant help and guidance, both before and after becoming my official supervisor. Thanks also go to Dr Claude Chan for his help with learning molecular biology techniques. I would like to thank CRUK for funding this work.

I am grateful to Dr Patrick Duriez for his help with scFv production and purification, and to the BRF staff for all their technical assistance and training. For allowing me to visit for technical training, and for providing cells and protocols, I am extremely thankful to Dr Martin Pule of UCL. I would also like to thank Dr Lydia Lee of UCL for teaching and technical demonstrations of the retroviral PBMC protocol.

Thank you to all the A&V group, you have always made me feel welcome and made this a lovely place to work for the duration of my PhD. Special thanks go to Robert and Kirstie, for helping out with experiments when life got in the way.

For their friendship and encouragement, and for reminding me of the world outside the lab, I would like to say a big thank you to Izzy, Sara, Sarah, Amy, Sheila and Chidi. For invaluable kindness and support, thank you to Johanne. This thesis would never have been finished without RMRK *et al*: Robert, Muchaala, Kirstie and Mike, you guys were the best PhD companions possible and I'm grateful for all the help, listening, advice and hilarity. Kirstie, your CFS advice and solidarity were invaluable. Likewise, John (Juan!), thank you for being a brilliant student-postdoc, feeder and friend.

I am grateful to my brother, Graham, for proofreading, being the only person I know to seemingly understand T cells, and for many other things.

To my Dad, thank you for everything (which is a lot). Your unwavering patience, kindness and listening are things I will always be grateful for. Make a space on the thesis shelf!

Whilst you haven't directly been a part of this time, I still want to say thank you to Mum for everything you taught and instilled in me.

To Harvey, for your confidence in me, your patience, cheerleading and friendship I am indebted. Thank you for listening to me talk about this thesis for more years than I care to count. Thank you for always seeing the positive and making me laugh. Thank you for all the cups of tea and bribing me to finish writing with the promise of a cat (worth it).

Abbreviations

ACT	Adoptive cell transfer	CAR	Chimeric antigen receptor
ADCC	Antibody dependent cell-mediated cytotoxicity	Carma-1	Caspase recruitment domain-containing membrane-associated guanylate kinase protein-1
ADCP	Antibody dependent cellular phagocytosis	Cas9	CRISPR associated protein 9
A/I	Activatory/inhibitory ratio	CCL	Chemokine ligand
AICD	Activation-induced cell death	CCR	Chemokine receptor
AID	Activation-induced deaminase	CD	Cluster of differentiation
AIRE	Autoimmune regulator	CDC	Complement dependent cytotoxicity
Akt	Protein kinase B	CDR	Complementary determining region
ALL	Acute lymphoblastic leukaemia	CEA	Carcinoembryonic antigen
AML	Acute myeloid leukaemia	c-FLIP	Cellular FLICE-like inhibitory protein
ANOVA	Analysis of variance	CFSE	Carboxyfluorescein succinimidyl ester
AP-1	Activator protein 1	CHO-S	Chinese hamster ovary-suspension
APAF-1	Apoptotic protease activating factor-1	cIAP	Cellular inhibitor of apoptosis protein
APC, flurophore	Allophycocyanin	CLL	Chronic lymphocytic leukaemia
APC, cell	Antigen presenting cell	CML	Chronic myeloid leukaemia
Arp2/3	Actin-related protein 2/3	CPRG	Chlorophenol red- β -D-galactopyranoside
ASK	Apoptosis signal-regulating kinase	C region	Constant region
BAK	Bcl-2 antagonist/killer	CRISPR	Clustered regularly interspaced palindromic repeats
BAX	Bcl-2 associated X	cSMAC	Central supramolecular activation complex
Bcl-2/6/10/XL	B cell lymphoma 2/6/10/XL	C segment	Constant segment
BCR	B cell receptor	cTEC	Cortical thymic endothelial cell
BID	BH3-interacting domain death agonist	CTL	Cytotoxic T lymphocyte
BIM	Bcl-2-like <i>protein</i> 11	CTLA4	Cytotoxic T-lymphocyte antigen 4
BiTE	Bispecific T-cell engager		
Bp	Base pairs		
BRCA	Breast cancer gene		
BSA	Bovine serum albumin		
BsAb	Bispecific antibody		
CAD	Caspase-activated DNase		

CXCR	Chemokine receptor	FSC-H	Forward scatter, height
DAG	Diacylglycerol	GEF	Guanine nucleotide exchange factor
DART	Dual-affinity retargeting antibody	GFP	Green fluorescence protein
DC	Dendritic cell	GM-CSF	Granulocyte-macrophage colony-stimulating factor
ddNTP	Di-deoxynucleotide triphosphate	Grb-2	Growth factor receptor bound protein 2
DMEM	Dulbecco's Modified Eagle Medium	GVHD	Graft versus host disease
DMSO	Dimethyl sulfoxide	Gy	Gray (ionizing radiation)
DN	Double negative	HA Tag	Human influenza haemagglutinin motif
dNTP	Deoxynucleotide triphosphate	HEK	Human embryonic kidney
DP	Double positive	Her2	Human epidermal growth factor receptor 2
D segment	Diversity segment	HSV-tk	Herpes simplex virus thymidine kinase
dSMAC	Distal supramolecular activation complex	HIF	Hypoxia-inducible factor
EBV	Epstein Barr virus	hIgG-Fc	Human immunoglobulin G, Fc portion
EDTA	Ethylenediaminetetraacetic acid	His Tag	Polyhistidine motif
EGFR	Epidermal growth factor receptor	HLA	Human leukocyte antigen
ELISA	Enzyme-linked immunosorbent assay	HPV	Human papilloma virus
EpCAM	Epithelial cell adhesion molecule	HRP	Horse radish peroxidase
ER	Endoplasmic reticulum	HSCT	Human stem cell transplant
ERK	Extracellular signal-regulated kinase	IAP	Inhibitor of apoptosis
E:T	Effector:target ratio	ICAD	Inhibitor of caspase-activated DNase
F(ab)	Fragment, antigen binding	ICAM-1	Intracellular adhesion molecule-1
FACS	Fluorescence-activated cell sorting	iCAR	Inhibitory chimeric antigen receptor
FADD	Fas-associated protein with death domain	ICOS	Inducible T-cell costimulator
Fc	Fragment, crystallisable	IDO	Indoleamine 2,3-dioxygenase
FcγR	Fc γ receptor	IFN	Interferon
FCS	Fœtal calf serum	Ig	Immunoglobulin
FDA	Food and drug administration		
FITC	Fluorescein isothiocyanate		
FKBP	FK506 binding protein		
FLICE	FADD-like IL-1β-converting enzyme		
FoxP3	Forkhead box protein 3		

IgSF	Immunoglobulin superfamily	MAP3K	Mitogen-activated protein kinase kinase kinase 7
I κ B	Inhibitor of NF κ B		
IKK	Inhibitor of NF κ B kinase	MAPK	Mitogen-activated protein kinase
IL	Interleukin	MART-1	Melanoma antigen recognized by T cells 1
IL- R	Interleukin - receptor		
IMDM	Iscove's Modified Dulbecco Medium	MDSC	Myeloid-derived suppressor cells
IP	Intraperitoneal injection	MEK	Mitogen activated protein kinase kinase
IP ₃	Inositol trisphosphate	MEKK1	Mitogen activated protein kinase kinase kinase 1
IRES	Internal ribosome entry site		
IS	Immunological synapse		
		MFI	Mean fluorescence intensity
ITAM	Immunoreceptor tyrosine-based activation motif	MHC	Major histocompatibility complex
ITIM	Immunoreceptor tyrosine-based inhibition motif	MICA/B	MHC class I chain-related protein A/B
ITK	Tyrosine protein kinase	MKK4/7	Mitogen activated protein kinase kinase 4/7
iTreg	Induced regulatory T cell		
		MPPs	Multipotent progenitors
ITSM	Immunoreceptor tyrosine-based switch motif	MSCV	Murine stem cell virus
		MT	Microtubule
IV	Intravenous injection	MTOC	Microtubule organising centre
J segment	Joining segment	mTOR	Mammalian target of rapamycin
JNK	c-Jun N-terminal kinase		
K _D	Dissociation constant	NCAM	Neural cell adhesion molecule
LAG3	Lymphocyte-activation gene 3	NEMO	NF κ B essential modulator
LAT	Linker for activation of T cells	NFAT	Nuclear factor of activated T cells
LB	Lysogeny broth	NF κ B	Nuclear Factor kappa-B
Lck	Lymphocyte-specific protein tyrosine kinase	NHEJ	Non-homologous end joining
LFA-1	Lymphocyte function associated antigen-1	NHL	Non-Hodgkin lymphoma
mAb	Monoclonal antibody	NIK	NF κ B inducing kinase
MAC	Membrane attack complex	NK	Natural killer cell
MAGE	Melanoma antigen gene	NKT	Natural killer T cell
MALT-1	Mucosa-associated lymphoid tissue lymphoma translocation protein 1	nTreg	Natural regulatory T cell
		NY-ESO-1	New York esophageal squamous cell carcinoma 1

OD	Optical density	RAG	Recombination activating gene
p53	Tumour protein 53	RIP	Receptor interacting protein
PAG	Phosphoprotein associated with glycosphingolipid enriched microdomains	ROR1	<i>Receptor tyrosine kinase like orphan receptor 1</i>
PARP	Poly ADP ribose polymerase	ROS	Reactive oxygen species
PBMC	Peripheral blood mononuclear cell	RPMI 1640	Roswell Park Memorial Institute 1640
PBS	Phosphate-buffered saline	RSS	Recombination signal sequence
PCD	Programmed cell death	RT	Room temperature
PCR	Polymerase chain reaction	SCF	Stem cell factor
PD-1	Programmed cell death 1	scFv	Single chain variable fragment
PDK1	3-phosphoinositide-dependent protein kinase-1	SCID	Severe combined immunodeficiency
PDL-1	Programmed cell death 1 ligand 1	SD	Standard deviation
PE	R-Phycoerythrin	SDS-PAGE	Sodium dodecyl sulfate - polyacrylamide gel electrophoresis
PHA-P	Phytohemagglutinin-P	SEM	Standard error of mean
PI3K	Phosphatidylinositide 3-kinase	SH2	Src homology 2 domain
PIP2	Phosphatidylinositol 4,5-bisphosphate	SHIP1	SH2 domain containing inositol polyphosphate 5 phosphatase 1
PIP3	Phosphatidylinositol 3,4,5-triphosphate	SHP	Src homology phosphatase
PKC	Protein kinase C	SLEC	Short lived effector cell
PLC	Phospholipase C	SOC	Super-optimal broth with glucose
PM	Plasma membrane	SOS	Son of sevenless
PMA	Phorbol 12-myristate 13-acetate	SSC-H	Side scatter, height
PP2A	Protein phosphatase 2A	STAT	Signal transducers and activators of transcription
pRb	Retinoblastoma protein	TAA	Tumour-associated antigen
PSCA	Prostate stem cell antigen	TALLEN	Transcription activator like effector nucleases
PSMA	<i>Prostate specific membrane antigen</i>	TAM	Tumour-associated macrophage
pSMAC	Peripheral supramolecular activation complex	T _{CM}	Central memory T cell
PTEN	Phosphatase and tensin homolog	TCR	T cell receptor

TdT	Terminal deoxynucleotidyl transferase
TEC	Thymic endothelial cell
T _{EM}	Effector memory T cell
T _{FH}	Follicular T helper cell
TGFβ	Transforming growth factor beta
Th	T helper cell
TIL	Tumour-infiltrating lymphocyte
TIM	TRAF-interacting motif
TIM-3	T-cell immunoglobulin and mucin-domain containing-3
TLR	Toll-like receptor
TNP	2,4,6- trinitrophenyl
TNFRSF	Tumour necrosis factor receptor superfamily
TRAF	TNF receptor-associated factor
Treg	Regulatory T cell
TRIM	T cell receptor-interacting molecule
VEGF	Vascular endothelial growth factor
VEGF-R	Vascular endothelial growth factor receptor
V _H	Variable heavy domain
V _k	Variable kappa light domain
VLP	Virus-like particle
V segment	Variable segment
WASP	Wiskott-Aldrich syndrome protein
WHO	World health organisation
WT	Wild type
WT-1	Wilm's tumour gene product-1
XIAP	X-linked inhibitor of apoptosis
ZAP-70	Zeta-chain-associated protein kinase 70

1 Introduction

1.1 Cancer

“Cancer” is a term used to describe a vast array of over 200 distinct diseases [1]. Furthermore, within these types great heterogeneity is seen in cause, progression and clinical presentation. Despite this extensive diversity, a set of well-defined hallmarks exist to describe cancer (**Figure 1.1**). These were originally summarised by Hanahan and Weinberg in 2000 [2] and later in 2011 [3] and describe the events that allow initiation and progression of oncogenesis.

Oncogenesis results from the accumulation of cellular mutations that allow escape from normal cell cycle control. Normally, the cell cycle is carefully regulated through a variety of checkpoints and molecular mechanisms. This ensures proliferation only occurs where and when necessary for growth or repair. Of equal importance, these processes also control apoptosis and so aberrant cell growth is inhibited. If any of these checkpoints fail, an alternative mechanism will usually compensate to correct the problem. However, if there is a breakdown at multiple checkpoints due to several mutations, uncontrolled cell growth can ensue leading to the unregulated expansion of a clonal cell population [4, 5]. The loss-of-function mutagenesis of a tumour suppressor gene such as p53 and pRb, results in uncontrolled entry into the active phases of the cell cycle, driving proliferation. Conversely, malignant transformation can be induced by mutagenesis resulting in constitutive activation of an oncogene, for example growth factor receptors and intracellular downstream signalling molecules [6].

Mutations occur in a cell when under stress or exposed to carcinogenic compounds. Well characterised cell stressors linked to malignancies include exposure to UV light and melanoma [7], and tobacco and asbestos exposure with lung cancers [8, 9]. Alternatively, mutations can arise due to genetic dispositions, such as in the case of the *BRCA1/BRCA2* genes. *BRCA1* and *2* are tumour suppressor proteins involved in DNA repair mechanisms [10]. Loss-of-function mutations in *BRCA1* and *BRCA2* genes are associated with a mean cumulative risk of developing breast cancer of 65 % and 45 % respectively, and 39 % and 11 % for ovarian cancers [11]. The failure to correctly repair DNA allows mutations to accumulate more rapidly. When these occur in important cell cycle control genes, such as tumour suppressors or oncogenes, there is a higher probability of oncogenesis initiation.

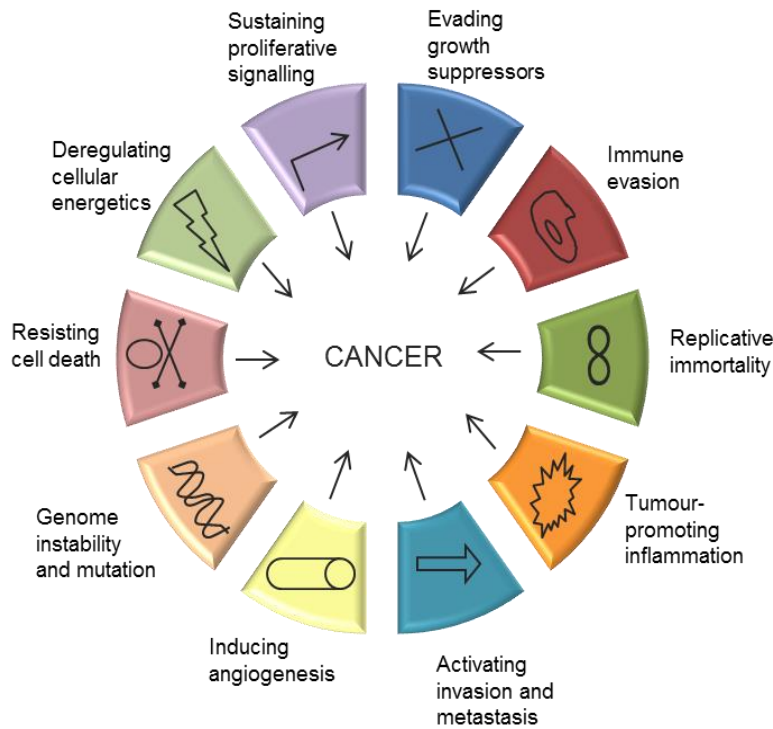


Figure 1.1: The hallmarks of cancer

As described by Hanahan and Weinberg [2, 3], these factors are characteristic of neoplastic tissue that proliferates in an uncontrolled manner and allow the tumour to expand further in a damaging way. The original 6 hallmarks described included evasion of apoptosis, induction of angiogenesis, sustained proliferative signalling, evasion of growth suppressors, tissue invasion and metastasis and replicative immortality. The other characteristics shown were later added as they were also observed to be defining features of cancer.

In addition to mutations resulting in altered function in particular genes, translocations of whole genes have been implicated in malignancies. The BCR/abl translocation (also known as the Philadelphia chromosome) is found in 95 % of all chronic myeloid leukaemia (CML) cases. It transpires when the *bcr* gene on chromosome 22 and the *abl* gene on chromosome 9 break, and translocation occurs, forming a BCR/abl fusion protein that has uncontrolled tyrosine kinase activity [12]. This results in dysregulated proliferation and enhanced survival of the transformed cell. The anti-apoptotic gene Bcl2 is translocated to the immunoglobulin (Ig) heavy chain locus in some cases of follicular lymphoma, resulting in its constitutive expression. This provides the transformed cell with increased survival and drives oncogenesis in cells with additional transformations [13].

Several viruses are linked to the development of particular cancers, including human papilloma virus (HPV) infection in cervical carcinoma and Epstein-Barr virus (EBV) in Burkitt's lymphoma. Both these viruses use the host cell machinery to generate proteins that have potent effects on cell proliferation. HPV protein E6 binds to the

essential tumour suppressor p53 and results in its degradation, whilst protein E7 interacts with and disrupts the function of pRb, another vital tumour suppressor. The consequence is loss of control of the cell cycle checkpoint at the entry into S phase, and uncontrolled proliferation of the transformed cells [14]. In a similar manner, EBV produces several proteins, the most potent of which is LMP1. This oncoprotein initiates multiple signalling pathways that drive cell division, including mitogen-activated protein kinase (MAPK), phosphatidylinositol 3-kinase (PI3K) and nuclear factor kappa B (NFκB) [15]. Chronic viral infection, and reactivation of latent infection in the case of EBV, results in the cells being exposed over an extended period to these mechanisms and so increases the likelihood of oncogenic transformation.

Once a transformed cell has overcome cell cycle control and avoided apoptosis, and proliferated to form a tumour, further survival pressures arise. The tumour microenvironment that develops has limited supplies of glucose and oxygen; if the tumour cells are to avoid death by necrosis they must adapt. Under hypoxic conditions, hypoxia-induced factor α (HIF- α) is stabilised and can enter the nucleus where it dimerises with HIF- β . This complex binds hypoxia-response elements in the promoters of pro-angiogenesis genes, including vascular endothelial growth factor (VEGF). VEGF signals to endothelial cells to induce the formation of new capillaries to provide the tumour with a continued blood supply [16].

Tumour cells also demonstrate an altered metabolism, involving high uptake of glucose and increased cytoplasmic glycolysis, known as the Warburg effects. This effect is seen even in the presence of oxygen and functional mitochondria. This ineffective but rapid generation of ATP is thought to allow the tumour cells to outcompete other cells present in the tumour microenvironment for the limited glucose available. The tumour cells can therefore produce sufficient energy for rapid biosynthesis and proliferation, whilst having the added advantage of restricting glucose access to immune cells present that may otherwise mount an anti-tumour response [17]. The resulting lactate produced from this metabolic pathway also promotes an acidic, pro-tumourigenic environment, skewing tumour-associated macrophages (TAMs) towards an anti-inflammatory phenotype and further dampening any immune response [18].

1.2 B-cell malignancies

Haematological malignancies are cancers originated from lymphoid or myeloid blood cells and can be categorised into lymphomas and leukaemias. Lymphomas usually present as a solid tumour in lymphoid organs, whilst leukaemias are observed in the blood and bone marrow. Haematological cancers have an extensive variability of

clinical presentation and prognoses, with over 60 different groups classified by the World Health Organisation (WHO) [19]. Of lymphoid cancers, B-lymphocyte malignancies account for several types, derived from B cells in many stages of differentiation. B-cell precursor malignancies such as acute lymphoblastic leukaemia (ALL) arise from naive, immature B lymphoblasts. Mature B-cell neoplasms include chronic lymphocytic leukaemia (CLL, the most common leukaemia in adults of the western world), Burkitt's lymphoma and follicular lymphoma. These arise from cells in the B-cell germinal centres of lymphoid organs. Multiple myeloma is a form of leukaemia that presents in the bone marrow, derived from B cells that have differentiated into plasma cells [19, 20]. This vast heterogeneity of B-cell malignancies presents many challenges for their diagnosis and treatment.

1.3 Traditional cancer therapy

Traditional treatment for solid tumours includes surgery, radiotherapy and chemotherapy. Surgery can remove a tumour bulk but is not effective in later stages of metastasis, and residual disease usually remains. Radiotherapy is used to induce apoptosis in tumour cells, often when surgery is a difficult option. This can be due to patient age, health and the lack of accessibility to the tumour whilst avoiding damage to surrounding tissues [21]. Because of its non-specific nature, radiotherapy causes side effects due to off-target damage to non-malignant cells. More recently, treatment has been performed guided by 3D tumour imaging to increase accuracy of targeted radiation, improve tumour reduction and minimise toxic side effects [22].

Chemotherapy agents, such as doxorubicin and cyclophosphamide, act to interfere with proliferating cellular processes. To achieve this, they are designed to cause DNA damage, disrupt the cell cycle or target the cytoskeleton [23-25]. The consequences of these actions are cell cycle arrest and induction of apoptosis. Not only malignant cells are targeted however, so toxic side effects are seen in any proliferating cell, including epithelial and endothelial tissue. Additionally, similar to surgery, chemotherapy often doesn't remove all the tumour cells leading to high rates of relapse. Frequently relapsed disease is chemo-resistant meaning treatment options are limited [26].

Haematological cancers have conventionally been treated with a combination of chemotherapy agents. Since the clinical approval of the anti-CD20 monoclonal antibody (mAb) rituximab in 1997 the survival rates of many B-cell malignancies have improved, when it is used in combination with chemotherapy drugs [27, 28].

1.4 Cancer and the immune system

The hypothesis that the immune system was capable of protecting against neoplastic cells was first proposed in 1909 by Paul Ehrlich [29]. This theory was confirmed through the use of tumour transplant animal models with various immune deficiencies [30]. The immunosurveillance hypothesis was later published stating that circulating cells, derived from the thymus, act as a patrol against transformed cells. They were observed to be capable of recognising and killing these tumour cells and controlling the background level of neoplastic transformation events in a multicellular complex organism [31]. Since these early discoveries, the theory of immunosurveillance has progressed significantly and now incorporates several aspects. The interactions of the immune system with transformed cells can be described by the “three Es” hypothesis; initial cancer elimination by the immune system, immunoediting of the tumour by the microenvironment in equilibrium and thirdly, tumour escape [32].

Initially, transformed cells can be cleared by the innate immune system, mediated by natural killer (NK) and natural killer T (NKT) cells [33]. Tumour-infiltrating macrophages, activated during tumour-induced remodelling of the extracellular matrix, can secrete interleukin-12 (IL-12) which activates infiltrating NK cells. A positive feedback loop allows production of high levels of interferon- γ (IFN γ), allowing IFN γ -dependent killing of tumour cells by NKs via the FasL/Fas or perforin pathways. Dendritic cells (DCs) attracted to the tumour microenvironment by cytokines can then process and present antigen to naive T cells in the lymph nodes. The newly-activated T cells then home to the tumour site and produce IL-2 and more IFN- γ , initiating an adaptive immune response [34]. Both $\alpha\beta$ and $\gamma\delta$ T cells are capable of recognising and killing tumour cells [35, 36]. Evidence from animal models has been supported by the more recent discovery of tumour infiltrating lymphocytes (TILs) playing an important role in anti-tumour immunity in a variety of cancer types. These T cells found within the intra-tumour environment are correlated with better prognosis in many cancers, implicating them as immuno-protective against neoplastic cells [37-39].

During the equilibrium phase, tumour progression is shaped by the immune response and the tumour microenvironment in a process known as immunoediting. The recognition of specific antigens by cytotoxic T lymphocytes (CTLs), whilst beneficial in early tumour clearance, becomes a selective pressure leading to the outgrowth tumour cells expressing alternative or lower levels of antigens. Random mutations can lead to cancer cells with reduced immunogenicity, and downregulation of major histocompatibility complex (MHC) protein expression resulting in reduced tumour

antigen presentation can also occur [40]. Additionally, expression of co-stimulation molecules can be decreased, inhibiting a successful immune response [41].

As less immunogenic tumours develop, growth starts to overcome the immune system, leading to tumour escape. The tumour and microenvironment can further directly impede the immune response via suppressive cell-cell signalling and the release of soluble immunosuppressive factors. Immature DCs in the tumour microenvironment express indoleamine 2,3-dioxygenase (IDO), which can activate T regulatory (Treg) cells [42]. Tregs can act to dampen the immune response via secretion of suppressive factors such as IL-10, and via cell-cell contact [43]. Soluble phosphatidylserine released from tumour cells stimulates tumour-associated macrophages to release further anti-inflammatory factors, including IL-10 and TGF- β , which act to prevent an anti-tumour inflammatory response [44]. The inhibitory signalling molecules cytotoxic T-lymphocyte-associated protein 4 (CTLA-4) and programmed cell death protein-1 (PD-1) are up-regulated on T cells after a period of chronic antigen exposure and lead to a reduced anti-tumour T-cell response. CD8+ve TILs have been shown to express high levels of PD-1, leading to inhibitory signalling and loss of T-cell function [45]. Moreover, tumour cells often upregulate programmed death ligand-1 (PD-L1), furthering this suppression [46].

1.5 Cancer immunotherapy

The development of cancer immunotherapy arose from the evidence demonstrating the ability of the immune system to recognise and kill neoplastic cells. There are now multiple avenues of immunotherapy in the clinic and in development. Immunotherapy is advantageous over traditional cancer therapies due to its higher specificity, reducing off-target toxicities. Immunotherapy is often most effectively given in combination with other chemotherapy or immunotherapy agents to exploit the potential for synergistic responses. The field of immunotherapy can broadly be split into active and passive arms.

1.5.1 Active immunotherapy

The principle of active immunotherapy is to initiate a response in the patient's own immune system by the administration of cytokines or vaccines. Whilst several attempts at active immunotherapy have shown limitations, some therapies are now demonstrating efficacy in animal models and in the clinic.

1.5.1.1 Cancer vaccines

Coley's toxin provided the first experimental evidence that the immune system can be stimulated against tumour cells when an immunogenic environment is created. This involved activation of a general immune response by injection of heat killed *Serratia* and *Streptococci* that led to tumour regression [47, 48]. Since then the field of cancer vaccines has expanded, targeting tumour-associated antigens (TAA) that are overexpressed or not usually found on differentiated cells, or tumour-specific antigens such as oncoviral and cancer neoantigens. The field of cancer vaccines is split into four major branches; cell-based, peptide, DNA/RNA and viral vector vaccines [49].

Cell-based vaccines involve the use of either whole tumour cells or tumour cell lysates, or antigen-presenting cells (APC) pulsed with cancer antigens. The GVAX vaccines employ irradiated whole tumour cells, also engineered to produce granulocyte macrophage colony stimulating factor (GM-CSF) to boost an immune response in the tumour microenvironment. These vaccines have shown promise in animal models [50], but the findings did not translate to patient trials. The vaccines were trialled against pancreatic, lung and prostate cancers and melanoma, and whilst immune responses were stimulated in patients this did not result in tumour control [51]. To avoid the issue of patient specific cell-based vaccines being expensive and time consuming to generate, allogeneic cell vaccines have been developed. An early example in mice used irradiated melanoma cells with engineered IL-2 expression which showed some success both as a treatment vaccine and a prophylactic vaccine prior to tumour challenge [52]. However an allogeneic, cell-based vaccine to melanoma, Canvaxin, was discontinued after clinical trials due to a lack of significant improvement in overall survival compared with a placebo [53].

APCs can be pulsed with tumour lysates or specific tumour antigens and given as a vaccine to prime a T-cell response to the tumour. DCs have also been targeted *in vivo* for peptide loading, using antigen-DC receptor fusion peptides, leading to robust antigen-specific T cell responses [54]. Sipuleucel-T is the first FDA-approved DC-based cancer vaccine for metastatic, hormone-refractory prostate cancer after showing improved survival times in stage III trials [55]. The DC are activated with GM-CSF and loaded with prostatic acid phosphatase antigen, expressed on the majority of prostate cancer cells [55].

Peptide vaccines can include whole tumour antigens or short epitopes, or mimetopes, designed to elicit a specific immune response. Strategies including multiple TAA epitopes are being implemented to try and avoid the outgrowth of tumour cells that undergo antigenic loss [56]. Synthetic long peptide (SLP) vaccines have also been

developed that contain both MHC I and II epitopes to induce a strong combined CD4 and CD8 T-cell response [49]. Peptide vaccines show greater efficacy when fused to inflammatory adjuvants [57], or TLR agonists [58] to induce large scale T-cell expansion and a stronger anti-tumour response. Despite much research into optimal peptide size and epitopes, no peptide-based treatment vaccines are approved for clinical use.

The most successful example of preventative cancer vaccination involves the use of peptides from human papilloma virus (HPV). Gardasil includes virus-like particles (VLP) from HPV 6, 11, 16, and 18, whilst Cervarix comprises VLP of HPV 16 and 18. Whilst not directly targeting a tumour, these prophylactic cervical cancer vaccines induce an immune response to the viral antigens that are responsible for the development of 70 % of cervical cancer cases. They have shown protective effects against persistent HPV infection and consequent cellular transformation, including in women with previous surgically-removed transformed cells [59-61]. A follow up study in 2019 on the impact of this vaccination has reported a >20 % drop in cases of HPV+ve cervical pre-cancers between 2008 and 2014 in women who received vaccination [62].

Similar to peptide vaccines, DNA and RNA vaccines can deliver tumour antigens to prime an immune response and provide the advantage of not requiring adjuvants. Plasmid DNA can be taken up by cells at the site of injection and will be transcribed and translated to produce the tumour antigens [63]. These are then processed for presentation to T cells via MHC molecules. DNA vaccines have had limited success, but recent developments in delivery techniques using microneedles, nanoparticles and on-site electroporation have helped improve cellular uptake of DNA vaccine leading to greatly enhance immune responses in animal models [64].

RNA vaccines involve the use of mRNA transcripts that, unlike DNA vaccines, do not require entry into the nucleus. Translation can occur directly in the cytoplasm and the resulting proteins are then processed by the proteasome for presentation to CD8 T cells [49]. To also induce a CD4 response, the RNA can be fused to signal peptides to direct it to the MHC II processing pathway. One of the major obstacles to RNA vaccines has been achieving sufficient transfection levels in the host cells and avoiding degradation by RNases. Several techniques have been investigated to improve the uptake and persistence of the mRNAs including encapsulation and vaccine delivery technique [65]. The development of RNA-LPX, an RNA vaccine encapsulated in liposomes for protection has shown anti-tumour effects in *in vivo* models and has now moved into clinical trials. A small phase I trial in melanoma patients has initially

demonstrated strong RNA-LPX induced T-cell expansion and resulted in disease stabilisation and regression of metastases [66].

The use of viral vectors to administer vaccines provides an enhancement to the immune response via viral pattern-associated molecular patterns present that are recognised by pattern-recognition receptors on APC [49]. Due to the immunogenic nature of viral vectors, repeated vaccinations with the same construct are not possible. A strategy has been developed to administer the gene for the desired tumour antigen in one viral vector, followed by repeated dosing using alternative vectors incorporating the same gene. A phase II trial of PROSTVAC, a vaccine incorporating PSA- initially given in a vaccinia viral vector and followed by a fowlpox vector- with GM-CSF, showed promising results in prostate cancer patients [67]. However, a larger-scale phase III trial was stopped as no clinical benefit was observed. The T cells were primed by the vaccine, but the immune response induced was insufficient to promote tumour clearance [68].

The field of cancer vaccines has overall been less successful than many other branches of immunotherapy due to issues with delivery techniques and insufficient immune responses, resulting in a lack of translation between data from animal models and clinical responses. Recent investigation using vaccines combined with immune checkpoint blockers suggests a synergistic response is seen and may provide a route to vaccine clinical successes [69]. For example, a phase II trial incorporating a HPV-16 vaccine with the anti-PD-1 mAb nivolumab demonstrated significantly increased survival in incurable HPV+ve oropharyngeal cancer patients, compared to those who received nivolumab alone [70].

1.5.1.2 Cytokine therapy

Cytokine therapies are designed to initiate an anti-tumour, pro-inflammatory environment to activate immune cells. Two cytokines, IL-2 and IFN α 2, are FDA approved. IFN α 2 has demonstrated success in treatment of several cancers including hairy cell leukaemia, melanoma and follicular lymphoma. IL-2 is used as a therapy for renal cell carcinoma and metastatic melanoma, although many patients do not get a clinically relevant response and toxic side effects are seen [71] [72]. IL-2 is often given more successfully in combination with adoptive cell transfer therapy (ACT) using tumour-infiltrating lymphocytes (TILs) [73].

Studies have also been performed using combination cytokine therapy, to try and mimic a true immune response with multiple cytokines that interact and develop the tumour microenvironment. This would potentially allow lower doses of each cytokine to be administered, limiting toxicity, whilst exploiting the synergistic effects of the combination [74, 75]. An alternative recent approach of using combined cytokines

involved generation of an IL-2-GM-CSF fusion protein which was reported to retain cytokine functions in addition to increasing cell-to-cell contacts between T cells and DCs to further promote immune activation [76]. The major issue seen with most cytokine therapies, including trials evaluating IL-12, IL-21 and IL-15, is that of toxicity. Use of cytokines in lower doses alongside other immunotherapies such as ACT and monoclonal antibodies (mAb) is proving to be a more effective strategy than the use of cytokine monotherapies [73].

1.5.2 Passive immunotherapy

Passive immunotherapy is designed to complement the immune system of the patient, by the introduction of immune components. A major arm of passive therapies is comprised of monoclonal antibodies (mAb), some of which have been very successful in the clinic. Alternatively, T cell-based therapies rely on expanded or modified T cells to elicit an anti-tumour response.

1.5.2.1 T-cell therapies

The development of ACT arose from the observations of tumour-specific T cells in the tumour microenvironment, as described in Chapter 1.4. TILs have been shown to elicit anti-tumour responses and can be used as a positive prognostic marker in several cancers [77-79]. ACT involves the expansion of autologous TILs *ex vivo*, before they are re-infused into the patient. Early attempts at ACT were impeded by poor T-cell proliferation and survival [80]. The discovery of IL-2 as the T-cell growth cytokine was a breakthrough in improving rates of division and survival of T cells, both *ex vivo* and upon reinfusion, when administered together [81]. Usually ACT is also administered in conjunction with chemotherapy agents to cause lymphodepletion, allowing further expansion of the infused cell population [82]. ACT of TILs has been particularly successful in the treatment of metastatic melanoma [83].

In addition to the use of mixed TIL populations, tumour-specific clonal populations of T cells can be generated by antigen priming *in vitro*. T cells are co-cultured with antigen-loaded APC and then the populations are expanded for infusion into the patient. This approach has proven successful in the treatment of metastatic melanoma [84]. ACT has also been successfully performed using EBV-specific CTLs to target EBV+ve lymphomas. The presence of these viral epitopes is advantageous, as selecting a specific target for immunotherapy is challenging and antigen loss can inhibit an effective T-cell response [85].

As an alternative to ACT of endogenous T cells, genetically engineered T cells can be generated. One approach to this is by endowing T cells with high-affinity tumour

antigen-specific T cell receptors (TCRs). To achieve this, antigen-specific TCR can be identified expressed on patient cells [86], or can be induced on healthy donor cells by MHC-restricted peptide exposure [87]. The TCR α and β chains recognising MHC-restricted tumour antigenic peptides are amplified from RNA, and these constructs are then transduced into T cells and expressed as the full TCR on the cell surface. These T cells can be expanded and infused into the patient to induce an anti-tumour response [88].

An advantage of TCR engineering is that the molecules signal by assembling with the endogenous CD3 complex so the consequent signalling is what would be triggered in a native TCR interaction, so can drive all aspects of T-cell activation and differentiation [89]. It has been shown that the number of CD3 molecules on the cell can limit engineered TCR abilities. This can be overcome by retroviral delivery of CD3, leading to improved T-cell anti-tumour efficacy [90]. A potential limitation of TCR engineering is that tumour cells often down-regulate both MHC molecules and costimulatory molecules that are required for TCR antigen recognition and complete T-cell activation [91].

Another issue with TCR engineering can be cross-pairing of the engineered TCR chains with the endogenous receptor subunits. This can lead to novel hybrid TCRs being expressed by the CTLs. Whilst this most commonly causes a loss of function, some studies have shown gain of function from this cross-pairing, leading to autoreactive TCRs [92]. There have been studies into preventing this occurring by including extra cysteine residues in the engineered chains to encourage self-binding or by using lentiviral-introduced zinc finger nucleases to edit the endogenous TCR to disable it [93]. More recently, CRISPR/cas9 has provided an efficient technique to knockout endogenous TCR expression in engineered T cells [94]. Alternatively, expressing the $\alpha\beta$ TCR DNA in $\gamma\delta$ T cells has been proposed, as these chains do not cross-pair [95] [96].

TCR-engineered T cells were first administered to a melanoma patient against the MART-1 TAA, and tumour regression was demonstrated [97]. TCR engineered to telomerase reverse transcriptase and Wilm's tumour gene product-1 (WT-1) antigens are now showing early clinical efficacy against acute myeloid leukaemia (AML) and B cell acute lymphoblastic leukaemia (B-ALL) [98], and AML and myelodysplastic syndrome respectively [99]. New York oesophageal squamous cell carcinoma-1 (NY-ESO-1) -targeted T cells are the subject of multiple clinical trials for synovial carcinoma and multiple myeloma [97, 100-102]. Anti-NY-ESO-1 TCR+ve cells have very low toxicity, as the antigen has restricted expression only on the germ cell lineage [103].

Toxicity of TCR-engineered T cells can be a major issue, as demonstrated by two independent trials against melanoma associated antigen (MAGE)-A3. In one, the autologous MAGE-A3-directed T cells also recognised an epitope of MAGE-A12, found to be expressed in the brain [104]. Patients suffered serious neurological damage from this off-target interaction and it was fatal in 2/9 patients. In a separate trial of melanoma and myeloma patients receiving MAGE-A3 TCR engineered T cells, the first two treated patients died of cardiovascular toxicity [58]. The affinity-enhanced TCR recognised an epitope of the protein titin, expressed on cardiomyocytes. This event went unpredicted as standard cultured cardiomyocytes do not express titin, only when beating cells generated from pluripotent stem cells were tested did the TCR interact and kill the cardiac cells. These examples highlight how critical antigen selection is in the design of engineered T cells.

The use of cancer neo-antigens has been proposed as a way to target only the tumour cells, with no off-target effects. Neo-antigens arise due to the somatic mutations that occur in all tumours. An average adult solid tumour contains around 50 mutations at time of diagnosis, although in carcinogen-exposed transformed cells this can be as high as 200 [105]. Neoantigen-specific TCR can be identified from patient TILs, or from donor cells primed with neoantigens, as identified by RNA and exome sequencing [106] [107]. Several studies are currently evaluating the generation and function of neoantigen-specific TCR [106, 108] [109, 110].

An important consideration in TCR engineering is that of affinity, as the endogenous TCRs do not undergo affinity maturation. Site directed mutagenesis can increase the affinity of a TCR from its original micro-molar range up to that nearer an antibody binding strength, of nano or picomolar levels [89] [111]. The binding half-life can also be improved from seconds to minutes or even hours to give an extended, robust interaction with the target antigen and rapidly activating the T cell [89]. However, engineering to increase TCR affinity has been shown to reduce avidity of the TCR, with 100-fold concentration of antigen required to successfully stimulate the mutated TCR compared with the native molecule. The lower affinity allows sequential TCR activation by antigen molecules, whilst raising the affinity and binding time of the TCR means the TCRs cannot “share” the antigens over time so need a higher expression level to trigger T cell activation. This can be an obstacle in circumstances of low target antigen expression [111].

Enhanced affinity can still be advantageous in the context of highly expressed antigens, promoting increased anti-tumour responses. Two amino acid substitutions were performed to generate high affinity anti-CEA TCR, which demonstrated increased

tumour recognition *in vitro* [112]. However, when this construct was trialled in colorectal cancer patients, serious on-target off-organ effects were seen with the development of autoimmune colitis [113]. This study reinforces the need for careful target selection, especially for high affinity T-cell therapies. A high affinity anti-NY-ESO-1 TCR, produced by a single amino acid substitution, demonstrated a higher level of antigen recognition and T cell reactivity than wild type (WT) TCR in preclinical evaluation [114]. A trial investigating the function of this high affinity TCR in melanoma and synovial cancers reported objective clinical responses in >50 % of patients. No toxicity was observed due to the restricted nature of NY-ESO-1 expression [115].

Similar to TCR engineering, chimeric antigen receptors (CARs) target a specific TAA and are expressed on T cells before infusion into a patient. CARs consist of an extracellular antigen-recognition domain, usually based on a single chain variable region (scFv) of a mAb, connected to a spacer, a transmembrane region and intracellular signalling domains of T-cell activatory molecules. This area of therapy is designed to combine the exceptional specificity of mAbs, with the cytotoxic efficacy of T-cell killing. These molecules are designed to mimic the endogenous TCR, but they recognise the specific target antigen in a MHC - independent manner and with the higher affinity of the scFv. This is particularly beneficial in the context of targeting tumour cells, which often down-regulate MHC cell-surface expression [116]. The signalling pathways activated via the CAR can initiate activation of the T cell in a similar manner to that of TCR signalling, resulting in cytokine production, proliferation and cytotoxicity against the tumour target. Chimeric antigen receptors are the focus of this project and are discussed in detail in Chapter 1.8.

1.5.2.2 Monoclonal antibodies

Antibodies comprise 4 immunoglobulin chains; 2 identical heavy (α , γ , ϵ , δ or μ) and 2 identical light (λ or κ) chains. Each light chain includes 1 variable and 1 constant domain, whilst heavy chains comprise 1 variable and at least 3 constant domains. In humans 5 classes of antibody are produced, IgG, IgA, IgM, IgE and IgD, dependant on the heavy chain incorporated. The heavy constant domains (C_H) 2 and 3 comprise the crystallisable fragment (Fc) domain, whilst the variable and C_H 1 domains of each chain make up the antigen binding fragment (F(ab)). In IgG, A and D a hinge region is present between the Fc and F(ab), the length and flexibility of which varies between antibody classes. IgM and E contain an additional C_H domain instead of a hinge region. The structure of the antibody is stabilised by disulphide bonds. Antigen binding specificity of an antibody is determined by the complementary determining regions

(CDRs), 3 of which are found in each variable domain. Together, these form the antigen binding site of each arm of the antibody.

IgG is the most abundant antibody class found in human serum and plays an essential role in adaptive immunity, and in immunotherapies. Four IgG isotypes exist, IgG 1, 2, 3 and 4, each with different FcγR and complement binding profiles, and consequently different functions [117] [118]. The structure of IgG is shown in **Figure 1.2**.

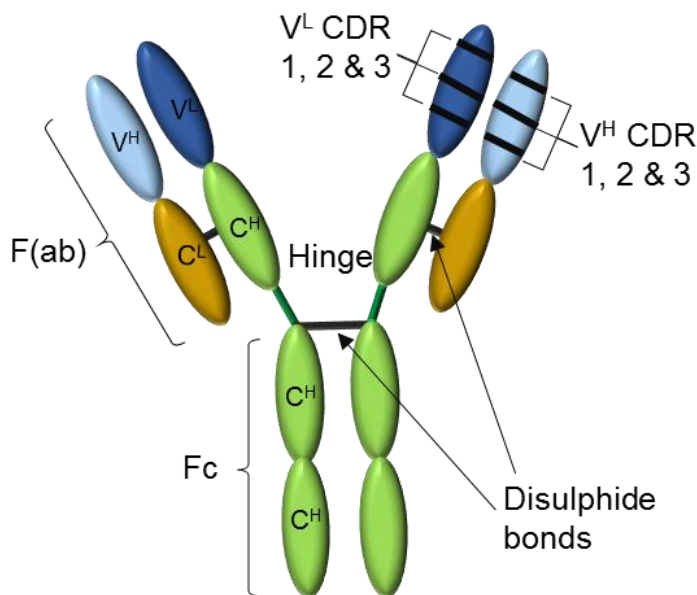


Figure 1.2: The structure of IgG

All antibodies comprise two identical heavy and two identical light chains. Each light chain is made up of a variable (V_L) and constant (C_L) domain, whilst each heavy chain includes a variable (V_H) and, in IgG, 3 constant (C_H) domains. IgG also contains a hinge region, instilling flexibility between the Fc and F(ab) regions. Antigen specificity is determined by the three complementary determining regions (CDRs), shown in black, present in each variable domain.

Antibody diversity is generated by the process of V(D)J recombination [119]. This is similar process by which T cells generate a wide TCR repertoire, described in Chapter 1.7.1. The variable (V), diversity (D) and junction (J) germline segments of the Ig locus undergo recombination, guided by flanking recombination signal sequences (RSS) comprised of a conserved heptamer-spacer-nonamer sequence. A coding region containing 1 V and 1 J segment for the V_L, and 1 each of V, D and J segments for the V_H is generated by this process. In humans there are 65 V, 27 D and 6 J heavy chain gene segments. For Lk chains 40 V and 5 J segments can be combined, whilst there are 30 V and 4 J Lλ gene segments. Additional constant (C) domains are incorporated

to generate the full chains. The class of the heavy chain is determined by the C coding region included, which is determined at the mRNA level.

During these recombination processes, several DNA cleavage and ligation events occur. These provide opportunities for increased diversity to be generated. The cleavage of the sequences at the RSS sites by the endonucleases RAG1 and RAG2 produces a hairpin structure of the coding region. This then undergoes a single stranded break via the RAG complex, the location of which is variable, increasing the sequence diversity. The open ends of the DNA are then edited by the addition and removal of nucleotides. RAG 1/2 can add “p” nucleotides to the ends whilst terminal deoxynucleotide transferase (TdT) adds “n” nucleotides to the ends of the recombined Ig genes, generating junctional diversity. The gene segments are then joined by DNA ligase IV, to form each section of the coding sequence for the Ig chain. As the CDR3 sequence is found between the V and J gene segment in the light chain and between the VD and DJ junctions in the heavy chain, this process produces increased diversity in the hypervariable CDR3 [118].

Antibodies undergo further development after antigenic stimulation. Stimulated B cells migrate and form germinal centres, where the processes of somatic hypermutation and class switching can further alter the antibody specificity. Somatic hypermutation occurs via random point mutations in the V segment, which can alter the binding characteristics of the antibody. Higher affinity mutations may be selected for in a process called affinity maturation. All antibodies are initially generated as IgM, incorporating the μ heavy chain, but the process of class switching, mediated by activation-induced deaminase (AID), allows splicing of the alternative heavy chains [120].

The production of therapeutic antibodies for immunotherapy can be performed using several techniques. Originally, immunisation of mouse models using a human protein was performed. This method generates a murine anti-human polyclonal antibody pool. The development of hybridoma technology allowed the isolation and production of single antibody clones [121]. To form a hybridoma, splenocytes from an immunised animal are fused via electroporation with a myeloma cell line. These cells are sub-cloned, and each can then produce a single antibody clone, with the advantage of the producer cells now having cell-line immortality. Whilst mAb produced in this way can be used in therapeutic studies, the administration of murine mAb into humans resulted in an immune response to the mAb itself [122].

Humanised mice can provide an effective way to avoid this anti-mAb response. These mice, when inoculated with an antigen, can produce fully human antibodies. Hybridoma

technology can then be employed as before to generate cell clones producing single mAbs [123]. Alternatively, post-production engineering can be employed to alter murine mAb to reduce an anti-mAb immune reaction. The Ig constant regions can be replaced with human domains using recombination, producing chimeric mAb. To generate humanised mAb, the CDR loops can be transferred into a full human Ig framework. Both of these techniques produce antibodies that are well tolerated by a human immune system, without the requirement for humanised mice [124].

A fully *in vitro* method of human mAb production involves the use of bacteriophage. The human Ig loci are edited to generate either scFv or F(ab) fragments and inserted into bacteriophage. These phage will consequently express a diverse range of human scFv or F(ab) fragments on their surface. Antigens are used to screen the phage library and those selected are eluted and amplified in bacteria. The specific Ig sequences are cloned out and these domains can then be modified to form full mAb constructs. Phage technology provides an efficient high-throughput, though costly, screening method without the need of animals [125] [126].

Therapeutic IgG mAb demonstrate a wide range of activity, including the targeting of cells for direct death via cell-intrinsic or FcγR-mediated mechanisms. Alternatively, mAb can block an antigen to inhibit signalling, or act as an agonist to promote a cellular response. The majority of mAb effector mechanisms require interactions with the FcγRs, either to mediate cell-based deletion of the target cell, or to provide crosslinking for the promotion of signalling cluster formation.

Early evidence for FcγR involvement in mAb mechanisms of action came from the observation that no anti-tumour immune response was seen after mAb treatment in mice lacking activatory FcγRs. Mice without the inhibitory receptor, FcγRIIB (CD32b), however, had improved cytotoxic responses from direct targeting mAb treatment [127]. In humans there are 5 activatory FcγR; FcγRI (CD64) is a high affinity receptor, whilst FcγRIIA (CD32a), IIC (CD32c) and IIIA (CD16a) are lower affinity. All can signal via immunoreceptor tyrosine-based activation motifs (ITAMs), either within the receptor itself (IIA and IIC) or by association with a common γ-chain (I and IIIA). FcγRIIIB is expressed via a GPI anchor and is classified as an activatory receptor despite the absence of ITAMs or association with the common γ chain. FcγRIIB (CD32b) includes an immunoreceptor tyrosine-based inhibition motif (ITIM) and is the only inhibitory FcγR in humans. The activation to inhibition (A/I) ratio of FcγRs can strongly affect the efficacy of direct targeting therapeutic antibodies [128].

The isotype of the mAb can influence the FcγR engaged [128]. Human IgG1 and IgG3 bind with high affinity to FcγRIIA and IIIA and elicit a strong effector response, so are

most effective at target cell deletion via ADCC and ADCP. Direct targeting mAb, such as rituximab and alemtuzumab, are usually produced as these isotypes to promote target cell deletion. Conversely to direct targeting mAb, human IgG1 and IgG2 are often used in the context of the immunostimulatory agonist mAb, described in Chapter 1.5.2.2.1. Whilst IgG1 interaction with the inhibitory FcγRIIB can be detrimental in the context of a direct-targeting mAb, an IgG1 immunostimulatory mAb can be crosslinked by FcRIIB, aiding the formation of a signalling complex which can augment its activity, seen for mAb targeting CD40 and death receptor 5 [128, 129]. Additionally an IgG1 isotype is beneficial for immunostimulatory mAb that act as both a ligand-blocking mAb and can also elicit direct targeting for example the anti-PD-L1 and anti-CTLA-4 mAbs [130]. The B form of IgG2 contains a restricted hinge region that can provide superagonistic properties, and so FcγR engagement is not required in this context [131]. Immunostimulatory blocking mAb, such as those targeted to PD-1, are often generated as IgG4, with minimal FcγR interactions to ensure that effector T cells are not deleted [128].

1.5.2.2.1 Immunostimulatory monoclonal antibodies

Immunostimulatory antibodies activate the immune system to improve anti-tumour responses, either by promoting co-stimulation or by blocking inhibitory molecules. Immune checkpoint antagonist mAb have been developed and have shown high levels of clinical success. The anti-CTLA-4 mAb ipilimumab has been successful in the treatment of metastatic melanoma patients, prolonging survival even in cases of advanced disease [132]. [133]. The mechanism of targeting CTLA-4 is proposed to involve both the blocking of inhibitory signals to effector T cells, and also the targeting of intra-tumoural Tregs, leading to their depletion and further potentiating the immune response [134]. Ipilimumab is now being studied as a therapy for other cancers including prostate and colon, and in combination with other chemotherapy or immunotherapy agents to try and improve efficacy and reduce toxicity [135].

PD-1, a T-cell exhaustion marker can be targeted by antagonist mAb, blocking interaction with the ligands PD-L1 and PD-L2, and augmenting T-cell anti-tumour activity. Nivolumab and pembrolizumab have been FDA approved for treatment of metastatic melanoma, and nivolumab is also approved as a therapy for squamous non-small cell lung carcinoma. These mAb are produced as the isotype IgG4 as crosslinking is not required, minimising FcγR interactions to reduce T-cell death. Both are in several ongoing trials investigating their efficacy against many cancer types [136]. Another PD-1 antagonist, cemiplimab, was also approved at the end of 2018 for the treatment of advanced cutaneous squamous cell carcinoma [137]. As with the majority of cancer therapeutics, combination therapy is often the most effective due to

synergistic effects. A combination of nivolumab and ipilimumab was shown to be more successful than either single agent in patients with untreated melanoma [138], and the dual therapy is now approved for metastatic melanoma, as well as renal cell carcinoma and colorectal cancer [139].

PD-L1 itself has also been targeted using blocking antagonistic mAb to inhibit interaction with PD-1. Several tumours express PD-L1, so this therapeutic approach can reduce T-cell suppression within the tumour microenvironment [140].

Atezolizumab, avelumab and durvalumab have been FDA approved for the treatment of locally-advanced or metastatic urothelial carcinoma, and atezolizumab for non-small cell lung cancer [139] [141]. PD-L1 can bind with PD-1 and also with CD80 *in cis*, inhibiting CD28-CD80 binding. PD-L1 antagonists have therefore been proposed to be a potential way to stop the inhibitory PD-1-PD-L1 signalling pathway, and prevent the blocking of CD28 co-stimulation [142]. The IgG1 isotype of these mAb also promotes the direct deletion of PD-L1+ve cells via FcγR+ve effector cells [130].

In addition to blocking inhibitory signalling molecules, the use of agonistic mAb targeted to co-stimulatory molecules on effector T cells can further activate them and overcome T-cell exhaustion. These mAb usually require cross-linking via FcγR interaction, promoting the formation of signalling complexes. CD137 stimulation can elicit a strong T-cell activation and survival signal, particularly in CD8+ve T cells, making it a favourable target to promote an anti-tumour T-cell response. Early models of CD137 agonistic mAb therapy in mice showed strong tumour control responses, including against some poorly-immunogenic tumours. The effects of anti-CD137 have been attributed to both an increased T-cell response, and to activation of NK cells on which CD137 is also expressed, resulting in enhanced antibody-dependent cellular cytotoxicity (ADCC) [143]. Combination studies using anti-CD137 with chemotherapy agents and radiation have shown a synergistic response, demonstrating higher T-cell infiltration of the tumour, corresponding with increased survival [144, 145].

Urelumab and utomilumab are the two CD137 agonists furthest in clinical development. Urelumab was first trialled as a monotherapy and showed some promise in patients with advanced solid tumours. However, dose-limiting liver toxicity was observed in some patients [146]. Use at a lower dose where toxicity is not observed is being investigated, in combination with other mAbs including rituximab, cetuximab and nivolumab. Utomilumab has shown reduced toxicity levels but also reduced efficacy. The engineering of this weaker anti-CD137 mAb to allow crosslinking via FcγIIB

provides a potential avenue to enhance its agonistic signalling abilities without inducing ADCC of the effector T cells, and avoiding liver toxicity [130].

OX40 is another member of the tumour necrosis factor receptor superfamily (TNFRSF), like CD137. OX40 agonistic antibodies have been shown to promote T-cell activation and differentiation into effector cells, and can reverse CD4+ve T-cell tolerance [147]. Further to augmenting an effector T-cell response, OX40 agonistic mAb can act to suppress Treg activity in the tumour microenvironment. Three mechanisms have been observed in which this can occur; the inhibition of Treg differentiation [148], suppression of Treg signalling [149], and direct FcγR-mediated deletion [150]. In mouse models, OX40 agonistic antibodies have been shown to synergise effectively with a CTLA-4 antagonist leading to Treg depletion and CD8+ve T-cell expansion, and with a PD-1 blocking antibody [151] [152]. Trials into melanoma and solid tumours are investigating OX40 agonism alone, or in combination with other immunotherapies or chemotherapy agents [153] [154].

1.5.2.2.2 Direct targeting monoclonal antibodies

Direct targeting mAb therapy involves the administration of an antibody to a specific TAA in order to elicit an anti-tumour response from the patient's immune system. Several effector functions can be induced by mAb interactions, depending on the characteristics of the antibody. The binding of the mAb to the antigen itself can sterically block the binding of survival or growth factors, or prevent receptor dimerization such as in the case of bevacizumab to VEGF and trastuzumab to Her2 [155] [156]. The interaction of some antibodies with the TAA can also induce a form of programmed cell death, dependent or independent of FcγR cross-linking [157].

Additionally, interaction of the Fc portion of the mAb with FcγR on NK cells and macrophages can initiate the major effector mechanisms of ADCC and antibody dependent cellular phagocytosis (ADCP) respectively. In humans ADCC is predominantly mediated via FcγRIIIA on NK cells [158]. ADCP is executed via the activatory receptors FcγRIIA and FcγRIIIA on macrophages and granulocytes that bind the Fc of mAb and engulf the tumour target cell [158, 159]. As FcγRI has such a high affinity it is usually bound by endogenous circulating IgG and is thought to have less of a role in immunotherapy. It has been shown that polymorphisms in the FcγR receptors that affect the affinity of binding to mAb can also alter the therapeutic outcome of mAb treatment, for example the V158 allele of FcγRIIIa has a higher affinity for IgG1 than the F158 allele, and has been associated with increased ADCC mediated via anti-CD20 mAb [160-162].

mAb can also elicit tumour cell lysis via the classical complement cascade in a process called complement dependent cytotoxicity (CDC). The complement cascade initiator protein, C1q can bind the Fc domain of mAbs, leading to activation of other complement proteins by proteolytic activation, culminating in formation of the membrane attack complex (MAC), and cell lysis [163]. Other complement cascade products can engage macrophages to enhance phagocytosis of apoptotic cells [164].

The chimeric anti-CD20 mAb rituximab demonstrated the first high clinical success of cancer mAb therapy. Since this time the field has expanded vastly, with many mAb now in the clinic or in development for a range of malignancies. mAb are particularly suited to the treatment of haematological disorders as their ability to penetrate a solid tumour and its microenvironment can be limited. Despite this there has been some success with solid tumour therapy, such as anti-GD2 dinutuximab for neuroblastoma and trastuzumab targeting Her2 +ve breast cancers [165, 166].

Other developments in the field include the glycoengineering of the Fc portion of mAb to increase the affinity of binding to FcγRs to improve efficacy or to select the mechanism by which the mAb will recruit effector cells. Obinutuzumab is a successful example of a glycoengineered mAb, whereby the Fc is partially afucosylated which improves its binding ability to FcγRIIIA, resulting in enhanced ADCC [167].

Obinutuzumab also has an engineered elbow-hinge region with enhanced flexibility, which increases the induction of direct cell death [168]. Additionally, some mAb have been developed to carry radioisotopes or pathogenic particles to the tumour to stimulate the immune response, or drugs to target the tumour cells [169].

Another category of therapeutic antibodies is bispecific antibodies (BsAb). These derivatives have two distinct epitope recognition domains to different antigens, to bind both a TAA and an effector cell receptor with one antibody, allowing the tumour cells to be brought into close contact with CTL or NK cells. Early bispecific antibodies were formed by fusion of one heavy and light chain of each targeting mAb, and demonstrated the ability of bispecific antibodies to form conjugates and to elicit target cell lysis [170] [171]. Several designs of bispecific mAb have been produced, including triomabs, appended IgG, and bispecific fragments such as dual affinity retargeting antibodies (DARTs) and bispecific T-cell engagers (BiTEs) [172].

Triomabs allow the targeting of CD3 and a TAA, whilst also retaining Fc-FcγR interactions. Catumaxomab, approved for therapeutic use for malignant ascites in 2009, is a triomab targeting epithelial cell adhesion molecule (EpCAM) and CD3. The Fc domain is designed to bind the activatory FcγR receptors, and not FcγRIIb, leading to the activation of macrophages, NK cells and DCs. These immune functions

collaborate with the activation of T cells via the CD3-targeting domain to provide a multi-faceted response [173].

The first therapeutically approved BiTE, Blinatumomab, was authorised in 2015 for the treatment of ALL, and targets CD19 and CD3. Even low doses (10-100 pg/ml) of this antibody have been shown in clinical trials to be capable of potent B-cell depletion with minimal toxicity [174, 175]. BiTEs do not require T-cell co-stimulation provided, rather they are thought to cluster into IS and induce native signalling. Alternatively, it has been proposed that memory T cells that do not require further co-stimulation play a major role in BiTE-mediated cytotoxicity [176]. Another benefit of BiTEs is their small size, bringing the effector and target cells into close contact and forming a close IS, known to be essential for effective T-cell cytotoxicity [177]. Other BiTEs in clinical trials include those targeting CD3, and CEA, PSMA or CD33 [178].

Similar to BiTEs, DARTs are small bispecific antibody fragments but in which the opposite VH and VL domains are linked, instilling a higher degree of conformational flexibility allowing optimal antigen-antibody interaction. DARTs targeting CD123, CD19, P-cadherin and B7H3 antigens, dually with CD3, are in clinical trials for a variety of malignancies, though none are yet approved for therapeutic use [178, 179].

1.6 CD20 and anti-CD20 mAb

CD20 was characterised by Stashenko *et al* as a cell surface antigen present on 95 % of healthy and most malignant B cells [180]. The exact physiological role of CD20 is not fully understood, but it is known to be involved in B-cell activation and signalling. It has been shown to generate a cytosolic Ca²⁺ flux in response to ligation. There is debate as to if this is via direct action as a calcium ion channel, or via an indirect mechanism [181]. CD20 spans the cell membrane four times and comprises two extracellular loops and cytosolic N- and C- termini. The molecular weight ranges between 33 and 36 kDa, dependent on levels of intracellular threonine and serine phosphorylation.

The antigen is highly expressed on the cell surface, thought to be as a homo-tetramer, and has historically been thought of as a stable molecule leading it to be selected as a mAb target antigen for B cell tumours [182] [183]. Extensive development in the area of immunotherapy has led to many advanced, humanised anti-CD20 mAbs now approved for use in the clinic or in clinical trials [184, 185] (**Table 1.1**).

Anti-CD20 mAb have been classified as either type I or type II, according to their binding and functional properties. Type II mAb bind to CD20 on the cell surface at

around half the maximal level of type I molecules at saturating concentrations, suggesting different binding configurations. It is proposed that two type I antibodies bind to every tetramer of CD20, whilst one type II binds in a diagonal conformation, as illustrated in **Figure 1.3 B**. Both types are known to most commonly bind the same extracellular region of CD20, incorporating an alanine-asparagine-proline (ANP) motif, but recently it has been shown they bind to different epitopes within this region (**Figure 1.3 A**). Type I mAb bind further towards the amino-terminal end of the motif, whilst type II bind towards the carboxy-terminal end, thus altering the conformation of binding [186]. Ofatumomab is classed as a type I anti-CD20 but is thought to bind an alternative epitope spanning both the large and small extracellular loops of CD20 [187].

	Antibody Name	Source, Isotype	
Type I	Rituximab	Chimeric, hIgG1 Fc	Glycoengineered Fc portions
	Ibritumomab I131	Murine, IgG1	
	Ocrelizumab	Humanized IgG1	
	Veltuzumab	Humanized IgG1	
	Ofatumomab	Fully human, IgG1	
	Ocaratuzumab	Humanized IgG1	
	PRO131921	Humanized IgG1	
	Ublituximab	Chimeric, hIgG1 Fc	
Type II	Obinutuzumab	Humanized IgG1	
	Tositumomab	Murine, IgG2a	

Table 1.1: anti-CD20 mAb

Current anti-CD20 mAb in the clinic (bold), or in clinical trials for B-cell cancers [188]. The source, isotype and type classifications are shown. Those that have undergone Fc glycoengineering to improve FcγR interactions are indicated (green box).

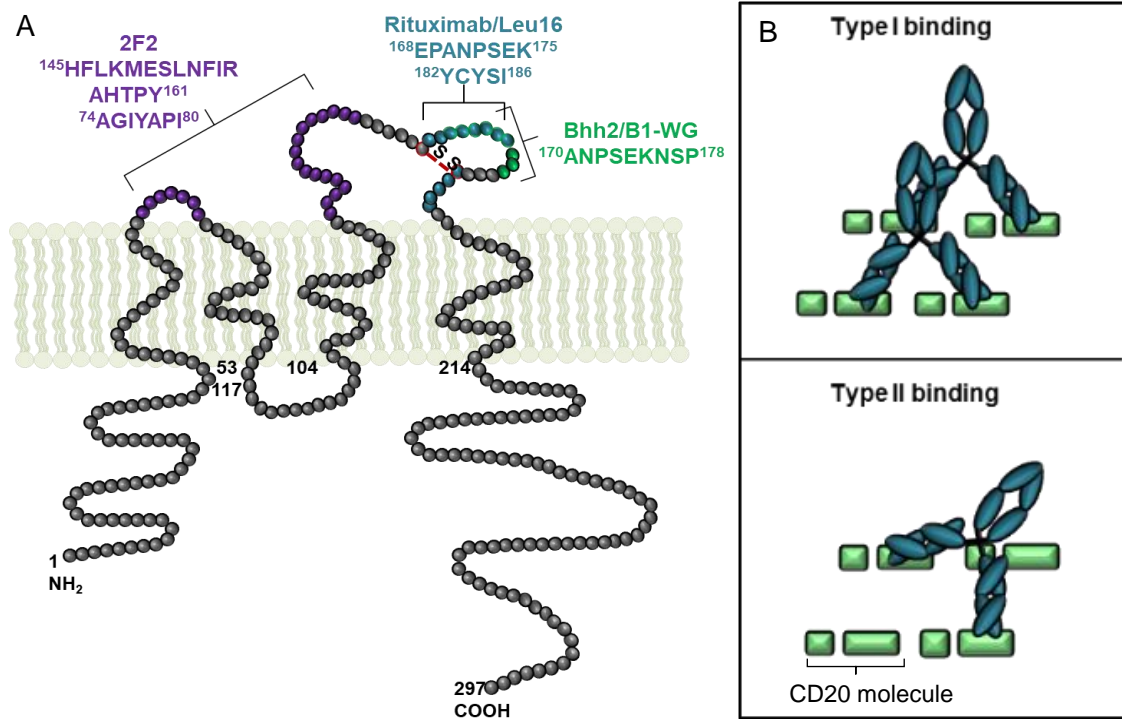


Figure 1.3: Epitopes bound by anti-CD20 mAb relevant to this project

A: The known epitopes of CD20 bound by ofatumumab (2F2; purple), rituximab and Leu16 (blue), and obinutuzumab (afucosylated BHH2) and tositumomab (similar to B1-WG; green) are shown in the context of the full CD20 molecule. S—S shows stabilising disulphide bond present in the large extracellular loop.

B: The proposed binding orientations of type I and type II anti-CD20 mAb. Type I mAb are known to bind at twice the maximal level of type II, and are thought to bind two mAb per CD20 tetramer, and in an inter-tetramer manner. Type II mAb are thought to bind as one molecule per CD20 tetramer, in a diagonal conformation.

The bivalent binding of anti-CD20 mAb to the CD20 tetramers increases the avidity and can enhance the instances of clustering, which allows cross-linking of the Fc portions. This can alter the signalling abilities of the mAb and improve efficiency. A study comparing monomeric rituximab to homodimers, introducing higher avidity without the need for *in vivo* hyper-crosslinking, demonstrated increased apoptosis and necrosis in target cells in the presence of the homodimers [189]. An anti-EGFR mAb was shown to have improved CDC when monovalent binding was forced, as the angle of binding was altered permitting hexamer formation. This was not found to enhance anti-CD20 mAb activity, although hexamer formation via mutagenesis may still influence those mAb that rely on CDC [190].

Another difference between type I and II anti-CD20 mAb is the ability of type I to redistribute CD20 into lipid rafts upon binding, whilst type II do not elicit this response. When a type I mAb, such as rituximab, binds to CD20 the molecules cluster into these

microdomains in the B-cell membrane. This is known to have considerable functional consequences [191-193]. Clustering of the rituximab-bound CD20, in a hexameric formation of the Fc domains, is thought to increase the ability of C1q to bind, leading to enhanced CDC [194].

A negative impact of distribution into lipid rafts on antibody function is the consequent internalisation seen of the type I antibody-CD20 complexes. This has been shown to be facilitated by CD32b *cis* interaction with the Fc portion of the antibody. The antibody-CD20-CD32b complexes are then trafficked to lysosomes for degradation and so the antibody is longer accessible to engage FcγR or complement proteins and CD20 is lost from the cell surface [195]. Type II anti-CD20 antibodies have been shown to bind to CD32b, but they do not become internalised like type I molecules. This could be due to the different orientation of binding of the antibody types to CD20 in relation to the CD32b molecules [196].

Whilst type I mAbs appear to rely extensively upon both the previously mentioned Fc:FcγR interactions and complement activation to kill B cells, type II mAbs exhibit high levels of ADCC and direct cell death. This cell death is not categorised as classic apoptosis, as DNA fragmentation is not seen, only low levels of caspase processing are involved, and Bcl2 overexpression cannot fully inhibit it [191]. Rather, a lysosome- and ROS-dependent mechanism has been proposed, involving the re-organisation of the actin cytoskeleton, induced by type II mAb binding [157].

Type II antibodies have been shown to have superior anti-tumour activity to type I in preclinical models [191] and in a clinical setting [197], [198], [199]. In preclinical studies, the differences seen could not be explained by affinity, isotype, binding density or half-life. Abrogation of complement engagement did not affect the outcome either. This may be explained by the alternative mechanisms engaged by the antibodies, particularly the ability of type II antibodies to initiate direct cell death, and the internalisation of type I antibodies after CD32b engagement. Additionally, the differential binding to the CD20 tetramers and the epitopes engaged may have a role in the enhanced efficacy seen with the type II antibodies.

Details on the anti-CD20 mAb key to this project (rituximab, Leu16, B1-WG [related to tositumomab], BHH2 [non-afucosylated obinutuzumab] and 2F2 [ofatumumab]) can be found in **Table A1.1** in the Appendix.

1.7 T cells

1.7.1 T-cell development

All blood cells are derived from a pool of haematopoietic stem cells in the bone marrow. These cells are capable of self-renewal and are undifferentiated. Multipotent progenitors (MPPs) develop from these stem cells and lose the ability to self-renew [200]. The classical view of haematological development is that two distinct lineages are derived from these MPPs, a myeloid and a lymphoid line [201, 202]. Common lymphoid progenitors are cells that have the ability to differentiate into NK cells, B or T lymphocytes. Some debate has occurred over the discovery of lymphoid-primed MPPs that have been seen to develop into B, T, or granular myeloid cells [203]. However, it has been shown *in vivo* that T lymphocyte progenitors are predominantly lymphoid-committed when they leave the bone marrow and migrate to the thymus, the site of T-cell development [204].

T lymphocyte progenitors enter the thymus via the cortico-medullary junction and migrate to the cortex. Here, the double-negative early (DN1) thymocytes are exposed to an environment that further restricts differentiation pathways other than that of T cells [205]. Notch signalling is essential in this process, shown by knockout experiments involving Notch1 or its regulators of expression [206]. A high rate of proliferation occurs at this stage and the cells migrate to the subcapsular zone of the thymus. Here, DN2 cells interact with thymic epithelial cells and fibroblasts and it is thought that this is the point from which all other differentiation potential is lost [207].

Two subsets are found at this stage, IL-7R^{hi} and IL-7R^{lo} thymocytes. This difference in receptor expression has been shown to play a role, independent of later TCR signalling, in the differentiation of cells into $\alpha\beta$ or $\gamma\delta$ T cells. IL-7^{lo} cells are biased towards $\alpha\beta$ T cell development and undergo T-cell receptor β chain rearrangement, whilst IL-7^{hi} cells initiate γ and δ chain rearrangement more often than $\alpha\beta$ [208]. Gene expression of a pre-TCR invariant α -chain and of recombination activating genes 1 and 2 (RAG1 and 2) increases, leading to germline rearrangement of β , γ and δ TCR genes [209]. This process is very similar to that of Ig recombination, described in Chapter 1.5.2.2, and allows gene segments encoding parts of the TCR to join in alternative ways to produce TCRs with a vast array of antigen specificities. In humans, there are 70 variable (V) and 61 joining (J) gene segments for the TCR α chain and 52 V, 2 D and 13 J segments in the β chain loci. The TCR gene recombination sites are flanked by RSS where RAG proteins bind and cleave the DNA to form hairpins. The D and J segments first undergo recombination under the control of the RAG 1 and 2 proteins,

followed by the V segment. These are then joined to a constant (C) segment to complete the chain [210, 211]. Junctional diversity is generated by RAG 1/2 and TdT, as for Ig recombination, before the gene segments are ligated together. If the addition of these extra nucleotides results in incomplete rehybridisation of the strands, the gaps are filled by DNA repair machinery. These processes increase the repertoire of antigens that the TCR library can recognise even further than that already generated by somatic recombination.

This process continues through the DN3 stage. The pre-TCR α invariant chain is expressed with the rearranged β -chain, and the $\gamma\delta$ TCR is also expressed. Notch signalling is upregulated again and Notch and β -invariant- α signalling are both required for progression of the cells into DN4 [212, 213]. Signalling via the pre-TCR at this point has been shown to be essential in final lineage commitment to $\alpha\beta$ T cells, or to the development into $\gamma\delta$ T cells [214]. CD4 and CD8 both become expressed on the cell surface, giving double positive (DP) cells. The cells migrate back towards the medulla of the thymus and RAG expression and recombination of α -chain genes are instigated in $\alpha\beta$ -destined cells, to produce the mature $\alpha\beta$ TCR molecule [215]. The α -chain V and J segments are rearranged and then joined to the C segment. The $\alpha\beta$ TCR with the accessory molecules of CD3 that it is expressed with on mature T cells is illustrated in **Figure 1.4**.

Once the T cells are expressing $\alpha\beta$ TCRs against antigens, thymic selection occurs. This process involves the presentation of a range of antigens in the context of MHC to the naive T cells to allow deletion of those that may recognise self-antigens with a high affinity and of those which are non-functional. Peptide-MHC complexes are presented to the T cells on cortical thymic endothelial cells (cTECs) in the first stage of positive selection. Those cells that can recognise the self-MHC, about 5 % of the cells generated, are selected for survival. Those cells that fail to recognise either MHC class I (MHC I) or MHC class II (MHC II) are deleted by apoptosis after approximately 4 days, known as death by neglect [216]. T cells recognising MHC I down-regulate CD4 and become CD8 single-positive T cells and those that interact with MHCII become CD4 single-positive. The majority of positive selection occurs in the cortex of the thymus. After positive selection, Bcl-2 and CCR7 are upregulated in the cells to promote survival and migration to the medulla respectively [217].

Negative selection then occurs, facilitated by medullary thymic endothelial cells (mTECs). These cells express a nuclear regulatory protein, AIRE, that enables processing and presentation of an extensive range of tissue-specific antigens [218]. Cells that have a high affinity for self-antigens are clonally deleted. Low affinity T cells

are selected for survival as CD4 or CD8 T cells. Some cells with higher affinities can undergo TCR editing to alter the binding [216]. Those cells that show a mid-level affinity for self-antigens can differentiate instead of undergoing apoptosis. These cells may up-regulate FoxP3 and develop into Tregs [219]. The successful T cells leave the thymus and enter circulation. This process is dependent on increased expression of S1P1 allowing the T cells to follow a S1P gradient out of the thymus into the periphery. CD62L upregulation is also required in this process [220] [217].

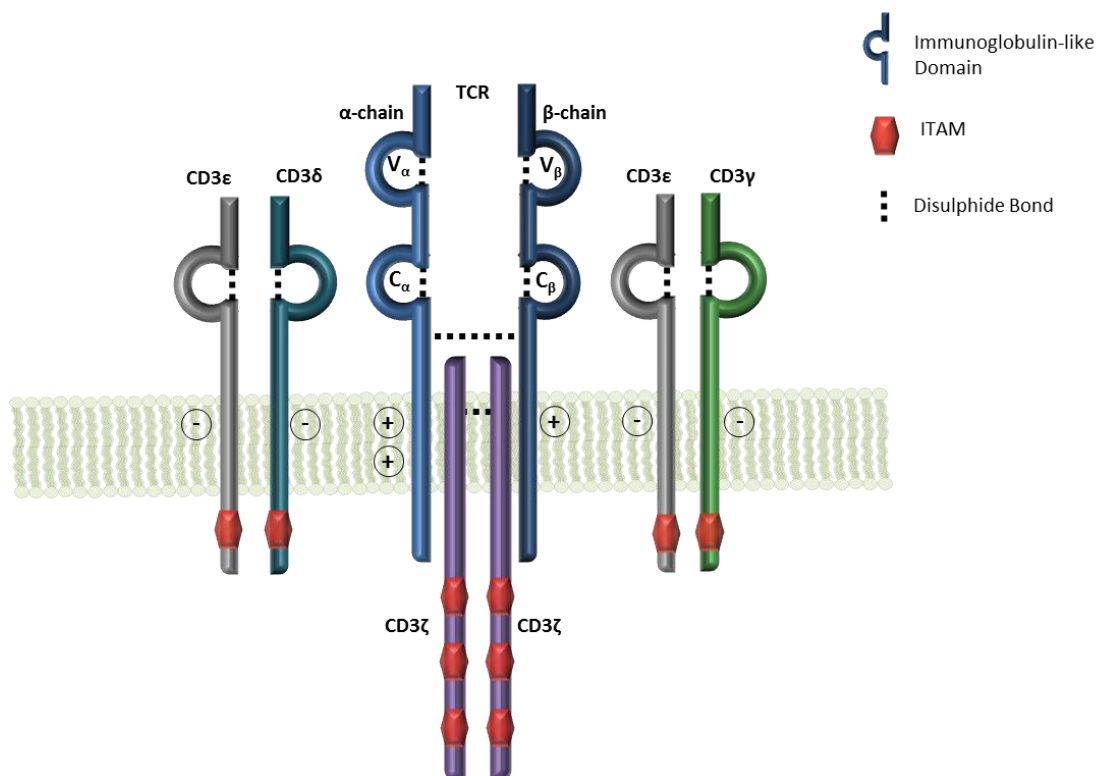


Figure 1.4: The structure of the $\alpha\beta$ TCR and associated CD3 molecules

Each chain of the TCR has 2 Ig domains; one constant (C) and one variable (V). The variable regions of the TCR are those that recognise and bind antigenic peptides, via the complementarity determining regions (CDRs). CDRs are hyper-variable sections responsible for increasing the vast antigenic repertoire of the TCR system. The CD3 γ , δ and ϵ chains each possess one Ig domain whilst the CD3 ζ homodimer has none. The ζ chains have cytoplasmic tails, each contains 3 immunoreceptor tyrosine-based activation motifs (ITAMs). The other CD3 chains have 1 intracellular ITAM each. ITAMs become phosphorylated upon antigen binding and initiate signalling cascades to activate the T cell.

T cells leaving the thymus are naive, meaning they have not yet encountered foreign antigen in the periphery and so are inactive. Naive T cells are CD4⁺ or CD8⁺ and express CCR7 and CD45RA. CCR7 is a chemokine receptor that elicits homing of the naive T cells to secondary lymphoid organs where they will encounter APCs [221]. Antigen from pathogens or self-antigen is processed by APCs such as DCs into

peptide epitopes. These are displayed upon the APC cell surface in the context of MHC molecules, allowing recognition by antigen-specific naive T cells. CD8+ve T cells recognise viral or self-antigens bound by MHC I, whilst MHC II presents exogenous antigens predominantly to CD4+ve T cells. If successful, these interactions combined with co-stimulation leads to T-cell activation and differentiation of effector and memory subsets that can act in a variety of ways to induce and support an immune response.

The strength of TCR signalling upon antigen recognition is thought to be key in deciding T-cell fates. Inappropriately strong TCR signalling will result in cell death to avoid the risk of an over-active immune response. Strong TCR signalling induces short lived-effector cells (SLECs) that demonstrate a terminally differentiated state. After the acute phase of infection is over, these cells will die by apoptosis as positive survival signals are no longer present. Intermediate strength TCR signalling also preferentially produces effector cells, but a subset of these become effector memory cells (T_{EM}) after the acute phase. These cells remain in the periphery and are capable of immediate effector responses upon antigenic re-stimulation. A weaker, but still activatory, TCR signal generates a population of central memory T cells (T_{CM}). The T_{CM} cells upregulate CCR7 and home to lymph nodes and do not immediately provide effector responses but have a high proliferative capacity. Memory cells are vital in the recognition and response of a secondary infection with a previously encountered pathogen [222-224].

1.7.2 T-cell receptor-mediated activation

To achieve full T-cell activation, sustained peptide-MHC (pMHC)-TCR interaction is essential. Upon specific antigenic epitope recognition by the TCR, steps are initiated to stabilise the binding between the APC and the T cell. The initial signalling via the TCR is thought to be induced by a combination of conformational change upon ligand binding, exposing CD3 motifs that were hidden in resting cells, and the grouping of signalling molecules in plasma membrane clusters, termed the kinetic segregation model [225-227]. T-cell polarisation is induced under control of the cytoskeleton, and the immunological synapse (IS) forms. The IS comprises the signalling and adhesion molecules required for T-cell activation, arranged in a specific way. The core of the IS is called the central supramolecular activation complex (cSMAC), where the TCR-pMHC interaction occurs with the CD3 accessory molecules associated with the complex, surrounded by CD4/8, CD28-CD80/CD86 and cytotoxic T-lymphocyte-associated protein 4 (CTLA4)-CD80/CD86. This microclustering of the TCR with CD28 has been shown to recruit signalling molecules and initiate signalling [228]. Around this signalling core, leukocyte function-associated antigen-1 (LFA1) and intercellular adhesion molecule 1 (ICAM-1) adhesion interactions comprise the peripheral (p)

SMAC. Further stability is provided by the distal (d) SMAC, incorporating CD43, CD44 and CD45 [229, 230].

The activation state of the src family kinase Lck is modulated by phosphorylation sites in resting T cells (**Figure 1.5**). Csk, another src family kinase docks to phosphorylated phosphoprotein-associated with glycosphingolipid-enriched microdomains (PAG) in the plasma membrane. Here, it acts to phosphorylate the inhibitory tyrosine, Y⁵⁰⁵, of Lck keeping it in the inactive form. The phosphatase CD45 removes this phosphate residue, transferring Lck into a primed state. Lck itself can then trans/auto-phosphorylate the activation residue, Y³⁹⁴, to form the fully active protein. CD45 reverses this process, retuning Lck to a primed state. Thus, CD45 has a dual role in the activation and inhibition of Lck [231] [232].

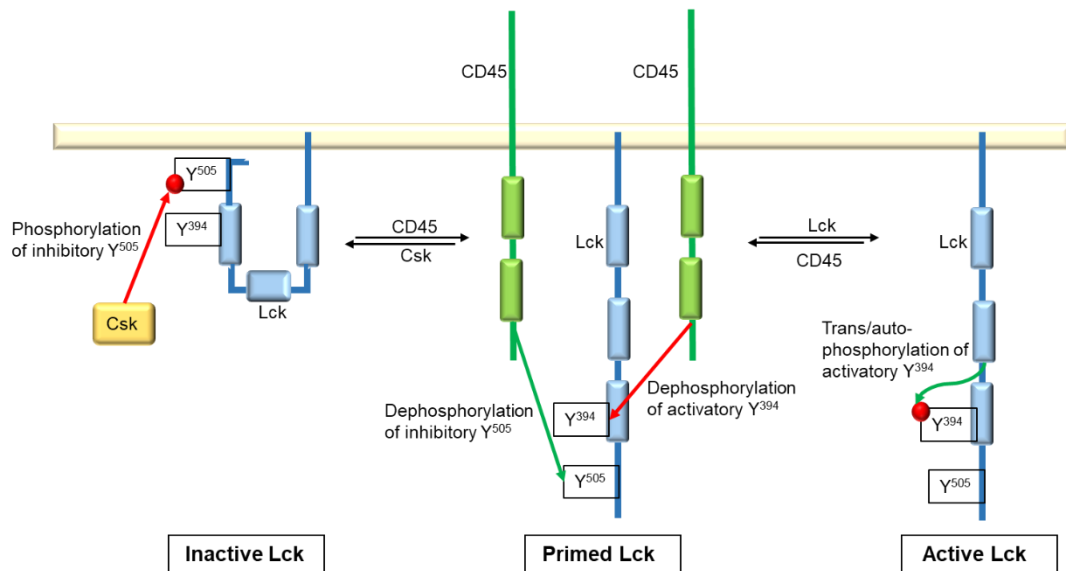


Figure 1.5: Control of Lck activation

Lck is phosphorylated on an inhibitory tyrosine residue (Y⁵⁰⁵) by the kinase Csk, keeping Lck in an inactive form. This phosphate is removed by CD45, priming Lck. Primed Lck can be auto-phosphorylated on the activatory tyrosine residue (Y³⁹⁴), transferring it to the active state. CD45 can again dephosphorylate this residue, returning Lck to a primed state. In this way CD45 has a dual role in activation and inhibition of Lck, and the outcome is thought to depend upon spatial segregation of the proteins, upon the formation of an IS [231, 232].

In an activated T cell, upon TCR-antigen binding and the formation of the IS, the large molecule CD45 is thought to be excluded from the protein cluster and PAG becomes dephosphorylated. Csk is therefore no longer membrane associated and cannot act to inhibit primed Lck. This process allows active Lck to be associated with the TCR signalling complex, where it acts to phosphorylate ITAMs in the CD3 chains [232]. Each ϵ , δ and γ chain possesses 1 ITAM motif, whilst the two ζ chains have 3 tandem

motifs. All the ITAMs follow the following consensus: YxxL/I-X7-YXXL/I, however each ITAM of the CD3 complex is distinctive [233]. Once both tyrosine residues in each ITAM are phosphorylated, zeta-chain-associated protein kinase 70 (ZAP-70) is recruited to the phosphorylation sites, binding via its Src homology-2 (SH2) domain [234]. Multiple T-cell activation signalling cascades are then initiated downstream (Figure 1.6).

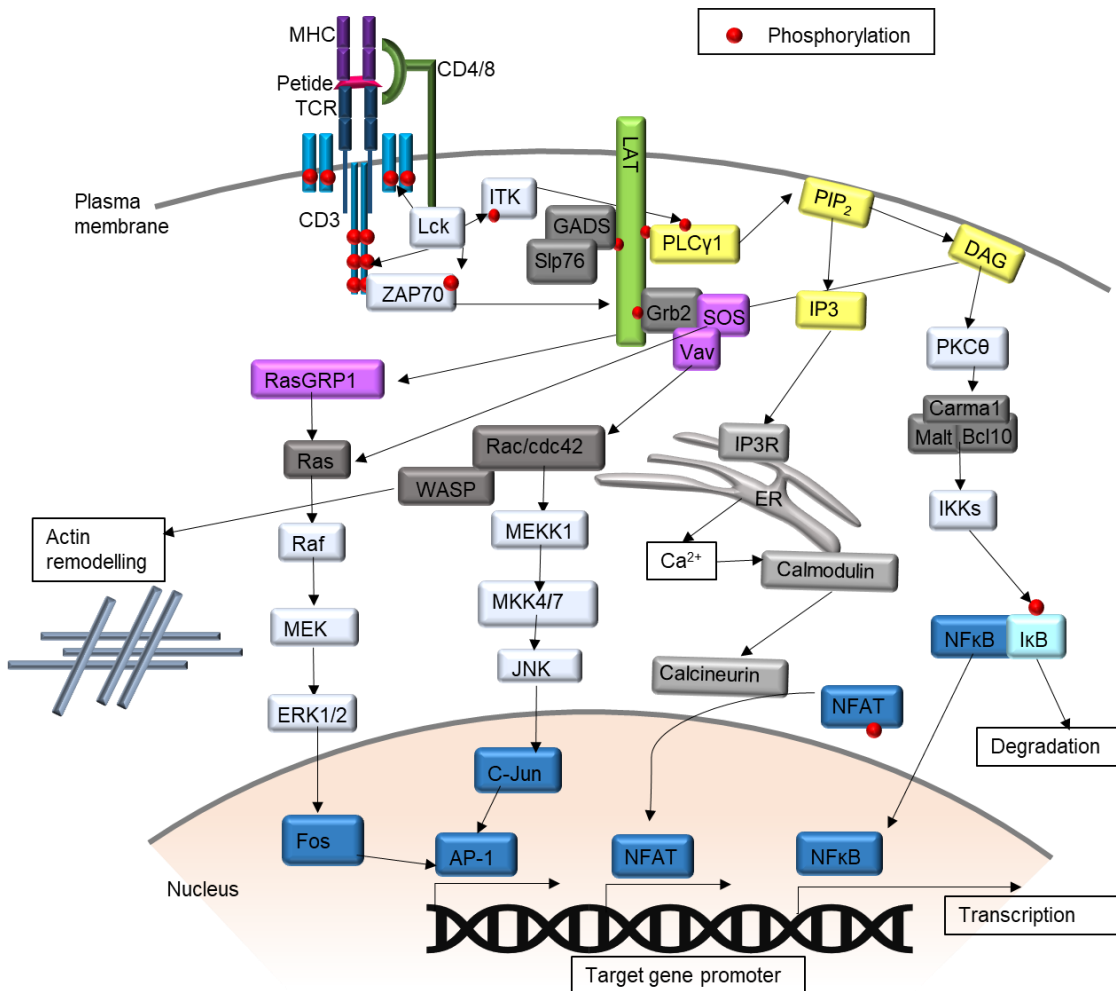


Figure 1.6: A schematic of T-cell signalling pathways induced upon antigen recognition

The interaction of the TCR with an antigen in the context of MHC results in the phosphorylation of CD3 chain ITAMs by the activated Lck kinase. ZAP-70 and ITK are recruited and phosphorylated leading to several downstream signalling cascades. PLC γ activation induces calcium-dependent NFAT dephosphorylation and PKC θ -mediated NF κ B activation. MAPK cascades are also activated leading to the activation and nuclear translocation of C-Jun and Fos, which dimerise to form the transcription factor AP-1. These transcription factors are all then able to bind target gene promoters to upregulate the production of activatory proteins such as IL-2. GTPase and WASP family signalling also leads to actin remodelling, essential for assembly and support of the IS [227, 235, 236].

ZAP-70 is phosphorylated by Lck at Y⁴⁹² and Y⁴⁹³ [234], and tyrosine protein kinase (ITK) is also phosphorylated at Y⁵¹¹. The linker for activation of T cells (LAT) signalosome assembles, comprised of ZAP-70-phosphorylated LAT, and adaptor proteins including growth factor receptor-bound protein 2 (Grb2), SH2 domain-containing leukocyte protein-76 (Slp76) and Grb2-related adaptor downstream of Shc (GADS) [235]. Phospholipase-C γ 1 (PLC γ 1) associates with phosphorylated LAT, where it is phosphorylated and activated itself, by ITK. Active PLC γ 1 is responsible for the initiation of the nuclear factor κ -B (NF κ B) and nuclear factor of activated T cells (NFAT) pathways [235] [227].

PLC γ 1 hydrolyses phosphatidylinositol 4,5-bisphosphate (PIP₂) to form inositol 1,4,5-trisphosphate (IP₃) and diacylglycerol (DAG). IP₃ binds to its receptor on the membrane of the endoplasmic reticulum and induces calcium release. Calmodulin is activated and in turn activates the serine/threonine phosphatase calcineurin. Calcineurin can act to dephosphorylate NFAT, allowing it to enter the nucleus and act as a transcription factor [227]. DAG recruits protein kinase C- θ (PKC θ), leading to the assembly of the caspase recruitment domain-containing membrane-associated guanylate kinase protein-1 (Carma1)/mucosa-associated lymphoid tissue-1 (MALT-1)/B-cell lymphoma-10 (bcl10) complex. This acts upon the inhibitor of κ B (I κ B) kinase (IKK) complex, comprised of catalytic IKK α , IKK β and the regulatory subunit NF κ B essential modulator (NEMO). Activated IKKs phosphorylate I κ B, leading to its degradation and revealing the nuclear localisation signal of NF κ B that is hidden when the inhibitor is bound. The canonical NF κ B subunits (RelA:p50 and c-Rel:p50 dimers) are then able to translocate to the nucleus to act as transcription factors [235, 237].

The GTPase Ras becomes activated downstream of both ras guanyl releasing protein-1 (RasGRP1) -activated by DAG- and the guanine nucleotide exchange factor (GEF), sons of sevenless (SOS). Ras activates the Raf/MEK/ERK MAPK cascade, resulting in activation of Fos. Another GEF associated with Grb2, Vav, activates the Rho-family GTPases Rac and cdc42, leading to activation of a second MAPK cascade involving MEKK1, MKK4/7 and JNK. JNK activates C-Jun [238], and the Fos and C-Jun proteins can dimerize to form the transcription factor activator protein-1 (AP-1). These transcription factors can all bind to target gene promoters and upregulate T-cell activation gene transcription, such as IL-2 [239].

The GTPases Rac and cdc42 are also involved in the activation of Wiskott-Aldrich syndrome protein (WASP) family proteins [236]. WASP family proteins interact with a protein complex known as Arp2/3 that are able to initiate actin polymerisation. This is essential in the formation and support of IS SMACs [240]. Additionally, microtubule

(MT) reorganisation and relocation of the MT-organising centre (MTOC) is a key part of T-cell activation signalling, to allow polarisation of organelles and secretory vesicles towards the IS. The reorganisation of the MT network is also regulated by Rac [240]. It has been demonstrated that Rac is upregulated by Hedgehog signalling upon TCR activation, which acts to increase Rac levels, promoting rapid cytoskeleton reorganisation and polarisation towards the target cells [241].

1.7.3 T-cell co-stimulation and co-inhibition

Further to the T-cell activation signal initiated by the TCR/CD3 complex, co-stimulation is essential for complete T-cell activation and to avoid anergy [242]. Two major families of costimulatory molecule are found expressed on T cells; the tumour necrosis family receptor superfamily (TNFRSF) and the immunoglobulin superfamily (IgSF). The TNFRSF molecules are transmembrane proteins that signal by binding to ligand trimers. Those involved in apoptotic signalling have intracellular death domains, whilst the activatory receptors have signalling factor-binding regions only [243]. The TNFRSF members signal via interactions with TNF receptor-associated factors (TRAFs), which associate via TRAF-interacting motifs (TIMs) on the internal signalling domains [244]. TRAFs can induce signalling cascades leading to JNK, ERK and NF κ B activation [245]. IgSF members each contain Ig domains, and the activatory proteins signal via PI3K and PKC θ . Inhibitory IgSF members recruit phosphatases that act to dephosphorylate activated proteins in the T-cell signalling cascades, attenuating the activation signal [246].

The traditional view of T-cell costimulatory signalling was the two-signal model. This involved the first signal for T-cell activation being induced by the TCR-pMHC interaction and a second signal, required for the activation to be complete, from CD28 on the T cell binding to B7-1 on the APC. The discovery of a second ligand for CD28, B7-2, and of another molecule CTLA4, expressed on T cells, that can bind both B7 ligands has led to a more complex view. This is often termed the “tide” model of signalling, requiring a threshold level of activation and control by suppression rather than the conventional on/off hypothesis [247].

CD28, a 44kDa IgSF member, is expressed on 50 % of CD8+ve and 80 % of CD4+ve naive T cells in humans, and 100 % of T cells in the mouse [248]. It has been shown that inside-out signalling mediated by the TCR causes the dimerization and activation of CD28. This may also induce a conformational change in the extracellular portion of CD28, allowing B7-1, B7-2 or the alternative ligand B7-H2 to bind to a MYPPPY motif, allowing signalling to commence [248, 249]. CD28-B7 interactions initiate upregulation of CTLA4 on the T cell. This molecule can out-compete CD28 to bind B7 as it binds

with a higher affinity (K_D 12 nM), compared with CD28 (K_D 200 nM) [250]. CTLA4 causes a suppressive signal to the T cell, and is also capable of removing B7 molecules from the APC cell surface by trans-endocytosis, into the T cell, thus preventing further CD28-B7 co-stimulation [251].

1.7.3.1 CD28 signalling

CD28 signalling acts to augment the TCR activation signals, to upregulate rates of IL-2 transcription and increased its post-transcriptional stability, along with the upregulation of survival and proliferation factors [252] [248]. The intracellular signalling motifs of human CD28 are shown in **Figure 1.7**. The tyrosine in the intracellular YMMN motif is phosphorylated by Src family kinases and forms a docking site for the SH2 domains of the p85 subunit of PI3K and the Grb2 adapter protein [248, 253, 254]. PI3K signalling induces PIP_3 production, which recruits 3-phosphoinositide-dependent protein kinase-1 (PDK1) and Akt (protein kinase B). Akt is phosphorylated and activated by PDK1, resulting in activation of downstream molecules mTOR and NF κ B, which act to promote cell division, and cell survival via upregulation of Bcl- $_{XL}$ [248]. This PI3K signalling is in turn regulated by SHIP1 and PTEN, that dephosphorylate PIP_3 to PIP_2 , attenuating downstream Akt activation [255].

The proline rich motifs of CD28 can also associate with Lck and Grb2. Lck can recruit PKC θ , leading to further NF κ B activation [259]. Similar to CD3 signalling, CD28-bound Grb2 recruits SOS and Vav. Grb2-SOS activates Ras, whilst Grb2-Vav can recruit the rac1-cdc42 dimer leading to MAPK cascade-mediated activation of JNK and ERK and consequent AP-1 assembly [256]. NF κ B signalling is also increased downstream of Grb2-Vav. These pathways combined have been shown to induce full activation of the CD28 response element [257].

ITK is recruited to the IS by PI3K-generated PIP_3 , where it also can interact directly with the PRRP motifs of CD28, furthering PLC γ 1 activation and signalling. In this way TCR-driven NFAT and NF κ B signalling is augmented by CD28, increasing IL-2 transcription [227].

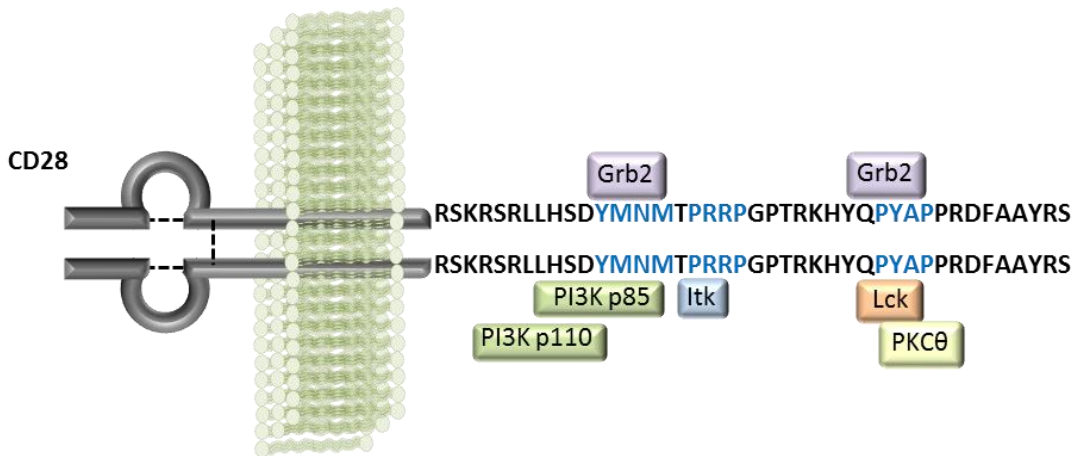


Figure 1.7 Structure of CD28 showing intracellular motifs that are bound by signalling proteins

The intracellular signalling motifs of CD28 are shown, along with the proteins known to bind to these domains. PI3K interacts with the YMNMT motif and is responsible for the activation of mTOR and NFκB. The adaptor protein Grb2 binds both the YMNMT and proline-rich motifs and recruits Vav and SOS, inducing MAPK signalling, and the assembly of AP-1. The kinases ITK and Lck interact with the proline-rich motifs, and augment PLCγ and PKCθ -dependent NFκB and NFAT activation [248].

1.7.3.2 Other key IgSF signalling molecules

Another key activatory IgSF molecule involved in T-cell stimulation is ICOS. This protein binds B7-H2 and induces PI3K signalling via an YMXM motif, as in CD28. This also leads to Akt activation and expression of subsequent cell growth and survival factors. However, PI3K subunits p50 and p85 are recruited by ICOS and as p50 is more active, higher Akt activation is seen compared to CD28 signalling [258]. ICOS also induces IL-4, IL-10 and IL-21 production via c-maf signalling which are involved in Th2 development, but minimal IL-2 [259].

Conversely to these activatory receptors, CTLA4 and the T-cell exhaustion markers PD-1, TIM-3 and LAG-3 are IgSF members involved in the inhibition of T-cell responses. As described in Chapter 1.7.3, CTLA4 binds the B7 ligands with higher affinity to CD28 and is upregulated when CD28 signalling is induced. It is only constitutively expressed on Treg cells. It has been shown that the majority of CTLA4 resides intracellularly, associated with T cell receptor-interacting molecule (TRIM) in the trans-Golgi network [260]. TRIM acts as a chaperone to regulate surface expression of CTLA-4. When surface CTLA-4 binds B7, a stable lattice-like structure of homo-dimers is formed [261]. By a combination of out-competing CD28, direct suppressive signalling and the ability to trans-endocytose B7, CTLA4 acts to inhibit T-cell activation and control the cytotoxic response. A YVKM motif of CTLA4 interacts

with SHP2 and PP2A phosphatases. SHP2 dephosphorylates the ITAMs of the CD3 complex, whilst PPA2 acts to dephosphorylate and inactivate Akt [262].

PD-1 contains an immunoreceptor tyrosine-based inhibition motif (ITIM) and an immunoreceptor tyrosine-based switch motif (ITSM) in its cytoplasmic tail. These motifs recruit SHP2, and SHP1 and 2 phosphatases respectively, which dephosphorylate activated CD3 chains, inhibiting their signalling and attenuating T-cell activation [263, 264]. PD-1 is upregulated rapidly after T-cell activation and interacts with its ligands, PD-L-1 (B7-H1) and PD-L-2 (B7-DC), on APCs. It is then downregulated on effector cells, to allow an acute immune response, but upregulated again upon chronic antigen exposure resulting in functionally exhausted T cells [265].

TIM-3 contains a Y²⁶⁵ motif that in the absence of TIM-3 interaction with its ligand, galectin-9, is not phosphorylated and allows the regulatory protein Bat3 to bind, inhibiting TIM-3 signalling. When the ligand binds, this tyrosine is phosphorylated by Lck, causing Bat3 to dissociate and TIM-3 to signal via undissected pathways to suppress T-cell activity [266].

Similar to TIM-3, LAG-3 doesn't contain any intracellular ITIM/ITSM motifs. Function relies upon a KIEELE motif via an undissected mechanism. LAG-3 is expressed on CD4+ve and CD8+ve T cells and binds MHC II with a high affinity. It is known that blockade of LAG-3 augments T cell activity, increasing proliferation and cytokine production, demonstrating the inhibitory characteristics of LAG-3 [262, 267].

1.7.3.3 CD137 Signalling

CD137 (4-1BB) is a member of the TNFRSF, expressed on T cells within 24 hours of initial activation, and upregulated as a consequence of TCR-mediated NFκB and AP-1 activation [268, 269]. It forms a trimer which binds a trimeric ligand, CD137L. As a TNFRSF molecule, it signals via interaction with TRAFs that associate via intracellular TIMs. CD137 can bind TRAF 1, 2, and 3 in humans, via glutamine-rich motifs, illustrated in **Figure 1.8** [270].

CD137 can activate the canonical and non-canonical NFκB pathways. In the canonical pathway, TRAF2 and cellular inhibitor of apoptosis protein (cIAP) are recruited to the receptor, along with RIP. RIP is ubiquitinated, and can then recruit MAP3K7, and IKK. These proteins form an IKK-activating complex, leading to phosphorylation and degradation of IκB, and allowing NFκB dimers RelA:p50 and c-Rel:p50 to enter the nucleus [271, 272]. This results in upregulation of anti-apoptotic genes c-FLIP, Bfl and Bcl_{XL}, leading to increased survival of cells, and of cytokines including IL-2 and IFNγ [273].

In the induction of the non-canonical pathway, TRAF2 and TRAF3 dimers associated with NFκB-inducing kinase (NIK) are recruited to the receptor. In resting cells, cIAP associates with this complex, and ubiquitinates NIK, leading to its degradation. However, upon receptor activation, cIAP ubiquitinates the TRAFs and they are degraded. This frees NIK, and allows it to phosphorylate and activate IKK proteins. The NFκB subunit p100 undergoes IKK-dependent phosphorylation and processing to generate the p52 subunit. This associates with RelB and enters the nucleus [274, 275].

Furthermore, TRAF1 activates ERK which leads to down-modulation of the pro-apoptotic protein BIM [276]. TRAF2 interactions also signal via MAPK pathways mediated by ASK1 association, to activate JNK. In conjunction with TCR signalling, this promotes IL-2 production as well as expression of IFNγ in humans [277-279]. CD137 can also induce Akt activation to promote cell division via mTOR activation [280].

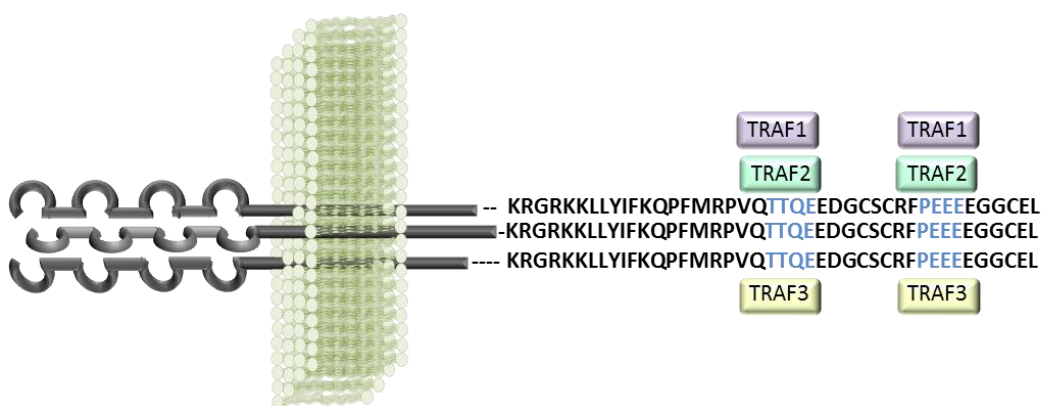


Figure 1.8: CD137 structure and intracellular TRAF-binding sites

The intracellular TIMs of CD137 are shown. TRAFs 1, 2 and 3 are known to interact with these, and can induce both the canonical and non-canonical NFκB pathways resulting in the upregulation of transcription of anti-apoptotic genes and activatory cytokines. MAPK cascades are also induced via ASK1 interactions, increasing the upregulation of IL-2 transcription [272, 275, 277, 279].

1.7.3.4 Other key TNFRSF signalling molecules

Other major TNFRSF T-cell costimulatory molecules include CD27 and OX40. CD27 has been shown to be necessary for the generation of long term T-cell immunity and in T-cell memory maintenance [281]. Its ligand, CD70, is inducibly expressed on APCs. Signalling via TRAF2, 3 and 5 binding initiates the upregulation of IL-2 and the anti-apoptotic factors c-FLIP, anti-apoptotic Bcl-2 family members and inhibitors of apoptosis (IAPs), via both canonical and non-canonical NFκB signalling [282]. Interestingly, in the context of a tumour, CD27 signalling has been shown to preferentially increase the number and survival of Tregs, promoting tumour growth [283].

OX40 is expressed only on activated T cells and binds the ligand OX40L on APCs. It is upregulated with delayed kinetics upon initial T-cell activation, from 12 h to several days [284]. It can act as a pro-survival receptor, inducing Bcl-2 family anti-apoptotic factors to increase the persistence of T cells, via NF κ B and NFAT signalling [285, 286]. These pathways also induce IL-2 and IFN γ upregulation [286].

1.7.4 T-cell subsets

1.7.4.1 Helper T cells

Helper T lymphocytes (Th) are so named for their roles in aiding and supporting immune responses. There are several subsets of Th cells with distinct roles, but all can be defined by $\alpha\beta$ TCR, CD3 and CD4 surface expression. The major functional branches of Th cells were first categorised as Th1 and Th2 subsets in 1986 [287]. Differentiation of Th1 cells, responsible for the promotion of immunity against intracellular pathogens, is induced in the presence of IL-12, produced by macrophages or DCs. The development of Th1 cells is enhanced by IFN γ production, which upregulates expression of the IL-12R β 2 subunit on the T cells [288]. The transcription factor STAT4 is induced by IL-12 signalling and T-bet is upregulated. T-bet itself promotes IFN γ production, producing a positive feedback loop for Th1 cells [289]. Th1 cells produce IL-2, IFN γ and TNF β , which promote an inflammatory response, activating DCs and macrophages and supporting T-cell proliferation [290].

IL-4 production early in an immune response, along with eosinophil and mast cell activation, initiates Th2 development as a defence to extracellular parasites [291]. This cytokine can be produced by other cells, or to a limited extent by the T cells themselves, mediated by TCR signalling [292]. The IL-4 receptor α subunit is upregulated and IL-4:IL-4R interaction on the T cell signals through STAT6, inducing transcription of GATA-3, driving commitment to the Th2 lineage [293, 294]. Th2 cells secrete IL-4, IL-5 and IL-13 and activate B-cell antibody responses, mast cells and eosinophils. In this way they have also been implicated in allergy, by the activation of IgE-producing cells [295].

The Th1 and Th2 lineages are polarised and the factors produced by each act to negatively regulate the alternative arm of differentiation. Th1 and Th2 pathways of IFN γ and IL-4 production respectively are inhibited by each other. Furthermore, IL-10 produced by Th2 cells inhibits Th1 development and IFN γ produced by Th1 cells inhibits proliferation of Th2 cells [292]. More recently there has been evidence to suggest some Th cells can develop into a hybrid Th1/Th2 dual phenotype subset [296, 297].

Other more recently characterised Th groups include Th9, Th17 and Th22 cells, and T follicular helper cells (T_{FH}). Th9 cells are thought to assist Th2 responses and have also been shown to have a role in allergic and autoimmune reactions [298]. Th17 cells have a role in protection against bacterial and fungal infection, particularly at mucosal surfaces, acting as first line of defence. They have been extensively implicated in tissue inflammation and autoimmune disorders [299]. Th22 cells were identified in skin inflammation and proposed to be involved in skin remodelling and inflammation [300]. Finally, T_{FH} are involved in promoting the development and maintenance of B-cell germinal centres. They can act in these areas to aid B cell Ig class switching and activation. This subset expresses CXCR5 to increase homing to secondary lymphoid organs where they carry out these functions [301].

The original model of Th cells was that the subsets have distinct, committed lineages. This is now contested, with evidence that the subsets can show plasticity in cytokine production and phenotype, rather than being fully committed to one terminally-differentiated state [302].

1.7.4.2 Regulatory T cells

Tregs are involved in immune control and are essential in prevention of autoimmunity by promoting tolerance. In this way they also inhibit anti-tumour responses. A naturally occurring Treg subset was first described in 1975, though the cell phenotype nor effector molecules were characterised [303]. Later, this subset was identified as CD4+ve CD25+ve FoxP3+ve [304]. Two main branches of Tregs exist, classified by their time and place of development; peripheral, or induced Tregs (iTreg) and thymic, or natural Tregs (nTreg).

nTregs develop in the thymus, from CD4+ve T cells that have a high affinity for self pMHC and are thought to protect from aberrant self-antigen responses. They require strong CD28 costimulation and the presence of IL-2 to develop, upon which FoxP3 is upregulated and conversion to the regulatory phenotype occurs. iTregs develop outside the thymus, in the periphery, differentiated from CD4+ve Th cells, in the presence of TGF β and IL-2. Within iTregs, there are further subsets, described based upon the conditions under which they are induced, and the subsequent molecules expressed. IL-10 can induce a Tr1 phenotype that are FoxP3-ve. The presence of TGF β results in a Th3 subset of iTreg, which are FoxP3+ve [305]. Together with nTregs, iTregs help to maintain peripheral tolerance and control immune responses. The complete pool of Tregs in humans makes up 5-10 % of circulating CD4+ve T cells [306].

Tregs can act to dampen the immune response via three avenues of suppression; cell-cell contact, release of soluble factors and by competition. Tregs release the suppressive cytokines IL-10, IL-35 and TGF- β that can act to inhibit effector T cells. Additionally Tregs can generate adenosine that binds to effector T cells, leading to suppression of TCR signalling and of IL-2R upregulation [307] [43, 308]. Direct cell death of effector T cells is also possible by the release of granzymes and perforin from Tregs [309]. APCs can be suppressed by direct cell contact with Tregs, via engagement of inhibitory receptors. CTLA-4 on Tregs can bind B7, blocking co-stimulatory signalling and upregulating indoleamine 2,3-dioxygenase (IDO) production in DCs. IDO acts to degrade tryptophan, causing a deficit for effector cells. LAG3 expression allows Tregs to suppress the antigen capturing ability of DCs through engagement of MHC II [309].

Competitive consumption of IL-2 has been shown to effectively suppress effector T and NK cells by the high expression of the IL-2R on Tregs, resulting in starved effector cells [43]. A regulatory CD8+ve T-cell subset has also been described, known to be involved in control of T-cell immune activity by the expression of the suppressive cytokines IL-10 and TGF β . CD8+ve Tregs can also secrete perforin and granzymes to directly lyse effector T cells [310].

1.7.4.3 Cytotoxic T cells

When successful antigen recognition and sufficient co-stimulation occurs, usually in a secondary lymphoid organ, naïve CD8+ve T cells become primed whereby they become activated and undergo rapid and extensive clonal expansion. The cells also undergo many metabolic changes to allow for this increased division. Uptake of glucose and amino acids is increased, and the cells switch to aerobic glycolysis, under the control of CD28-driven mTOR expression and TCR-ERK signalling. mTOR upregulation also increases ribosomal translation rates to prepare for high rates of cell division [311].

A high proportion of CD8+ve T cells differentiate into short lived effector cells (SLECs) that have a terminally differentiated effector cell phenotype and demonstrate high levels of cytotoxic ability. Two main transcription factors, eomesodermin and t-bet, are involved in driving the differentiation of CD8+ve SLECs [312]. The upregulation of CXCR3 then allows the differentiated SLECs to migrate to the periphery, where additional interactions with antigen drive further proliferation, cytokine production and cytotoxic effector function [311].

Similar to Th cells, although more recently characterised, CD8+ve T-cell subgroups have been described [310]. A large proportion of CD8+ve T cells produce IFN γ and

have been termed Tc1, whilst a Tc2 phenotype secretes IL-4 and IL-5. Both these subsets also express granzymes and perforin and so are capable of cytotoxicity. Tc1 cells develop in the presence of IL-2 and IL-12, and their function involves cytotoxicity against virus-infected or transformed cells, and the promotion of an inflammatory response. Tc2 cells develop in the presence of IL-4 and are often involved in allergy responses and supporting the Th2 response. As with Th cells, a Tc9 and Tc17 phenotype have also been described, expressing IL-9 and IL-17 respectively. Both of these subsets are thought to have a role in anti-tumour immunity, whilst Tc9 cells have been shown to also support allergy responses [313]. Tc17 cells also have a role in anti-viral responses and have been implicated in autoimmunity [314].

The majority of classic anti-viral and anti-tumour cytotoxic responses are therefore mediated by the well-characterised Tc1 CTLs. The cytoplasm of these CTLs contains cytolytic granules; vesicles containing perforin and serine proteinases. These are involved in the first pathway of cytotoxic killing, the lytic granule pathway. The second pathway of CTL killing involves cell contact via Fas and Fas Ligand (FasL), which induces apoptotic signalling. Both of these pathways induce a controlled cell death with minimal inflammation. Apoptosis is characterised by membrane blebbing, nuclear fragmentation, chromatin condensation and cell shrinkage. Apoptotic bodies form from the cells which are cleared by phagocytosis, mediated by macrophages [315].

1.7.4.3.1 Perforin/Granzyme pathway of cytotoxicity

The perforin/granzyme pathway was the first mechanism discovered of how CTLs and NK cells kill target cells, mediated by the polarised release of factors to induce apoptosis across a narrow IS gap. Perforin is only found within lytic granules and is required for this pathway of cell death. Mice deficient in perforin show defective killing of target cells and a higher susceptibility to infection and tumours due to lowered CTL responses [316].

Perforin pores are formed by lateral aggregation of perforin molecules in the outer leaflet of the target membrane, which form circular structures through the membrane where the serine proteinases, granzymes, can enter [317]. Granzymes can also enter independent of perforin, via receptor mediated endocytosis [316]. Granzyme B performs this using the mannose-6-phosphate receptor, entering into an intracellular vesicle [318]. Perforin damage to the membrane encourages uptake of the granular components as part of a “wound-healing” response [319]. It has more recently been shown that perforin can actively induce clathrin- and dynamin- controlled endocytosis of granzymes. This method does not involve damage to membrane integrity, avoiding inflammatory necrotic responses [320]. Protease inhibitor-9 acts to inhibit granzyme B

activity and cathepsin B is also released from CTLs following granule exocytosis and is thought to bind the outside of the effector cell to prevent it from perforin-induced damage [321, 322]. The granules also contain other factors involved in inducing apoptosis, including granulysin and FasL. Granulysin is involved in lipid and membrane degradation and is known to be capable of anti-microbial and anti-tumour activity [323]. Once the granule contents are within the cytoplasm of the target cell, apoptotic pathways are initiated.

In humans there are 5 granzymes, A, B, H, K and M. The two major granzymes are granzyme A and B. Granzyme A induces apoptosis in a caspase-independent manner via mitochondrial mechanisms [324]. The enzyme is transported from the cytoplasm into the mitochondrial matrix and leads to disruption of the electron transport chain and ATP production, resulting in the production of superoxides [324, 325]. The subsequent oxidative stress activates the SET complex, comprising several endonucleases and DNA repair enzymes, which are transported to the nucleus where they cause DNA damage in the form of single strand nicks [326]. This method of mitochondrial damage does not include the release of cytochrome C or loss of mitochondrial membrane integrity. Granzyme A can also cleave histones and lamins directly [324].

Granzyme B cleaves BID, a Bcl-2 pro-apoptotic family member. Activated BID translocates to the mitochondria whereby it activates BAX- and BAK- induced release of cytochrome C. This induces APAF-1 to aggregate and activate the initiator caspase 9, as part of the apoptosome. Caspase 9 can then cleave downstream caspases, such as the major executioner caspase 3. Granzyme B can also directly cleave and activate procaspase 3 and 9. Caspase 3 cleaves the inhibitor of CAD ([caspase-activated DNase] ICAD) [327, 328]. CAD then translocates to the nucleus, where DNA fragmentation is mediated [329]. When the mitochondria lose membrane integrity, apoptosis-inducing factor (AIF) and endonuclease G are also released. These factors migrate into the nucleus to perform additional DNA condensation and fragmentation. Additionally, second mitochondria-derived activator of caspases (smac/diablo) is released. This protein binds inhibitors of apoptosis (IAPs), suppressing their activity and so promoting cell death [330].

1.7.4.3.2 Fas/FasL pathway of cytotoxicity

This pathway of CTL-induced death is triggered by Fas-FasL interactions between a target cell and a CTL. FasL is upregulated on cytotoxic cells upon their activation. Prior to activation, FasL is found in cytoplasmic granules, which are translocated to the cell membrane and expressed to increase induction of the Fas/FasL pathway.

Sequestering the FasL in these granules until they are released during CTL activation

may protect other bystander cells that may come into contact with the T cells [331],[332]. Fas and FasL are both expressed as trimers. Fas is a TNFRSF member containing an intracellular death domain, which associates with FADD, an adapter protein, in the target cell which can recruit pro-caspase 8. The aggregation of inactive caspase 8 leads to self-cleavage and activation [315].

There are two downstream pathways of Fas-induced caspase 8 activity, dependent upon the target cell and thought to be regulated by X chromosome-linked inhibitor of apoptosis (XIAP) [333]. In type I cells, such as thymocytes, caspase 8 cleaves caspase 3 to activate it directly. As in the perforin/granzyme pathway, caspase 3 cleaves ICAD. CAD is then active and free to move to the nucleus where it performs DNA fragmentation. In type II cells, including B cells, BID cleavage by caspase 3 is also required. As in the perforin/granzyme pathway, the result of this is the cytochrome-c mediated assembly of the apoptosome, activating caspase 9. This further drives the activation of caspase 3, and so promotes its catalytic degradation of apoptotic substrates [334].

1.8 Chimeric antigen receptors

As briefly described in Chapter 1.5.2.1, CARs usually consist of an extracellular scFv targeting a specific TAA, linked via a spacer to a transmembrane domain and one or more intracellular signalling domains. These comprise signalling motifs from costimulatory molecules to activate the effector cells on which the CARs are expressed in a tumour-directed manner. An illustration of the construction of a CAR is shown in **Figure 1.9**. Some CAR have been generated using NK cells, expressing CAR modelled on either a scFv or an NK cell receptor such as NKG2D [335, 336], however this chapter will focus on CARs designed for expression on T cells.

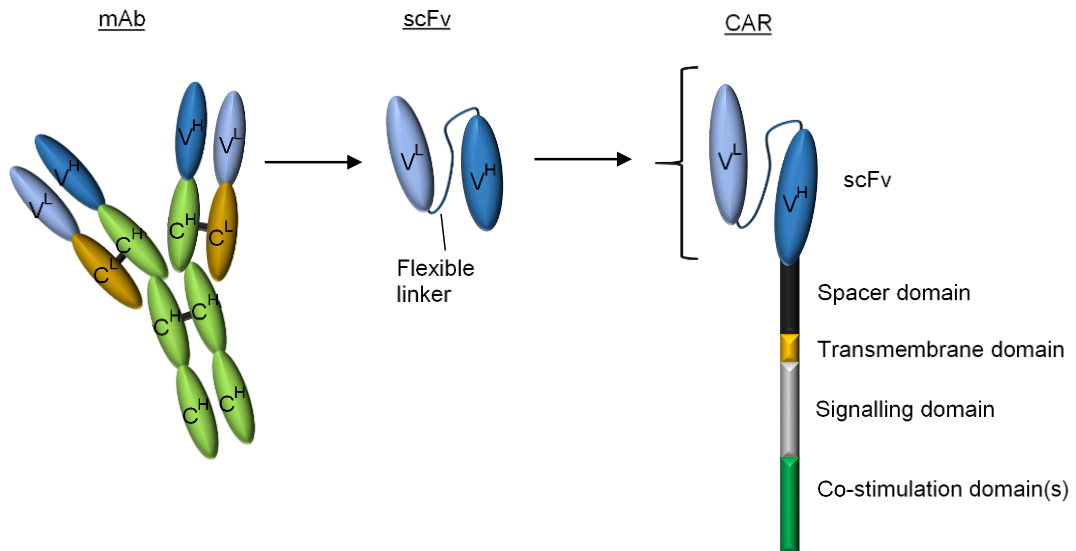


Figure 1.9: The domains of a CAR

The antigen binding domain of a CAR consists of a scFv, with the heavy and light variable regions connected by a flexible linker to allow correct conformational folding. The scFv is adjoined to a spacer domain, transmembrane region, and intracellular signalling and often co-stimulation domain(s). V_L: variable light chain; V_H: variable heavy chain; C_L: constant light chain; C_H: constant heavy chain.

1.8.1 The development of CAR design

The first CAR was designed in 1989, comprising the variable regions of an anti-TNP (2,4,6- trinitrophenyl) antibody spliced to part of a TCR α or β chain [337]. Transfection of this construct into a CTL hybridoma induced IL-2 production and cytotoxicity upon stimulation with TNP-modified cells, demonstrated in a [⁵¹Cr] release assay. The chimeric receptors were shown to be capable of associating with the native TCR molecules, permitting signalling via the endogenous signalling molecules. The same group expanded on this work by the inclusion of signalling molecules within the chimeric constructs [338]. The γ chain of activating Fc receptors or the CD3 ζ chain were incorporated into the intracellular portion of the receptor, allowing T-cell activation and IL-2 production directly via the chimeric molecule.

The first anti-CD20 CAR to target B cells was constructed in 1998, incorporating the variable region of the anti-human CD20 mouse antibody Leu16, a hIgG hinge-CH2-CH3 spacer and the human CD4 transmembrane region linked to the intracellular signalling human CD3 ζ chain [339]. This study demonstrated the ability of these CAR+ve T cells to become activated and produce IL-2 upon target recognition, which could be blocked by the addition of an anti-CD20 soluble antibody, showing the antigen-specific response. Specific target cell lysis was also seen, demonstrating

the potential for *in vitro* CAR activity. These early studies paved the way for the extensive development of CAR design.

CARs are now classified into four groups, or generations, based on the additional intracellular domains included (**Figure 1.10**). First generation CARs comprise only the CD3 ζ signalling domain, and consequently do not expand or survive effectively *in vivo*. The addition of a co-stimulation domain, often from CD28, to the cytoplasmic tail led to the development of second generation CARs, which promote increased proliferation and cytokine production. Third generation CARs are characterised by the inclusion of two or more domains from different co-stimulation molecules, often including CD137 which bestows the CAR+ve T cells with improved survival and persistence *in vivo*. Fourth generation CAR have now emerged, encompassing extra intracellular domains. These often comprise either constitutively-expressed or CAR-inducible cytokine transgenes for improved survival and anti-tumour effects. Additionally, some fourth generation CAR include suicide genes, such as caspase 9, for enhanced safety [340].

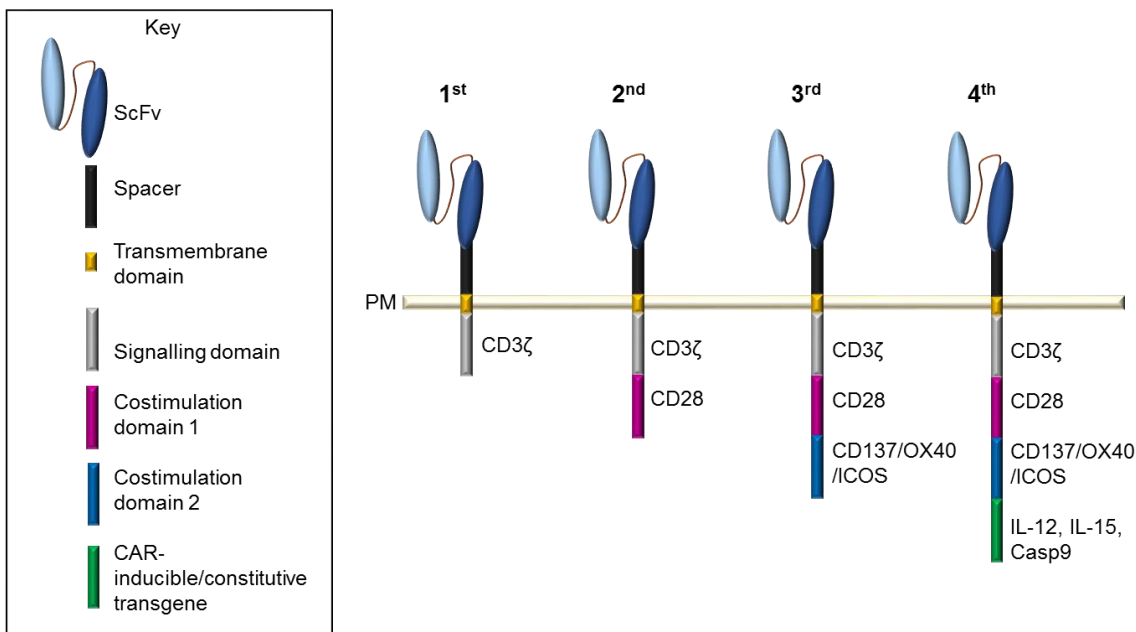


Figure 1.10: First, second, third and fourth generation CAR constructs.

Early CARs comprised a scFv linked to the CD3 ζ signalling domain. The addition of a co-stimulatory domain, often from CD28, to the CAR construct confers higher cytokine production and cytotoxicity and are classed as second generation CAR. Inclusion of two such domains from co-stimulatory molecules provides third generation CARs, with increased cell proliferation and persistence *in vivo*. Fourth generation CAR comprise all these domains along with additional transgenes conferring cytokine production, or suicide safety genes. PM, plasma membrane.

1.8.2 CAR signalling

1.8.2.1 Signalling domains

The principle of CAR design is to incorporate all the signalling domains in the same construct, *in cis*. This allows full activation of the T cell via one antigen interaction and helps to avoid anergy. Two classes of molecules have previously been used in CAR generation; those from the IgSF such as CD28 and the CD3 ζ chain, and TNFRSF members, including OX40, CD27 and CD137. The fact that CARs include such signalling domains may prove advantageous over TCR engineering, as tumour cells can down regulate the costimulatory molecules necessary to engage the T-cell IS fully [341, 342].

Pule *et al* demonstrated that a first generation anti-GD2 CAR comprising a scFv region linked to a CD3 ζ chain intracellular signalling domain could initiate target cell killing and some IFN γ production but that full T-cell activation was not achieved [296]. Whilst a response can be seen *in vitro*, it is unlikely that these CAR would be effective *in vivo*. When the CD28 signalling domain was incorporated into the same CAR, enhanced IL-2 production was reported [343]. Similarly, a xenograft tumour study demonstrated enhanced CD19 CAR+ve T-cell persistence and upregulation of Bcl-X_L with the inclusion of the CD28 signalling domain compared to CD3 ζ alone [344]. T-cell proliferation was seen to increase both *in vitro* and in *in vivo* models when CD28 signalling domains were included in an anti-Ig light chain CAR, compared to constructs with only the CD3 ζ chain [345]. Moreover, significantly higher CAR+ve T-cell expansion was observed in NHL clinical trial patients when CD3 ζ and CD28 signalling domains were included into an anti-CD19 CAR construct when compared to those containing CD3 ζ alone [346].

Second generation CARs incorporating CD3 ζ and CD137 signalling domains have also been shown to promote T-cell persistence in an *in vivo* model of human ovarian tumours. Additionally, higher levels of tumour localisation and subsequent anti-tumour activity were seen with CD137-containing CAR compared to those incorporating CD3 ζ alone [347]. An anti-CD19 CAR construct comprising CD3 ζ and the intracellular signalling domain of CD137 was studied *in vitro* targeting acute lymphoblastic leukaemia (ALL) cells. Potent cytotoxicity against the patient samples was reported, with 1% transduced CAR+ve T cells capable of eliminating the ALL cells in co-culture within 5 days. CD137 was shown to be responsible for significant expansion of the CAR+ve T cells, along with increased production of IL-2 [348].

Interestingly, a metabolic study comparing second generation CAR incorporating CD28 or CD137 showed marked differences in the promotion of T-cell subsets. CD28 was found to drive an effector T-cell memory phenotype, with decreased T-cell persistence. Conversely CD137 skewed the T cells towards a central memory phenotype, with an increase in oxidative phosphorylation and mitochondria biogenesis, and a higher level of T-cell persistence [349].

By incorporating both these signalling domains into one third generation CAR, the potent anti-tumour effects of CD28 can be combined with enhanced T-cell survival promoted by CD137. Anti-mesothelin CAR constructs including CD28 alone, or in conjunction with CD137 were compared. It was demonstrated that CD28 was sufficient for cytotoxic killing of the target cells, but the T cells had low survival levels [299]. When both co-stimulatory molecules were included in the CAR construct the tumour burden of the xenograft model used was removed completely or significantly reduced, even at low effector:target ratios, and robust engraftment and persistence of the CAR+ve T cells was reported. Similarly, the inclusion of both costimulatory domains in an anti-PSMA CAR resulted in higher tumour clearance and cytokine production in an *in vivo* model. Additionally, increased PI3K signalling and enhanced expression of Bcl-X_L was mediated by this third generation CAR compared to those comprising only one co-stimulatory domain [350].

A recent clinical trial directly compared an anti-CD19 CAR comprising CD28 or CD28 and CD137 in the treatment of B-cell leukaemias and lymphomas [351]. Patients were infused simultaneously with CAR+ve T cells expressing both constructs, and clinical outcome was assessed along with CAR+ve T-cell expansion and persistence. The third generation CAR+ve T cells were shown to proliferate to a higher degree and showed improved T-cell survival. The difference between second and third generation CAR numbers was particularly marked in patients with low disease burden. As all patients received both therapies, survival and ongoing disease burden cannot be directly compared between the second and third generation CAR.

Alternative to CD28 and CD137, other T-cell co-stimulation domains have been incorporated in CAR design. Inclusion of OX40 in an anti-GD2 CAR elicited potent T-cell activation with an increased NFκB response and sustained clonal expansion of the CAR+ve T cells compared to that comprising CD28 alone [343]. However, another study comparing a third generation anti-GD2 CAR comprising CD28 with either OX40 or CD137 found that the production of IL-2 and IFN-γ was higher with the inclusion of CD137. The anti-tumour effects seen were also greater with CD137 than

OX40, and CD137 promoted enhance T-cell survival and a reduction in T-cell exhaustion [352].

CARs including the signalling domain of inducible T-cell costimulator (ICOS) have also been described. This co-stimulatory molecule promotes a Th1/Th17 polarisation, and was incorporated into an anti-mesothelin CAR [353]. Th17-skewed CAR+ve T cells were shown to have strong anti-tumour effects and higher levels persistence than CD28 or CD137 CAR constructs. Further investigation revealed that CD137 and ICOS together promoted T-cell persistence in solid tumour models. This was attributed to ICOS signalling promoting CD4+ve Th17 cells, and a CD8+ve CTL population driven by the inclusion of CD137 that together enhanced the anti-tumour response [354].

Whilst most CAR signalling domains are designed *in cis* within one construct, an alternative method involves the use of a bi- or multi-cistronic vector. This allows the transduction of the CAR construct alongside extra co-stimulation genes. The expression of the CD40L gene in this way, additional to a second generation anti-CD19 CAR, was shown to enhance Th1 cytokine production, T-cell proliferation and tumour lysis in a xenograft lymphoma model [355]. The authors also noted that the interaction of this constitutively-expressed CD40L with CD40 on the tumour cells led to an increase in the tumour cell immunogenicity with the upregulation of other co-stimulatory molecules on their surface, further promoting an anti-tumour immune response.

The CD40 signalling domain has also been tethered to Myd88 and constitutively expressed alongside a CAR construct [356] or inducibly expressed, controlled by the presence of a small molecule [357]. When expressed constitutively, the construct was shown to promote pro-inflammatory cytokine production in an antigen-independent manner. In a xenograft leukaemia model, anti-tumour responses and survival were significantly enhanced by the presence of the Myd88-CD40 construct, compared to a first generation anti-CD123 CAR alone [356]. The inducible system incorporated a first generation anti-Her2 CAR, and a construct comprising Myd88, the CD40 intracellular domain and two tandem FKBP dimerization domains. The addition of the small molecule AP1903 dimerises the co-stimulatory construct and results in signalling, additional to that from the CD3 ζ CAR domain. In solid tumour models, the Myd88/CD40 system demonstrated a superior anti-tumour response and increased survival than both the CD3 ζ CAR alone, and interestingly a second generation CAR also containing the CD28 domain. This system holds potential for CAR design, not only due to the anti-tumour responses seen but in that it provides a mechanism of remote control post-CAR+ve T-cell infusion [357].

1.8.2.2 The CAR immunological synapse

The CAR IS has not been fully characterised. However, marked differences to that of the endogenous IS have been observed. A study using an anti-CEA CAR revealed a more disordered arrangement at the synapse of CAR molecules, with clustered Lck and an absence of the ordered rings of the adhesion molecule LFA-1 that usually stabilises the outer regions of the IS. LFA-1 was still present in CAR IS but it was observed that the adhesions between the T cell and target cell were less reliant on this than in an endogenous IS. The interactions between CAR+ve T cells and target cells have also been observed to be more transient, with T-cell signalling being induced faster leading to more rapid lytic granule recruitment. A higher percentage of CAR+ve T cells were shown to bind to target cells within a 10-40 min period than TCR+ve T cells, and a higher proportion had detached by the end of this observation period [358].

Xiong *et al* [359] investigated the immunological CAR synapse in relation to functional efficacy. By analysing clustering of F-actin, target antigen and phosphorylated CD3 ζ , they were able to show a correlation between the synapse quality and long-term CAR lysis capabilities. Short-term *in vitro* cytotoxicity and cytokine assays did not show a difference between constructs, but the response in long-term *in vitro* assays and tumour control in xenograft models were both higher in those CAR shown to have improved quality of IS clustering. Thus, IS evaluation is a potential method for predicting CAR efficacy, even when differences may not be apparent in the commonly used short-term assays.

Some investigation has been performed into downstream intracellular CAR signalling, but again this is not fully characterised. ZAP70 phosphorylation has been observed, along with CD45 exclusion from the IS upon antigen engagement of an anti-CD19 CAR [360]. Third generation CAR constructs including signalling domains from CD28 and CD137 have been shown to induce high levels of activated PI3K, phosphorylated Akt and Bcl-XL [350]. A tyrosine kinase array performed on third generation anti-CD19 CAR+ve T cells revealed increased levels of activation in CAR+ve cells, with signalling components involved in endogenous TCR signalling being phosphorylated including CD3 ζ , LAT, Lck and ZAP70 [361]. All these studies suggest that CAR signalling employs the endogenous TCR signalling pathways, despite differences observed in the IS binding arrangements.

1.8.3 CAR Spacer domains

Along with the intracellular signalling domains, the extracellular spacer region can influence aspects of expression and functionality of CAR molecules. In the majority of

CAR designs, this spacer comprises domains from the IgG Fc region, although CAR constructs incorporating CD8 and NGFR spacers have also been produced [362] [363]. Moritz and Groner first demonstrated that including a spacer region in an anti-Erb2 CAR allowed for increased flexibility and receptor access to the target antigen. This resulted in increased signalling and cytokine production in the CAR+veT cells, compared to CAR without the spacer domain [364]. Other studies have supported this finding, with results suggesting that a spacer is required for optimal expression and function of many CAR constructs [365, 366].

Cartellieri *et al* [116] reviewed the spacer regions used in previous studies and concluded that different spacer domains can cause otherwise similar CAR to have different functional abilities. This paper supported previous findings that the need for a full spacer region such as the IgG hinge-CH2-CH3 domains, rather than a shorter region such as part of the CD8 α chain depends upon the distance of the target antigen from the membrane [367]. A comparison between the same CARs with and without such IgG spacer regions to different antigens showed that CARs targeting antigen 5T4 and NCAM (CD56) induced enhanced responses when an extracellular spacer domain was included, eliciting higher levels of specific cytotoxicity. In contrast, the inclusion of the same spacer domain in an anti-CEA (carcinoembryonic antigen) CAR actually reduced the IFN γ response seen. It is now thought that a longer spacer domain is preferential in CARs targeting antigens that reside proximal to the membrane, whilst this region is less important for membrane-distal epitopes.

Whilst a spacer region derived from IgG Fc is commonly used in CAR constructs, Hombach *et al* [368] investigated the idea of inadvertent immune activation via this domain. It was shown that binding of this region to Fc γ R could activate NK cells and monocytes and initiate pro-inflammatory cytokine release. The T cells could be activated by these interactions and lyse the innate immune cells. The Fc region can be modified by site-directed mutagenesis to remove cross-activation via Fc γ R, whilst retaining the CAR binding ability and equivalent *in vitro* lysis. Two studies using CARs incorporating an IgG4 Fc spacer domain demonstrated that FcR interaction resulted in significant AICD of the CAR+ve T cells and consequent lack of *in vivo* anti-tumour efficacy [369, 370].

Mutagenesis of the FcR binding domains of IgG1 and IgG2-derived spacer domains to inhibit interaction has now been attributed to increased *in vivo* tumour localisation of CAR+ve T cells, and higher tumour lysis [371]. Moreover, this study demonstrated that tonic signalling of CAR constructs can be induced by the IgG Fc spacer domain. This tonic signalling was linked to increased CAR+ve T-cell aging and senescence. The

deletion of the whole Fc domain or of just the CH2 portion reduced these effects and improved CAR+ve T-cell function. This finding poses a potential issue with CAR design as many require the longer spacer region for optimal target antigen binding and function.

1.8.4 Target antigen selection and scFv properties

In the construction of a CAR, a tumour-specific antigenic target is selected to minimise off-target effects, as there is a risk of CTLs enabled with CARs demonstrating potent on-target off-organ effects. A trial of an anti-Her2 CAR highlighted the potential consequences of this, where serious, fatal adverse effects were reported due to the recognition by CAR+ve T cells of low-level Her2 expression on the lung epithelium [372]

The other important consideration when a TAA is chosen as a CAR target, is that the epitope itself can affect the efficacy of the treatment. Hombach *et al* [373] constructed anti-CEA CARs, targeting two different epitopes of the antigen. T cells expressing CARs targeting the membrane-proximal A3 domain of CEA demonstrated superior cytotoxic potency than those targeting the more distal N-domain. This difference was only seen when the antigen was present on target cells, not when the target was immobilised, indicating a role for cell-cell interaction. When the N-epitope was grafted nearer to the membrane of the target cell, the anti-N-domain CAR performed more effectively.

Similarly, the targeting of CD22 with CAR constructs has been shown in two independent studies to be greatly influenced by the distance of the targeted epitope from the membrane. In both cases, the targeting of membrane-proximal epitopes elicited improved CAR+ve T-cell responses, as compared to more distal binding domains [374, 375]. A comparison of two CARs targeted to either a membrane-proximal or -distal epitope of mesothelin also revealed superior cytokine production and cytotoxicity when the closer epitope was engaged [376]. Likewise, when a membrane-proximal epitope of the melanoma antigen MCSP was targeted using a BiTE, a more potent cytotoxic effect was seen than when the antibody was directed to a membrane-distal binding domain [377].

A published conference abstract reports the influence of epitope membrane proximity on anti-CD20 CAR function. Whilst no data is published, and the authors mis-categorise the parental mAb used (obinutuzumab as type I, ofatumumab as type II) confusing the conclusions drawn, it is reported that a CAR encompassing a scFv from ofatumomab (2F2) showed superior cytokine production and cytotoxicity to other anti-

CD20 CAR. The authors suggest that the membrane proximity of the ofatumumab binding site on the smaller extracellular loop of CD20 contributes to this increased activity.

In addition to the position of the targeted epitope, binding affinity can impact CAR function. Haso *et al* [374] studied the consequence of affinity on the efficacy of the same anti-CD22 CAR. They compared two scFv derived from anti-CD22 mAb RFB-4; BL22 (affinity 85 nM) and HA22 (high affinity mutant, affinity 6 nM) incorporated in CAR constructs. This study was based on previous findings [378] that binding affinity impacts potency of these scFv, when they are used as monomeric constructs to deliver immunotoxins. It was found however, that when included in a CAR, affinity does not alter the efficacy of these scFv. Both these scFv bind to a membrane distal site (domains 2-3 of CD22) When a scFv of similar binding affinity to HA22 (m971) that binds a membrane proximal site (domains 5-7) was included, CAR function was seen to improve both *in vitro* and *in vivo*, demonstrating that membrane proximity was more important than affinity.

Similarly, the work by Hombach *et al* [373] discussed above showed that the membrane proximity of the targeted epitope was more important than affinity on CAR effector function. The scFv (H10) to the distal N-terminal domain of CEA has a higher affinity than the membrane-proximal A3 domain targeting scFv (BW431/26). Despite this, lower levels of target cells lysis and cytokine production were observed when the H10 scFv was included in the CAR design.

Chmielewski *et al* [379] showed that increasing the binding affinity of an anti-Her2 CAR had no impact upon the CAR efficacy, above a certain threshold. A wide range of affinities were investigated *in vitro*, using the same scFv mutated to have K_D values from 0.015 nM - 320 nM. It was shown that affinity only had a small impact on CAR function at the lowest affinity (320 nM), when target antigen was expressed to a low level. In this circumstance, a higher effector to target ratio was required of the lowest affinity CAR+ve T cells to achieve equivalent function to the others. However, above the threshold (affinity < ~100 nM) no differences were seen. The authors note that the low affinity construct demonstrates a higher specificity due to a reduced response to cells with a low target antigen density, which may be advantageous to avoid on-target off-organ effects of healthy tissue.

Furthermore, two anti-Her2 CARs incorporating scFv targeting the same epitope, but with very different affinities (1616 nM and 1 nM) demonstrated functional differences [380]. When high target antigen density was present, the lytic abilities of the two

constructs was similar. Interestingly in this study, the low affinity CAR demonstrated superior target cell lysis when target antigen density was low.

Function of a CAR targeting the MAGE1-A1 peptide in the context of HLA-A1 was shown to be affected by affinity of target binding [381]. Two scFv with K_D values of 250 nM and 14 nM were investigated and CAR function was found to be affinity-dependent. This finding is supportive of the work by Chmielewski *et al*, that scFv may require affinity above a threshold (affinity < ~100 nM) for optimal activity. As the study on anti-MAGE-A1 CARs didn't include additional higher affinity scFv it is unknown if any further impact would be seen for this target antigen.

CAR expression levels were also shown to have an influence on function between the two constructs. The low affinity scFv achieved increased target cell lysis compared to the high affinity, when the CAR density was low. It can be hypothesised that this may be attributed to the reported difference between TCR-mediated "serial killer" T-cell cytotoxicity, and the prolonged interactions usually observed in CAR-induced target lysis [382]. Whilst CAR have been shown to be capable of "serial killing" [383], with reduced CAR expression, the prolonged interaction of a higher affinity construct may slow the rate at which target cells can be bound and lysed, whereas a lower affinity CAR may allow a quicker interaction and thus increased level of cell interactions within a time frame.

Conversely, anti-CD123 CAR constructs encompassing the scFv 7G3, mutated to have affinities ranging from 1 nM – 300 nM were found to have equivalent functional activity [384]. These scFv had similar off-rates and varied on-rates, altering the overall K_D values. Target cell lysis and T-cell activation were shown to be entirely affinity-independent. Longer-term effector function was also not influenced by affinity, although CAR expression levels did have an impact. It may be that the similar off-rates allow sufficient duration of CAR-target interactions for all the constructs. Likewise, it has been reported that anti-Tyrb-1 CAR constructs incorporating affinity mutated scFv with K_D values ranging from 0.74 nM – 54.3 nM demonstrated no correlation between affinity and function [385]. However, these receptors all have relatively high affinities, and are above the potential threshold discussed above.

A comparison of two anti-ROR1 CAR reported that the higher affinity receptor had increased functional efficacy compared to the lower affinity one, when both were otherwise identical [386]. 2A2 scFv (affinity 65 nM [387]) and R12 scFv (affinity 1.3 nM) both target the same membrane distal domain but differ in their dissociation rates. *In vitro* the CARs lysed target cells to a similar extent, but the higher affinity scFv induced much higher levels of cytokine production. When compared *in vivo*, the higher affinity

construct demonstrated superior anti-tumour responses and overall survival. The lower affinity construct still has a relatively high K_D value and is above the proposed threshold discussed above. It may be that the difference in off-rates between these scFv is responsible for the affinity-dependent efficacy, as the constructs discussed above targeting CD123 with much lower overall affinity, but similar off-rates maintained equivalent function [384].

Interestingly, it has been reported in a published conference abstract that affinity does play a role in anti-CD20 CAR function [388]. Five scFv with affinities ranging from 7.07 nM – 14.66 nM were compared. Despite this relatively small range, functional differences were reported, with the two lowest affinity constructs requiring higher effector to target ratios to achieve equivalent levels of target cell lysis. The levels of cytokine production were also stated to be affected, with increased IL-2 and IFN- γ secretion induced by the highest affinity scFv. However, the author reports that the highest affinity construct had much reduced proliferation and *in vitro* survival due to increased AICD. They conclude that affinity above a threshold is required for optimal CAR efficacy, but high affinity may also inhibit some function. There is however no published data yet of this work, so conclusions are difficult to draw.

As discussed in the context of anti-Her2 CARs [379, 380], the influence of CAR affinity can be exploited to avoid on-target off-organ effects. This was demonstrated using anti-CD38 CARs [389]. The lowering of the scFv affinity included in the constructs resulted in preservation of function and specific lysis of high-CD38 multiple myeloma cells, and the sparing of healthy low-CD38 cells. This provides a potential method of avoiding serious damage when target TAA that are also expressed at a lower level on healthy tissues.

Whilst some hypotheses can be proposed of affinity thresholds and the influence of on- and off-rates on CAR function, the role of affinity on CAR efficacy remains unclear and may depend upon the target antigen and context. The reduction of affinity can be employed to avoid damage to healthy tissues but may also allow the escape of low-antigen expressing tumour cells and can impact overall CAR function in some cases.

Dual-targeting CARs provide a potential solution to the problem of low-antigen tumour cell escape. Tumour cells can undergo mutations that lead to antigen loss or the expression of isoforms of the target antigen that can no longer be recognised or bound by the CAR [390, 391]. Additionally, relapse can occur with a genetically-related but differentiated tumour, for example that seen in a case of anti-CD19 CAR treated CLL whereby escaped tumour cells underwent a phenotypic switch and outgrowth occurred as a CD19-ve plasmablastic lymphoma [392]. CAR+ve T cells can be targeted to more

than one antigen, in either a single bispecific tandem-CAR, with bi-cistronic CAR+ve T cells or by co-administration of two populations of CAR+ve T cells [390].

Dual-targeting to date commonly incorporates an anti-CD19 CAR with either an anti-CD20 or anti-CD22 construct. Preclinical studies of a bicistronic [393], and bispecific tandem [394] anti-CD19/CD20 CARs have shown improved tumour control, and a reduction in CD19-ve cell outgrowth in tumour models. Early clinical trial results investigating the efficacy of a bicistronic anti-CD19/CD20 CARs reported 3/6 patients achieving partial or total recovery [395]. Of those patients who relapsed, either CD20 or CD19 expression was maintained, meaning that the therapy failure was not due to antigen loss. A bispecific anti-CD19/22 CAR was shown to be able to clear tumours in preclinical models of ALL, including xenografted CD19-ve tumour cells from a patient with relapsed refractory disease [396]. Bispecific anti-CD19/CD22 CAR are in early clinical trials [397], along with co-administration of a mixed population of anti-CD19 CAR+ve and anti-CD22 CAR+ve T cells [398]. The first results of this co-administration trial showed high levels of initial complete responses. In those patients that relapsed, again the outgrowing cells were CD22+ve and CD19+ve, showing that antigenic escape was not responsible.

Furthermore, trivalent CARs have also been designed to attempt to prevent any tumour escape. T cells expressing three CARs, targeting CD19, CD20 and CD22 have been described [399]. In preclinical models of CD19-ve ALL, the T cells were shown to be able to clear the tumours, avoiding tumour cell escape, whilst the single anti-CD19 CAR +ve T cells were ineffective. In addition to targeting leukaemia and lymphoma, bi- and tri-cistronic CARs have been developed targeting glioblastoma antigens. CAR+ve T cells targeting Her2 and IL-13R α 2 were shown to have an increased duration of tumour control in a xenograft model, and to exhibit stronger activation signalling than either CAR alone [400]. *In vitro* escape and expansion of single-antigen expressing cells was also ablated by the dual-targeting cells. The addition of a third CAR targeting ephrin-A2 attenuated the tumour response seen, and the survival of xenograft-bearing mice [401]. Glioblastoma has been shown exhibit a heterogenous antigenic expression profile, both between patients, and within a single tumour [400]. Thus, antigen escape with single-targeting therapies is common. This multi-targeting CAR+ve T cell approach provides a potential mechanism to avoid these treatment-resistant relapses.

1.8.5 CAR targeting solid tumours and the microenvironment

Whilst there has been some success reported in targeting solid tumours with CAR+ve T cells, the majority have been in the treatment of leukaemia and lymphoma. One of the major reasons for this is the challenge of accessing a solid tumour and its

microenvironment. In order to improve targeting of solid tumours, fourth generation CARs equipped with transgenes for enhanced tumour infiltration and T-cell survival have been developed.

Tumour antigen-specific CTLs co-expressing IL-12 have been shown to induce tumour regression in mice [402]. Pmel TCR gene constructs to the TAA gp100 were transduced into T cells along with the IL-12 gene. This cytokine is pro-inflammatory and can promote the anti-tumour response in a tumour microenvironment. In this study, even low doses of the co-expressing engineered T cells could kill solid tumour cells. Usually, very high doses are required to penetrate the tumour environment and persist.

Another study using IL-12 compared co-expression of an anti-VEGF-R2 CAR with either constitutively expressed IL-12 or an inducible IL-12. The inducible cytokine gene was under the control of an NFAT promoter meaning the gene was only expressed when the T cells were activated, via CAR+ve-TAA interaction within the tumour microenvironment. The CAR targeting VEGF-R2 preferentially targets solid tumours which are highly vascularised and are consistently undergoing angiogenesis. Whilst tumour regression of an established B16 solid tumour was mediated by the constitutive IL-12 CAR+ve T cells, dose limiting toxicity was observed. The inducible IL-12 CAR+ve T cells elicited tumour regression without the toxicity as the IL-12 was only expressed within the tumour microenvironment, upon T-cell activation.

IL-7 has also been employed in CAR design to enhance T-cell expansion and survival. An anti-CD20 CAR with both IL-7 and CCL19 genes included in the vector, separated by short linker peptides, demonstrated improved tumour infiltration and control, and significantly increased survival in an *in vivo* model [403]. Similarly, an anti-GD2 CAR, also expressing IL-7Ra in a bi-cistronic vector was evaluated *in vitro* and in a neuroblastoma xenograft model [404]. The CAR+ve T-cell expansion, tumour infiltration and persistence were greatly improved by the expression of the IL-7R in the presence of IL-7, whilst IL-2 did not improve the responses. Crucially, Treg cells lack IL-7R, so the cytokine was able to act to expand the CAR+ve CTL population in the tumour microenvironment, without enhancing this inhibitory population.

CARs have also been designed to co-express chemokine receptors to improve T-cell homing and infiltration into a solid tumour. Two studies have co-expressed CCR2, with either an anti-GD2 CAR or an anti-mesothelin CAR [405, 406]. In both cases the targeted tumours expressed high levels of CCL2, but the CAR+ve T cells lacked significant chemokine receptor expression. When CCR2 was co-expressed with each CAR construct, a >10 fold increase in CAR+ve T-cell migration and tumour infiltration

was observed in *in vivo* tumour models. This corresponded with enhanced anti-tumour activity in both cases, as compared to CAR+ve T cells alone.

A major obstacle for solid tumour CAR+ve T-cell therapies is the expression of multiple inhibitory molecules in the tumour microenvironment that can lead to diminished T-cell activation and function. To circumvent this, CAR design has been developed to include methods of blocking these inhibitory signals. Several CAR therapies have been evaluated in combination with checkpoint blocker mAb against PD-1, PDL-1 and CTLA4 [407]. In the first example of this combination therapy, Her2+ve tumours were targeted with CAR+ve T cells in combination with an anti-PD-1 mAb. The tumour cells, expressing PDL-1 were capable of inhibiting the T cells, but blocking PD-1 led to enhanced tumour regression with the combined therapy. Significantly, a decreased number of tumour-associated MDSCs were observed in the tumour microenvironment after treatment with the mAb and CAR+ve T cells [408]. Several trials are now investigating the clinical potential of CAR+ve T cell and checkpoint blocker mAb combined therapy, including anti-CD19 CAR combined with either ipilimumab to block CTLA4 [409], pembrolizumab to block PD-1 [410], or atezolizumab against PD-L1 [411].

CAR constructs have also been designed that incorporate the gene for an anti-PD-1 scFv into the vector [412]. The transduced T cells then express these soluble blocking mAb as the CAR is expressed, allowing a more targeted approach to inhibitor blockade. The anti-PD-1 scFv was shown to act in both a paracrine and autocrine manner, enhancing the CAR+ve T-cell anti-tumour function, and the anti-tumour response of non-transduced TILs against PD-L1+ve tumours leading to augmented survival in an *in vivo* model. Importantly, this method resulted in the anti-PD-1 scFv only being detected in the tumour microenvironment which may help to reduce the known toxicities of checkpoint blockade therapies.

An alternative approach involves the use of “switch” CAR constructs, whereby the external domain binds an inhibitory molecule, but the intracellular domains are T-cell activatory. A truncated extracellular domain of PD-1 was linked to the CD28 signalling domain and co-expressed with anti-mesothelin and anti-PSCA CARs [413]. The addition of the “switch” CAR allowing inhibitory PD-1/PD-L1 interactions to be redirected into further CAR+ve T-cell co-stimulation resulted in increased tumour control in *in vivo* models bearing large, established PD-L-1+ve tumours. Similarly, an extracellular domain of IL-4R was linked to the intracellular domain of IL-7R and co expressed with an anti-Her2 CAR [414]. In a breast cancer tumour model, where the microenvironment milieu contained high levels of IL-4, this “switch” receptor enhanced

CAR+ve T-cell expansion and persistence and subsequent tumour control, whilst CAR+ve T cells without it became exhausted and failed to control tumour growth.

The recent advancements in gene editing techniques such as CRISPR/Cas9 have now allowed the total knock out of PD-1 in anti-CD19 CAR+ve T cells. Preclinical study has demonstrated increased CAR+ve T-cell function and tumour control than with unedited CAR+ve T cells [415], and this combination is now being evaluated in a phase I clinical trial [416].

1.8.6 T-cell subsets in CAR therapy

The role of CD8 T cells in CAR therapy has been well defined, as the major cytotoxic response to tumour target cells. CD8 CTLs directly lyse target cells upon antigen engagement with the CAR, via the perforin/granzyme pathway (described in Chapter 1.7.4.3.1). In addition to this degranulation, CAR+ve T cells have been shown to kill via the Fas/FasL pathway (described in Chapter 1.7.4.3.2) [417]. The majority of CAR+ve CD8 CTLs provide an acute, robust anti-tumour response, culminating in T-cell exhaustion and death. In some cases, memory CAR+ve T cells have been described, providing longer term protection [418] [419, 420].

More recently, the key roles that CD4 Th cells play in the support of CAR-induced tumour eradication have been described. CAR-transduced Th cells produce cytokines including IL-2, IFN- γ and TNF- α which act to promote the proliferation and anti-tumour responses of CAR+ve CTLs [421]. The presence of CD4 CAR+ve T cells was observed to enhance tumour clearance in a glioblastoma xenograft model and the ability of the CAR+ve CTLs to perform “serial killing”, where several target cells are engaged and lysed sequentially, was improved [422].

In addition to the supportive role, tumour-infiltrating CD4 T cells have been observed to elicit direct cytotoxic activity. Th1 cells, upon the upregulation of the transcription factors T-bet and Blimp-1, were able to directly lyse B16 melanoma cells in an *in vivo* model [423-425]. Further to this, CAR+ve CD4 T cells have also proved capable of direct cytotoxic activity. In a xenograft leukaemia model, CAR+ve CD4 T cells proved as effective at target lysis as the CD8 CTLs, though the rate of killing was slower (2 d Vs 4 d). This delay was attributed to lower levels of cytosolic granzymes and perforin present in the CD4 cells. The CD4 cells were seen to persist for a longer time period, whilst the CD8 CTLs succumbed to exhaustion. In a syngeneic murine model using the same CAR constructs, the CD4 cells provided a more supportive, cytokine-producing role when in the presence of CD8 CAR+ve cells. When infused alone, the CD4

CAR+ve cells elicited a cytotoxic response and were able to clear the tumour cells [426].

Similarly, when CD4 and CD8 CAR+ve T cells were challenged with glioblastoma cells, the Th cells were skewed away from a cytotoxic effector role, whilst the CD8 CTLs executed a rapid, but short-lived anti-tumour response. The CD4 T cells were again observed to persist longer, whilst the CD8 cells became exhausted and expired. Interestingly, in this study the CD4 CAR+ve cells out-performed both CD8 cells and a combination of both subsets in a glioblastoma xenograft model. The CD4 cells, in the absence of CD8 cells, were capable of robust direct cell lysis and consequent tumour clearance [422].

A comparison between 1:9 and 1:1 ratios of CAR+ve CD4:CD8 T cells in a breast carcinoma xenograft also highlighted the importance of the Th subset. The inclusion of 10 % CD4 CAR+ve T cells resulted in 20-50 % survival, whilst the 1:1 ratio achieved 100 %. The infusion of CD8 or CD4 CAR+ve cells alone did not provide a significant anti-tumour response, with a 30 % survival rate seen only when a double dose of CD8 cells was administered. Additionally, the mice that received the 1:1 CAR+ve T-cell ratio were protected from a secondary tumour challenge, demonstrating the robust immune response generated by the infusion of the mixed pool of cells [427].

A synergistic anti-tumour response was observed in NSG mice bearing Raji tumours, when a 1:1 ratio of CD4 and CD8 CAR+ve T cells was administered. Further investigation revealed that the inclusion of T cells from the T_N or T_{CM} differentiation states elicited a superior response, to those from the T_{EM} state [428]. The natural variation in differentiation states in the T cells of patients may therefore affect the efficacy of a CAR therapy, even within a trial cohort. This pre-clinical study was expanded upon into a clinical trial of B-cell ALL patients. Administration of a 1:1 ratio of T_{CM} CD8 and CD4 CAR+ve T cells resulted in 93 % of patients achieving bone marrow remission [429].

Supporting these findings, the analysis of leukapheresis products of multiple myeloma patients prior to CAR modification, showed that a higher CD4/CD8 T-cell ratio correlated with increased CAR+ve T-cell expansion *in vivo* and an improved clinical outcome [430]. These data together clearly show that the role of CD4 CAR+ve T cells can be as important as that of the traditional cytotoxic CD8 T cells forming an essential part of the anti-tumour responses, and that a mixed T-cell subset pool is beneficial to maximise CAR efficacy.

1.8.7 CAR Safety

As discussed in Chapter 1.8.4, CAR target selection is important for both optimal performance and for therapeutic safety. Even in the absence of on-target off-organ or off-target effects, a potent CAR+ve T-cell response can induce tumour lysis syndrome or a cytokine storm. Tumour lysis syndrome occurs when extensive cell lysis occurs in a short timeframe, releasing cellular contents into the extracellular space. This induces an inflammatory response and induces side effects of aberrant immune activation. A cytokine storm is characterised by immune over-stimulation, leading to massive cytokine and pro-inflammatory mediator release. This can cause organ damage and in severe cases can be fatal [372, 431]. Two main methods have been employed to improve the safety of CAR therapy; the inclusion of suicide genes and dual-targeting CAR constructs.

The first suicide gene system developed employed the herpes simplex virus thymidine kinase (HSV-tk) [432]. This enzyme converts ganciclovir to GCV-triphosphate in the CAR+ve T cells, and is toxic to DNA replication, killing proliferating cells [433]. However, whilst this method is effective at T-cell ablation, the expression of HSV-tk in human cells has been observed to be immunogenic itself resulting in an immune response to the transduced cells. More recent developments in suicide genes have involved the use of inducible caspase 9 and Fas dimer systems. These functional proteins are linked to FKBP12 domains, which allow homo-dimerisation upon the addition of the small molecule AP1903, leading to the induction of apoptosis in the T cells. An inducible caspase 9 (iC9) suicide system was shown to ablate >90% of CAR+ve T cells in patients within 30 minutes of a single dose of AP1903 [434]. An inducible Fas system eliminated 80% of expressing T cells *in vitro* in 2 hours at a single sub-nanomolar dose [435]. However, this small molecule is not a licensed drug and so may limit the translation of this system to the clinic. To circumvent this, Stavrou *et al* designed a similar system of iC9 using rapamycin as the dimerization agent [436]. Caspase 9 domains were linked to FKBP12 and the rapamycin-binding domain of mTOR. Rapamycin forms heterodimers of these constructs, bringing the caspase 9 domains together and inducing apoptosis.

Alternatively, molecules have been co-expressed on the T-cell surface with CAR constructs, that can be targeted for cell deletion. EGFR and CD20 can be targeted with cetuximab and rituximab respectively and allow the removal of a CAR+ve T-cell population. A non-signalling truncated EGFR (tEGFR) was evaluated and found to be functionally inert and provide an effective method of T-cell deletion in an *in vivo* model [437]. A study using CD20 demonstrated that the co-expression did not interfere with

T-cell function and these cells were efficiently eliminated *in vitro* by the addition of rituximab [438]. A short peptide, RQR8, has been designed containing both CD20 and CD34 epitopes [439]. This construct functions both as a method for CAR+ve T-cell detection and selection using a clinically approved anti-CD34 system, and a suicide gene upon the addition of rituximab. This study demonstrated effective T-cell clearance in an *in vivo* model after rituximab treatment.

Dual-targeting CAR systems involve the co-expression of two constructs, targeted to two different antigens. Both can contain complementary signalling domains targeted to TAA, which can also help to treat relapsed/refractory tumours that have decreased antigen expression, as discussed in Chapter 1.8.4. Alternatively, one may target a molecule that leads to an inhibitory signal to provide an “off switch”.

In a dual-targeting study, T cells were transduced to express a CAR with the CD3 ζ signalling domain and incorporating a low affinity scFv targeting PSCA, and a second CAR with a high affinity scFv to PSMA, containing the signalling domains from CD137 and CD28 [440]. When both the receptors expressed on the T cell bound both the antigens on the tumour cell, activation via both receptors is induced and the CAR cell could kill the target. Cells expressing only one of the antigens, such as healthy tissues, were avoided.

Recently the principle of dual CAR targeting has been further developed using a synthetic notch (synNotch) system [441, 442]. Upon antigen binding to a CAR with a notch core, a custom transcription factor is cleaved and can induce production of desired cytokines, mAb, BiTE or a second CAR construct. Thus, a second co-stimulatory CAR to a second TAA can be induced to enhance target cell lysis in a controlled way.

Inhibitory CAR (iCAR) provide a system to control an activatory CAR response in the presence of a non-target antigen. iCAR have been generated using intracellular domains from CTLA4 and PD-1. These were targeted to PSMA, whilst a antigen-specific TCR or activatory CAR was expressed on the same cell to CD19. In this study, the iCAR could control the activatory response induced by the anti-CD19 CAR when the T cells were co-cultured with artificial antigen presenting cells expressing CD19 and PSMA. When CD19 alone was expressed on the target cells, T-cell activation and target lysis was observed. Crucially, it was shown that the iCAR controlled T-cell activation in a fully reversible manner so when the T cells encountered a target cell with only the activatory tumour antigen on, activation was induced again [443].

1.8.8 Universal CAR

A major hurdle in the progression of CAR therapy into mainstream clinical treatment is that each patients' T cells must be harvested, expanded, genetically altered and re-infused in an expensive and time-consuming manner. To attempt to overcome this, "universal" CAR+ve T cells are being developed that remove the requirement for autologous cells for each individual. Additionally, donor cells from a healthy patient may be advantageous over those from a patient who has undergone previous therapies which can result in immune system defects. The first "universal" CAR were developed using zinc finger nucleases to prevent the expression of the endogenous TCR α and β chains in CAR+ve T cells [444]. The CAR directed T cells retained their anti-CD19 function, but no longer responded to TCR stimulation.

The development of the TALEN and CRISPR/Cas9 gene editing systems now allow the efficient generation of "universal" CAR+ve T cells, often in conjunction with other modifications. The TALEN system employs transcription-activator like effector (TALE) nucleases, containing a DNA-binding domain, which is easily customisable due to the repeat variable diresidues present in the TALEs, linked to the nuclease domain [445]. Anti-CD19 CAR+ve T cells were modified using TALEN to knockout the CD52 gene, eliminating sensitivity to alemtuzumab, used as a co-therapy, and to disrupt TCR expression [446]. The edited "universal" CAR+ve T cells were given to two ALL patients, both of whom achieved remission.

CRISPR/Cas9 involves a similar system of specific DNA targeting and enzymatic editing. Guide RNA are used to target the gene of choice, whilst the Cas9 enzyme can then cleave both strands of the DNA. The cellular mechanisms of double-strand repair can then be allowed to insert a gene of interest using homology directed repair, or make smaller gene alterations via non-homologous end joining (NHEJ) [447]. CRISPR/Cas9 has been used to target the TCR α chain gene in anti-CD19 CAR+ve T cells, resulting in "off-the-shelf" CAR+ve T cells generated from healthy donor cells that demonstrated strong anti-cancer responses in a humanised *in vivo* model. The same technique has been employed in conjunction with disruption of the β 2M and PD-1 genes, generating TCR and HLA-I -deficient anti-CD19 CAR+ve T cells that can be produced from a healthy donor [415]. This study showed enhanced anti-tumour responses in an *in vivo* model compared to PD-1-unedited CAR+ve T cells, and significantly reduced GVHD as compared to HLA-I-unedited CAR+ve T cells.

Induced pluripotent stem cells have now been edited using CRISPR/Cas9, with an anti-CD19 CAR gene construct being inserted into the TCR α locus [448]. The cells can then be differentiated into CAR+ve TCR-ve T cells and could provide a continuous supply of

“off-the-shelf” CAR+ve T cells. The CD16 (FcγRIII) gene was also inserted into these cells, producing dual-targeting cells via the addition of mAb. An early study reports successful differentiation into CD8+ve T cells of these cells, and *in vitro* anti-tumour function.

Another aspect of “universal” CAR development has been the design of “universal” CAR constructs rather than of the CAR+ve T cells. CAR constructs targeting fluorescein isothiocyanate (FITC) and avidin have been developed. These allow the targeting of these CAR+ve T cells to any labelled mAb, itself targeting the desired antigen. EGFR+ve human pancreatic cells grafted into mice were cleared even when thoroughly established by the administration of anti-FITC CAR+ve T cells and FITC-labelled Cetuximab. A colon cancer line in an *in vivo* model was also delayed, although outgrowth of EGFR-ve tumour cells was observed[449]. A small “switch” molecule comprised of FITC-labelled folate has also been used in the same way to link folate receptor+ve tumour cells to anti-FITC CAR+ve T cells, forming an effective immunological synapse [450]. The requirement of the presence of the small molecule also provides a potential safety switch for CAR activation. Similarly, a CAR incorporating avidin as the extracellular binding domain allows interaction with a biotinylated mAb to the desired TAA and has shown to be functional against several different antigens [451, 452]. The advantage of these systems is that different labelled mAb could be used against an alternative TAA in one tumour in the case of antigen downregulation, or against several tumours in conjunction with the same CAR, providing a “universal” system.

1.8.9 CARs in the clinic

The first clinical success for CAR therapies was a trial carried out by Carl June’s group in 2011 using anti-CD19 second generation CAR+ve T cells to treat a patient with refractory CLL [453]. The construct comprised CD3ζ and CD137 signalling domains, and a CD8α hinge and transmembrane domain. This trial was remarkable due to the very low dose of CAR+ve T cells administered. A total of 1.42×10^7 transduced cells were infused over a 3 day period and these proliferated 1000-fold, depleting malignant and normal B cells. Delayed tumour lysis syndrome was a side effect, along with hypogammaglobulinemia. Two further patients were treated with the CAR+ve T cells, one also achieving full remission, and the other partial remission [453]. A proportion of the CAR+ve T cells were seen to persist in the patient as a memory CAR+ve T-cell subset. These cells showed sustained effector capabilities at 6 months after transfusion.

Two anti-CD19 CAR are currently FDA approved and used in the treatment of relapsed/refractory B-cell malignancies in the US, UK and Japan. Tisagenlecleucel (Kymriah; Novartis) [454] is of the same design as the CAR used in the original trial described above, and is licenced for the treatment of paediatric and young adult ALL. Axicabtagene ciloleucel (Yescarta; Kite/Gilead) [455], incorporating CD3 ζ and CD28 signalling domains and an IgG1 spacer domain, is used for large B-cell lymphoma [456].

Several other CAR constructs against haematological malignancies and solid tumours are being evaluated in ongoing clinical trials. Anti-CD19 CAR+ve T cells have shown the highest clinical success and there are several continuing trials targeting this antigen in multiple B-cell cancers [457]. Additionally, CARs targeting CD20, CD22 and CD30 are also in assessment for the treatment of diffuse large B-cell lymphoma, ALL and Hodgkin lymphoma respectively. Initial data demonstrate that a proportion of patients have achieved complete recovery in each case [458-460]. Two trials using universal TCR/CD52 KO anti-CD19 CAR+ve T cells are also currently ongoing [461] [462], whilst an anti-CD19 CAR in conjunction with CRISPR/Cas9 knock out of PD-1 in the T cells is entering phase I trials [416] .

Whilst no CAR targeting solid tumours have been approved for clinical use, there are several early trials targeting TAA commonly used in mAb therapies. These include GD2 for neuroblastoma, Her2 for breast cancer, EGF2 for glioblastoma, PSMA for prostate cancer and mesothelin for ovarian and pancreatic carcinomas [463]. However, at the current time these trials include very small numbers of patients and all show very varied responses. The majority of patients in solid tumour CAR trials achieve a partial response or stable disease outcome at best, in comparison to the complete recovery responses seen in trials for haematological malignancies [457]. As fourth generation CAR constructs with associated cytokine production and tumour microenvironment targeting capabilities are further developed, there is great potential for improvement in the outcome of clinical trial patients with solid tumours.

1.9 Aims and Objectives

As discussed in Chapters 1.8.3 and 1.8.4, it is known that the IS distance can affect CAR function, whether due to the length of the spacer domain included or the position of the targeted epitope. Additionally, scFv affinity for the target antigen can impact CAR efficacy. CD20 is a well-established immunotherapy target, for mAb and CAR therapies. However, the role of epitope and binding strength of the scFv in anti-CD20 CARs has not been thoroughly evaluated. The impact of inclusion of a type I or type II anti-CD20 scFv is also unknown. Therefore, the aim of this thesis was to produce and compare the function of a panel of anti-CD20 CARs, differing only in the scFv included. The hypothesis of this thesis was that the scFv included in an anti-CD20 CAR will influence the functional efficacy, due to differences in antigen binding characteristics.

To investigate this, the following objectives were designed:

1) Produce a panel of anti-CD20 CAR constructs.

- Generate anti-CD20 scFv from parental mAb sequences and determine protein expression of the soluble fragments.
- Incorporate these scFv into full CAR constructs using molecular biology techniques.
- Confirm mammalian cell surface expression of the CARs.
- Determine if the constructs can bind the target antigen, and if this interaction is specific.

2) Test the functional characteristics of the CARs in cell line systems.

- Generate CAR-expressing stable cell lines for use in functional assays.
- Compare the T-cell activation levels achieved for each CAR using a reporter cell line.
- Compare the cytotoxic function of each CAR using a cytotoxic cell line in *in vitro* killing assays.
- Employ the previously generated Rp3-CD137 constructs [464] to further investigate the role of the epitope position in anti-CD20 CAR function.

3) Investigate the function of the CARs in murine and human primary systems.

- Establish CAR expression in primary murine T cells, to examine *in vivo* CAR efficacy for each construct.
- Express CARs in primary human T cells and compare in *in vitro* functional assays.

2 Materials and methods

2.1 Cell Culture

2.1.1 Cell culture conditions

Cells were grown as described in **Table 2.1**. Roswell Park Memorial Institute 1640 (RPMI 1640), Dulbecco's Modified Eagle Medium (DMEM), FreeStyle CHO expression, FreeStyle 293 expression and Iscove's Modified Dulbecco Medium (IMDM) media were all purchased from Life Technologies. Supplemented media included 10 % (v/v) foetal calf serum (FCS; Sigma Aldrich), 2 mM glutamine and 1 mM sodium pyruvate (GP), and 100 U/ml penicillin and 10 µg/ml streptomycin (PS; all Life Technologies) unless otherwise stated. Other additional supplements are listed in **Table 2.1**.

Cell type	Media	Supplemented	Growth conditions	Density/ml
A20	RPMI 1640	10 % FCS, GP, PS	37 °C, 5 % CO ₂	5 x 10 ⁵ - 1 x 10 ⁶
BWZ.36	RPMI 1640	10 % FCS, GP, PS, 10 mM Hepes buffer (Fisher), 50 µM β-mercaptoethanol, 0.5 mg/ml hygromycin (Sigma Aldrich)	37 °C, 5 % CO ₂	1 x 10 ⁵ - 1 x 10 ⁶
CHO-S	FreeStyle CHO expression	8 mM Glutamine	37 °C, 5 % CO ₂	3 x 10 ⁵ – 3 x 10 ⁶
CTLL-2	RPMI 1640	10 % FCS, GP, PS, 10 % T-stim (Corning)	37 °C, 5 % CO ₂	< 2 x 10 ⁵
HEK 293F	FreeStyle 293 expression	None	Shaking, 37 °C, 8 % CO ₂	1x10 ⁵ - 1x10 ⁶
HEK 293T	IMDM +veL-Glu	10 % FCS, GP	37 °C, 5 % CO ₂	Split 1:5-1:7 3x a week

Human peripheral blood mononuclear cells (PMBC)	RPMI 1640	10 % FCS, GP, PS	37 °C, 5 % CO ₂	Plated at appropriate density for immediate use
K562	RPMI 1640	10 % FCS, GP, PS	37 °C, 5 % CO ₂	2 x 10 ⁵ - 1 x 10 ⁶
Murine bone marrow	DMEM	20 % FCS, GP, PS, 50 µM β-mercaptoethanol	37 °C, 5 % CO ₂	Plated at appropriate density for immediate use
Murine Splenocytes	RPMI 1640	10 % FCS, GP, PS, 50 µM β-mercaptoethanol	37 °C, 5 % CO ₂	Plated at appropriate density for immediate use
NIH3T3	DMEM	10 % FCS, GP, PS	37 °C, 5 % CO ₂	Split 1:5-1:7 3x a week
Phoenix-ECO	DMEM	10 % FCS, GP, PS	37 °C, 5 % CO ₂	Split 1:5-1:7 3x a week
Raji	RPMI 1640	10 % FCS, GP, PS	37 °C, 5 % CO ₂	5 x 10 ⁵ - 2 x 10 ⁶
Ramos	RPMI 1640	10 % FCS, GP, PS	37 °C, 5 % CO ₂	2 x 10 ⁵ - 1 x 10 ⁶
RPMI 8226	RPMI 1640	10 % FCS, GP, PS	37 °C, 5 % CO ₂	5 x 10 ⁵ - 2 x 10 ⁶

Table 2.1: Growth conditions and media used for the culture of each cell type used in this thesis.

All cells originally obtained from ATCC.

2.1.2 Isolation of human peripheral blood mononuclear cells (PBMCs)

Platelet-depleted whole blood cones from the NHS Blood Service were used as the source of human PBMCs. 2 mM ethylene-diamine-tetra-acetic acid (EDTA) 5 % (v/v) FCS phosphate buffered saline (PBS) was added to 15 ml blood to a total volume of 50 ml. 25 ml diluted blood was layered onto 12.5 ml lymphoprep (Axis-Shield) and separated by density gradient centrifugation at 800 xg for 20 min with the brake off.

The separated lymphocyte layer was removed with a Pasteur pipette into a fresh tube and washed 3x in 2 mM EDTA 5 % FCS PBS at 300 xg, 5 min. Supernatant was discarded, and cells were resuspended in complete RPMI 1640 media.

2.1.3 Isolation of murine splenocytes

Spleens were harvested from wild type C57BL/6 mice into 10 ml PBS. A single cell suspension was generated by passage through a 100 µm cell strainer, using the end of a sterile 5 ml pipette plunger. Cells were washed through with PBS and collected into a universal. Splenocytes were centrifuged at 300 xg for 5 min and resuspended. 5 ml erythrocyte lysis buffer (155 mM NH₄Cl, 10 nM KHCO₃) was added and cells were washed again in PBS after 5 min. Splenocytes were then resuspended in complete RPMI 1640 with the addition of 2 µg/ml anti-CD3 (KT3) and 2.5 µg/ml anti-CD28 (37.51) to activate T cells for retroviral transduction. Cells were plated at 1.5 x 10⁶/ml and incubated for 48 h prior to use.

2.1.4 Isolation of murine bone marrow

Donor mice were treated with 150 mg/kg 5-fluorouracil, by intraperitoneal injection (IP). After 4 d, bone marrow was harvested from the hind legs of wild type C57BL/6 mice and pooled. Erythrocytes were lysed by addition of lysis buffer (155 mM NH₄Cl, 10 nM KHCO₃), then centrifuged at 300 xg for 5 min. Cells were resuspended in complete DMEM with the additional of 50 ng/ml each of mIL-3, mIL-6 and murine stem cell factor (mSCF; all Gibco), to promote a stem cell phenotype. Cells were plated at 3.8 x 10⁶/well in 6-well plates (Corning) for 48 h prior to use.

2.1.5 Freezing and thawing cells

2.1.5.1 Freezing

1 x 10⁷ cells were resuspended in 1 ml FCS with 10 % (v/v) dimethyl sulfoxide (DMSO). Cells were transferred to a cryovial and transferred to -80 °C storage, in polystyrene boxes to slow the freezing process. Cells were transferred after 48 h to liquid nitrogen storage.

2.1.5.2 Thawing

To maintain viability, cells were thawed from -80 °C or liquid nitrogen by addition of pre-warmed media and gentle mixing using a Pasteur pipette. Cells were then transferred to a universal and centrifuged to wash away the DMSO. Cells were resuspended in media and seeded at the appropriate density for culture.

2.1.6 Harvesting adherent cells

Adherent cells were harvested by removal of media and the addition of 10-15 ml pre-warmed 15 mM filter-sterilised ethylenediaminetetraacetic acid (EDTA) in PBS. Cells were incubated at 37 °C for 10 min before collection using a Pasteur pipette. Cells were then pipetted up and down to ensure a single cell suspension, before being washed in media or PBS, centrifuged at 300 xg for 5 min, and resuspended in appropriate media for re-plating.

2.1.7 Cell counting

All cell counts were performed using Coulter Industrial D Cell Counter (Beckman Coulter). Cells were diluted 1:500 in Coulter Isoton diluent (Beckman Coulter) prior to counting. Where required, 1-2 drops of Zapoglobin lytic reagent (Beckman Coulter) was also added using a Pasteur pipette to lyse erythrocytes.

2.2 Molecular biology techniques

2.2.1 Polymerase chain reaction (PCR)

Primers were generated to order by Invitrogen. PCRs were performed in a total volume of 25 µl, comprising 2.5 µl 10x Buffer (Promega; including 4 mM MgSO₄), 0.2 mM dNTPs (Promega), 100 ng 5' and 3' primers in TE buffer (10 mM Tris-HCL pH7.5, 1 mM EDTA), up to 1 µg DNA template, 1 µl PFU polymerase (Promega) and distilled H₂O (dH₂O). Where indicated, some PCRs were performed using Q5 polymerase (NEB). All PCR primer sequences can be found in **Table A2.1**, in the Appendix.

The basic PCR protocol used is detailed in **Table 2.2**. The annealing temperature of each reaction was altered based on the melting temperature (T_m) of the primers used and the number of cycles was varied as necessary. Reactions were carried out using a PTC-200 thermal cycler with a heated lid (MJ Research).

Step	Temperature	Time (min:sec)	
1	94°C	05:00	
2 Denaturing	94°C	00:30	X 25 cycles
3 Annealing	60°C	01:00	
4 Elongation	72°C	02:00	
5 Extension	72°C	10:00	
6 Hold	4°C	∞	

Table 2.2: PCR protocol used to generate DNA constructs.

Annealing temperature and cycle number were altered as required.

2.2.2 Overlap PCR

PCR reactions were performed as described in Chapter 2.2.1 for 30 cycles, to generate DNA fragments with complementary overlapping 5' or 3' ends. The two products to be joined were extracted and purified and a second round of PCR was performed for 15 cycles without the addition of primers, to allow the fragments to fuse via the complementary sections. Finally, a third reaction including 5' and 3' primers and additional dNTPs generated an improved yield of the final fused product. Additional rounds of overlap PCR were carried out to adjoin further fragments to the DNA construct as required.

2.2.3 Gel electrophoresis

PCR products were separated by gel electrophoresis on 0.7 % (w/v) agarose gels, unless otherwise indicated. Gels were made by dissolving agarose powder in 1x TAE buffer (2 M Tris base, 0.95 M glacial acetic acid, 50 mM EDTA (pH 8) in dH₂O) in a microwave. 5 µl Gel-Red (Biotium) was added and gels were poured into moulds and allowed to set. Samples were run with 6X orange loading buffer (Promega) in 1x TAE buffer at 120-140 V in electrophoresis tanks to allow separation of DNA bands. Gels were visualised under UV light using a Molecular Imager Gel Doc XR (BioRad) and Quantity One software (BioRad).

2.2.4 DNA gel extraction

DNA bands were predominantly extracted and purified from gels using a QIAEX II Gel Extraction Kit (Qiagen) following the manufacturers' protocol. Briefly, after band excision, QX1 suspension buffer and QIAEX II DNA-binding beads were added. The gel slice was solubilised, and the DNA bound to the QIAEX II by incubating at 50 °C

for 10 min. The sample was centrifuged at 17,000 xg for 30 sec, and the supernatant removed. The pellet was washed with QX1 buffer to remove residual agarose and twice with 70 % (v/v) ethanol to remove salt contamination. DNA was eluted by the addition of TE buffer or water, incubation at 50°C for 10 min and centrifugation. The supernatant containing the purified DNA was transferred to a sterile tube.

In some instances, a QIAquick Gel Extraction Kit (Qiagen) was used, according to the manufacturers' instructions. In brief, electrophoresis gel fragments containing DNA were solubilised by incubation at 50 °C for 10 min in suspension buffer QG. Isopropanol was added and the sample centrifuged before the supernatant was transferred to a spin column. Samples were centrifuged at 17,000 xg. Once DNA was bound to the column, samples were washed with buffer QG to remove residual agarose and 70 % ethanol to remove salt contamination. DNA was eluted from the column in EB buffer or water.

2.2.5 Restriction enzyme digestion

Restriction enzyme digests were performed using 10 U of enzyme (Promega) per µg of DNA. Single digests were carried out in a total volume of 10 µl, double digests in 20 µl. Suitable restriction buffers (Promega) were used at 10 % of the total reaction volume. Reactions were incubated at 37 °C for varying times, depending on the compatibility of the enzymes and buffers used together. Digested products were separated by gel electrophoresis.

2.2.6 Ligation reaction

Ligations of blunt end PCR products into pCR-Blunt II-TOPO were performed using a Zero Blunt TOPO PCR Cloning Kit (Invitrogen). 0.5 µl salt solution (1.2 M NaCl, 0.06 M MgCl₂), 0.5 µl vector and 2 µl PCR DNA product were mixed and incubated for 5 min at room temperature (RT).

Ligations into pcDNA/HisMax4B and pcDNA3.1(-) vectors were performed using T4 DNA ligase and ligase buffer (both Promega). Each reaction was performed in a total volume of 30 µl containing 3 µl DNA ligase, 3 µl 10x buffer, and the insert and pcDNA vector at a molar ratio of 3:1. The reaction was incubated at 4 °C for 16 h.

Ligations into pMIGR1 and SFG retroviral vectors were performed using T4 DNA ligase and ligase buffer (both Promega), as for pcDNA vectors. The ligation reactions were then incubated at 16 °C for 6 h.

2.2.7 Site-directed mutagenesis

Mutagenesis reactions were run in a total volume of 50 μ l, comprising 5 μ l 10x buffer (Agilent Technologies), 300-600 ng target DNA, 10 mM each mutagenesis primer (generated to order by Invitrogen), 0.2 mM dNTPs, 1.5 μ l QuikSolution reagent (Agilent Technologies), 1 μ l QuikChange Lightning Enzyme (Agilent Technologies) and dH₂O. The reaction was performed in a PTC-200 thermal cycler (MJ Research) following the protocol outlined in **Table 2.3**.

Step	Temperature ($^{\circ}$ C)	Time (min:sec)	
1	95	02:00	
2 Denaturing	95	00:20	X 18 cycles
3 Annealing	60	00:10	
4 Elongation	68	00:30 per kb	
5 Extension	68	05:00	
6 Hold	4	∞	

Table 2.3: Protocol of site-directed mutagenesis.

After the mutagenesis reaction was complete, the parental (non-mutated), methylated dsDNA was digested by addition of 2 μ l DpnI (Agilent Technologies) and incubation at 37 $^{\circ}$ C for 45 min. All mutagenesis primers are listed in **Table A2.2**, found in the appendix.

2.2.8 Recombination

A sequence- and ligation- independent cloning (SLIC) approach was used to insert BHH2 scFv into pFUSE-hIlgG1-Fc2 vector, performed by Patrick Duriez (Southampton Protein Core Facility). Briefly, the vector and scFv DNA were amplified by PCR using Phusion polymerase (NEB). The scFv primers used contained 23-24 bps complementary to the sequence of the vector, with the addition of a C-terminus haemagglutinin (HA) tag. The vector PCR product was treated with DpnI (Promega), before both products were run on a gel and purified. A recombination reaction was performed with a 3:1 insert/vector molar ratio in the presence of RecA (NEB) for 30 min at 37 $^{\circ}$ C.

2.2.9 Heat shock bacterial transformation

Bacterial transformations were carried out using competent strains of *E. coli* (Promega). Constructs ligated into pCR-Blunt TOPO-II were transformed into Top10,

all other ligations into JM109, and products of mutagenesis reactions into XL-Gold cells. 3 µl of pCR-Blunt TOPO-II plasmid DNA was mixed with 30 µl Top10 *E. coli*, 30 µl plasmid DNA was mixed with 300 µl 2:1 CaCl₂ and JM109 *E. coli* or 2 µl β-mercaptoethanol (Promega) and 2 µl mutated DNA was added to 45 µl XL-gold *E. coli*. All cells were incubated on ice for 30 min, then heat-shocked at 42 °C for 30 sec (XL-Gold) or 45 sec, and incubated on ice for 2 min. 0.5 ml RT SOC media (Super Optimal Broth +veglucose; Invitrogen) was then added. All cells were then incubated, shaking for 1 h at 37 °C, before being plated on antibiotic-containing Lysogeny Broth (LB) agar plates and grown overnight.

To avoid the issue of a methylation site that blocked an essential restriction site in some scFv constructs in pCR-Blunt TOPO-II, SCS110 dcm⁻/dam⁻ *E. coli* were used. 2 µl β-mercaptoethanol was added to 100 µl cells and incubated on ice for 10 min, mixing every 2 min. 1 µl DNA was added and the cells incubated for 30 min on ice before being heat-shocked for 45 seconds at 42 °C. 0.9 ml SOC media, pre-heated to 42 °C, was added before these cells were incubated and plated as described for the other cell types.

2.2.10 Bacterial culture

Antibiotic plates were made by melting LB agar before the addition of 100 µg/ml Ampicillin (Amp) or 50 µg/ml Kanamycin (Kan) (both Sigma Aldrich). Once cooled, the plates were poured and allowed to solidify. Bacterial transformation reactions were plated on to appropriate plates and incubated at 37 °C overnight. Individual bacterial colonies were picked and grown up in 10 ml LB +veAmp or Kan for 16 h. To extract DNA from these, minipreps were performed. Alternatively, these cultures were used to inoculate large volumes of LB to obtain high quantities of DNA.

2.2.11 Plasmid DNA purification from bacterial cells

Plasmid isolation was performed using Qiaprep Spin Miniprep or HiSpeed Plasmid Maxi Kits (both Qiagen) according to the manufacturer's protocols. Briefly, bacterial cultures were harvested by centrifugation at 6000 xg and the supernatant was removed. Cell pellets were resuspended and lysed using an alkaline buffer for 5 min. Neutralisation was performed allowing the DNA to enter into solution. The lysate was applied to small spin columns for minipreps and centrifuged at 17,000 xg for 1 min. For maxi preps the lysates were applied to equilibrated filter tip gravity columns. In both systems, as the solution passes through the column the DNA is bound to the filter, whilst all other cellular components and buffers pass through. The bound DNA was then washed in a medium-salt buffer to remove remaining RNA, proteins and

other impurities by centrifugation (miniprep) or gravity flow (maxiprep). Miniprep DNA was eluted into 50 µl water or elution buffer. For maxiprep DNA, a further step was performed to desalt and concentrate the eluted DNA by the addition of isopropanol. This solution was then passed through a Qiaprecipitator module, washed in 70 % ethanol and the DNA was eluted into 1 ml elution buffer. Plasmid DNA concentration and quality (260:280 ratio) was ascertained using a nanodrop spectrometer (Thermo Scientific).

2.2.12 Short-chain termination DNA sequencing

Each in-house sequencing reaction comprised 300-500 ng DNA, 10 ng appropriate sequencing primer(s) (generated to order by Invitrogen), 2 µl Big Dye (containing dNTPs, fluorescent dye conjugated-ddNTPs and DNA polymerase) and 2 µl 5x sequencing buffer (both AB Sciences), made up to 10 µl with dH₂O. Reactions were run in a PTC-200 thermal cycler (MJ Research) using a heated lid. The protocol for the reactions is shown in **Table 2.4**. Sequencing primer sequences are detailed in **Table A2.3**, found in the Appendix.

Step	Temperature (°C)	Time (min:sec)	
1	96	2:00	
2	96	2:00	X 24 cycles
3	50	0:05	
4	60	4:00	
5	4	∞	

Table 2.4: Thermocycler sequencing reaction protocol

After the sequencing reaction, DNA was precipitated by the addition of 1 µl 3 M sodium acetate (pH 5.4) and 25 µl 100 % ice-cold ethanol. Tubes were incubated on ice for 5 min before being centrifuged at 4 °C, 17,000 xg for 30 min. The supernatant was removed and 125 µl 70 % ice-cold ethanol was added. Samples were spun for 5 min and the supernatant was removed. Pellets were air dried for 15 min, 10 µl formamide was added to each, and the samples were assessed using a 3130xl Genetic Analyser (Applied Biosystems) by the in-house sequencing service. On occasion sequencing was outsourced to Source Bioscience Sanger sequencing service. All DNA sequencing results were analysed using Lasergene8 SeqManPro software (DNASTar).

2.3 Mammalian cell transfection

2.3.1 HEK 293F transient transfection

2.3.1.1 Soluble protein expression

5x10⁸ cells were resuspended in 25 ml FreeStyle293 expression media in a large flask. 500 µg DNA was added to 10 ml 150 mM autoclaved NaCl, and 1.5 mg polyethylenimine to 7.5 ml 150 mM autoclaved NaCl. These were combined and incubated at RT for 10 min before being added to the cells. The flask was incubated, shaking at 37 °C for 4 h. 3.75 ml 0.5 M valproic acid (Sigma Aldrich) was added, and the culture made up to 500 ml with FreeStyle293 expression media. Cells were incubated, shaking at 37 °C, for 7-10 d. At this time, cells or supernatant were harvested by spinning cultures twice for 30 min, 800 xg. Supernatant was filtered and stored at 4 °C or -20 °C, dependent upon immediacy of use. Cell pellets were used immediately.

2.3.1.2 Membrane-bound protein expression

20 µl 293Fectin transfection reagent (Invitrogen) and 10 µg DNA were added to 330 ml Opti-MEM serum-free media (Life technologies) each, and both were incubated at RT for 5 min. The diluted DNA was transferred into the 293Fectin mix and incubated to form complexes, at RT for 15-20 min. 10 ml HEK 293F cells were seeded at 1x10⁶/ml in Freestyle293 expression media in a flask and the DNA-293Fectin was added dropwise before cells were incubated, shaking at 37 °C. Cells were harvested from the culture at 24 and 48 h to determine membrane-bound protein expression.

2.3.2 CHO-S transient transfection

10 µl FreeStyle MAX transfection reagent (Invitrogen) and 10 µg DNA were added to 200 µl OptiPro serum-free media (Life Technologies) each. The diluted FreeStyle MAX was immediately added to the DNA and incubated for 10 min at RT, to allow the formation of complexes. This mixture was added dropwise to 10 ml CHO-S cells at a density of 10⁶/ml in FreeStyle CHO expression media. The cells were returned to the incubator, shaking at 37 °C. Cells were harvested from the culture at 24 and 48 h to determine membrane-bound protein expression.

2.3.3 Nucleofection of CTLL-2 cells

Nucleofections were performed using a Mouse T cell Nucleofection Kit (Amaxa). For each nucleofection, 1 x 10⁶ CTLL-2 cells were centrifuged at 200 xg for 10 min and resuspended in 100 µl Mouse T cell nucleofector solution. 4 µg plasmid DNA was

added and the cells transferred to a cuvette. 2 µg pmaxGFP vector was used as a positive control. The cells were placed in a nucleofector machine (Amaxa) and shocked using the X-001 program before transferr to 12-well plates (Corning) containing pre-warmed complete RPMI 1640 media. Cells were assessed at 24 and 48 h for membrane-bound protein expression.

2.3.4 Sub-cloning and antibiotic selection

To select stably-expressing CTLL-2 cells, 0.3 µg/ml G418 (Life technologies) was added 48 h post-nucleofection. The total cells from each nucleofection were then sub-cloned across 2 96-well plates, in a volume of 100 µl/well. Cells were supplemented with G418 once a week and T-stim twice a week. After 21 d cells were visualised to see growth of colonies and when present, samples were analysed by flow cytometry for CAR expression. Positive wells were expanded, with continued addition of G418, to generate CAR+ve CTLL-2 populations.

2.4 Retroviral transduction

Throughout all retroviral transduction work, Virkon (Du Pont) was used to disinfect all potentially virus-contaminated equipment before disposal.

2.4.1 Ecotropic retroviral transduction

2.4.1.1 Generation of retroviral supernatants

Phoenix-ECO cells were seeded in 6-well plates at 0.5×10^6 /well in 5 ml complete DMEM media. When cells were 60-80 % confluent, transfection was performed using Effectene transfection reagent and buffers (Qiagen). For each well, 1 µg DNA and 0.4 µg pCL ECO retroviral packaging vector was added to buffer EC to a total volume of 150 µl before 11.2 µl enhancer was added. Samples were incubated at RT for 5 min, then 31.1 µl Effectene reagent was added to each. After a further 10 min incubation, 1 ml complete DMEM media was added. Old media was removed from the Phoenix-ECO cells and replaced with 4 ml fresh complete DMEM. Each effectene sample was then added drop-wise to the appropriate well. Media was changed at 23 h to 3 ml fresh DMEM or appropriate target-cell media. Viral supernatants were harvested at 48 h or 72 h post-transfection and used immediately to transduce murine target cells.

2.4.1.2 Transduction of murine cells

2.4.1.2.1 NIH3T3 cells

NIH3T3 positive control target cells were plated at 3×10^5 /well in 5 ml complete DMEM. Media was removed at 24 h and replaced with viral supernatant and 4 μ g/ml polybrene (Millipore). Plates were covered with parafilm and centrifuged for 1 h at 32 °C at 800 xg. At 24 h post-transduction, viral supernatants were removed and replaced with complete DMEM. Cells were screened for GFP and CAR expression from 48 h post-transduction.

2.4.1.2.2 BWZ.36 cells and murine splenocytes

Splenocytes activated with anti-CD3 and anti-CD28, as described in Chapter 2.1.3, or BWZ.36 cells were centrifuged at 300 xg and resuspended in viral supernatant with the addition of 4 μ g/ml polybrene. Cells were plated at 6×10^5 /well in 24-well plates (Corning) and centrifuged for 1 h at 32 °C at 800 xg. Cells were returned to the incubator for 6-7 h, then a second spin transduction was performed. At 24 h post-transduction, viral supernatants were removed and replaced with complete RPMI 1640 media. For splenocytes, 10 ng/ml mIL-2 (R&D Systems) or mIL-7 (Cell signalling) was added. Cells were screened for GFP and CAR expression from 48 h post-transduction.

2.4.1.2.3 Murine bone marrow cells

Murine bone marrow cells, described in Chapter 2.1.4, were centrifuged at 300 xg for 5 min and resuspended in viral supernatants, supplemented with 2 μ g/ml polybrene, 50 ng/ml each of mIL-3, mIL-6 and mSCF, and an additional 10 % (v/v) FCS. Cells were centrifuged for 1 h at 32 °C at 800 xg. Cells were returned to the incubator for 6-7 h, then a second spin transduction was performed. Cells were screened for GFP and CAR expression at 48 h post-transduction and subsequently used to generate bone marrow chimeras.

2.4.2 Amphotropic retroviral transduction

2.4.2.1 Generation of retroviral supernatants

2.5×10^6 293T cells were plated in 100 mm cell culture dishes in 10 ml complete IMDM. When cells were 50-60 % confluent transfections were performed using Genejuice (Novagen). For each dish, 470 μ l plain IMDM was mixed with 30 μ l Genejuice transfection reagent. After 5 min, retroviral plasmid DNA (4.7 μ g), RD114 envelope plasmid (3.1 μ g) and pEQPAM gag/pol plasmid (4.7 μ g) were added and mixed gently by pipette. After a 15 min incubation at RT, the mixture was added dropwise to the HEK 293T cells. At 48 h post transfection, supernatants were harvested and stored at 4 °C. Fresh media was added to the HEK 293T cells, and a

second harvest was performed at 72 h post-transfection. The two harvests of each transfection were pooled and either used fresh or snap frozen using an ethanol and dry ice bath, followed by storage at -80 °C. When required, these supernatants were thawed on ice.

2.4.2.2 Transduction of human PBMCs

PBMCs, collected as described in Chapter 2.1.2, were resuspended at 1×10^6 /ml in complete RPMI 1640 media, containing 5 µl/ml of phytohemagglutinin-P (PHA-P; Sigma Aldrich) and plated 1 ml/well in 24-well plates. After 24 h, 100 U/ml recombinant human IL-2 (hIL-2; Peprotech) was added. Non-treated 24-well plates were coated with 4 µg retronectin (Takara) per well in 0.5 ml PBS and stored overnight at 4 °C. 24 h after the addition of hIL-2, PBMCs were checked for rosetting using light microscopy, and harvested using Pasteur pipettes. Retronectin was aspirated from the coated plates and 250 µl of fresh or thawed retroviral supernatant was added to each well for 30 min. PBMCs were centrifuged at 300 xg and resuspended at 4×10^5 /ml in complete RPMI 1640 containing 400 U/ml hIL-2. Retronectin-coated plates were aspirated again and PBMCs were plated at 2×10^5 /well. 1.5 ml retroviral supernatant was added to each well and cells were spun at 1000 xg for 40 min at RT. At 48-72 h post-transduction cells were harvested and centrifuged at 400 xg for 5 min and resuspended at 1×10^6 /ml in complete RPMI 1640 with 50-100 U/ml hIL-2. Transduction efficiency was screened 24-48 h later.

2.5 Flow cytometry

Cells were run on a FACScan or FACSCalibur (both BD biosciences) using the associated BD CellQuest Pro software for data acquisition. 10,000 live-gated events were collected for each sample and data were analysed using FCS express (De Novo Software). Samples were expressed as either percentage positive, gated based upon relevant isotype controls, or using the geometric mean of fluorescence intensity (MFI).

2.5.1 Staining with fluorescent antibodies

$1-2 \times 10^5$ cells in 200 µl media or PBS were stained with 10 µg/ml antibody to detect surface protein expression. Cells were incubated with antibodies at 4 °C for 30 min. Cells were then washed in FACS buffer (PBS containing 1 % (w/v) BSA and 10 mM sodium azide), centrifuged at 300 xg, 5 min, and resuspended in 200 µl FACS buffer. All antibody stains were compared to relevant isotype controls. All antibodies used are detailed in **Table A3.1**, in the Appendix.

2.5.2 Intracellular staining with fluorescent antibodies

1-2 x 10⁵ cells were spun at 300 xg for 5 min and fixed in 200 µl 1 % (v/v) paraformaldehyde in PBS for 10 min at RT. Cells were washed twice in FACS buffer. Antibodies were diluted in 0.3 % (w/v) saponin (Sigma Aldrich) in PBS to permeabilise and stain the cells. Cells were incubated on ice for 30 min with required antibody, then washed in FACS buffer with 0.03 % (w/v) saponin. Cells were spun at 300 xg for 5 min and samples were resuspended in FACS buffer.

Alternatively, intracellular staining was performed using Intracellular Fixation and Permeabilization kit (eBioscience). 1x working dilutions of fixation/permeabilization solution and permeabilization buffer were made by addition of fixation/permeabilization diluent and dH₂O respectively. Cells were pelleted in FACS tubes and resuspended in 100 µl FACS buffer. 1 ml fixation/permeabilization solution was added to each and incubated for 1 h at RT in the dark. 2 ml of permeabilization buffer was added and cells were centrifuged at 400 xg for 5 min. Cells were resuspended in residual buffer, staining antibody was added, and cells were incubated for 30 min at RT. Cells were washed twice in permeabilization buffer and resuspended in FACS buffer for analysis.

2.5.3 Cell sorting

Transduced BWZ.36 cells were sorted on a FACSAria (BD Biosciences) to select pure and comparable populations of CAR+ve cells to use in *in vitro* assays. Cells were stained with PE-anti-human IgG-Fc as detailed in Chapter 2.5.1 and double GFP+ve and CAR+ve cells were selected for expansion.

2.6 Microscopy

Cells were visualised for confluency, rosetting and for GFP expression using an Olympus CKX41 microscope and images were captured using CellB software (Olympus). Where cells were to be directly compared, identical settings were used to visualise and capture all images.

2.7 Soluble protein analysis

2.7.1 Protein purification

Purification of HA-tagged scFv was performed using an anti-HA antibody covalently linked to agarose in a 1 ml column (Sigma Aldrich). All buffers used are shown in **Table 2.5**. Equilibration buffer was applied to the column prior to the supernatant containing

the secreted scFv. The supernatant was allowed to flow through the column by gravity flow. This flow through was collected, then the column was washed with 20 ml of wash buffer. The bound scFv was eluted with a solution of 1 mg/ml HA peptide in equilibration buffer (EB) at 37 °C. Four elution steps were performed with 1 ml HA-EB each time, incubated for 15, 10, 5 and 5 min respectively, before each elution was collected. The unpurified supernatant, the flow through and the elution fractions were run on SDS-PAGE gels for Coomassie Blue staining and for Western blot analysis.

Equilibration buffer	20 mM Tris-HCl pH 7.5, 0.1 M NaCl, 0.1 mM EDTA
Wash buffer	20 mM Tris-HCl pH 7.5, 0.1 M NaCl, 0.1 mM EDTA, 0.05 % (v/v) Tween 20
Elution buffer	1 mg/ml HA peptide (GL Biochem Shanghai) reconstituted in equilibration buffer.
Regeneration buffer	0.1 M Glycine, pH 2.5

Table 2.5: The buffers used in HA-scFv purification

2.7.2 SDS-PAGE

Supernatant or cells were harvested as described in Chapter 2.3.1.1. Purification of scFv from supernatant was performed as described in Chapter 2.7.1. Cell pellets were lysed using ONYX lysis buffer (10 mM Tris-HCl pH 7.4, 0.5 mM MgCl₂, 67.5 mM NaCl, 0.5 mM ethylene glycol tetraacetic acid (EGTA), 5 % (v/v) glycerol and 0.5 % (v/v) Triton X-100) containing 1 % (v/v) protease inhibitor (Sigma Aldrich), 50 mM NaF and 2 mM Na₃VO₄ for 30 min on ice. 1.25 ml lysis buffer was used for every 1 x 10⁸ cells. Cells were then centrifuged at 13,000 xg for 15 min and the lysate removed.

All samples to be analysed by SDS-PAGE were mixed at a 2:1 ratio with reducing loading buffer and heated to 95 °C for 5 min to denature the protein. 25 µl of each sample and 10 µl of protein standard ladder (Novex) were loaded onto a pre-cast NuPage 10 % Bis-Tris polyacrylamide gel (Invitrogen). Electrophoresis was performed in 1 x 3-(N-morpholino) propanesulfonic acid (MOPS) buffer (50 mM MOPs, 3.5 mM SDS, 50 mM Tris, 1 mM EDTA in 1 L dH₂O) at 150 V for 1 h. When required, the gel was incubated in Coomassie blue stain, rocking at RT for 10 min. The gel was then washed in de-stain until protein bands were clear.

2.7.3 Western blot

2 sheets of filter paper and a 0.2 µm nitrocellulose membrane were soaked in 20 % (v/v) methanol in transfer buffer (5 % (v/v) 20 x NuPage buffer (Invitrogen), 20 % (v/v) methanol in dH₂O) for 10 min. A Western blot module was loaded from the cathode side as follows; 2 sponges, filter paper, the SDS-PAGE gel, the nitrocellulose membrane, filter paper and 2 further sponges. The transfer was run in transfer buffer at 30 V for 80-90 min. After transfer, the membrane was extracted and stained with Ponceau Red as a non-specific protein stain to check transfer. The membrane was then washed in TBS-tween (50 mM tris, 150 mM NaCl, 0.05 % [v/v] Tween) and blocked in 3 % (w/v) BSA in PBS for 1 h, rolling. The membrane was then again washed in TBS-Tween.

Primary antibody (mouse anti-HA tag [Sigma Aldrich], mouse anti-His tag [Abcam]) was diluted in 3 % BSA PBS and the membrane was stained overnight, rolling at 4 °C. The membrane was washed 3 x with PBS-tween (PBS, 0.05 % [v/v] Tween) for 5 min, rocking at RT. The secondary antibody (rabbit anti-mouse horse radish peroxidase [HRP]-conjugated, in 3 % BSA PBS), was added for 1 h, rolling at RT. The membrane was washed again in PBS-tween for 3 x 5 min, followed by once in PBS. The membrane was incubated in 2 ml Immobilon Western chemiluminescent HRP substrate (Merck Millipore) and then affixed between acetate sheets. A UVP bioimager (Analytik Jena) was used to capture images.

2.8 *In vitro* functional assays

2.8.1 Binding and blocking assay

HEK 293F cells were transfected as described in Chapter 2.3.1.2 with CAR constructs, and after 48 h expression was analysed by flow cytometry. Cells were then labelled with 0.5 µM carboxyfluorescein succinimidyl ester (CFSE) for 10 min at RT in the dark. Raji target cells were stained with APC-anti-CD32. Cells were all washed in FACS buffer before co-cultures were set up. Transfected HEK 293F cells were combined with target cells at required ratios and incubated at 4 °C for 30 min. Flow cytometry was performed without further washing to avoid mechanical disturbance of CAR-CD20 interactions. To establish the percentage binding of CAR+ve transfectants, PE-anti-hIgG-Fc staining was included in some assays.

To perform the blocking assay, CD20+ve target cells were pre-incubated with excess (50 µg/ml) unlabelled rituximab (Roche) for 30 min at 4 °C prior to the addition of CAR+ve HEK 293F cells. The target cells were not washed before the CAR+ve HEK

293F cells were added. The co-culture was then performed as for the binding assay. In the case of the rituximab CAR, the assay was also performed by pre-incubating with 50 µg/ml anti-rituximab idiotype (MB2A4; in-house).

2.8.2 CPRG assay

CAR+ve transduced BWZ.36 T cells, described in Chapter 2.4.1.2, were co-cultured at required ratios with CD20+ve or CD20-ve cells in hygromycin-free RPMI 1640 media for 16 h at 37 °C in U-base 96-well plates (Corning). 50 ng/ml phorbol myristate acetate (PMA, Abcam) and 750 ng/ml ionomycin (Sigma Aldrich) were added to positive control wells. Mock-transduced (empty vector) BWZ.36 cells were used as a control cell population. After 16 h, plates were centrifuged at 300 xg for 5 min and the media was aspirated. 100 µl 155.5 mM chlorophenol Red-β-D-galactopyranoside (CPRG; Sigma Aldrich) in lysis buffer (0.125 % [v/v] NP-40, 9 mM MgCl₂, PBS) was added to each well and gently mixed to lyse the cells. The reactions were left at RT to develop for 5 h and subsequently read on a BioRad microplate reader at absorbance 595 nm, minus the reference wavelength 655 nm.

2.8.3 Calcein release cytotoxicity assay

Target cells were resuspended in PBS and labelled with 1 µl Calcein-AM (Life technologies) per 2 x 10⁶ cells by incubation in the dark with periodic mixing. Cells were washed 3 x with RPMI 1640 at 300 xg, resuspended to 1 x 10⁶ /ml and plated at 1 x 10⁵ /well in a 96-well plate. CAR and mock -transduced PBMCs (described in Chapter 2.4.2.2) or CAR+ve and -ve CTLL-2 cells (described in Chapters 2.3.3 and 2.3.4), were added to the labelled target cells at required effector to target ratios and plates were pulsed for 1 min at 100 xg. Target cells alone were also included, to determine background levels of calcein release. Co-cultures were incubated at 37 °C for 2, 4 or 24 h. 4 % Triton X-100 was used to induce maximal lysis in control wells. Plates were centrifuged at 400 xg for 5 min, before 60 µl of supernatant from each well was carefully transferred to a white opaque 96-well plate. Calcein release was measured using a Varioskan Flash (Thermo Scientific) at the excitation wavelength 485 nm and the emission wavelength 530 nm. Data was analysed and presented as percentage maximal lysis using the following calculation:

$$\% \text{ Maximal lysis} = \frac{\text{Sample} - \text{background}}{\text{Triton X} - \text{background}} \times 100$$

2.8.4 Sandwich enzyme-linked immunosorbent assay (ELISA)

For murine IFN γ ELISA untransfected, Leu16 CAR+ve and BHH2 CAR+ve CTLL-2 cells were co-cultured with or without Ramos target cells, for 4 d. Cells were pelleted by centrifuging at 500 xg for 5 min and supernatants were harvested and stored short-term at -20 °C. For human IFN γ and IL-2 ELISAs mock-transduced, Leu16 and BHH2 CAR+ve human primary T cells were co-cultured with Raji or K562 target cells for 24 h. Cells were pelleted by centrifuging at 500 xg for 5 min and supernatants were harvested and stored at -80 °C.

Murine ELISA was performed using an ELISA MAX Standard Set Mouse IFN γ kit (Biolegend). Human ELISAs were performed (by Dr Robert Oldham) using ELISA MAX Standard Set Human IFN γ and IL-2 kits (Biolegend). For each, the capture antibody was diluted 1:200 in coating buffer (100 mM NaHCO $_3$, 33.5 mM NaCO $_3$, dH $_2$ O, pH 9.5). 100 μ l was added to all wells of a 96-well plate. The plate was sealed with parafilm and incubated overnight at 4 °C. Wells were washed 4 x in 300 μ l wash buffer (PBS +ve0.05 % [v/v] Tween-20) using a SkanWasher 300 microplate washer (Skatron) and residual buffer was removed by blotting. 200 μ l RT assay diluent (10 % [v/v] FCS in PBS) to block non-specific binding. Plate was re-sealed and incubated at RT for 1 h, shaking. Mouse IFN γ Standard was prepared to 1000 pg/ml (Murine) or 500 pg/ml (Human) and two-fold serial dilutions were performed in assay diluent to provide the standard curve controls.

Plates were washed 4 x in wash buffer as before and 100 μ l Standard dilutions were added to required wells. The CTLL-2 cell supernatant samples were diluted 1:4 in assay diluent, the human T cell supernatant samples were diluted at either 1:4 or 1:5, and each was added to the appropriate wells. Two-fold dilutions of each sample were then performed using assay diluent. The plates were again sealed, and incubated at RT for 2 h, shaking. Plates were washed 4 x as before, and 100 μ l of the biotinylated detection antibody was added (diluted 1:200 in assay diluent) to all wells, before plates were sealed and incubated at RT for 1 h, shaking. Plates were subsequently washed 4 x and 100 μ l Avidin-HRP solution (diluted 1:1000 in assay diluent) was added to all wells. Plate was incubated for 30 min at RT, shaking, and then washed 5 x allowing wells to soak for 1 min each time.

For Murine ELISA, substrate solution was prepared fresh (24.7 ml 0.1 M citrate, 25.5 ml 0.2 M Na $_2$ HPO $_4$, 50 ml dH $_2$ O, 0.4 mg/ml o-Phenylenediamine dihydrochloride and 40 μ l 30 % hydrogen peroxide). 100 μ l was added to each well, and plate was incubated in the dark for 30 min, or until colour developed. The reaction was stopped

by the addition of 100 μ l 3 M H₂SO₄ to each well. Plates were read on an Epoch plate reader (BioTek) at the absorbance wavelength 495 nm.

For Human ELISAs, 100 μ l TMB substrate solution (Biolegend) was added to each well and plates were incubated in the dark for 20 min, or until colour developed. Reaction was stopped by the addition of 100 μ l Stop Solution (Biolegend) and plates were read on an Epoch plate reader (BioTek) at 450 nm minus 570 nm.

Data from all ELISAs were analysed by use of the reference standard curve generated, to determine quantified concentrations of cytokine from the absorbance readings. Values were multiplied by the dilution factor of samples.

2.9 *In vivo* techniques

All *in vivo* work was conducted in accordance with the Animals (Scientific Procedure) Act 1986, under the project licence 30/2964 and personal licence 30/10432.

2.9.1 CTLL-2 cell tracking

2 x 10⁷/ml CTLL-2 cells in PBS were labelled with 5 μ M CFSE for 10 min at RT in the dark. FCS was added to an equal volume and cells were washed twice in PBS by centrifuging at 300 xg, 5 min. The majority of labelled cells were resuspended at 3 x 10⁷ in 600 μ l. The remainder were cultured overnight *in vitro* for use as control cells. 1.5 x 10⁷ CFSE+ve CTLL-2 cells each were given by intraperitoneal injection (IP) to two severe combined immunodeficient (SCID) mice.

The mice were culled, one each at 24 h and 72 h. Blood was collected into tubes containing heparin. Following this, a peritoneal wash was performed by injecting 5 ml sterile PBS into the exposed intact peritoneal membrane and then collecting the contents of the cavity using a syringe. The axial and inguinal lymph nodes, spleen and liver were collected into sterile PBS and single cell suspensions were generated for each by use of a 100 μ m cell strainer. Erythrocytes were lysed in each blood, spleen and lymph node sample by incubation with lysis buffer (155 mM NH₄Cl, 10 mM KHCO₃) for 5 min, before cells were washed in PBS. The liver cells were treated with 33 % (v/v) percoll to allow spin separation of the hepatocytes prior to erythrocyte lysis. 15 ml 33 % percoll was added to the cells and they were centrifuged for 15 min at 500 xg, the hepatocyte layer was removed using a Pasteur pipette and the remaining cells were washed in PBS. All cells were resuspended in media and then analysed by flow cytometry for CFSE+ve cells, and by using PE-anti-CD3 (KT3).

2.9.2 Bone marrow chimeras

C57BL/6 mice were ear tagged for identification, anaesthetised using Hypnorm given IP, and irradiated (total body) at 5.5 Gy (Gulmay D3225 Orthovoltage X-ray system; settings 210kV, 12.9mA, filter 3, applicator F). After 24 h this was repeated, and mice then received $0.75\text{-}1.125 \times 10^6$ transduced donor cells, described in Chapter 2.4.1.2, administered intravenously (IV; by Vicki English). Mice were given acidified water (pH 2.5) with the addition of 1 % (v/v) enrofloxacin. Mice were taken off acidified water after 2 weeks, and screening was performed at 6 and 10 weeks by the collection of tail blood samples. Mice were warmed to increase vasodilation at 37 °C and lidocaine cream was administered to the tail tips. Mice individually were restrained in a tube, and <1 mm of the tail tip was removed using a sharp blade. Vaseline was applied to the tail and the tail was gently massaged towards the tip to encourage blood flow. Blood was collected into tubes containing 50 µg/ml heparin. Erythrocytes were lysed and the cells were then stained using fluorescently labelled antibodies for analysis by flow cytometry. Blood collection and flow cytometry of these samples were performed by Dr Robert Oldham and Dr Kirstie Cleary.

2.10 Statistical analysis

All statistical analysis was carried out using GraphPad Prism software. One-way ANOVA was used to compare pairs of data sets when different numbers of data points existed. Where equal data point totals were present, two-way ANOVA was used to compare between data sets. F test was used to determine whether a correlation existed within a data set. P values of <0.05 were considered significant. Stars were used to denote p values (* shows $p < 0.05$; ** shows $p < 0.01$; *** shows $p < 0.001$; **** shows $p < 0.0001$).

3 Molecular Generation and Expression of Chimeric Antigen Receptor Constructs

3.1 Introduction

The overall aim of this thesis was to compare the functional efficacy of CAR constructs comprised of different anti-CD20 scFv. As discussed in Chapter 1, studies into other antigens have shown that the target epitope and its position within the target molecule can strongly influence CAR efficacy [373-375]. There has also been conflicting data produced as to how the affinity of the CAR-antigen interaction affects CAR function [373, 374, 379-381, 384, 385, 388, 389]. A CAR incorporating a Leu16 scFv has shown success both *in vitro* and *in vivo*, however it is not known if this is the optimal design [465, 466]. This project aimed to investigate the importance of binding strength and the targeted epitope to the functioning of an anti-CD20 CAR, using Leu16 scFv as a control construct.

CD20 was chosen as the target antigen as it has been validated as a strong immunotherapy target. This membrane tetra-spanning molecule has two extracellular loops that have been targeted successfully by several mAb. CD20 is highly expressed on more than 95% of B lymphocytes, at all developmental stages, meaning it is a strong target for the treatment of all B-cell cancers [187]. Whilst internalisation has been seen as a consequence of some mAb therapies, CD20 is usually found as a stable cell surface molecule [467].

It is known that the binding characteristics of anti-CD20 mAb can influence their function, independent of the Fc portion [191]. The different binding configurations seen between type I and type II anti-CD20 mAb may play a role in their functional efficacy. Whilst the binding action of a bivalent mAb differs to that of a scFv, the binding angle and nature of target antigen interaction could still impact the activity of a CAR.

This chapter describes the production of five constructs containing equivalent spacer, transmembrane and signalling domains, but with different scFv incorporated, to allow investigation into how the binding domain can affect the expression and function of the CARs. The constructs were based on the Leu16 CAR design described by Oliver Press' group [466], including the human IgG1 hinge-CH2-CH3 domains as a spacer and the CD4 transmembrane domain (amino acid residues 372-393 of the mature peptide). The intracellular portion comprises the CD28 signalling domain (aa162-202 of

the mature peptide), CD137 signalling domain (aa191-232 of the mature peptide) and CD3 ζ signalling domain (aa31-142 of the mature peptide) (**Figure 3.1**). A double leucine motif (L¹⁸⁴ and L¹⁸⁵) in the signalling domain of murine CD28 has previously been shown to reduce surface expression of chimeric receptor constructs, and it is proposed that the same effect would occur in human CD28. Accordingly, this was altered to a diglycine motif prior to protein generation [468]. The human IgG1 hinge-CH2-CH3 domain was selected due to the evidence showing that a longer spacer region is advantageous when targeting smaller or more membrane proximal target antigens [367]. A glycine- and serine-rich (G/S) linker peptide was included in the design of each scFv to adjoin the variable heavy (V_H) and light (V_L) chains and allow correct folding of the scFv, forming the antigen binding site.

To evaluate the role of the scFv, the five anti-CD20 mAb selected for use in this study have different binding characteristics, affinities and epitopes, and belong to either the type I or type II categories of anti-CD20 mAb [193]. The binding epitopes of the mAb used - rituximab, BHH2, B1-WG, Leu16 and 2F2 - are shown in **Figure 1.3**, and information about each is listed in **Table A1.1** in the Appendix.

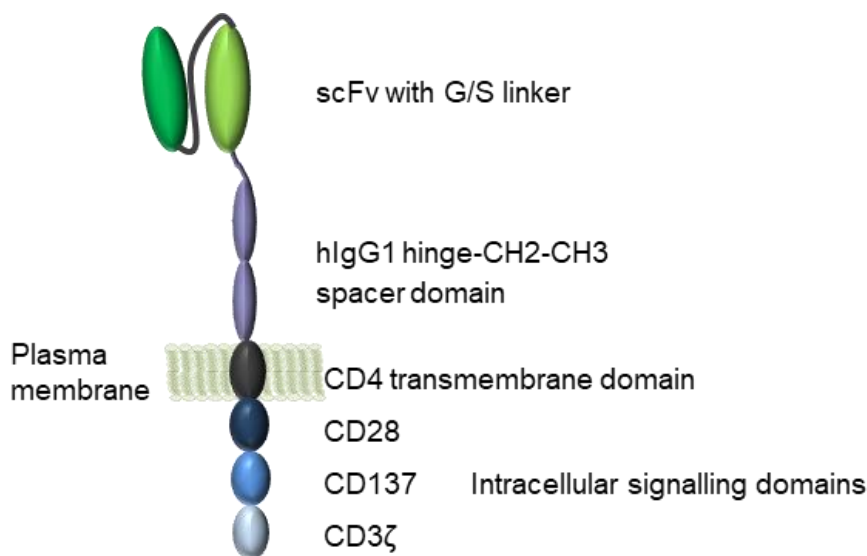


Figure 3.1: An Illustration of the CAR constructs generated.

A graphic showing a CAR construct expressed on the cell surface, illustrating the peptide domains incorporated. The intracellular signalling domains include those from CD28 (aa162-202 of the mature peptide), CD137 (aa191-232 of the mature peptide) and CD3 ζ (aa31-142 of the mature peptide). The design of CAR constructs produced was based on that from Wang *et al* [466].

3.2 Cloning and expression of anti-CD20 single chain variable fragments

3.2.1 Production and cloning of single chain variable fragments

To produce scFv, variable heavy (V_H) and light kappa (V_K) chain fragments of the anti-CD20 mAb rituximab (Ritux), B1-WG and BHH2 were first generated using PCR (Chapter 2.2.1). The rituximab and BHH2 mAb template DNA used were previously generated as custom oligonucleotides (GeneArt) from the published sequences [469, 470] and cloned into a pEE6.4 vector by Dr Claude Chan. The B1-WG sequence was previously generated using a combination of mass spectrometry, sequencing and mutagenesis by Dr Claude Chan, and was also cloned into the pEE6.4 vector.

Half of the G/S linker was amplified at the 3' end of each of the V_K fragment and at the 5' of the V_H fragments. Restriction enzyme recognition sites were also incorporated at each 5' and 3' end. A schematic of the scFv constructs is shown in **Figure 3.2**. All PCR primer sequences may be found in **Table A2.1**, in the Appendix.

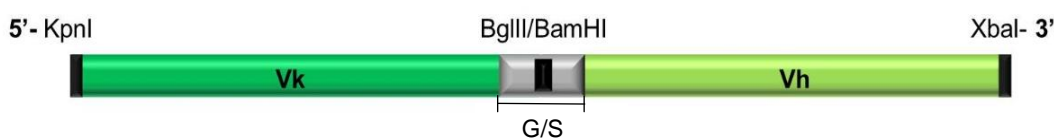


Figure 3.2: An illustration of a single chain variable fragment structure.

Each scFv comprises a variable light (V_K) and a variable heavy (V_H) anti-CD20 mAb fragment, joined by a flexible glycine- and serine- rich linker (G/S) to allow proper folding of the protein. Restriction enzyme sites used in cloning are labelled. The recognition sequences of BglII and BamHI sites overlap, allowing ligation, and are consequently destroyed.

The PCR-generated variable fragments were assessed on an agarose gel by electrophoresis (Chapter 2.2.3) to confirm product size and cloned into the pCR-Blunt-II-TOPO vector (Chapter 2.2.6). This vector is pre-linearized and has topoisomerase annealed at the 3' end to inhibit self-ligation and allow an efficient, single-step ligation of PCR products. As the PCR products are blunt-ended and encompass the restriction sites required for subsequent steps, the orientation of the fragment within this vector was not important. The ligated DNA was transformed in to Top10 chemically competent *E. coli*, before the amplified product was extracted using a Qiagen miniprep kit

(Chapters 2.2.9 and 2.2.11). An EcoRI enzymatic digest of the recognition sites flanking the ligation site in the vector confirmed insertion (**Figure 3.3**), and positive ligations were sequenced using the vector primers Sp6 and T7 (Chapter 2.2.12).

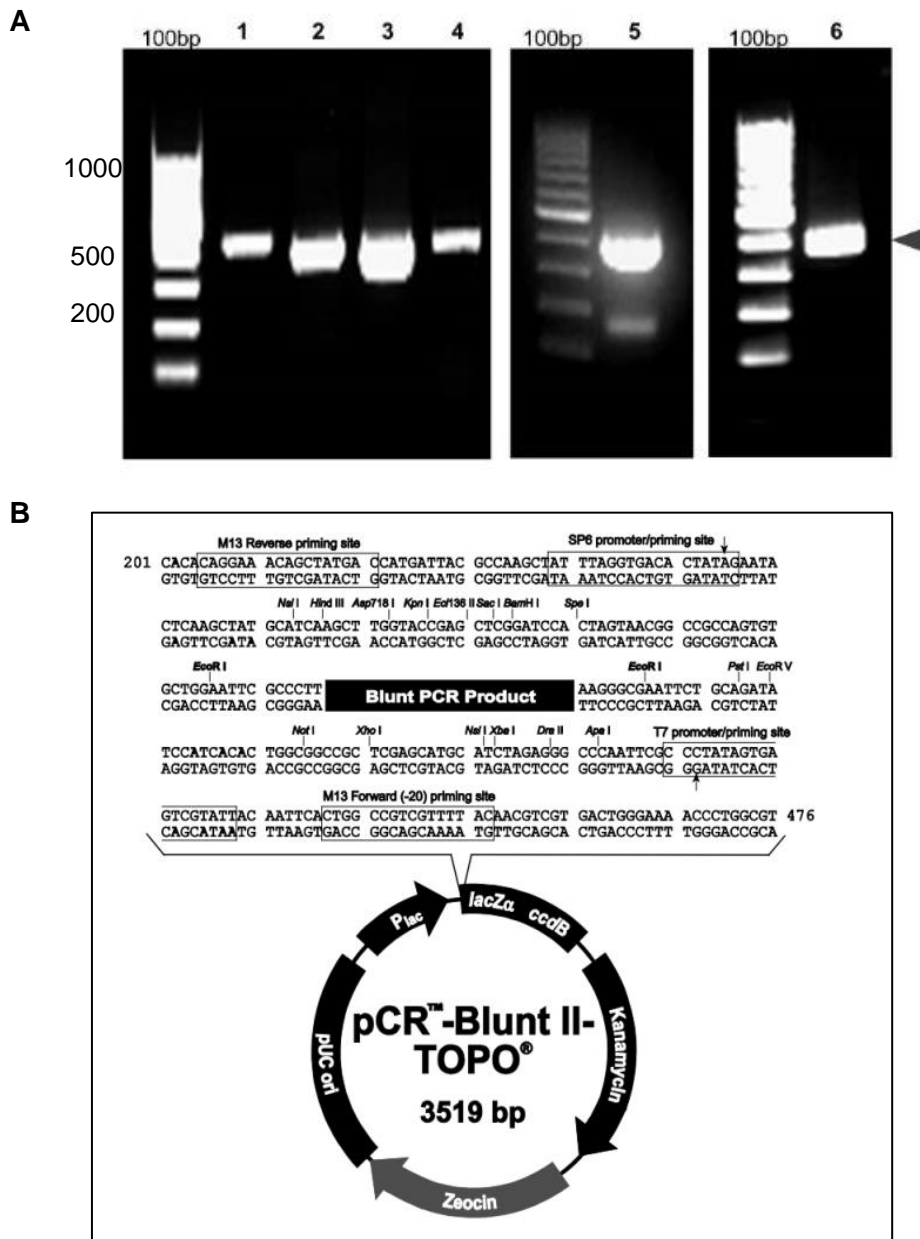


Figure 3.3: scFv fragments were produced by PCR and products were ligated into pCR-Blunt-II-TOPO.

A: PCR-generated V_K and V_H chain anti-CD20 mAb fragments were assessed by agarose gel electrophoresis. DNA was stained with GelRed dye, run on a 0.7 % gel at 120 V, and visualised under UV light. Lane 1, B1-WG V_H ; 2, B1-WG V_K ; 3, BHH2 V_H ; 4, BHH2 V_K ; 5, rituximab V_H ; 6, rituximab V_K . Grey arrow indicates bands at expected size. Ladders shown are 100 bp.

B: Map of the pCR-Blunt II-TOPO vector. Blunt-end PCR products from **A** were cloned into the vector and transformed into Top10 chemically competent *E. coli*. The replicated DNA was extracted, digested using the EcoRI sites shown flanking the ligation site, and sequenced. The sequencing primer annealing sites of Sp6 and T7 are also shown.

Upon sequence confirmation, V_K and V_H fragment pairs were cloned together to form the full scFv. For each scFv, the V_K fragment was first excised from pCR-Blunt-II-TOPO and ligated in to pcDNA4/HisMax B, via the KpnI and BglII restriction sites. This vector was chosen as it allows construction of the scFv using the appropriate restriction enzymes, whilst maintaining the correct DNA reading frame (**Figure 3.4 A**). The V_H fragment was cloned at the 3' end of the V_K chain using BamHI and XbaI, connecting the two halves of the G/S linker and forming the scFv (Chapter 2.2.6).

The sequence surrounding the XbaI site contained a deoxyadenosine methylation site that blocked activity of the restriction enzyme. Therefore prior to excision, these fragments were transformed in to SCS110 dcm-/dam- chemically competent *E. coli* to generate partially non-methylated DNA. Where necessary, site directed mutagenesis, detailed in Chapter 2.2.7, was used to remove extra restriction sites that would interfere with the restriction digests. The BHH2 scFv sequence contained additional XbaI, BglII and KpnI sites, and B1-WG contained a BglII site which were all removed using targeted mutagenesis, without altering the subsequent protein sequences.

At each stage, the ligated DNA was transformed into JM109 chemically competent *E. coli* and grown in culture. DNA was extracted using a Qiagen miniprep kit and digested to confirm insertion of a fragment at the correct size (**Figure 3.4 B, C**). Positive colonies were sequenced using the vector primers T7 and BGH reverse.

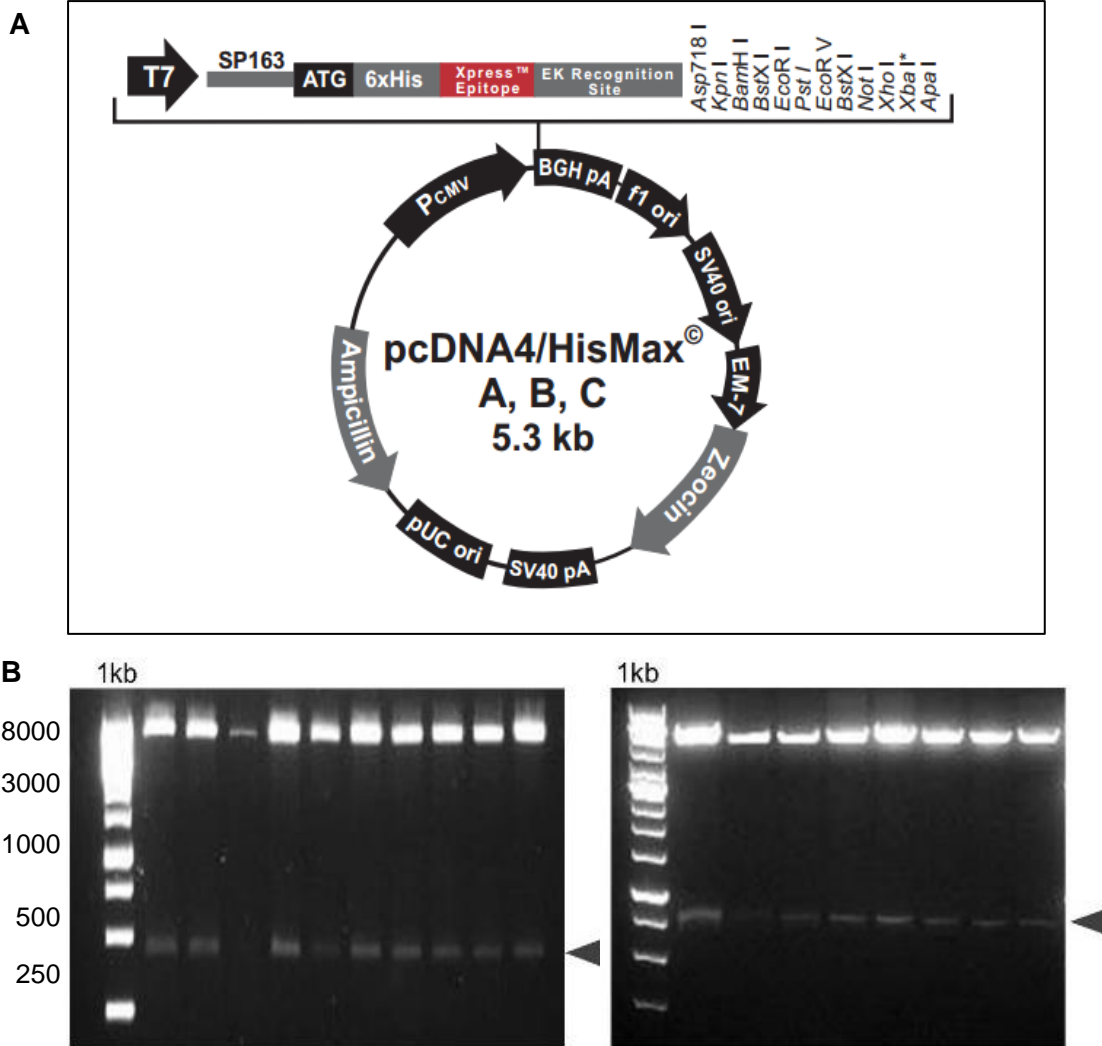


Figure 3.4: scFv sections were cloned together into the pcDNA4/HisMax B vector.

A: Vector map of the pcDNA4/HisMax B vector used in construction of the full scFvs. The restriction enzymes site used are shown, along with the poly-histidine “6xHisTag” and Xpress epitope both of which can be used for protein detection.

B: PCR-generated V_K fragments of each mAb were excised from the pCR-Blunt-II-TOPO vector and ligated into pcDNA4/HisMax B. Example shown is rituximab V_K fragment, digested to confirm insertion and analysed by agarose gel electrophoresis.

C: V_H fragments were excised from PCR-BLUNT-II-TOPO and ligated at the 3’ end of the corresponding V_K fragment in pcDNA4/HisMax B. The BglIII and BamHI recognition sites overlap, joining the full scFv together via the G/S linker. Example shown is B1-WG scFv, digested to confirm insertion and analysed by agarose gel electrophoresis.

B and C: DNA was stained with GelRed, separated on a 0.7 % agarose gel by electrophoresis at 120 V, and visualised under UV light. Grey arrow indicates bands at expected size. Ladder shown is 1 kb. Lanes are separate bacterial colonies of the same ligation.

3.2.2 Expression of scFv in mammalian cells

Production of soluble scFvs was first proposed, to determine their expression and binding abilities prior to their inclusion in CAR constructs. Expression of two representative scFvs was first assessed in mammalian cells to confirm protein production at the expected molecular weight. HEK 293F cells were transfected with two scFv constructs in pcDNA4/HisMax B, detailed in Chapter 2.3.1. This vector contains an N-terminal poly-histidine tag (His Tag) upstream of the multiple cloning site to allow protein detection via an anti-His Tag mAb.

At 8 d post-transfection, the cells were pelleted and lysed. Lysate was run on an SDS-PAGE gel under reducing conditions before transfer to a nitrocellulose membrane (Chapter 2.7.2). A Western blot was performed using an anti-His Tag mAb, described in Chapter 2.7.3 (**Figure 3.5**). Protein bands were visualised at the expected scFv weights, as estimated using the ExPASy compute pI/Mw online tool (estimates including His Tag and upstream cloning sites: BHH2, 30.49 kDa; Ritux, 29.68 kDa), demonstrating that the proteins can be expressed in mammalian cells and the products are of the expected size.

Due to the lack of a stably folding soluble CD20 molecule, surface plasmon resonance analysis to determine the scFv affinities was not possible. However, scFv expression levels were investigated to determine if the proteins could be produced in high enough quantities to perform cell-based target binding experiments. These would be designed to investigate firstly if the scFv could fold correctly and bind CD20, and secondly to determine the ability of each scFv to outcompete an anti-CD20 mAb bound to a CD20+ve target cell. A comparison could then be made between the scFv in terms of binding strength. In order to outcompete a bivalent bound mAb, a high concentration of scFv would be required.

BHH2 scFv was cloned into the pFUSE-hlgG1-Fc2 vector (**Figure 3.6**). Unlike pcDNA4/HisMax B, this vector contains a secretion sequence to allow transit of the protein product from the expressing cell. A stop codon was incorporated at the 3' end of the sequence, prior to the Fc portion of the vector, to allow only scFv production. A HA tag was also included in the sequence to allow purification and detection of the expressed protein. Cloning of the BHH2 scFv sequence into the pFUSE vector was performed using overlapping recombination sites, described in Chapter 2.28) by Dr Patrick Duriez (Southampton Protein Core Facility).

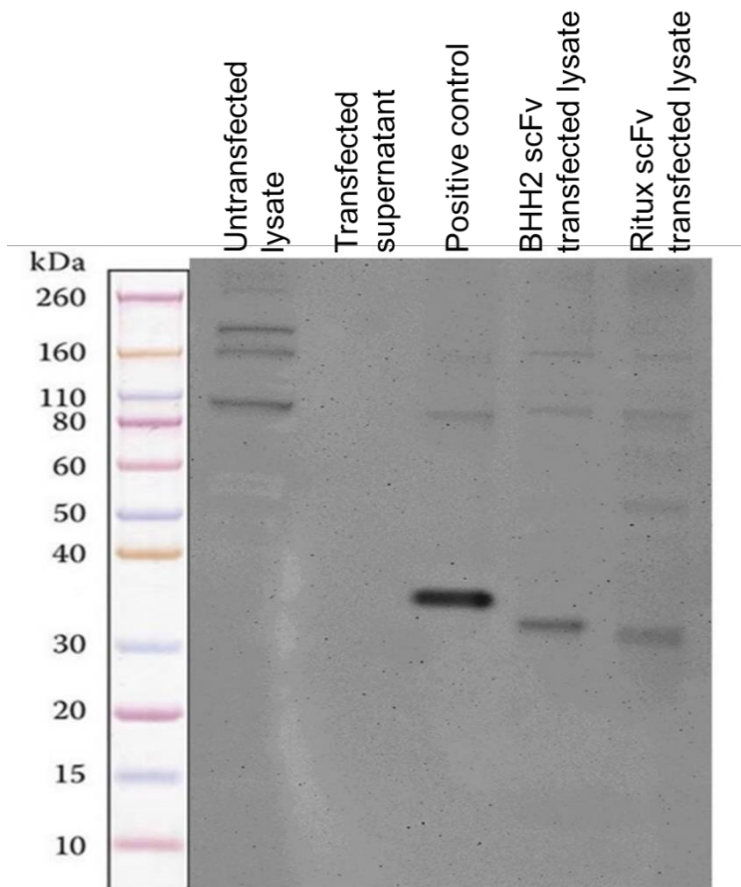


Figure 3.5: Western blot for His-tagged scFvs, expressed intracellularly by transfected HEK 293F cells.

HEK 293F cells were transfected with pcDNA4/HisMax B vectors containing rituximab and BHH2 scFv constructs to confirm protein production at the correct weight. At 8 d post-transfection cells were harvested and lysed, and lysates were run on an SDS-PAGE gel at 150 V under reducing conditions. After transfer to a nitrocellulose membrane, protein expression was probed using an anti-His Tag mAb and an HRP-conjugated secondary mAb. Lane 1, untransfected HEK 293F cell lysate; 2, transfected cell culture supernatant; 3, an irrelevant purified His Tag protein as a positive control for the Western blot and mAb; 4, BHH2 scFv transfected cell lysate; 5, rituximab scFv transfected cell lysate. Ladder shown is Novex protein standard. N=1.

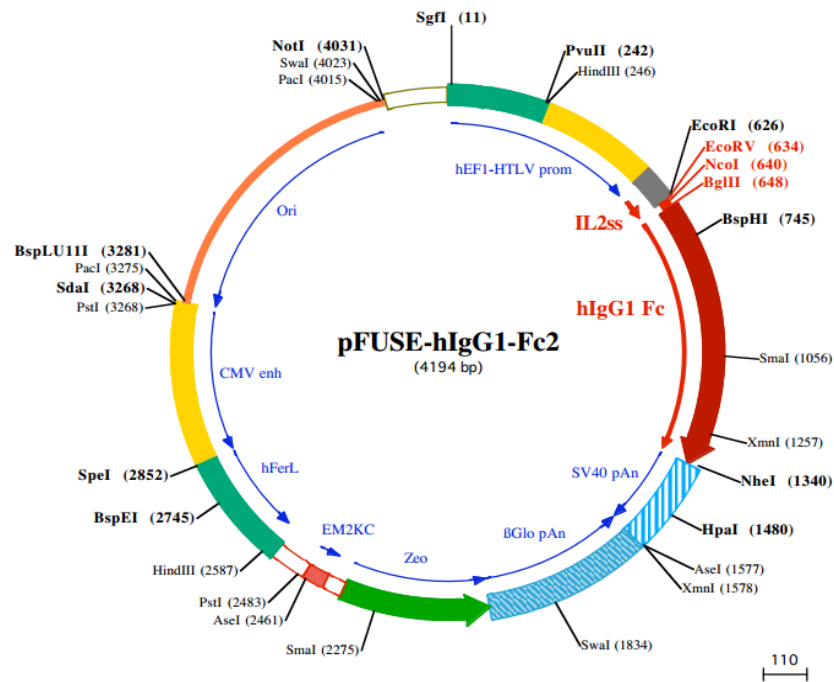


Figure 3.6: Vector map of pFUSE-hIgG1-Fc2

The pFUSE vector contains the IL-2 secretion sequence upstream of the cloning site to allow transit of the protein product out of the cell. BHH2 scFv was cloned into this vector using overlapping recombination sites by Dr Patrick Duriez (Southampton Protein Core Facility). A stop codon was included prior to the Fc portion of the vector to produce only the scFv. Additionally, a HA tag was incorporated into the sequence to allow protein purification on an anti-HA column.

HEK 293F cells were transfected and at 5 d post-transfection, the supernatant was harvested. An anti-HA column was used to bind the protein product. This was subsequently eluted in a series of washes through the column. This method is described in Chapter 2.7.1. The elutions were run on an SDS-PAGE gel and a Western blot was performed using an anti-HA mAb (**Figure 3.7**). This confirmed that the scFv was successfully expressed and secreted from the cells. However, a Bradford Assay (performed by Dr Patrick Duriez) demonstrated very low initial yields of protein. This indicated that in order to make a high concentration of scFv for binding experiments, very large transfection volumes would be required. For this reason, it was decided the project would proceed with the generation of full CAR constructs and investigation into their function.

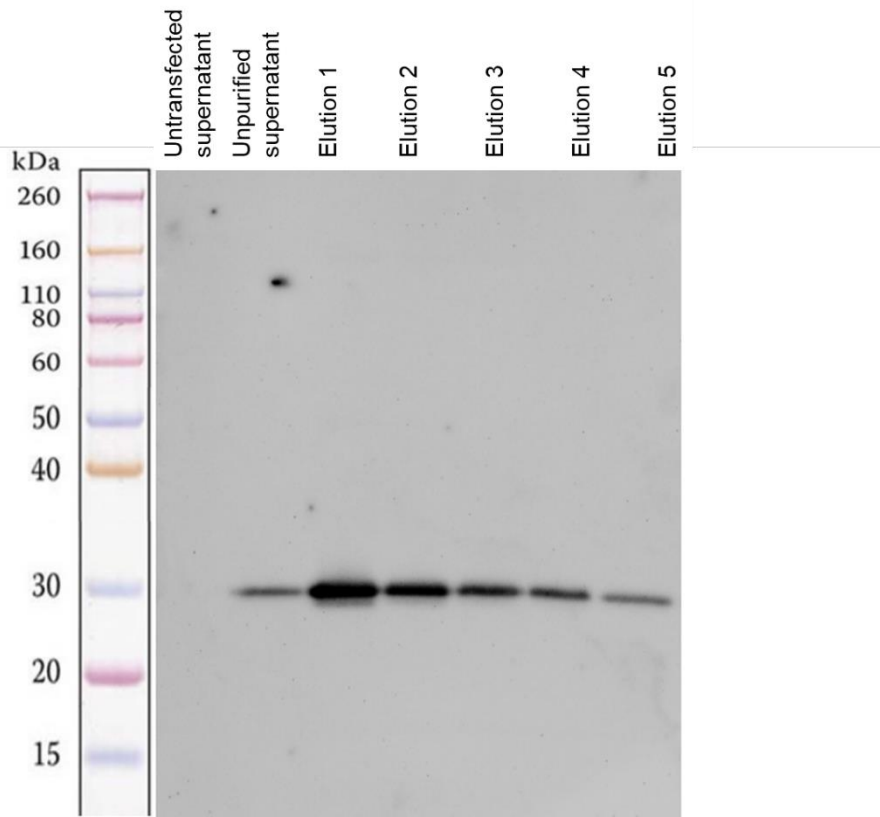


Figure 3.7: Western Blot of secreted soluble HA-tagged BHH2 scFv expressed by transfected HEK 293F cells.

HEK 293F cells were transfected with pFUSE-hlgG1-Fc2 containing the BHH2 scFv construct. At 5 d post-transfection supernatant was harvested and run on an SDS-PAGE gel at 150 V under reducing conditions. After transfer to a nitrocellulose membrane, protein expression was probed using an anti-HA mAb and an HRP-conjugated secondary mAb. Lane 1, untransfected HEK 293F supernatant; 2, unpurified transfected HEK 293F supernatant, prior to use of the anti-HA column; 3-7, subsequent elutions from the purifying anti-HA column. Ladder shown is Novex protein standard. N=1.

3.3 Cloning of chimeric antigen receptors

To generate CAR constructs, the anti-CD20 scFv were cloned upstream of the other required molecular domains, into the pcDNA3.1(-) expression vector (Chapters 2.2.5 and 2.2.6). These include the spacer, transmembrane and intracellular sections. An illustration of these domains and the restriction enzyme sites involved in the CAR constructions is shown in **Figure 3.8**.

The first CAR generated was the control construct comprising the Leu16 scFv. This scFv was produced commercially to specification as an extended oligonucleotide (GeneArt), encompassing enhancer and leader sequences upstream, and 5' and 3' restriction enzyme recognition sites. After sequence verification, this fragment was digested from the commercial vector and ligated into the pcDNA3.1(-) expression vector via the NheI and XhoI restriction sites.



Figure 3.8: An illustration of the CAR molecule structure

The CAR constructs were produced by the cloning together of all required molecular domains into the pcDNA3.1(-) expression vector. The CAR structure is shown, with the restriction enzyme cloning sites incorporated in these domains labelled and shown in red. The SP163 enhancer region is also shown, incorporated upstream to increase expression [466], additional to a leader sequence to allow protein trafficking to the cell surface.

The human IgG1 hinge-CH2-CH3 spacer domain, incorporating a 5' XhoI site and 3' BamHI site, was generated by PCR (**Figure 3.9**). The template DNA used was previously generated using PCR by Dr Claude Chan from human cDNA, and cloned into the pEE6.4 vector. The PCR product was ligated into PCR-BLUNT-II-TOPO and sequenced using the vector primers, before being cloned into pcDNA3.1(-), downstream of the Leu16 scFv via the XhoI and BamHI restriction enzyme sites.

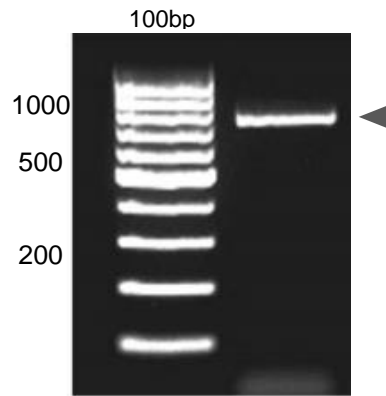


Figure 3.9: PCR was used to generate the IgG1 hinge-CH2-CH3 spacer region

The PCR-generated human-IgG1 hinge-CH2-CH3 spacer domain was assessed by agarose gel electrophoresis. DNA was stained with GelRed dye, run on a 0.7 % gel at 120 V, and visualised under UV light. The PCR primers used incorporated XhoI and BamHI restriction recognition sites at the 5' and 3' ends respectively, to allow cloning of this spacer region into the CAR constructs. Gray arrow indicates band at expected size. Ladder shown is 100 bp.

The transmembrane and intracellular domains included were generated commercially to specification as one custom oligonucleotide chain (GeneArt), incorporating 5' BamHI and 3' HindIII restriction sites. This was digested from the commercial vector and ligated downstream of the spacer domain to produce the full Leu16 CAR construct. Restriction enzyme digests and sequencing with T7 and BGH reverse primers were used to ensure all the fragments were correct. **Figure 3.10** depicts digests of each CAR fragment and the whole construct in pcDNA3.1(-). Upon confirmation of the fragment sizes and correct sequences, the construct was transformed in to JM109 chemically competent *E. coli*. Amplified DNA was extracted using a Qiagen maxiprep kit for use in cellular transfection.

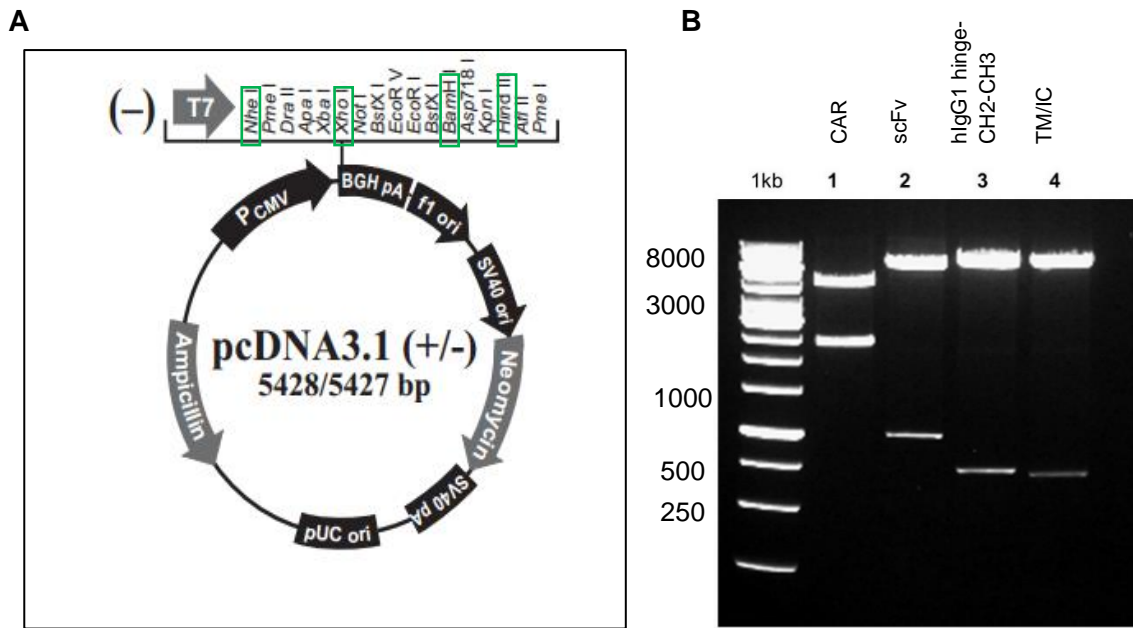


Figure 3.10: CAR constructs were generated by cloning DNA fragments together into pcDNA3.1(-).

A: Vector map of pcDNA3.1(-). Shown in green are the restriction enzyme sites of the multiple cloning site, used in construction of the CAR constructs.

B: Confirmation of Leu16 CAR construct correctly inserted into the vector, analysed by restriction enzyme digests and gel electrophoresis. DNA was stained with GelRed, separated on a 0.7 % agarose gel at 120 V and visualised under UV light. Lane 1, full CAR construct (2334 bp) digested with NheI/HindIII; 2, SP163 enhancer/Leu16 scFv fragment (964 bp) digested with NheI/XhoI; 3, hIgG1 spacer fragment (706 bp) digested with XhoI/BamHI; 4, transmembrane and intracellular fragment (TM/IC; 664 bp) digested with BamHI/HindIII. Ladder shown is 1 kb.

The first stage of construction of the BHH2, Ritux (rituximab) and B1-WG CARs used overlap PCR (Chapter 2.2.2) to produce fragments comprising each previously generated scFv, and the SP163 enhancer and leader sequences. Each overlap PCR was performed in three sections to avoid self-annealing of the primers used (**Figure 3.11**). For each scFv, the three sections were generated individually, using either the CAR backbone in pcDNA3.1(-) or the appropriate scFv DNA in pcDNA4HisMaxB as a template. The sections were joined in subsequent overlap reactions in two stages; a 15 cycle PCR to anneal the complementary regions and generate the joined construct, and a 20 cycle PCR with additional 5' and 3' primers to amplify yield of the finished product. Each PCR product was ligated into pCR-Blunt-II-TOPO and sequenced as before. The fragments generated by overlap PCR were flanked at the 5' and 3' end with NheI and XhoI recognition sites respectively. The XhoI recognition sequence was replaced by a Sall site in the BHH2 construct due to an additional XhoI site present in the scFv. Sall and XhoI restriction enzyme recognition sites overlap, allowing ligation.

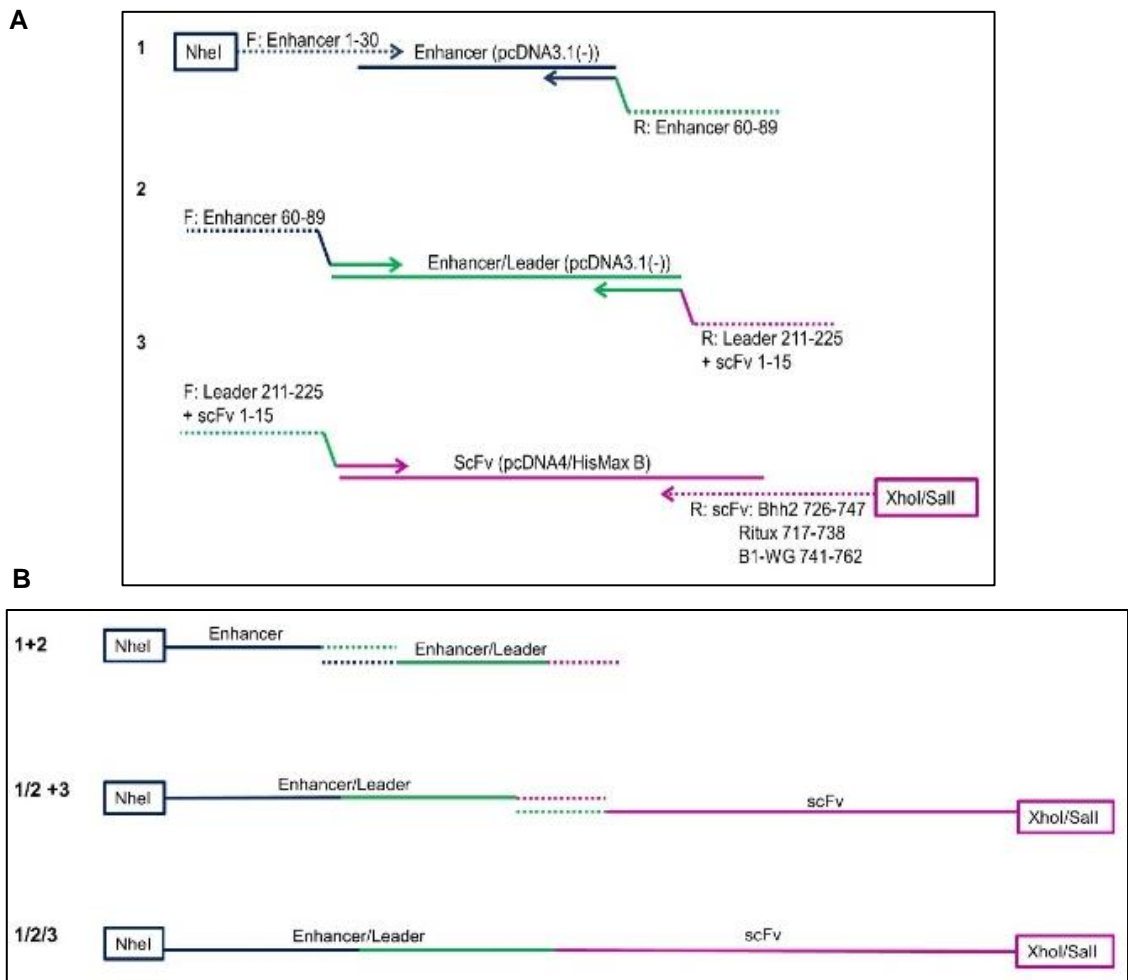


Figure 3.11: An illustration of the overlap PCR used to generate fragments comprising the SP163 enhancer, leader sequence and each scFv

A: Three PCR reactions of 30 cycles were performed to generate fragments with short overlapping complementary sequences at the 3' (fragment 1, blue), 5' (fragment 3, pink) or 3' and 5' (fragment 2, green) ends. Arrows represent primers used in the reactions, encompassing overlapping sequences. Fragments 1 and 2 were generated using template DNA of the scFv in pcDNA4HisMaxB. Fragment 3 used the CAR backbone in pcDNA3.1(-) as template DNA. The incorporated restriction enzyme sites are shown in blue (5') and pink (3').

B: The DNA sections were adjoined via the complementary overlapping sequences generated in A, using further PCR reactions. Fragments 1 and 2 were joined, followed by the addition of fragment 3. Each overlap PCR was performed in two stages. Firstly, the complementary sequence sites were allowed to anneal in a 15 cycle PCR, to form the joined product. Additional 5' and 3' primers were then added into another 20 cycles of PCR to increase the yield of the completed DNA strand.

After confirmation of correct sequences by sequencing, the fragments comprising each scFv and the upstream enhancer and leader sequences were excised from PCR-BLUNT-II-TOPO using NheI and XhoI/SalI restriction enzyme digests. The Leu16 scFv, enhancer and leader fragment was also excised from the CAR-pcDNA3.1(-)

backbone using the same technique. Ligations were performed using T4 ligase to insert the alternative scFv fragments in the place of Leu16 scFv, producing the panel of full CAR constructs. Each ligation was performed once, if successful, and only repeated in cases of failed ligation. As previously, the ligated DNA was transformed into chemically competent JM109 *E. coli* and DNA was purified from the cultures using a Qiagen miniprep kit. Insertion of each scFv into the full construct was confirmed by restriction digests using NheI and HindIII enzymes (**Figure 3.12**). Constructs were sequenced using the vector primers and PCR primers were also used for internal sequencing.



Figure 3.12: Additional CAR constructs were generated by cloning overlap PCR products into pcDNA3.1(-).

Insertion of each scFv into the construct was confirmed by restriction enzyme digests using NheI/HindIII and analysis by gel electrophoresis. DNA was stained with GelRed, separated on a 0.7 % agarose gel at 120 V and visualised under UV light. The example of B1-WG CAR is shown here. Bands at the expected size of the complete CAR are indicated by grey arrow. Lanes show several colonies of the same ligation reaction. Ladder shown is 1 kb.

At this stage, an additional 2F2-based CAR was also generated. The mAb 2F2 has a unique epitope within CD20, binding more proximally to the membrane on the smaller extracellular loop (**Figure 1.3**). This made it an interesting potential CAR to further investigate the relationship between scFv characteristics, binding and CAR function. The scFv 2F2 was generated as a commercial extended oligonucleotide to specification (GeneArt), including part of the leader sequence flanked by a 5' KpnI site and a 3' XhoI site. Commercial production inclusive of the complete enhancer and leader sequence was not possible due to the high GC content. A complementary KpnI site was mutated into an existing CAR construct at the same point in the leader sequence, allowing cloning of the 2F2 fragment into the CAR backbone in pcDNA3.1(-), completing the panel of five CARs.

For each CAR, one positive bacterial colony was selected based on the quantity and quality of DNA produced, as determined by nanodrop analysis. These were used to inoculate a 100 ml LB culture, from which amplified DNA was extracted using a Qiagen maxiprep kit, detailed in Chapter 2.2.11. The resulting DNA was used in cell transfections to investigate construct expression.

3.4 Expression of CARs by mammalian cells

To investigate CAR expression CAR-pcDNA3.1(-) constructs were transfected into HEK 293F cells and assessed for transient surface expression, as described in Chapters 2.3.1.2 and 2.5.1. These cells are adapted to high density culture and have superior transfection efficiency making them ideal to transiently express high surface levels of CAR proteins. Flow cytometry was used to assess expression at 48 h post-transfection. A polyclonal Phycoerythrin (PE)-conjugated F(ab')₂ anti-human IgG-Fc antibody (PE-anti-hIgG-Fc) was used throughout to detect CAR protein expression via the spacer domain with a polyclonal PE-conjugated F(ab')₂ anti-mouse IgG-Fc antibody (PE-anti-mIgG-Fc) as the isotype control. Flow cytometry plots showing positive staining for expression of three of the CAR constructs is shown in **Figure 3.13**.

Interestingly, Ritux CAR was consistently expressed at a lower level than Leu16 or BHH2, both in percentage of cells positive and expression levels as measured by the mean fluorescent intensity (MFI). This is likely due to this sequence being expressed less efficiently with lower protein production. It is also possible that the way the protein folds is limiting detection of the Ritux CAR protein, rather than actual lowered expression.

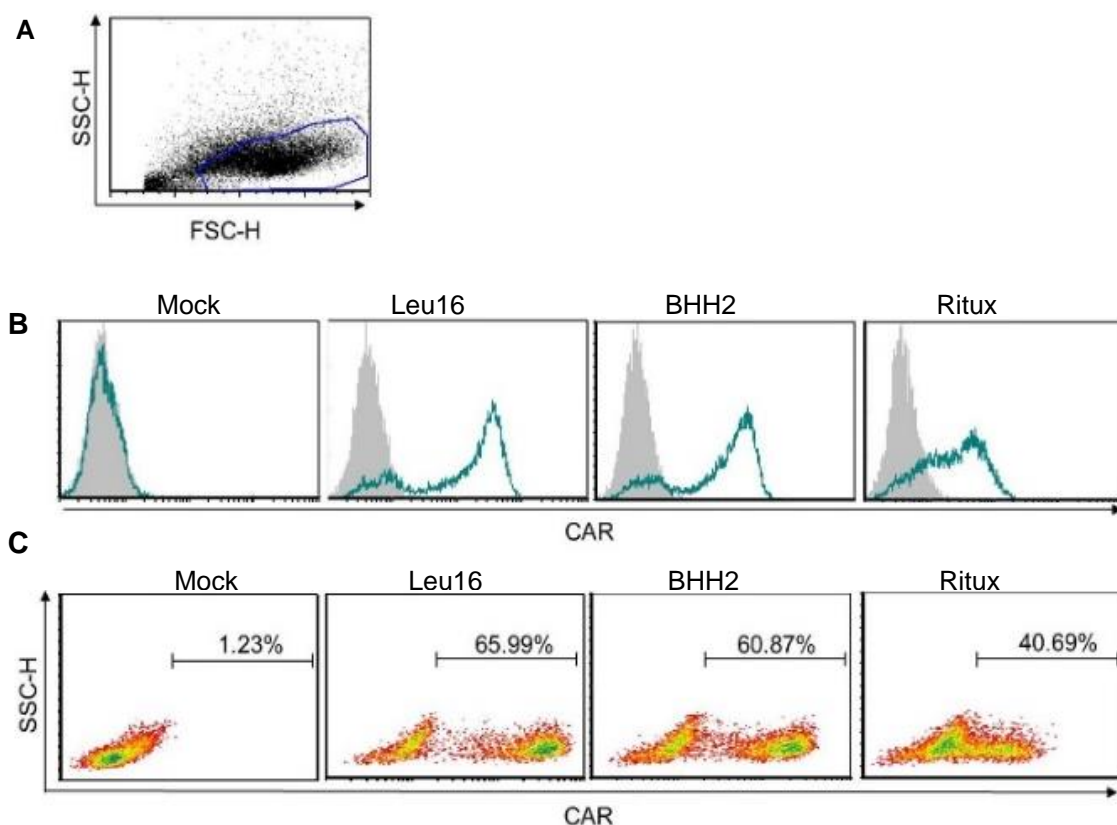


Figure 3.13: Mammalian cell surface expression of Leu16, BHH2 and Ritux CARs.

Transient surface expression of CARs was assessed on transfected HEK 293F cells.

A: Live cell populations were gated based on FSC-H and SSC-H. Representative of 2 trial transfections.

B: Histogram plots showing HEK 293F expression of Leu16, BHH2 and Ritux CARs assessed by flow cytometry at 48 h post-transfection. Mock transfection was performed with empty vector. Grey shows isotype control (PE-anti-mIgG-Fc), teal shows anti-CAR (PE-anti-hIgG-Fc).

C: Density plots showing data from **B** to illustrate the CAR+ve shift for each transfection. Marker shows percentage of CAR+ve cells.

B1-WG and 2F2 CAR constructs were also transfected into HEK 293F cells however no surface CAR expression was detected. Ritux CAR expression was used as a positive control for the transfections. Anti-idiotypic staining was additionally used to investigate whether misfolding of B1-WG CAR was inhibiting interaction of PE-anti-hIgG-Fc with the spacer region, but neither antibody could detect any surface CAR expression (**Figure 3.14 A**). The constructs were re-sequenced to rule out any errors in the protein, start codon, or in the enhancer or leader sequences that would inhibit successful protein expression. Staining using saponin (detailed in Chapter 2.5.2) showed that both B1-WG and 2F2 constructs were both expressed intracellularly (**Figure 3.14 B**).

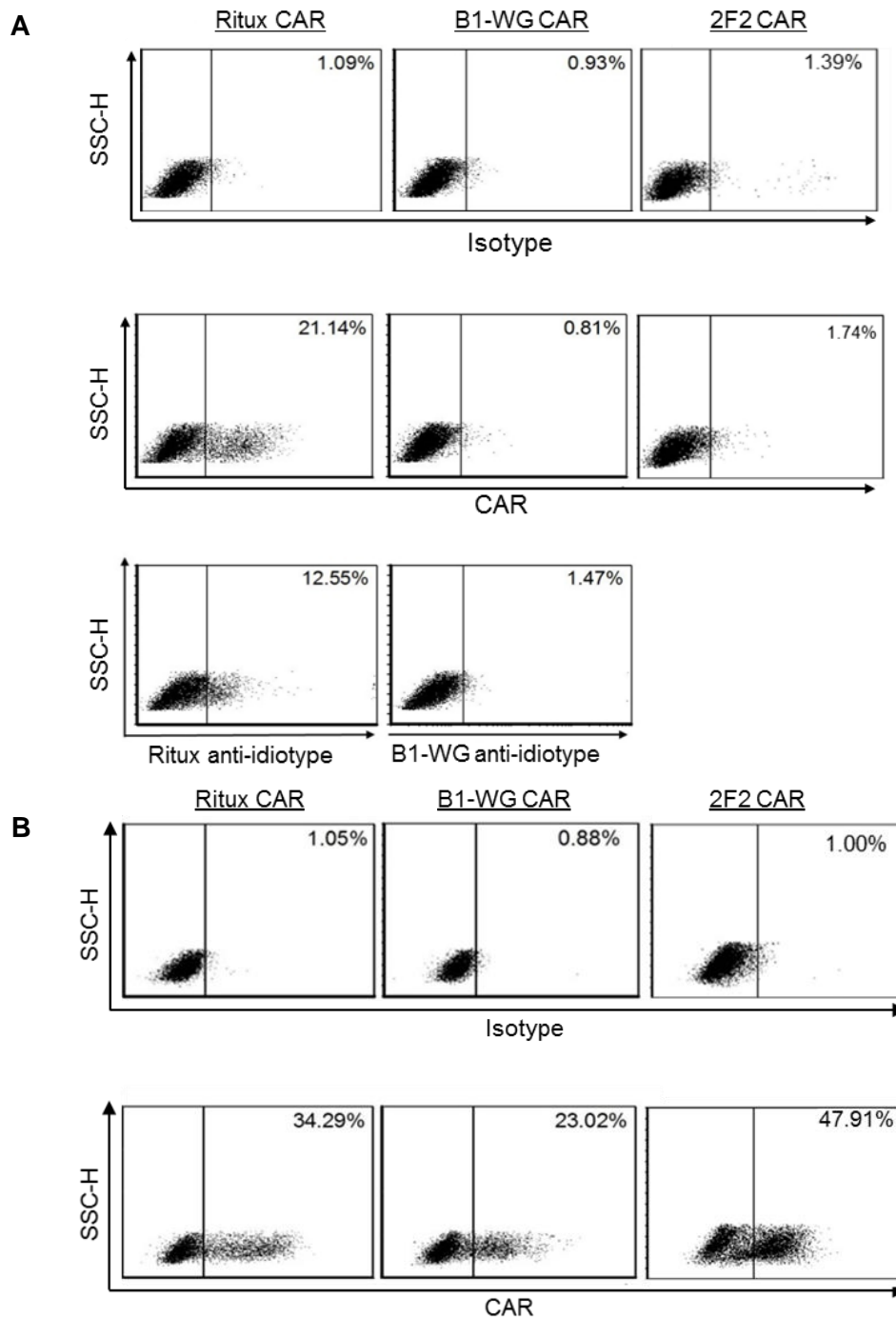


Figure 3.14: Surface and intracellular expression of B1-WG and 2F2 CARs on HEK 293F cells.

HEK 293F cells were transfected with Ritux, B1-WG and 2F2 CARs. At 48 h post-transfection, surface (A) and intracellular (B) expression were assessed by flow cytometry. Live cell populations were gated based on FSC-H and SSC-H.

A: Surface expression of Ritux, B1-WG and 2F2 CARs. Top row: isotype control (PE-anti-mIgG-Fc); middle row: anti-CAR (PE-anti-hIgG-Fc); bottom row: Ritux and B1-WG CAR stained with anti-idiotypic mAbs. Representative of N=2.

B: Cells were fixed and permeabilised using saponin prior to incubation with antibody to investigate intracellular protein expression of the CARs. Top row: isotype control intracellular (PE-anti-mIgG-Fc); bottom row: anti-CAR (PE-anti-mIgG-Fc).

Representative of N=2.

The sequences of 2F2 and B1-WG CAR were examined further. When B1-WG was compared to the other CAR sequences, a clear difference was seen. With Ritux, BHH2, Leu16 and 2F2, two cysteine residues are present in each variable domain, allowing the formation of disulphide bonds that form and strengthen the immunoglobulin domains. The sequence of B1-WG V_H comprises three cysteine residues, the additional one identified by comparing the framework regions of the scFv (**Figure 3.15**). It was hypothesised that this extra cysteine could be forming an aberrant disulphide bond, leading to improper folding of the protein (**Figure 3.16**) and either protein degradation, or misfolding at the cell surface, inhibiting any binding of the detection antibody.

Ritux

KVPQIVLSQSPAILSASPGEKVTMT**C**RASSSVSYIHWFFQQKPGSSPKWIYATSNLASGVPVRFSGSGSGTSYSLTISRVEAEDAATYY**C**QQWTSNPPTFGGGTKLEIKGGGGSIEGRSGGGGSQVQLQ QPGAELVKPGASVKMS**C**KASGYTFTSYNMHWVKQTPGRGLEWIGAIYPGNGDTSYNQKFKGKA TLTADKSSSTAYMQLSSLTSEDSAVYY**C**ARSTYYGGDWYFNVWGAGTTVLVSA

B1-WG

KVPQLVLTQSSSASFSLGASAKLT**C**TLSSQHSTYTIIEWYQQQLKPPKYVMELKKDGSHTGDGI PDRFSGSSSGADRYLRISNIQPEDEAIYI**C**GMGNKIQEFVYVFGGGTKVTVLGGGGGSIEGRSG GGGSQIQLVQSGPVLKPKGETVKLS**C**KASGYTFTNYGMNWKQAPGKGLKWMGWINTYTGEST YADDFKGRFSMSLETSVTTA**C**LQINNLKNETATYF**C**ARWGPHTAPYSMDNWGGQTLVSA

Figure 3.15: B1-WG scFv contains an additional cysteine residue in the VH domain.

Comparison of the sequences of each scFv demonstrates that all contain the four cysteines required for formation of the disulphide binds that strengthen the immunoglobulin domains, shown in green. B1-WG contains an extra cysteine (pink), shown here compared to the example of Ritux scFv. Comparison of the framework regions of each scFv identified which is the additional residue. It was hypothesised that this cysteine could be forming an aberrant disulphide bond, leading to improper folding of the immunoglobulin domains. This could be responsible for either protein degradation due to misfolding, or inhibition of antibody binding at the cell surface, meaning the construct cannot be detected.

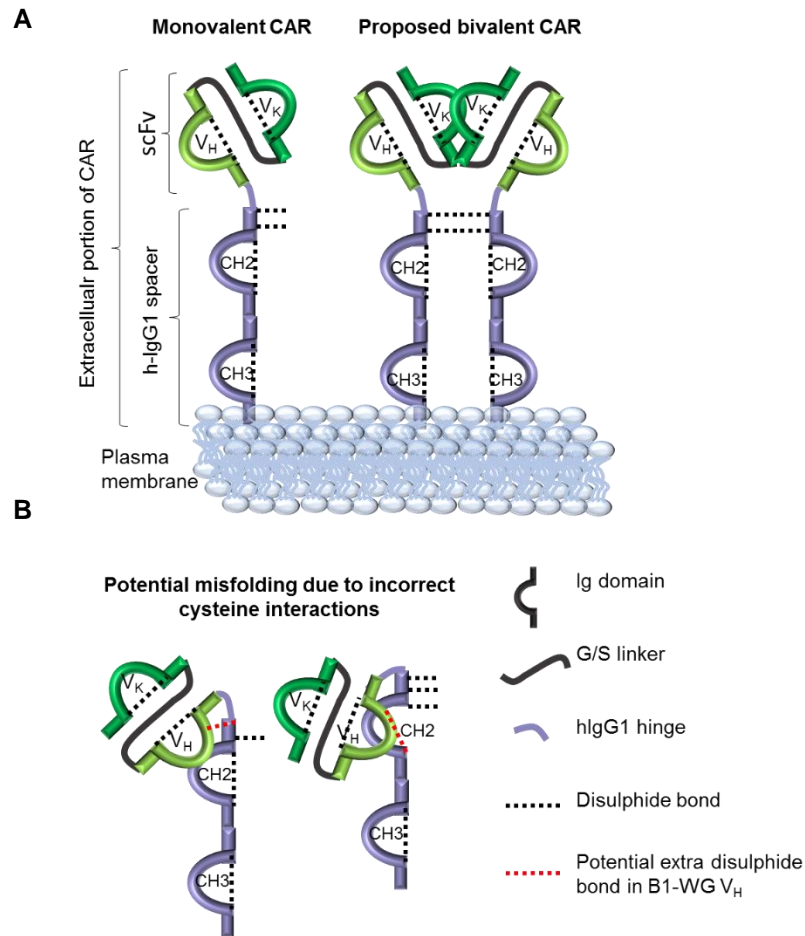


Figure 3.16: Disulphide bond formation in the extracellular domains of CAR constructs

The extracellular IgG1 spacer and scFv portion of a CAR is shown, with the disulphide bonds that stabilise the immunoglobulin (Ig) domains illustrated.

A: The monomeric construct is shown next to the proposed cell surface dimeric CAR.

B: Two examples of the hypothesised misfolding of B1-WG CAR are illustrated. The extra cysteine residue was proposed to interact incorrectly, disrupting the stabilising disulphide bonds and leading to protein misfolding and a subsequent failure in cell surface expression.

3.4.1 Mutagenesis of B1-WG scFv

Site-directed mutagenesis was performed to investigate whether removal of the additional cysteine residue in the sequence of B1-WG would allow surface protein expression and detection. The cysteine was mutated into a serine residue, to ensure minimal disruption to the protein sequence. The mutated DNA was transformed into XL-GOLD chemically competent *E. coli* and the amplified DNA was extracted using a Qiagen miniprep kit. Sequencing confirmed the mutation (**Figure 3.17 A**).

The B1-WG C²⁸⁸S CAR DNA was transfected into HEK 293F cells, and surface and intracellular protein expression was assessed at 48 h. Intracellular staining was performed as previously using saponin. As before, B1-WG CAR was shown to be expressed intracellularly but failed to be detected upon the cell surface (**Figure 3.17 B**). This showed that the additional cysteine residue was not the reason for undetected CAR expression of the B1-WG construct.

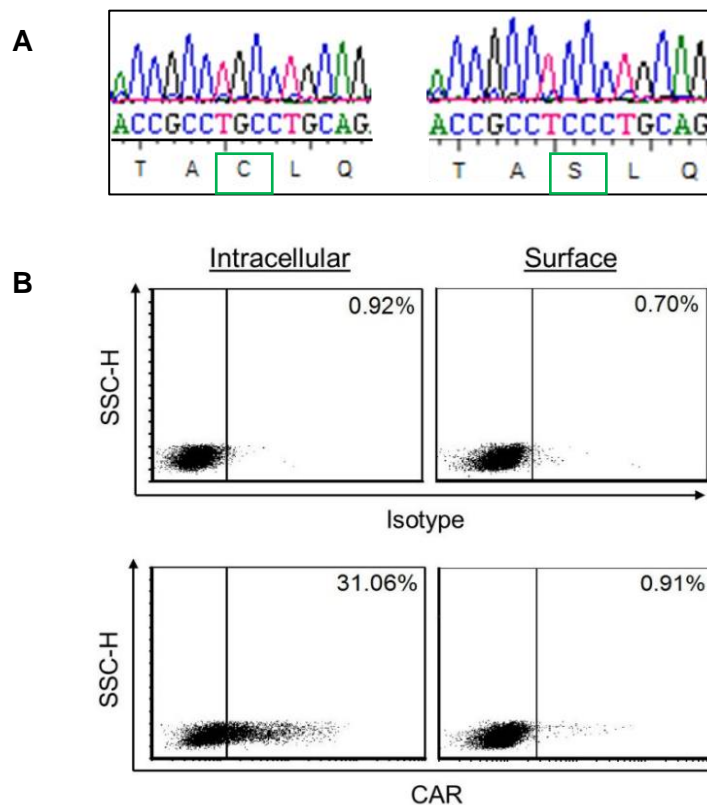


Figure 3.17: Site-directed mutagenesis was used to convert the additional cysteine in B1-WG to a serine residue.

A: Sequence traces of B1-WG before (left) and after (right) the mutagenesis, showing the change from a cysteine to serine residue.

B: HEK 293F cells were transfected with the mutated B1-WG C²⁸⁸S CAR. At 48 h post-transfection, surface and intracellular expression was assessed by flow cytometry using isotype control (PE-anti-mIgG-Fc) and anti-CAR (PE-anti-hIgG-Fc). For assessment of intracellular expression, cells were fixed and permeabilised using saponin, prior to incubation with antibody. Live cell populations were gated based on FSC-H and SSC-H as previously. Representative of N=2.

3.5 Discussion

In this chapter five DNA constructs of anti-CD20 scFv were successfully designed and generated comprising V_H and V_K mAb domains adjoined by a G/S linker. Ritux, BHH2 and B1-WG scFv were generated by PCR and comprised the GS15 linker. 2F2 and Leu16 scFv were generated as custom oligonucleotides to order (GeneArt) and contained the GS15 linker and GS18 linker respectively. Leu16 scFv was generated as the published control construct [465, 466].

Expression of selected scFv proteins was then confirmed at the expected molecular weight by Western blot of transfected cell lysates. Furthermore, a soluble secreted scFv was produced and purified through use of the pFUSE vector and an anti-HA column. The intention was to produce each scFv as such a soluble protein to allow investigation into the stability of antigen binding for each. Ideally, surface plasmon resonance is used to accurately assess mAb-antigen binding affinities. However, due to the lack of a stably folding soluble CD20 molecule, this was not possible for the scFv.

An alternative assay was proposed to compare relative anti-CD20 binding strengths of each construct, similar to that used by Hombach *et al* [373]. This would involve a cell-based binding competition assay of the soluble scFv, with a fluorescently-labelled parental mAb, such as rituximab. The rate at which the scFv at different concentrations can outcompete the bivalent mAb could then be compared to produce a hierarchy of binding strengths. To be capable of outcompeting the bivalent mAb, high concentrations of scFv would be required. Consequently, large yields of soluble scFv would need to be produced and purified. The initial yields seen from the transfections performed by Patrick Duriez (Southampton Protein Core Facility) were very low, showing inefficient protein production. Extremely large transfection volumes would be necessary to produce sufficient quantities of scFv for use in this assay. As the main aim of this thesis was to determine if the scFv affected CAR binding and function, it was decided to proceed with the generation of the full constructs. Once it had been established if a difference in CAR binding and function was observed, investigation as to whether the binding strengths of the scFv were responsible would be more relevant.

The scFv were successfully converted into a panel of five CAR constructs. The hIgG1 hinge-CH2-CH3 spacer was included to allow optimal CAR activation upon binding the small target molecule of CD20 [367]. Additionally, this domain allowed detection of CAR expression at the cell surface using a PE-anti-hIgG-Fc antibody, with the murine equivalent used as an isotype control. The signalling domains included were based

upon the published Leu16 CAR and are those standardly incorporated into a generation three CAR construct (**Figure 1.10**) to elicit T-cell activation, proliferation and survival. The CAR domains were cloned into an expression vector to produce the complete constructs.

Of the five CARs generated, three were shown to be expressed readily on transiently transfected mammalian cells; Ritux, BHH2 and Leu16 CAR. Ritux CAR consistently exhibited lower expression than the other two CARs, in both percentage of CAR+ve cells, and level of expression measured by the mean fluorescence intensity (MFI). There are a number of possible causes for this, at the DNA, RNA or protein levels. There may be sequence-specific elements leading to a reduction in transcription or translation. At the protein level, the peptide produced may be subject to misfolding, leading to a reduced trafficking to the plasma membrane, or a lack of stability in cell surface expression. As the Ritux CAR was detected at a higher intracellular level than surface expression (**Figure 3.14 B**), it is likely that protein misfolding and reduced trafficking is at least partly responsible.

Cells maintain their proteome and avoid the build up of misfolded proteins via a series of quality control measures. Accumulation of misfolded proteins and consequent aggregates in the cytosol can result in cell damage and death. Firstly, any misfolded proteins are identified by chaperone proteins of the Hsp40/70 families which recognise exposed areas of hydrophobic residues in the proteins. These chaperones can then direct the proteins for refolding via cycles of ATP hydrolysis, or if this is not possible E3-Ubiquitin ligases are recruited to tag the misfolded protein for proteasomal degradation. Large aggregates of protein can be cleared by an autophagy process [471]. In these ways, cells can clear misfolded proteins to maintain cell health. If the Ritux CAR has a higher rate of misfolding in the cytosol, these mechanisms will recognise and remove those molecules, resulting in reduced successful Ritux CAR trafficking to the cell surface.

It is also possible that the nature of folding of surface Ritux CAR could be responsible for inaccessibility of binding the detection antibody. If the scFv spatially blocks some of the IgG1 spacer domain, a reduced level of detection by the anti-spacer antibody could be seen. It would be beneficial for future CAR design to identify the mechanism responsible for the lower expression detection of surface Ritux CAR. A Western blot could be used to compare protein levels between the CAR-transfected cell lysates to determine relative protein production. This would reveal whether the cause of the reduced expression of Ritux CAR lies at the protein production level or is an issue of protein stability.

The other two CAR constructs, 2F2 and B1-WG did not express on the mammalian cell surface. Both were detected intracellularly, showing that protein production occurs for both, albeit at a comparatively low level. No obvious issues were found regarding protein retention sequences or other problematic motifs that may inhibit surface expression of the CAR for either [472, 473]. The low intracellular expression levels and absence of detectable surface CAR may be attributed to similar mechanisms as discussed for Ritux CAR. The reduced intracellular expression can likely be explained by a lower rate of transcription or translation of these proteins. It is hypothesised that these proteins then do not stably fold and thus are not successfully trafficked to the cell surface for detectable, stable expression.

When the sequences were examined in detail, the extra cysteine in the V_H domain of B1-WG was discovered. It was proposed that this may be responsible in the case of B1-WG for protein misfolding leading to either failure to be expressed on the cell surface, or an expression that blocks antibody detection. As no cell surface expression was detected with either the anti-hlgG-Fc or anti-idiotypic, it is more likely that the protein is failing to achieve stable cell surface expression. **Figure 3.16** shows the usual disulphide bond interactions seen in the extracellular portion of the CAR constructs. The monomeric construct is shown, alongside the proposed bivalent CAR expressed on a cell surface (**A**). Previous studies have shown it is probable that CAR molecules interact via their IgG1 spacer regions to form dimers at the cell surface [474]. Two examples of hypothesised aberrant disulphide bonds in B1-WG are illustrated (**B**). The extra cysteine in B1-WG was mutated into a serine residue, chosen to minimise disruption to the scFv structure due to its similar size and properties to cysteine. Transfection of the mutated construct demonstrated intracellular expression only, revealing that the additional cysteine was not responsible for lack of surface expression of B1-WG CAR.

The three CAR constructs capable of cell surface expression, comprising scFv from rituximab, BHH2 and Leu16, were taken forward into functional studies, discussed in the next chapter.

4 Antigen-Specific Binding of CAR Constructs

4.1 Introduction

In the previous chapter it was determined that three of the generated CAR constructs could be successfully expressed transiently on a mammalian cell surface. Furthering this, the ability of the CARs to bind the target antigen in a specific manner was investigated. Cellular rosetting assays have been previously described, used in measuring levels of phagocytosis [464]. This assay was adapted to allow the interrogation of CAR-CD20 interactions.

Transient transfection of the CAR constructs was used to generate short-term high expression on HEK 293F cells. Binding ability for each of these to CD20+ve cells was investigated and compared to the CAR expression levels to determine if the binding levels differed between constructs. It is essential that CAR constructs bind target antigen in a specific manner. Off-target effects of targeted T cells *in vivo* can be catastrophic, as healthy tissues can be severely damaged. Whilst scFv-directed CARs are unlikely to bind non-specifically, it is essential to confirm that the binding of the molecule is correct to ensure this [475]. Therefore, CAR binding to CD20+ve cells was compared to that of CD20-ve populations. Whilst this does not exclude all off-target antigenic interaction, it allowed assessment of binding specificity in the presence and absence of the target antigen.

4.2 Confirmation of CAR-CD20 interactions

HEK 293F cells were transiently transfected with each of the CAR constructs as described in Chapter 2.3.1.2. Expression was determined at 48 h post-transfection and the cells were labelled with 0.5 μ M CFSE. Mock-transfected (transfected with empty vector) HEK 293F cells were also CFSE-labelled as a control population. CD20+ve Raji target cells were labelled with an APC-anti-CD32 mAb to allow identification of this population via their CD32b expression. Effector and target cells were incubated together for 30 min at 4 °C and samples were analysed by flow cytometry without further washing to avoid disruption of cellular interactions.

The double positive conjugate population of CD32b+ve target cells associated with CFSE+ve HEK 293F cells was identified (**Figure 4.1 A**). **Figure 4.1 B** illustrates the gating strategy used; live cells were gated based on FSC-H/SSC-H, then the

percentage of CAR-transfected CFSE+ve cells that were also APC+ve was determined as a readout for CAR-CD20 interactions.

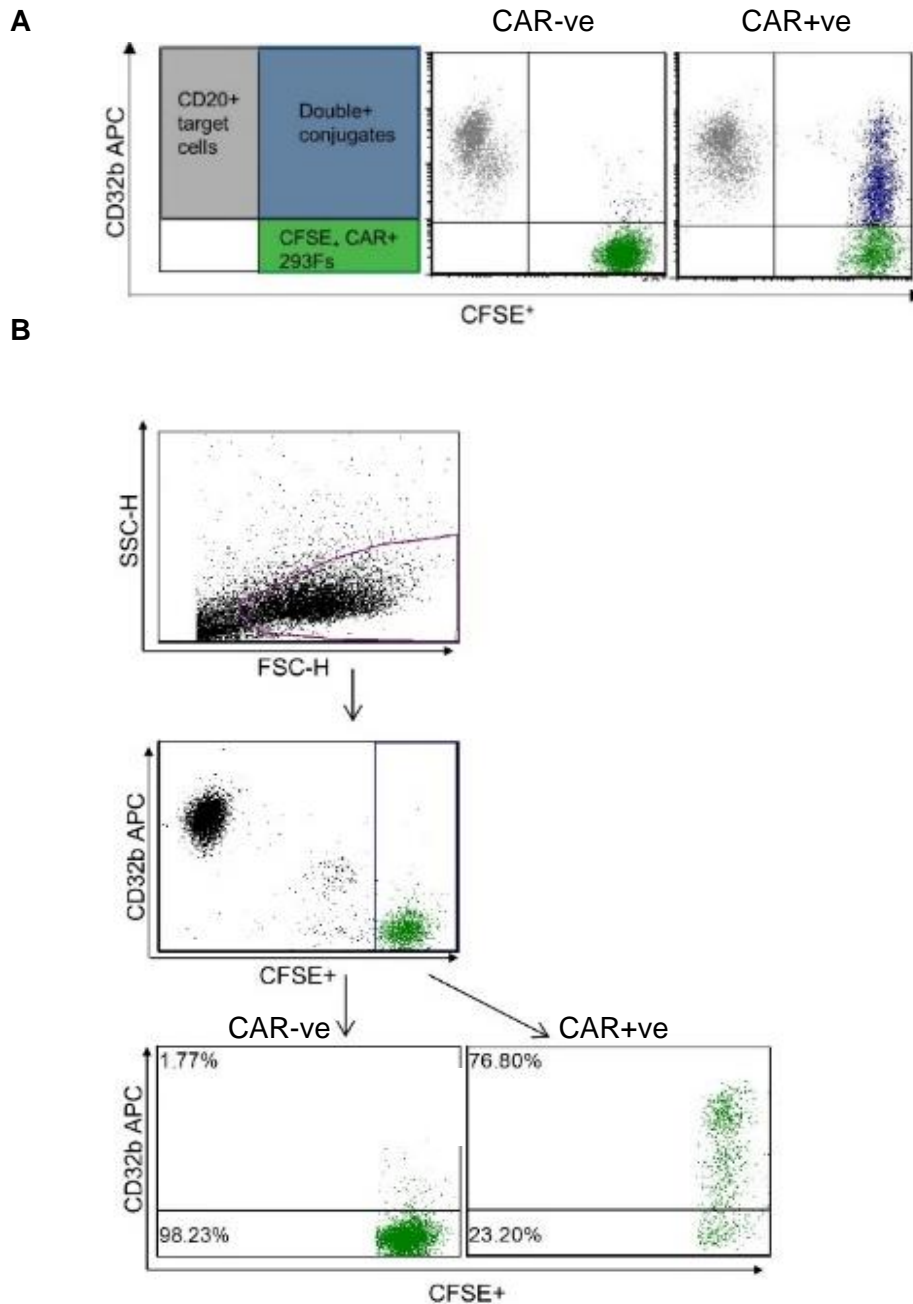
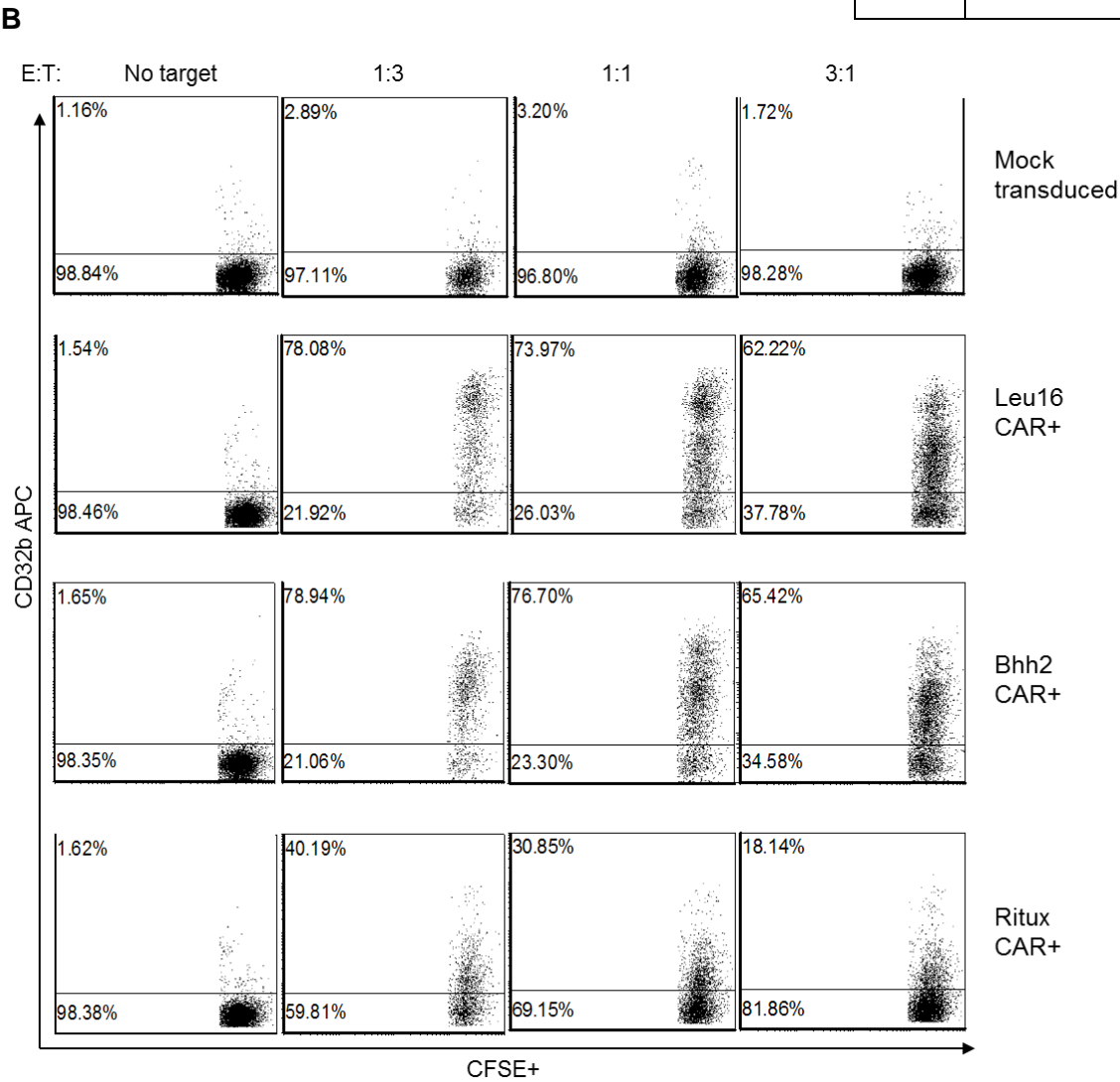
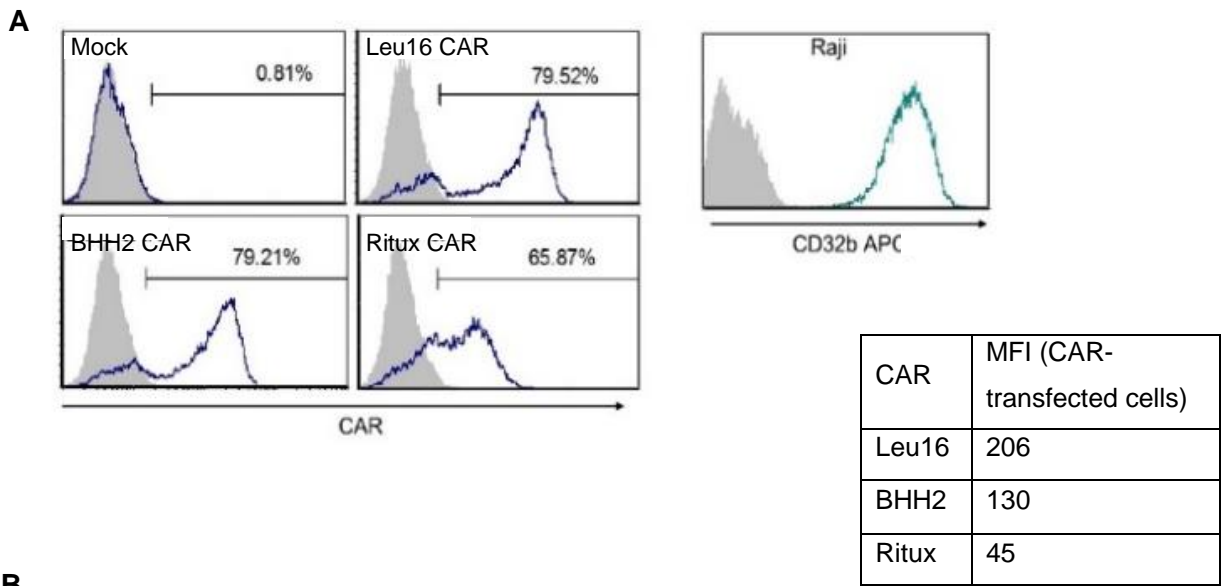


Figure 4.1: Flow cytometry gating strategy employed to assess binding interactions between CAR+ve HEK 293F cells and CD20+ve target cells.

A: A schematic to illustrate the principle of the binding assay. CAR-transfected HEK 293F cells were CFSE-labelled and co-cultured with CD20+ve Raji target cells. These were labelled with APC-anti-CD32 to identify the target population. When no CAR is present, only two distinct cell populations are seen. CAR+ve transfected cells can interact with the target cells, forming APC+ve CFSE+ve cell conjugates.

B: A live-cell gate based on SSC-H/FSC-H was drawn to exclude debris. CFSE+ve HEK 293F cells were then gated on (green), to allow calculation of the percentage of CAR transfected cells binding to APC-labelled target cells.

The initial binding assay demonstrated interactions between the CAR-transfected HEK 293F cells and the CD20+ve targets, whilst no double positive population is seen in the absence of CAR expression (**Figure 4.2**). As seen previously (**Figure 3.13**), the Ritux CAR was expressed at a lower level on HEK 293F cells than the other constructs, and the percentage of positive cells was also lower (**Figure 4.2 A**). Consistent with this they showed a lower level of interaction with the CD20+ve target cells (**Figure 4.2 B and C**). To investigate whether this lowered interaction was due purely to the reduced expression levels of Ritux CAR, the data were normalised to percentage CAR+ve HEK 293F cells (**Figure 4.2 D**). Ritux CAR was still observed to be interacting at a lower rate with the target cells than BHH2 and Leu16 CAR.



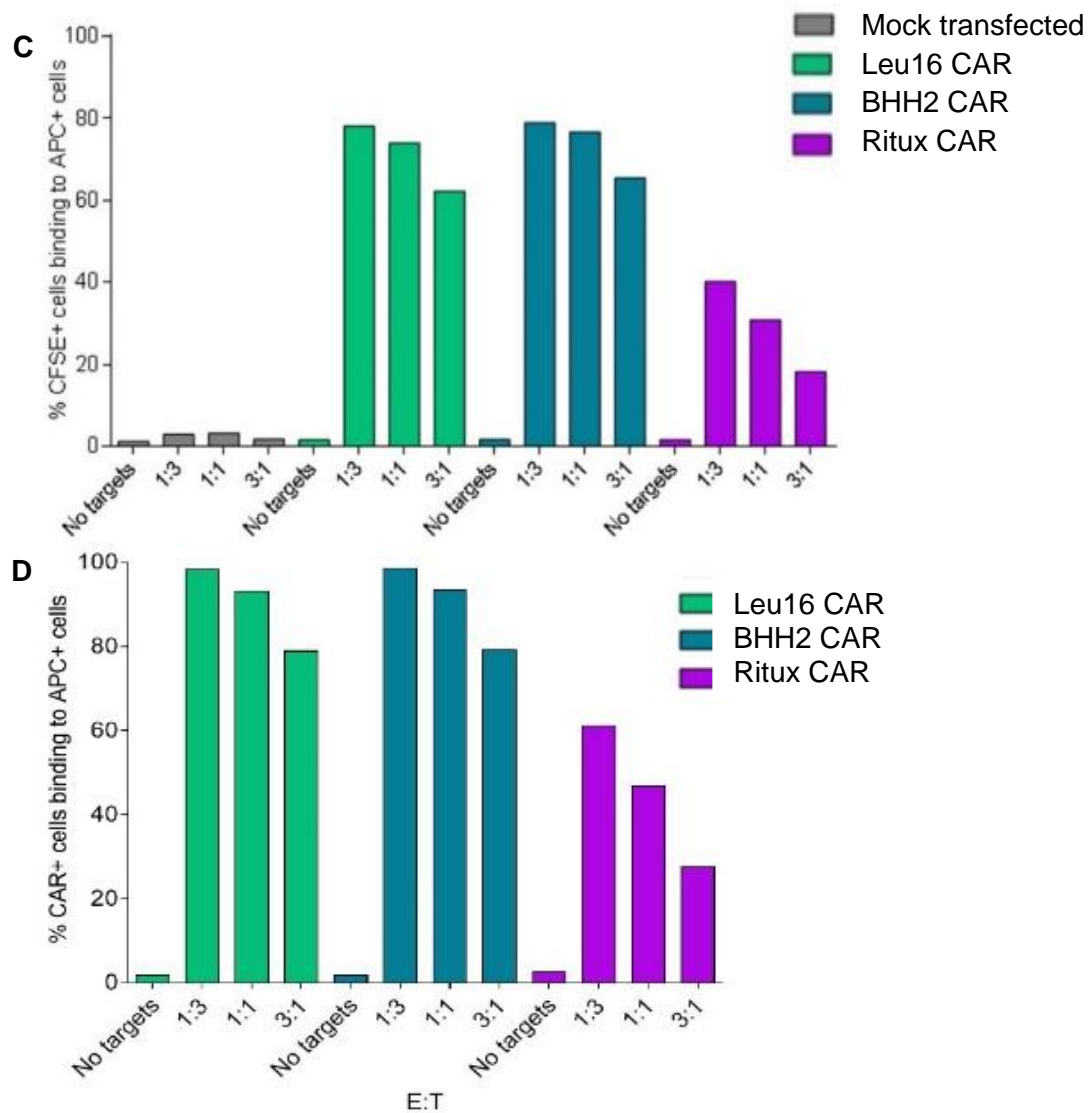


Figure 4.2: Binding assay to determine interactions between CAR-transfected HEK 293F cells and CD20+ve target cells.

HEK 293F cells were transfected to express Leu16, BHH2 and Ritux CARs or with empty pcDNA3.1(-) vector (Mock). At 48 h post-transfection, cells were labelled with 0.5 μ M CFSE. CAR expression was confirmed by staining with PE-anti-hIgG-Fc. CD20+ve Raji target cells were labelled with APC-anti-CD32. Co-cultures were performed in flow cytometry tubes for 30 min at 4 $^{\circ}$ C and run without further washing. Representative of n=2.

A: Expression of CAR constructs on transfected HEK 293F cells and CD32b labelling of Raji target cells. Isotype control, PE-anti-mIgG-Fc (grey); anti-CAR, PE-anti-hIgG-Fc (blue). Percentage of CAR+ve cells shown above markers on histogram plots. Table below denotes geometric mean fluorescence intensity (MFI) of CAR-transfected cells for each population.

B: Flow cytometry plots of binding assay. Gating was performed as shown in **Figure 4.1**. Percentages of CFSE+ve CD32b+ve conjugates are shown for each transfected HEK 293F population at the effector:target ratios labelled.

C: Graphical representation of percentage data shown in **B**. Data presented as percentage CD32b+ve of CFSE+ve cells, showing CAR-CD20 interactions.

D: Data from **C** normalised to percentage CAR expression, to show an estimate of percentage CAR+ve cells binding to target cells.

Data from this assay were also analysed to look at the size of the double positive cell populations to confirm that they were cellular conjugates. The CFSE+ve CD32b-ve, CFSE+ve medium-CD32b+ve, and CFSE+ve high-CD32b+ve populations were back-gated onto plots showing FSC-H/SSC-H for each CAR construct (**Figure 4.3**). The CD32b-ve and medium-CD32b+ve populations were shown to be smaller, as determined by the FSC-H, suggesting single non-bound cells, or small numbers of interacting cells. The high-CD32b+ve populations were revealed to be positioned further along the FSC-H axis, showing they are of a larger size and supporting the hypothesis that they are multiple cell conjugates, formed from CAR-CD20 interaction.

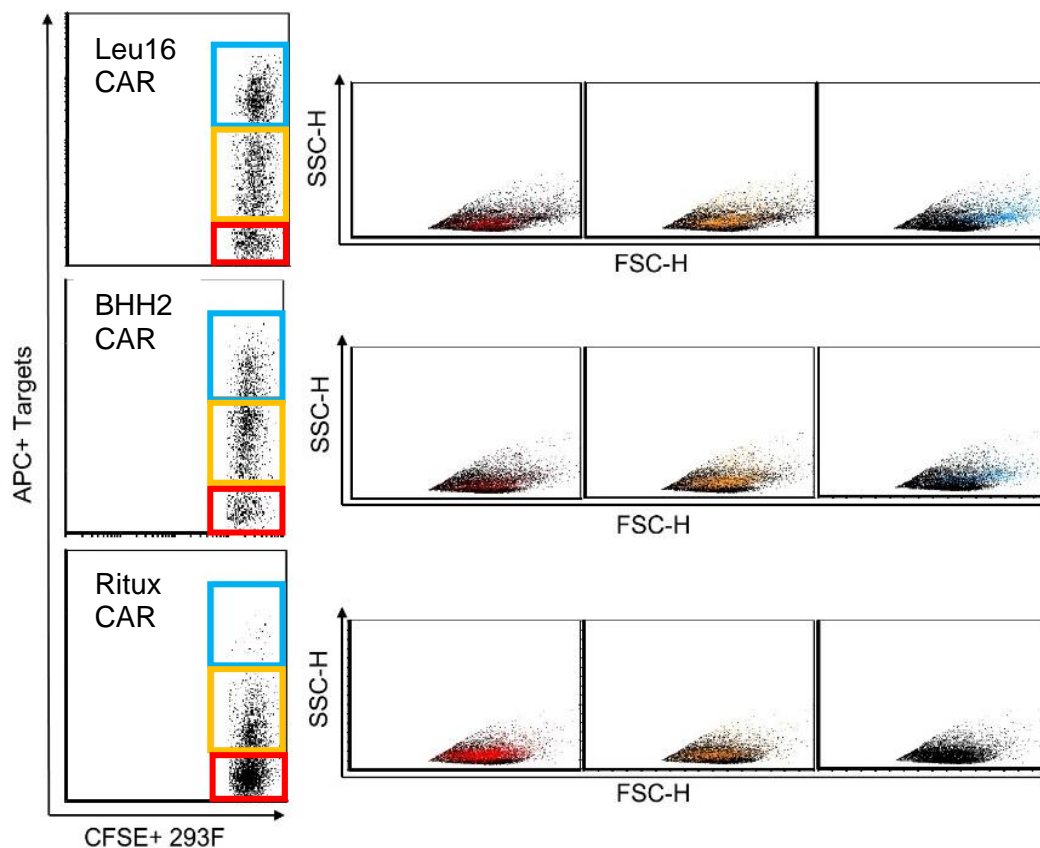


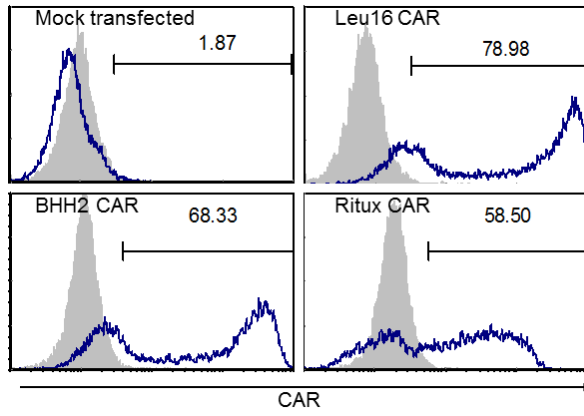
Figure 4.3: Determination of size increase of effector-target conjugates from single non-bound cells.

Data from each CAR-transfected HEK 293F binding co-culture (1:1 E:T ratio) was analysed using FSC-H/SSC-H to assess size of conjugates. This was to confirm that the double positive staining seen was due to cell-cell interactions, demonstrated by increase in FSC-H size. CFSE+ve cells were gated then these divided these into three populations, APC-CD32b-ve (red), medium +ve (yellow) and high +ve (blue). These were then shown on FSC-H/SSC-H colour plots to reveal changes in size, representing increase from single non-binding cells to conjugates of interacting cells.

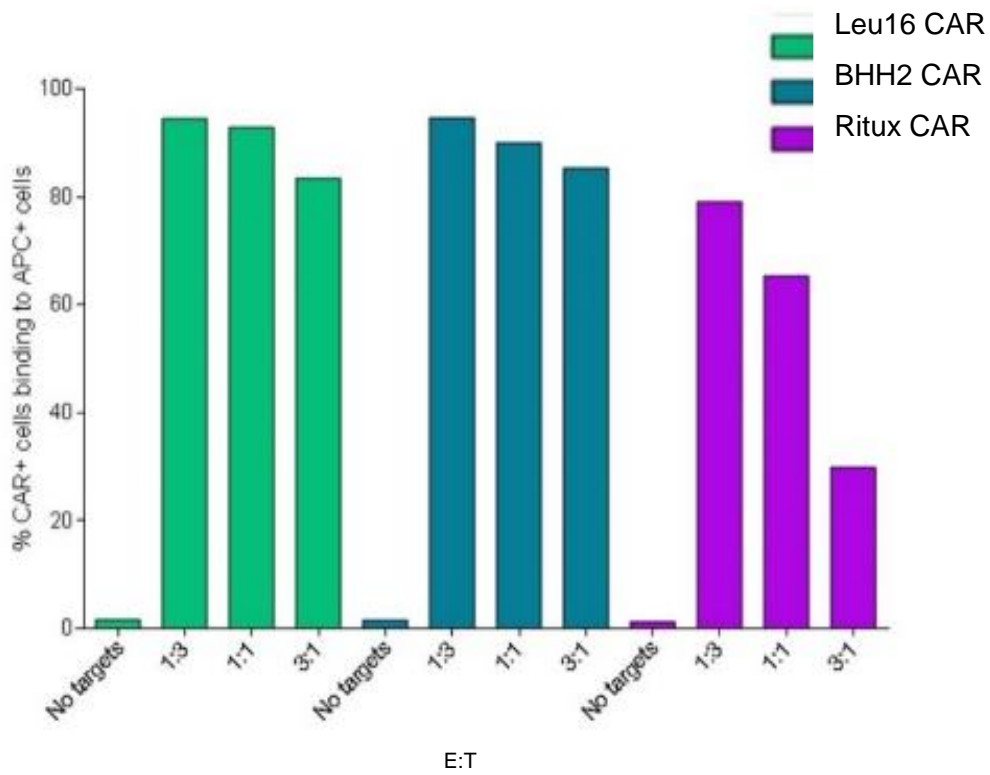
Having shown that the CAR-transfected cells were capable of binding to CD20+ve Raji cells, the assay was repeated with the addition of the anti-CAR antibody (PE-anti-hlgG-Fc). This allowed the identification of CAR+ve cell populations and provided a more accurate insight into their interactions with CD20+ve cells. HEK 293F cells were transfected with CAR constructs as previously, and expression ascertained at 48 h (**Figure 4.4 A**). The cells were labelled with CFSE, and then stained with PE-anti-hlgG-Fc antibody before the co-culture was performed. The data were analysed by gating upon the CFSE+ve CAR+ve population, before determining the percentage of these that were also APC+ve indicating target binding.

It was revealed that a very high percentage of Leu16 CAR+ve and BHH2 CAR+ve cells were binding to the CD20+ve Raji cells. High numbers of Ritux CAR+ve cells were also seen to be interacting, though at a lower level than the other two CARs (**Figure 4.4 B**), as seen previously. This may be attributed to the nature of the construct itself or may be influenced by the construct expression. The density of Ritux CAR expression was shown to be lower than that of the other two constructs, as determined by the geometric MFI (**Figures 4.2 A, 4.4 A**).

To investigate the potential effect of CAR expression density on target binding, medium and high CAR+ve transfectants were gated based on a PE-anti-hlgG1-Fc labelling (**Figure 4.4 C**, red and blue respectively) and the interaction of each population with APC+ve targets compared. It was shown that the higher expressing CAR+ve populations also demonstrated high APC fluorescence, suggesting several target cells interacting with the highly-expressing CAR+ve cells. The medium density CAR+ve populations showed a lower level suggesting the interaction with fewer target cells. In this analysis, Leu16 CAR+ve and BHH2 CAR+ve cells showed similar binding characteristics, whilst Ritux CAR+ve cells were once again found to express and bind at lower levels. The high Ritux CAR+ve population was comparable to the medium expression populations gated for the other CARs, in both expression density and target cell interaction, indicating that CAR density has an effect on the number of target cells able to bind. However, the overall CAR+ve percentage of cells does not fully account for the different rates of CAR+ve cells binding with the target cell population.

A

CAR	MFI (CAR-transfected cells)
Leu16	2215
BHH2	1625
Ritux	383

B

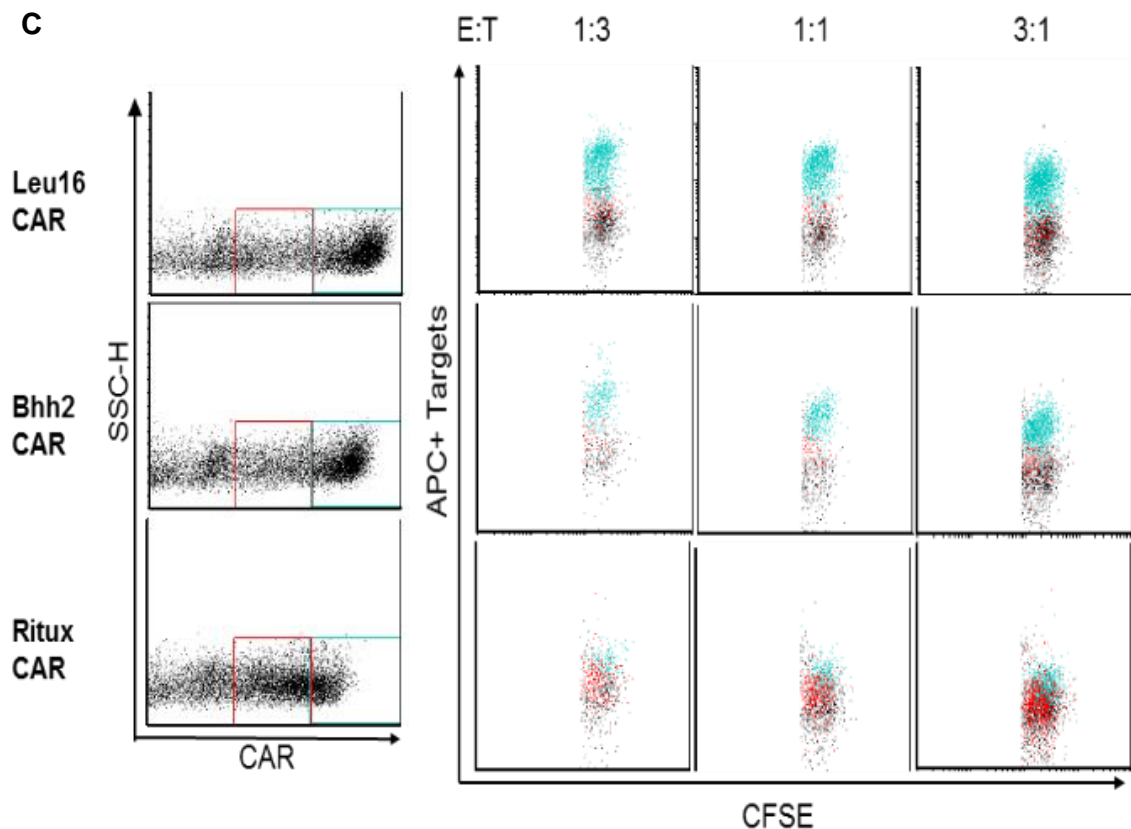


Figure 4.4: Binding assay to determine interactions between CAR+ve HEK 293F cells and CD20+ve target cells.

HEK 293F cells were transfected to express Leu16, BHH2 and Ritux CARs, or with empty pcDNA3.1(-) vector (Mock). At 48 h post-transfection, cells were labelled with 0.5 μ M CFSE, and stained for CAR expression. CD20+ve Raji target cells were labelled with APC-anti-CD32b. Co-cultures were performed in flow cytometry tubes and run without further washing to avoid disturbance of cell interactions. N=1.

A: Expression of CAR constructs on transfected HEK 293F cells. Isotype control, PE-anti-mIgG-Fc (grey); anti-CAR, PE-anti-hIgG-Fc (blue). Percentage CAR positive cells shown above markers on histogram plots. Table below denotes geometric MFI of CAR-transfected cells for each population.

B: Cells were gated on CFSE+ve as previously, then on CAR+ve cells. Percentage CAR+ve CD32b+ve cells is shown for each transfected HEK 293F population, at the effector:target ratios labelled.

C: Cells were gated on CAR+ve mid expression (red) and high expression (blue) and analysed on colour plots to investigate the relationship between level of CAR expression and extent of interaction with target cells.

4.3 Confirmation of Antigen Binding Specificity

It was important to confirm that the interactions observed between CAR+ve and target cells were CD20-specific. Prior to inclusion in a binding assay, Raji cells were incubated with either rituximab to block the CD20 binding epitope, or an irrelevant IgG mAb. The assay was performed as previously with CAR+ve HEK 293F cells.

Additionally, a population of the Ritux CAR+ve HEK 293F cells were pre-incubated with an anti-Ritux idiotype to block the scFv epitope binding domain, restricting the ability of the CAR to bind to CD20. The percentage of CFSE+ve CAR+ve cells forming conjugates with APC+ve targets was determined as previously and expressed as a percentage of maximum binding in the absence of blocking antibodies (**Figure 4.5**).

The binding level for each CAR transfectant to the target cells was not affected by the addition of irrelevant IgG. However, in the presence of rituximab, all of the CAR interactions were significantly reduced consistent with the blocking of CD20 on the target cells. Additionally, the inclusion of the anti-Ritux idiotype to the scFv of Ritux CAR also blocked target-CAR interactions. These data demonstrate the CAR+ve cell interactions with target populations are CD20-dependent and CD20-specific.

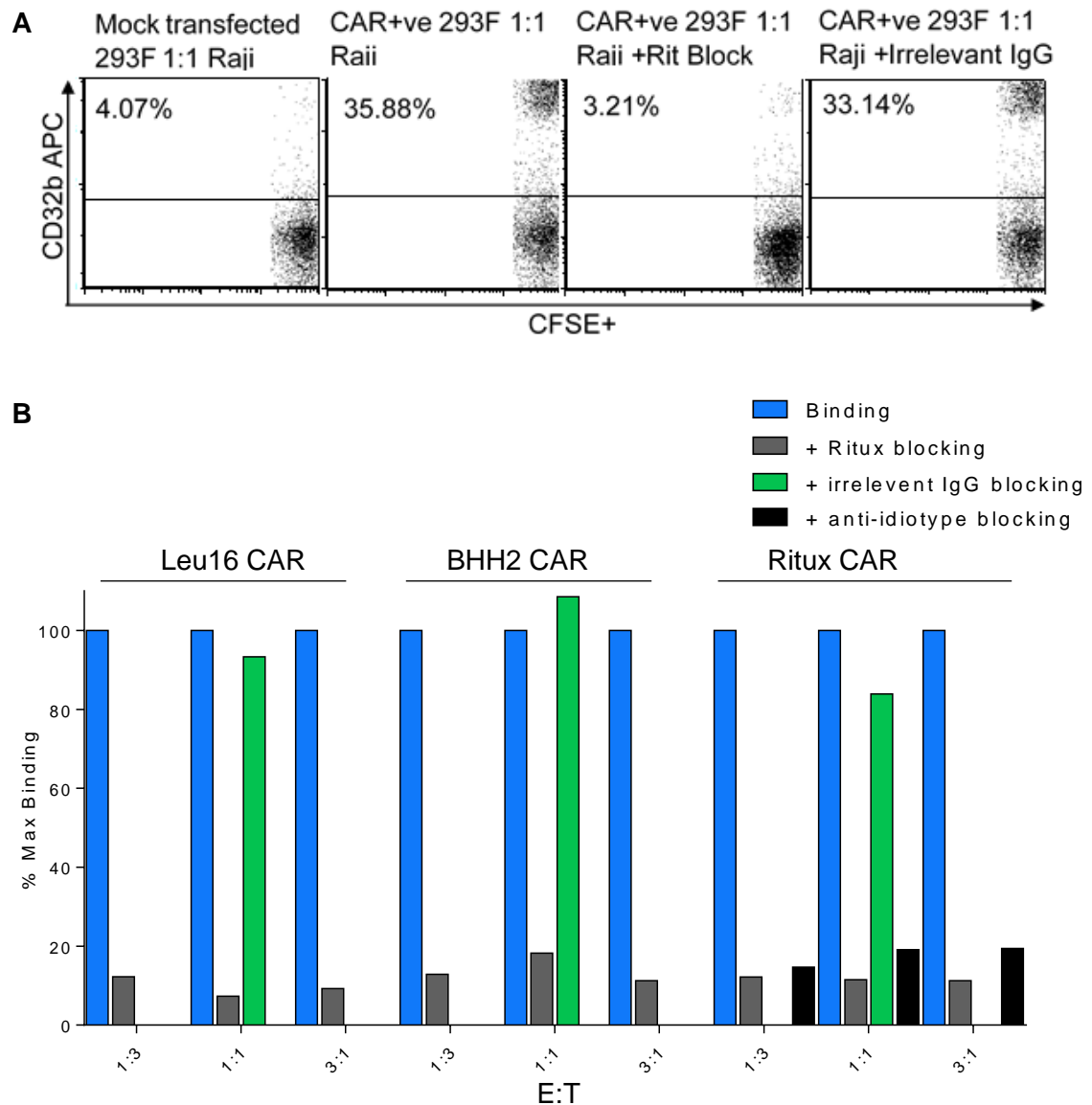


Figure 4.5: Binding and blocking assay to assess specificity of CAR-CD20 interactions.

HEK 293F cells were transiently transfected to express Leu16, BHH2 and Ritux CARs, or with empty pcDNA3.1(-) vector (Mock). At 48 h post-transfection, cells were labelled with 0.5 μ M CFSE, and stained for CAR expression with PE-anti-hIgG-Fc. CD20+ve Raji target cells were labelled with APC-anti-CD32b. For investigating specificity of CAR-CD20 interaction, the Raji target cells were incubated with excess (50 μ g/ml) unlabelled rituximab mAb or irrelevant IgG for 30 min, prior to co-culture with the CAR+ve cells. To investigate blocking of the Ritux CAR binding to CD20, the transfected HEK 293F cells were incubated with excess (50 μ g/ml) unlabelled anti-Ritux idiotypic (MB2A4) for 30 min, prior to co-culture with target cells. Co-cultures were performed in flow cytometry tubes and run without further washing to avoid disturbance of cell interactions.

A: Example flow cytometry plots of CAR+ve 293F cells co-cultured with labelled Raji cells showing binding interactions to unblocked, rituximab-blocked and irrelevant IgG-blocked target cells.

B: Data is shown as a percentage of maximal binding for each CAR where no blocking or irrelevant mAb was included. Representative of two independent experiments.

4.4 Discussion

In this chapter it was confirmed that the antigen-binding scFv of the three CAR constructs all fold correctly, allowing interaction with CD20. Leu16 and BHH2 CAR were seen to express at a consistently higher level than Ritux CAR on the HEK 293F cells, as observed in Chapter 3, in terms of their level on the cell surface (MFI) and percentage transfection (**Figures 4.2 A** and **4.4 A**). The binding efficiency of Ritux CAR to the target cells was also reduced compared to the other two constructs. The reduced expression may influence the level and strength of interactions between Ritux CAR and the target antigen. However, the second transfection of HEK 293F cells with each of the CAR constructs yielded higher MFI levels (**Figure 4.4 A**). When expressed at a more equivalent MFI in the second assay to the other CARs in the first assay (**Figure 4.2 A**), Ritux CAR is still observed to interact with CD20+ve cells at a lower level (**Figures 4.2 D** and **4.4 B**). This suggests that the expression levels are not wholly responsible for the differences observed in binding efficacy. The Ritux scFv may have a reduced affinity for the target, leading to a decreased level of sustained interactions. Importantly, none of the CAR+ve cells bound to CD20-ve target cells, demonstrating specific antigen interaction.

5 Generation of CAR-Expressing Cell Lines and Evaluation of Functional Characteristics

5.1 Introduction

In the previous chapter a transient-transfection cell system was used to confirm that each of the three surface-expressing CAR constructs are capable of binding the target antigen CD20, in a specific manner. In this chapter, these findings are expanded to examine the CD20-specific functional capabilities of each CAR. To accommodate this, several stably-expressing CAR+ve cell lines were generated. These permitted repeated, comparable assessments of CAR function, firstly in a T-cell activation reporter cell line and secondly in a cytotoxic T-cell line.

The first part of this chapter employs an IL-2 reporter cells line, BWZ.36. IL-2 is produced upon T-cell activation and is involved in a vast array of immune functions [476]. Notably in the case of T cells, including CAR+ve T cells, it enables rapid differentiation into cytotoxic T cells (CTL) and proliferation. It also aids in the induction of IFN γ and granzyme B production in CTL, factors essential in the function of target cell lysis [477]. An IL-2 reporter cell line therefore provides a representative readout of overall T-cell activation, and representative comparable levels of production of a cytokine that plays a vital role in CAR+ve T-cell function.

BWZ.36 T cells are a murine hybridoma fusion cell line, originally generated by Sanderson and Shastri [478], with the *lacZ* gene inserted downstream of four replicate NFAT enhancer elements. The presence of this construct is maintained by cell culture in media containing hygromycin. When the BWZ.36 cell becomes activated by antigenic stimulation, β -galactosidase is produced in the cell and, upon cell lysis, can catalyse a colour-change reaction of the substrate chlorophenol red β -D galactopyranoside (CPRG). The level of T-cell activation can be assessed by the extent of the colour change and resultant photospectrometer absorbance reading. In this chapter the BWZ.36 cells were used in CPRG assays based upon Chen *et al* [479] to investigate and compare the abilities of the CAR constructs to induce T-cell activation, represented by the IL-2 reporter cell response.

BWZ.36 T cells have a rapid proliferation rate, allowing efficient retroviral transduction without the need for prior stimulation. To enable this, the CAR constructs were cloned into a retroviral vector, pMIGR1 (**Figure 5.2**; first described by Pear *et al* [480]). This

vector is derived from murine stem cell virus (MSCV) and is capable of protein expression in a range of mammalian cells. It has the advantage of containing an IRES-eGFP reporter gene to assess transduction efficiency, separate to CAR protein expression. Additionally, it is considered a safe retroviral vector, requiring the additional gag-pol and ecotropic envelope genes to be expressed by the packaging cell line. CAR+ve BWZ.36 cell lines were generated using retroviral spin transduction, and antigen-specific CAR-induced T-cell activation of each was investigated and compared.

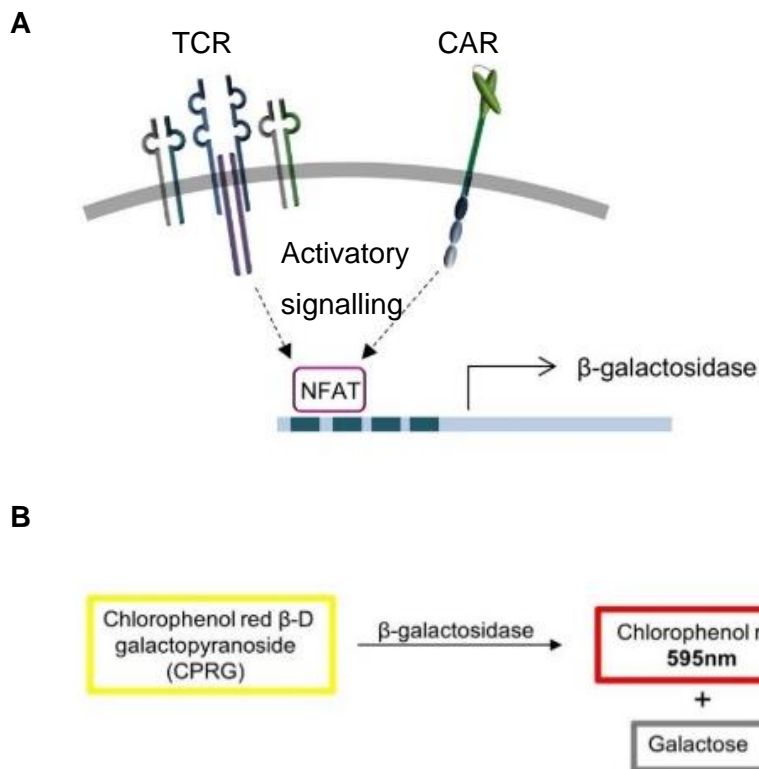


Figure 5.1: An illustration of β -galactosidase production and the catalysis reaction of the BWZ.36 CPRG assay

A: T-cell signalling via the TCR complex, or an expressed CAR construct, leads to dephosphorylation and nuclear translocation of the transcription factor NFAT. In the BWZ.36 reporter cell line, four copies of the NFAT enhancer element precede the *lacZ* gene. T-cell activation therefore results in expression of β -galactosidase within the BWZ.36 cell.

B: β -galactosidase catalyses the hydrolysis of substrate chlorophenol red β -D galactopyranoside (CPRG) to galactose and chlorophenol red. BWZ.36 activation can therefore be ascertained by cell lysis and substrate addition, followed by quantification of chlorophenol red accumulation by reading the absorbance at 595 nm, minus the reference wavelength 655 nm.

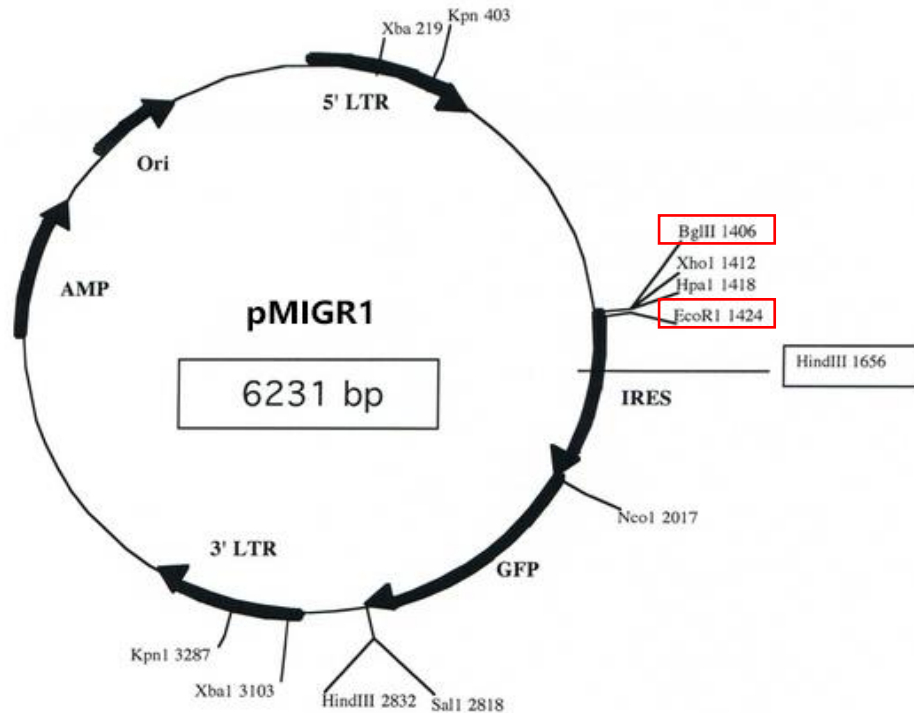


Figure 5.2: Vector map illustrating the retroviral vector pMIGR1

The retroviral vector pMIGR1 is shown, illustrating the enzymatic restriction sites- BglIII and EcoRI- used in CAR construct cloning (red). Also shown is the IRES-eGFP gene that allows independent transcription of the reporter gene. The AMP gene provides a method of prokaryotic selection using ampicillin.

Additionally, studies using the Ritux CAR+ve BWZ.36 reporter cell line were designed to probe the role of antigenic epitope distance from the membrane upon CAR function. It has previously been shown that the membrane proximity of a CAR-targeted epitope can strongly influence the consequent T-cell activation response [373-375]. To directly compare this aspect of CAR design against CD20, a panel of constructs containing the Rp3 cyclic rituximab epitope were employed. The Rp3 epitope (ACPYSNPSLC) was previously described [481], and is effectively bound by rituximab (**Figure 5.3 A**). A panel of fusion proteins containing the Rp3 epitope were previously generated by Dr Kirstie Cleary [464]. Different numbers of CD137 domains were included in these constructs to provide a comparable CD20 epitope, at membrane proximal and distal locations (**Figure 5.3 B**).

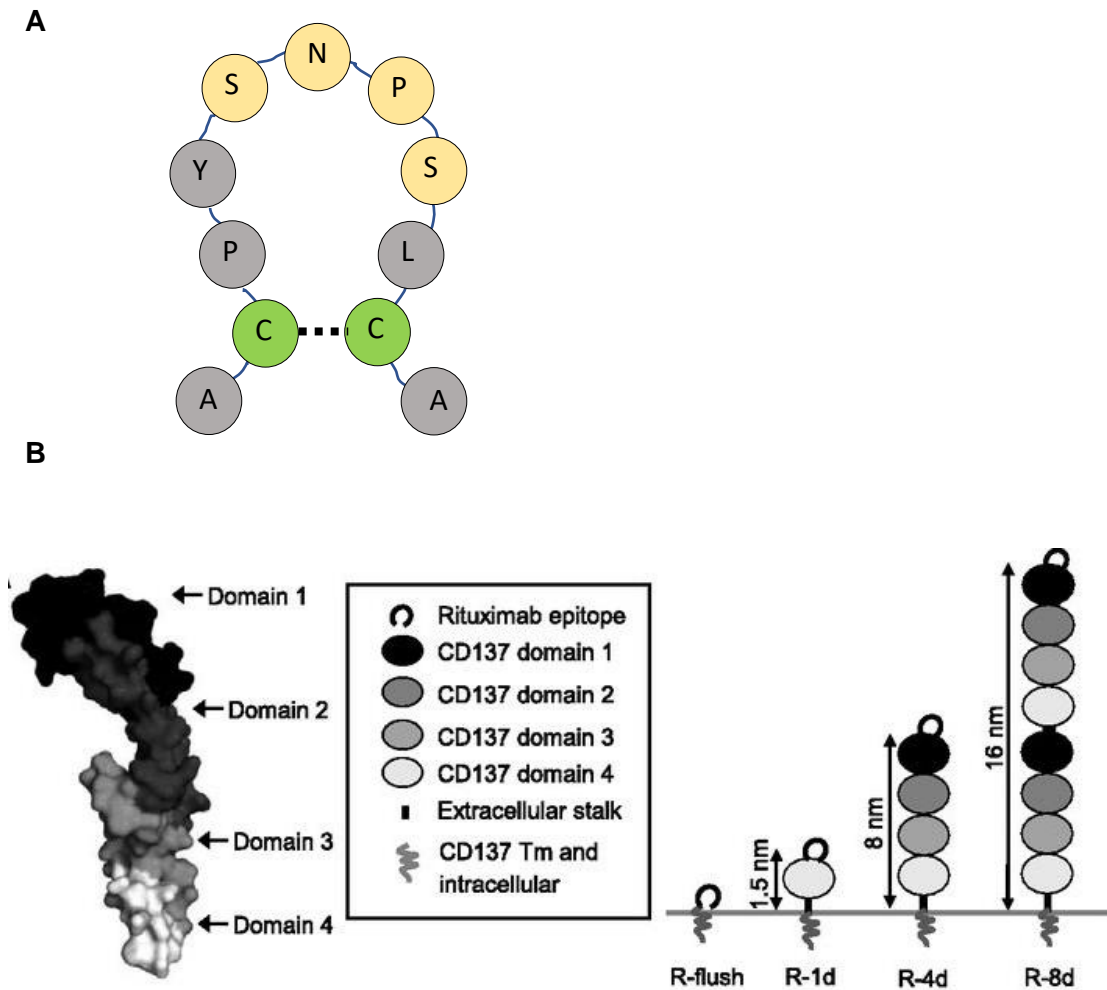


Figure 5.3: Illustration of the Rp3 epitope and CD137 fusion protein constructs

A: An image of the CD20 cyclic Rp3 mimetope. This short epitope contains the ‘SNPS’ motif (yellow), similar to the ‘ANPS’ CD20 epitope bound by rituximab, and is recognised by this mAb. The cyclic nature is maintained by the disulphide bond formation (dashed line) between the two cysteine residues (green).

B: Image taken from Cleary *et al* [464]. The panel of fusion proteins generated by Dr Kirstie Cleary is illustrated. Each contains a different number of CD137 domains, producing the panel of constructs that position the Rp3 epitope at a range of distances from the plasma membrane. R-flush comprises the Rp3 epitope adjoined directly to the transmembrane domain of CD137. R-1d, R-4d and R-8d contain 1, 4 and 8 CD137 domains respectively. Estimated distances between the membrane and the Rp3 epitope are shown in nm.

The final part of this chapter employed another T-cell line, CTLL-2. These cells were the first described example of successful long-term culture of cytotoxic T cells (CTLs) [482]. *In vitro* cytotoxicity assays using CTLL-2 have previously been shown to be an effective way to distinguish between the effects of fusion proteins on killing efficacy [483]. Additionally, it was intended to use CTLL-2 in *in vivo* cytotoxicity experiments. Short-term *in vivo* cytotoxicity assays can be performed by co-injecting high/low CFSE labelled target/non-target cells and T cells into the peritoneal cavity of mice. If the cell populations remain in the peritoneal cavity, they will interact, and specific cytotoxicity of the target cells can occur. The cells are subsequently harvested and the ratio of high/low CFSE analysed to deduce the level of target-specific cell death [484]. For a successful assay, the effector cells must persist short-term *in vivo*, and it was important to determine whether they remain in the peritoneal cavity or track to the blood or internal organs. Thus, the ability of CTLL-2 to survive *in vivo* and the locations that the cells tracked to were characterised in SCID mice. Stably-expressing CAR+ve cell lines were once again generated, using nucleofection and sub-cloning techniques, and the cytotoxic capabilities of CAR+ve CTLL-2 were probed.

5.2 Investigation of CAR-specific T-cell activation

5.2.1 Generation of CAR+ve IL-2 reporter cell lines

Mutagenesis was performed upon the CAR constructs in pcDNA3.1(-) to add additional BglII and EcoRI restriction digest sites at the 5' and 3' ends respectively of each (**Figure 5.4 A**). The presence of an extra BglII site within the pcDNA3.1(-) vector was discounted, as the vector would not be required subsequently. The mutated DNA was transformed into XL-GOLD chemically competent *E. coli* and the amplified DNA was extracted using a Qiagen miniprep kit. After successful mutagenesis was confirmed by enzymatic digestion (**Figure 5.4 B**) and sequencing, each CAR construct was cloned from the pcDNA3.1(-) vector into pMIGR1. Insertion was confirmed by further restriction digests (**Figure 5.4 C, D**) and by sequencing. Each CAR-pMIGR1 plasmid was transformed into JM109 chemically competent *E. coli*. DNA was then extracted using a Qiagen maxiprep kit for use in retroviral transduction.

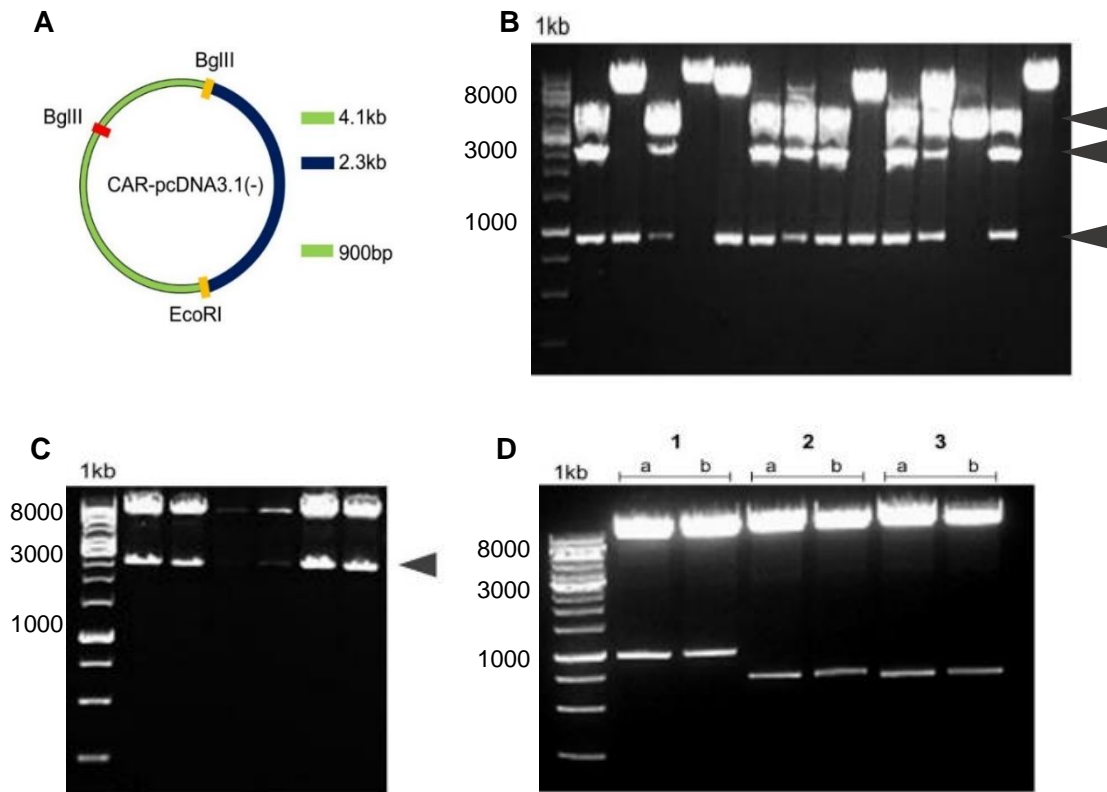


Figure 5.4: Molecular cloning to transfer CAR constructs into the retroviral vector pMIGR1

A: pcDNA3.1(-) vector illustration showing where BglIII and EcoRI sites (yellow) were mutated at the 5' and 3' ends respectively of each CAR. Also shown is the existing BglIII site in the pcDNA 3.1(-) vector (red) and the subsequent DNA band sizes expected after successful mutagenesis.

B: Confirmation of mutagenesis of BglIII and EcoRI sites in an example CAR construct. Lanes show several colonies of the same reaction. Successful mutagenesis is shown by bands at 4.1, 2.3 and 0.9 kb (grey arrows).

C: Confirmation of ligation of an example CAR construct into pMIGR1 via the BglIII and EcoRI sites. Grey arrow indicates bands at expected size for CAR insertion.

D: Restriction digests of each section of an example CAR in pMIGR1 to confirm each fragment remains correctly inserted. Lane 1, leader, enhancer and scFv fragment; 2, IgG spacer; 3, transmembrane and intracellular domains. For each, A: maxiprep DNA, B: miniprep DNA.

B, C, D: DNA was analysed by restriction digests and gel electrophoresis. DNA was stained with GelRed, separated on a 0.7% agarose gel at 120 V and visualised under UV light. Ladders shown are 1kb.

BWZ.36 cells underwent retroviral spin transduction with each of the three CAR constructs, using the Phoenix-ECO packaging system described in Chapter 2.4.1.2.2. Two spin transductions were performed 7 h apart for each, with the addition of polybrene (Millipore) to maximise transduction efficiency. CAR expression was observed at 48 h post transduction by incubation with PE-anti-hIgG-Fc and analysis by flow cytometry. Additionally, due to the presence of the IRES-eGFP in pMIGR1, GFP expression was also observed as a marker of transduction. Pure GFP+ve CAR+ve populations were obtained by cell sorting using a BD FACSAriaII (Chapter 2.5.3). Positive populations were then expanded for use in assays.

Initially Leu16 CAR was transduced into the cells. This transduction was not efficient (**Figure 5.5 A**), so these cells underwent two rounds of cell sorting to generate the pure CAR+ve population required (**Figure 5.5 B**). Prior to subsequent transductions BWZ.36 cells were checked for optimal health to ensure high levels of proliferation required for effective transduction. The second transductions were more efficient, providing higher expression levels for BHH2 CAR and Ritux CAR (**Figure 5.5 C**). The highest expressing GFP+ve CAR+ve populations for each were cell sorted and expanded (**Figure 5.5 D**).

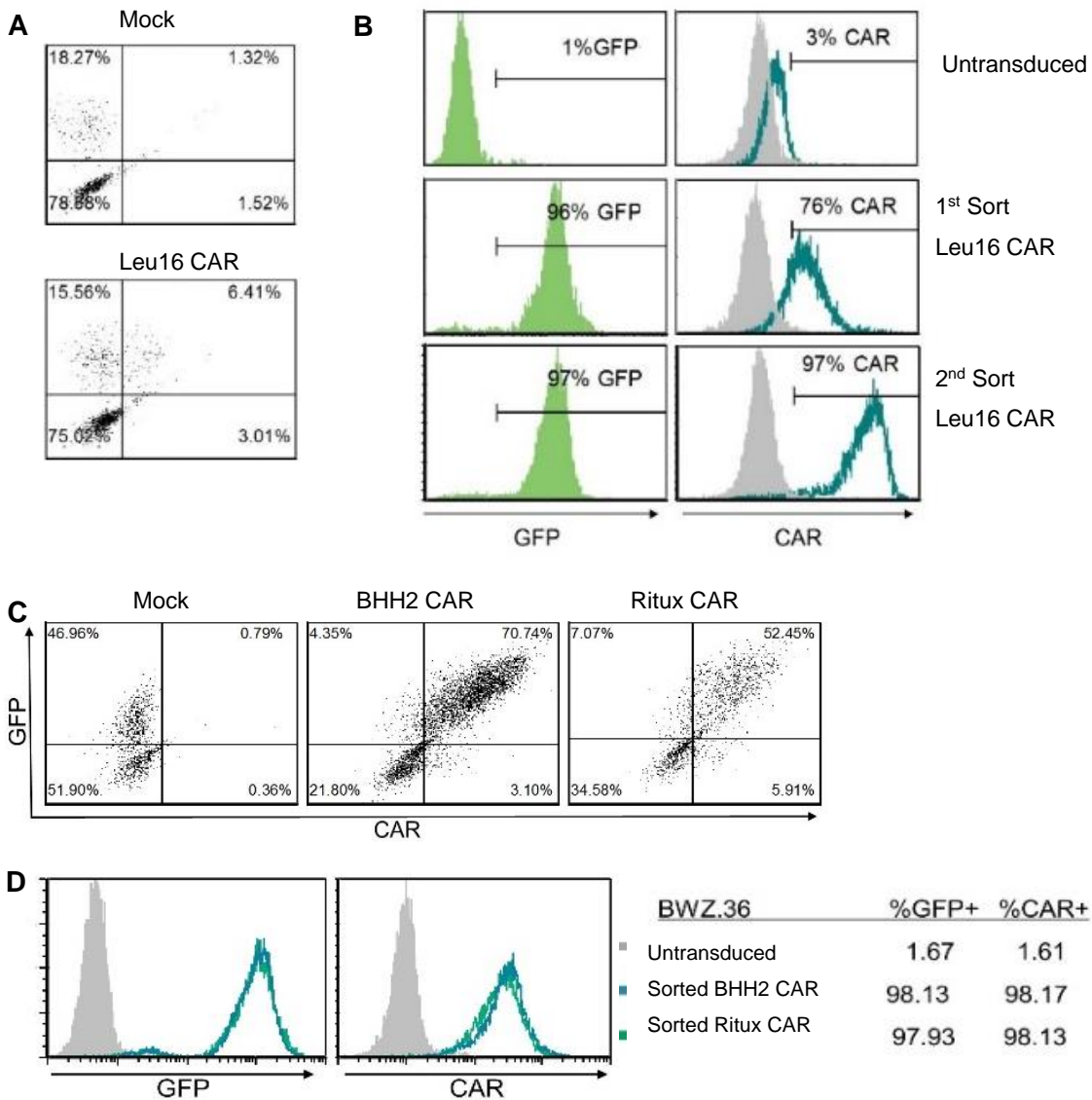


Figure 5.5: Retroviral transduction of BWZ.36 cells

BWZ.36 cells were spin transduced with retroviral supernatant produced by CAR-transfected Phoenix-ECO cells. Media was changed 48 h post-transduction and cells were screened for expression 5-7 d post-transduction. GFP+ve CAR+ve cells were selected by cell sorting using a BD FACSAriaII.

A: Retroviral transduction of BWZ.36 cells with empty vector control and Leu16 CAR. Cells were gated based on FSC-H/SSC-H to exclude debris. CAR+ve and GFP+ve percentages are shown.

B: Positive cell populations from **A** were selected using cell sorting and expanded. 1, untransduced BWZ.36; 2, Leu16 CAR+ve cells sorted once to enrich the positive population; 3, results from a second cell sort of the highest expressing CAR+ve cells. GFP expression, green; isotype control (PE-anti-mIgG-Fc), grey; anti-CAR (PE-anti-hIgG-Fc), teal.

C: Retroviral transduction of BWZ.36 cells with empty vector control and BHH2 and Ritux CARs. Cells were gated based on FSC-H/SSC-H to exclude debris. CAR+ve and GFP+ve percentages are shown.

D: Positive cell populations from **C** were selected using cell sorting and expanded. Untransduced cells (grey) and sorted populations of BHH2 CAR+ve (blue) and Ritux CAR+ve (green) BWZ.36 are shown as percentage positive GFP and CAR.

5.2.2 Assessment of CAR-mediated BWZ.36 activation

To assess the ability of each CAR to activate T cells when expressed on the cell surface, the transduced BWZ.36 reporter cells were used in CPRG reporter assays based upon that by Chen *et al* [479] and detailed in Chapter 2.8.2. Briefly, BWZ.36 cells were incubated for 16 h with target cells in wells of a 96-well plate. Cells were pelleted and lysed, and CPRG substrate was added. After 5 h, the absorbance of each well was read at 595 nm minus the reference wavelength of 655 nm.

Firstly, a CPRG assay was performed to select an effective positive control for subsequent assays. Two clones of anti-murine CD3 mAb, KT3 and 145-2C11, were tested, and also phorbol myristate acetate (PMA)/ionomycin. PMA/ionomycin can elicit a non-specific T-cell activation response, acting as a PKC activator and an ionophore to induce Ca²⁺ signalling respectively. PMA/ionomycin elicited a strong activation response in both mock-transduced and CAR+ve cells (**Figure 5.6**) and was selected as the positive control for use in following CPRG assays. It is likely that the absence of a secondary source of crosslinking of the anti-CD3 mAb lead to their lack of a response.

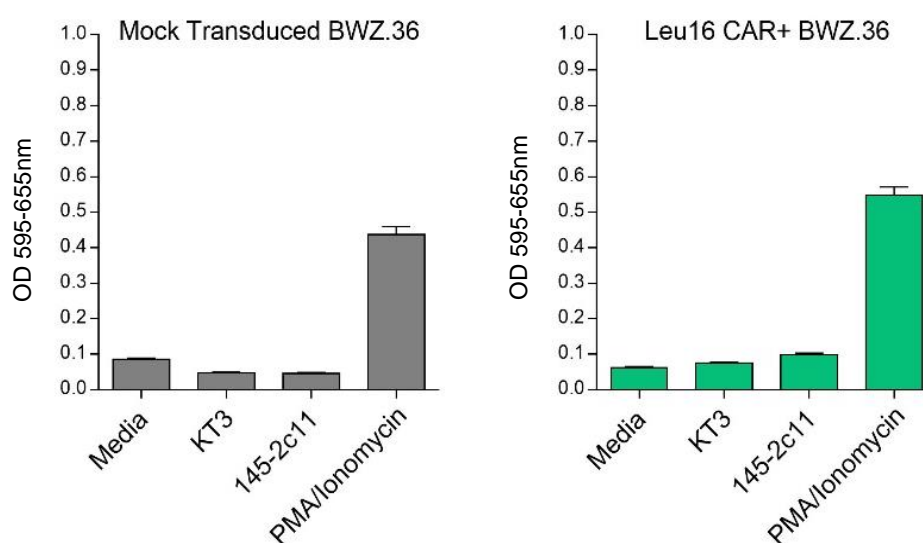


Figure 5.6: Selection of a positive control for CPRG assays

Mock-transduced and Leu16 CAR+ve BWZ.36 cells were incubated for 16 h with either media alone, KT3 (2 µg/ml), 145-2C11 (2 µg/ml), or PMA (50 ng/ml) and ionomycin (750 ng/ml) in wells of a 96-well plate. Cells were pelleted and lysed, and the CPRG substrate was added. Plates were read after 5 h. Shown is the absorbance for each well at 595 nm minus the reference wavelength, 655 nm, representing T-cell activation for each condition; mean +/- range of duplicates.

A preliminary CPRG assay was performed to compare the ability of the three CAR constructs to activate T cells upon target antigen interaction (**Figure 5.7**). Mock

transduced cells were also included in the assay to confirm that any activation was CAR-specific. The assay used the same effector:target ratios as in the CAR-CD20 binding assays (**Figures 2.2, 2.4 and 2.5**). CAR+ve cells were incubated with a CD20+ve target cell line, a CD20-ve cell line or PMA/ionomycin, and the BWZ.36 activation level observed. Each BWZ.36 population responded to the positive control, although the level of activation differed between the CAR+ve cell lines. This may be due to the health of the cells at the time of the assay dictating their ability to produce a maximal response. Alternatively, it must be noted that the cell sorting process to generate the pure CAR+ve populations may have selected certain cells and skewed the populations away from the untransduced native cell line. However, even in this case, the comparison between the positive control response and the CD20+ve target cell response is still a valid report of CAR-specific activation for each cell line.

The highest T-cell activation was seen with BHH2 CAR, despite a reduced response from incubation with PMA/ionomycin, whilst Leu16 CAR produced a much lower level of activation (**Figure 5.7**). Ritux CAR+ve BWZ.36 was seen to have a slightly raised background activation level when incubated with media alone, or a CD20-ve cell line, whilst BHH2 and Leu16 CAR BWZ.36 did not show such a response. Ritux CAR was shown to be capable of stimulating the T cells upon CD20 interaction and, taking into account the increased background observed and the activation level from the positive control, was shown to elicit an intermediate response. **Figure 5.8** shows a photographic image of the CPRG assay plate. The different levels of activation produced by the three CAR constructs interacting with CD20+ve target cells are clear by the colour change reaction upon CPRG substrate addition.

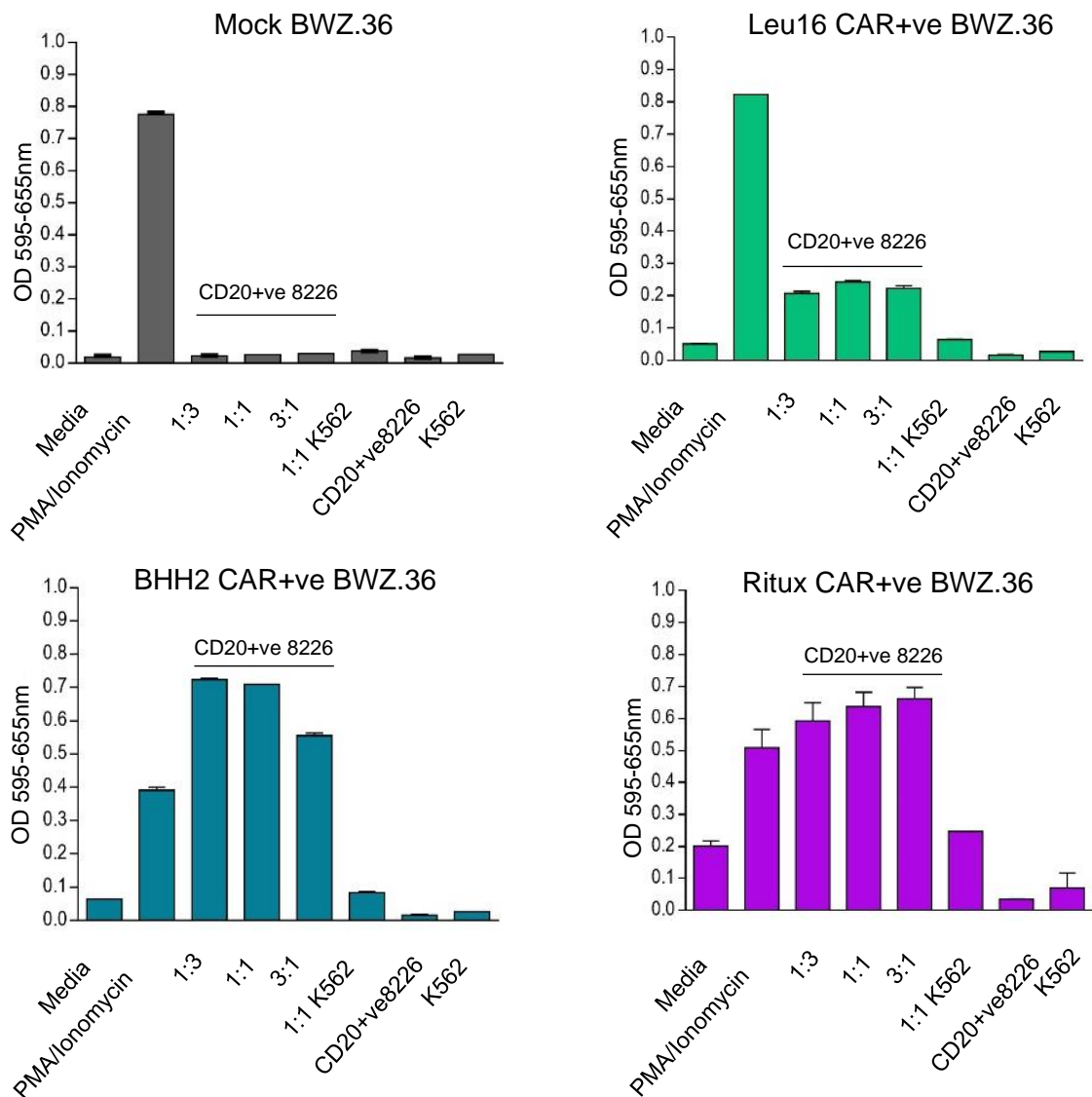


Figure 5.7: CPRG assay with CAR+ve BWZ.36 cells and CD20+ve target cells to investigate CAR-induced T-cell stimulation.

Co-cultures were performed for 16 h at 37 °C of CAR-ve and each CAR+ve BWZ.36 cell line with CD20+ve RPMI8226 (CD20+ve8226, at effector:target ratios shown on x-axis) or CD20-ve K562. Incubations were performed in a total volume of 200 µl, before cells were pelleted and lysed. CPRG substrate was added to each well and plates were read after 5 h at 595 nm minus the reference wavelength of 655 nm. Negative controls included incubating BWZ.36 with media alone. PMA/Ionomycin was used as a positive control for T-cell stimulation. CD20+ve RPMI 8226 and K562 cells alone with no BWZ.36 cells were also included, to exclude any background absorption. Mean +/- range of duplicates.

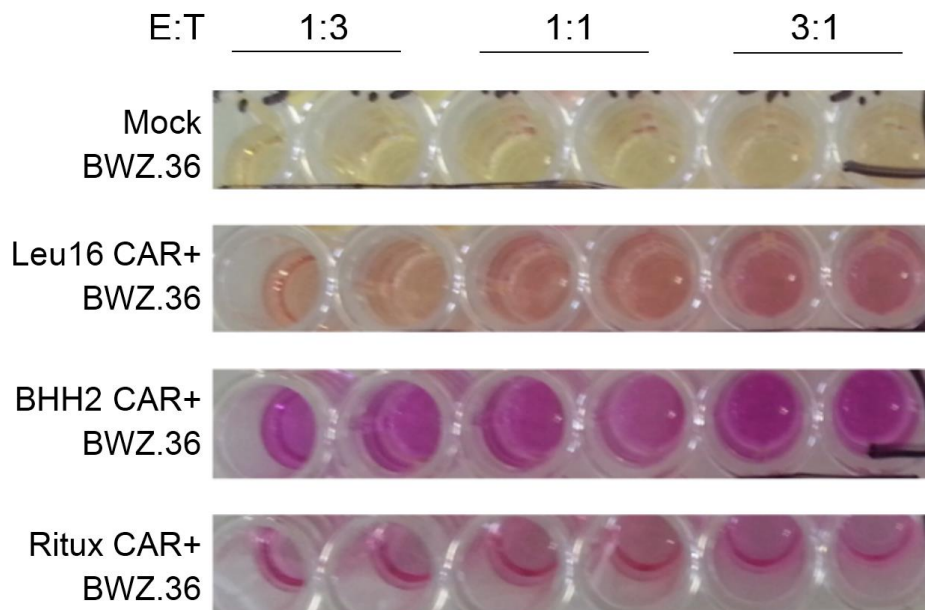


Figure 5.8: Photographic image of a CPRG assay plate

The CPRG substrate is hydrolysed by β -galactosidase- produced by activated BWZ.36 cells- resulting in a colour change from yellow to red/purple. This change is quantified by reading the absorbance at 595 nm, minus the reference wavelength 655 nm, and is representative of T-cell activation levels. E:T, effector:target ratio. Shown are wells from an assay including Mock-transduced and Leu16, BHH2 and Ritux CAR+ve BWZ.36 cells co-cultured for 16 h with CD20+ve RPMI 8226 cells at the ratios shown. Cells were pelleted and lysed, CPRG substrate added and plates read after 5 h.

To confirm that the T-cell activation seen in the previous assay was CD20-specific, CHO-S cells were transiently transfected with CD20, providing a direct comparison of the effect of the presence or absence of the antigen (**Figure 5.9 A**). In a CPRG assay with Ritux CAR+ve BWZ.36 co-cultured with CD20+ve and CD20-ve CHO-S cells, CD20 was proved to be essential for T-cell activation (**Figure 5.9 C**). Additionally, an assay was performed comparing responses to CD20+ve and CD20-ve RPMI8226 target cells, a CD20 negative human B lymphocyte cell line [485]. Previous nucleofection (performed by Dr Andrew Vaughan) established a population expressing CD20 (**Figure 5.9 B**). In the absence of CD20, no BWZ.36 response above background is observed with any CAR. In the presence of CD20+ve RPMI8226, the CAR+ve BWZ.36 cells are activated (**Figure 5.9 D**).

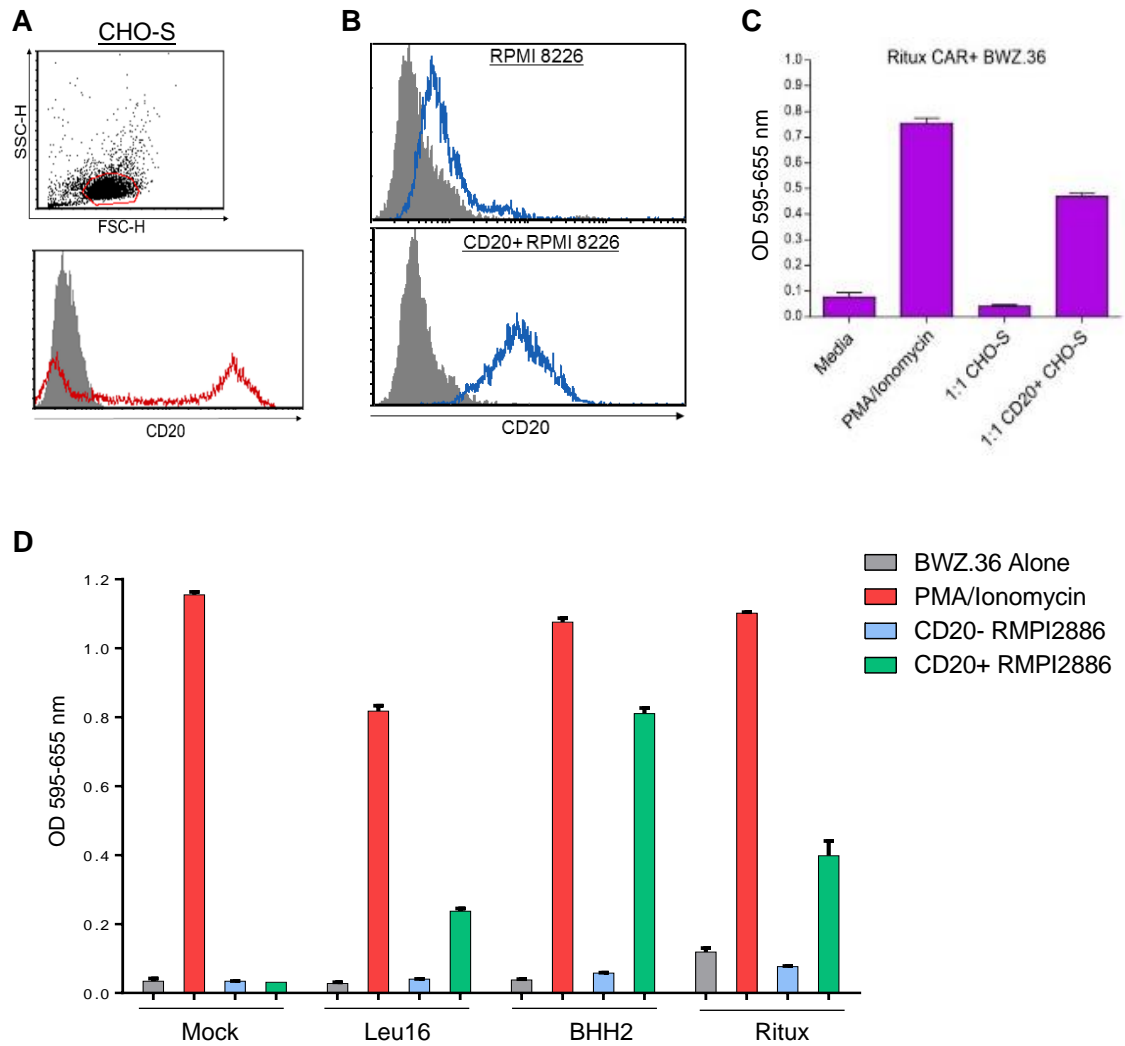


Figure 5.9: CPRG assay to investigate the specificity of CAR-induced T-cell activation.

A: Flow cytometry plots showing CD20 expression on transiently transfected CHO-S cells at 24 h post-transfection. Gate excluding cell debris based upon FSC-H/SSC-H is shown. Grey, isotype control; red, rituximab.

B: Flow cytometry plots showing CD20 expression on untransfected RPMI 8226 cells, and those previously nucleofected by Dr Andrew Vaughan to express CD20. Grey, isotype control; blue, rituximab.

C: Ritux CAR+ve BWZ.36 cells were co-cultured with mock-transfected CHO-S cells or CD20-transfected CHO-S cells. N=1.

D: Mock-transduced and each CAR+ve BWZ.36 cell line were co-cultured with CD20+ve or CD20-ve RPMI 8226 cells. Representative of n=2.

C and D: OD 595-655nm depicts assay absorbance readout, representing T-cell activation response. Mean+/- range.

The CPRG assay was repeated multiple times to compare the T-cell responses with the three CAR constructs (**Figure 5.10 B**). For these repeat experiments, the CD20+ve RPMI8226 cells and Ramos cells were used as the target populations. The comparative CD20 expression of these lines is shown in **Figure 5.10 A**.

BHH2 CAR consistently elicited the highest BWZ.36 reporter response, similar to that with PMA/ionomycin. The Ritux and Leu16 CARs showed a considerably lower level of activation. Interestingly, in the case of the two lower-activating CAR constructs, CD20+ve RPMI8226 cells stimulated the BWZ.36 cells more strongly than Ramos target cells. This difference was not seen with BHH2 CAR.

When the means of these data (from **Figure 5.10**) are normalised to percentage of maximal response, the differences remain clear (**Figure 5.11**). Analysing the data in this way allows BWZ.36 cell health, CAR background reactivity levels, and the selection process of cell sorting all to be taken into account. When observed as percentage maximal response, Leu16 and Ritux CAR were shown to be capable of similar levels of antigen-specific BWZ.36 activation.

Figure 5.12 shows statistical analysis of the same data (from **Figures 5.10** and **5.11**). BHH2 CAR elicited a significantly higher BWZ.36 activation level compared to both other CARs when Ramos cells were the target population. A significant difference is also seen when BHH2 CAR+ve and Leu16 CAR+ve BWZ.36 cells are incubated with CD20+ve RPMI8226 cells. BHH2 CAR+ve cells showed a significantly superior response to Ritux CAR+ve BWZ.36 cells incubated with CD20+ve RPMI8226 at the effector:target ratio of 1:3. With the exception of an effector:target ratio of 1:1 with CD20+ve RPMI8226 cells, no significant difference was observed between Ritux CAR+ve and Leu16 CAR+ve BWZ.36 cells.

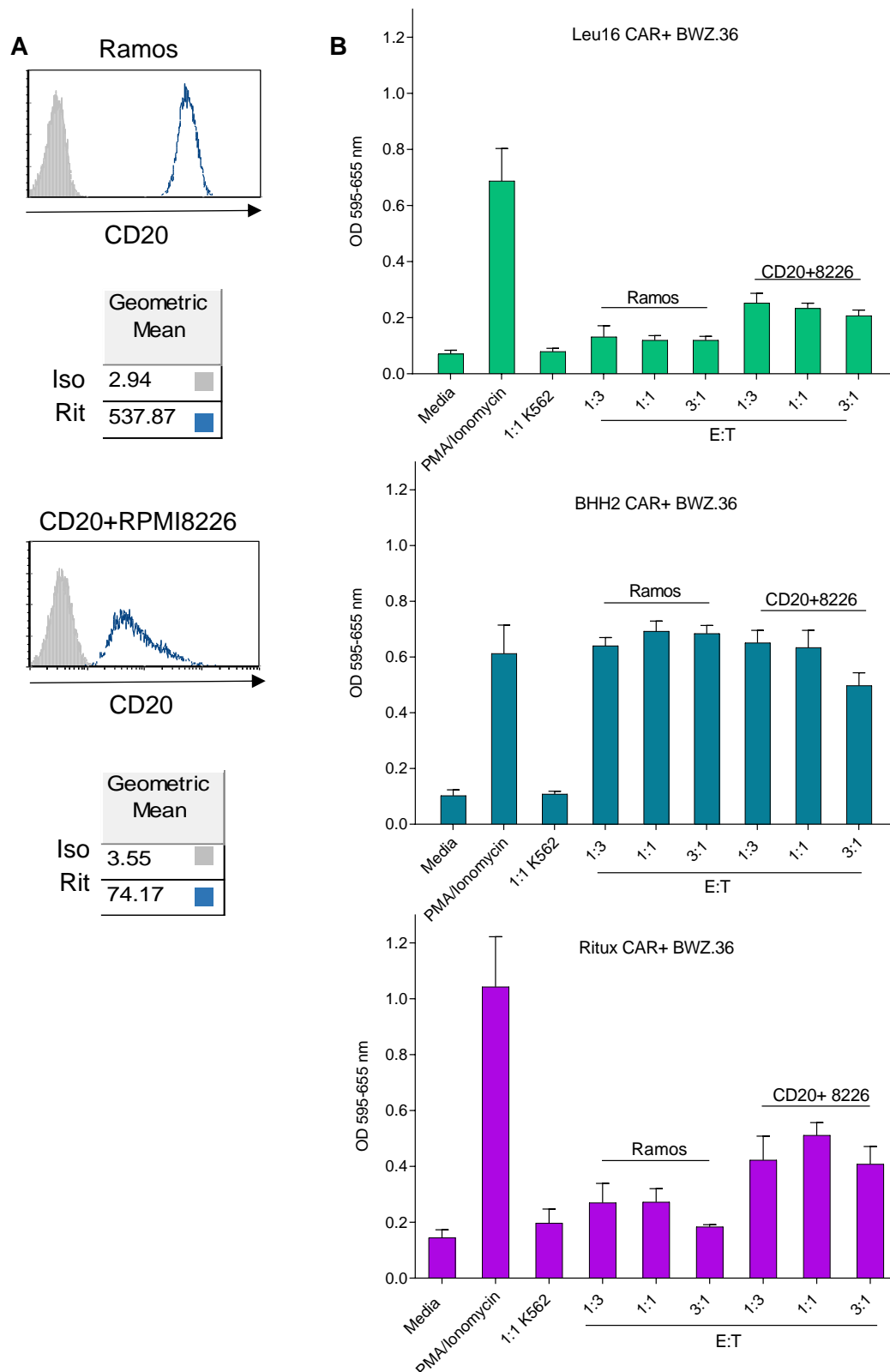


Figure 5.10: Combined data of CPRG assay repeats

A: CD20 expression profiles of target cells used in repeat CPRG assays, as assessed by rituximab staining (blue). Isotype is shown in grey.

B: Data from repeated CPRG assay repeats were combined to compare consistent differences between T-cell activation elicited by the CAR constructs. OD 595-655nm depicts assay absorbance readout, representing T-cell activation response. E:T, effector:target ratio. Target cells shown are Ramos and CD20+ve transfected RPMI8226 (CD20+8226). Mean +/- SEM of 3-7 independent experiments.

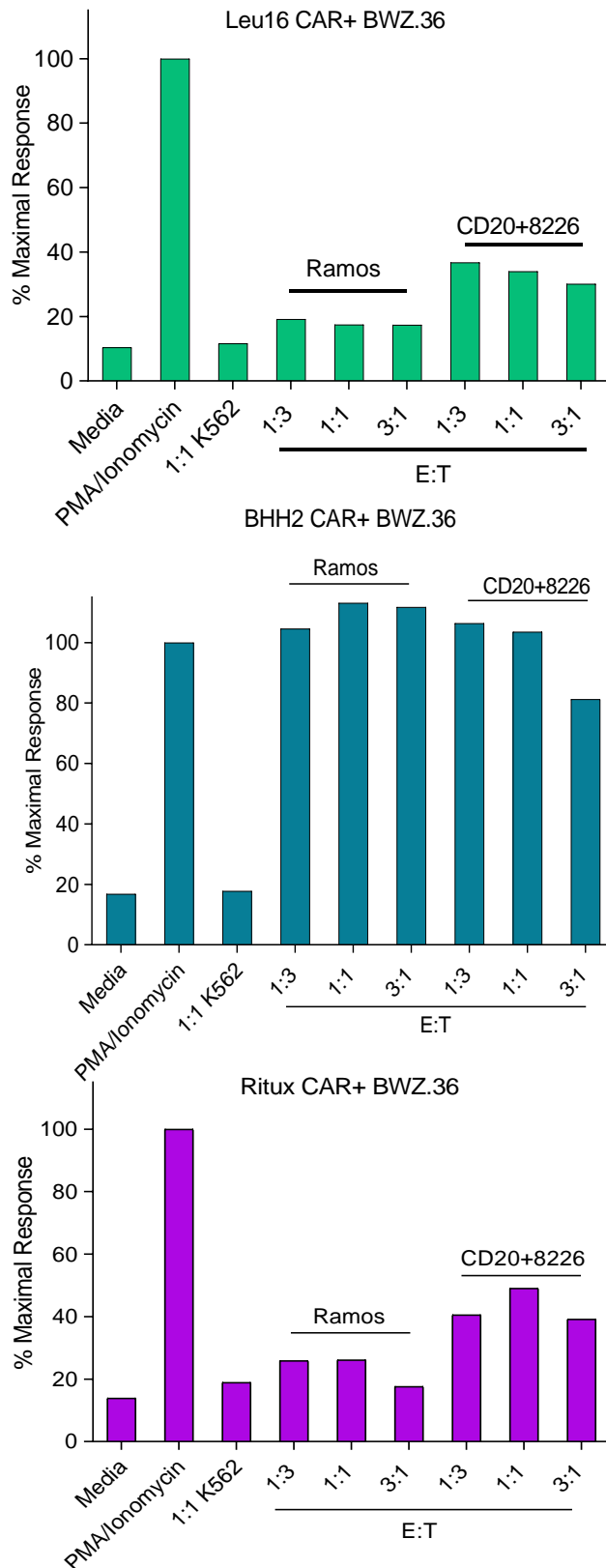


Figure 5.11: Combined data of CPRG assay repeats shown as percentage maximal response

The mean responses from **Figure 5.10** are shown for each CAR as a percentage response of that seen with the positive control of T-cell stimulation (PMA/ionomycin). OD 595-655nm depicts assay absorbance readout, representing T-cell activation response. E:T, effector:target ratio. Target cells shown are Ramos and CD20+ve transfected RPMI8226 (CD20+ve8226).

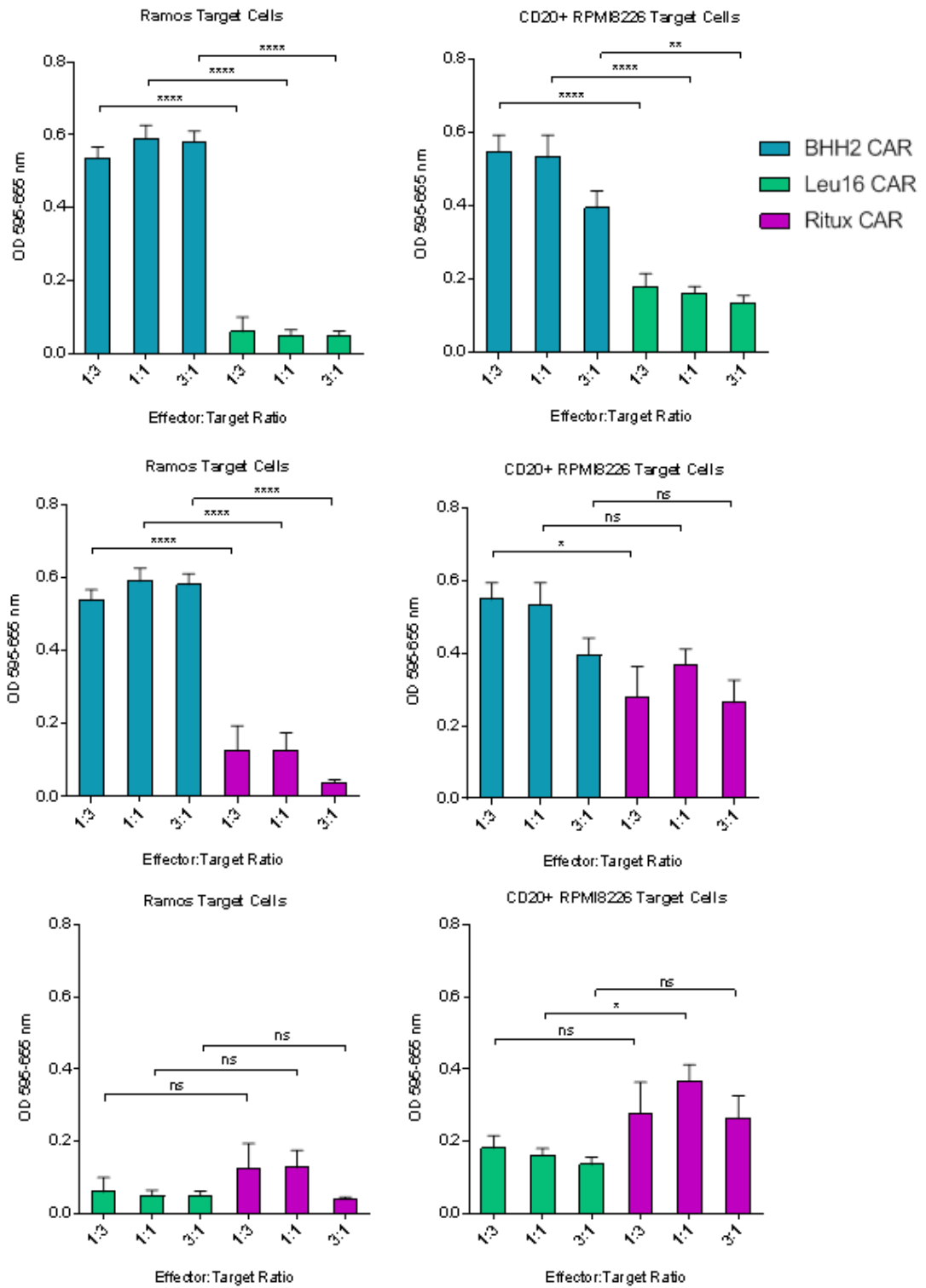


Figure 5.12: Combined data of CPRG assay repeats compared using one-way ANOVA tests

Data from **Figure 5.10** are shown for each CAR co-cultured with CD20+ve target cells, compared to the equivalent ratios of each other CAR+ve BWZ.36-CD20+ve target co-culture. The mean background absorbance from incubation with media alone for each CAR was subtracted before one-way ANOVA tests were performed to determine statistical significance. OD 595-655 nm depicts assay absorbance readout, representing T-cell activation response. Stars show significance (* p<0.05; ** p<0.01; *** p<0.001; **** p<0.0001). ns= not significant.

5.2.3 Investigation of the relationship between CAR expression and T-cell activation level

The effect of CAR expression levels upon BWZ.36 activation responses was investigated to determine if this was responsible for the differences observed. Initially CPRG assays were performed comparing BHH2 CAR+ve BWZ.36 cells with Leu16 CAR+ve or Ritux CAR+ve BWZ.36 cells at equivalent expression levels, as determined by the geometric MFI measured by flow cytometry (**Figure 5.13**). At similar expression levels, BHH2 CAR was observed to elicit a superior BWZ.36 activation response compared to both the other two CARs, with both Ramos and CD20+ve transfected RPMI8226 target cells. This demonstrated that the differences in T-cell responses seen between the CAR constructs were not due to different expression levels.

Repeated CPRG assays were performed to compare BHH2 CAR+ve and Leu16 CAR+ve BWZ.36 cells at varying expression levels (**Figure 5.14**). It was observed that BHH2 CAR elicited a high BWZ.36 activation response irrespective of the CAR expression level with a strong response even at a very low level of expression. The T-cell activation responses produced by Leu16 CAR were consistently lower than for BHH2 at each expression level. In each case no correlation is seen between MFI and T-cell activation response, as assessed using an F test ($p > 0.2$ for each point).

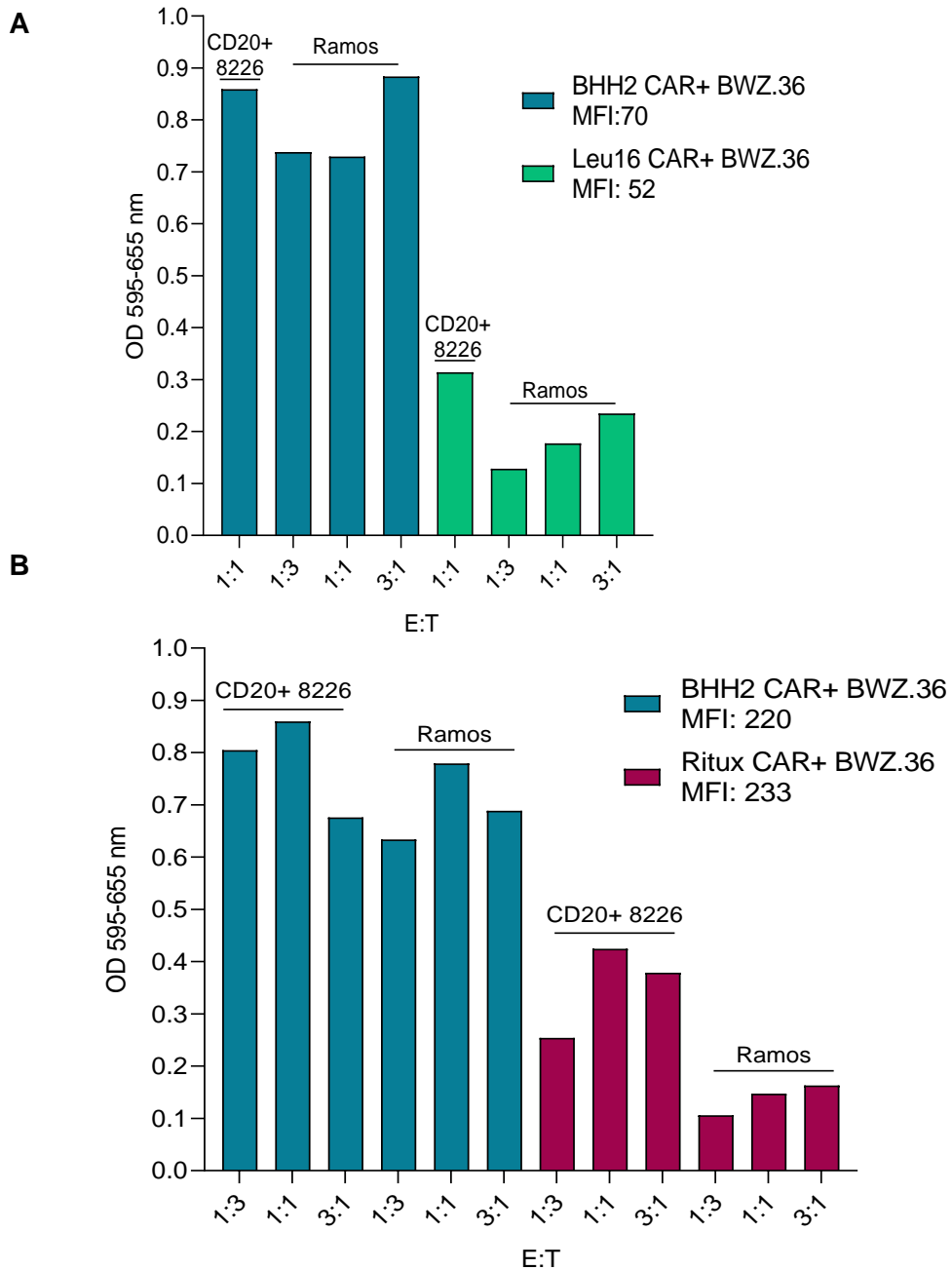


Figure 5.13: CPRG assays comparing CAR+ve BWZ.36 cells with equivalent CAR expression levels.

CPRG assay co-cultures were performed using CAR+ve BWZ.36 cells with similar expression levels with CD20+ve RPMI8226 (CD20+8226) and Ramos cells as target populations.

Expression levels (geometric MFI) of CARs were assessed immediately prior to the assay co-culture. OD 595-655 nm depicts CPRG assay absorbance readout. E:T, effector:target ratio. Mean of duplicates.

A: BHH2 CAR+ve BWZ.36 cells, MFI 70; Leu16 CAR+ve BWZ.36 cells, MFI 52. N=1.

B: BHH2 CAR+ve BWZ.36 cells, MFI 220; Ritux CAR+ve BWZ.36 cells, MFI 233. N=1.

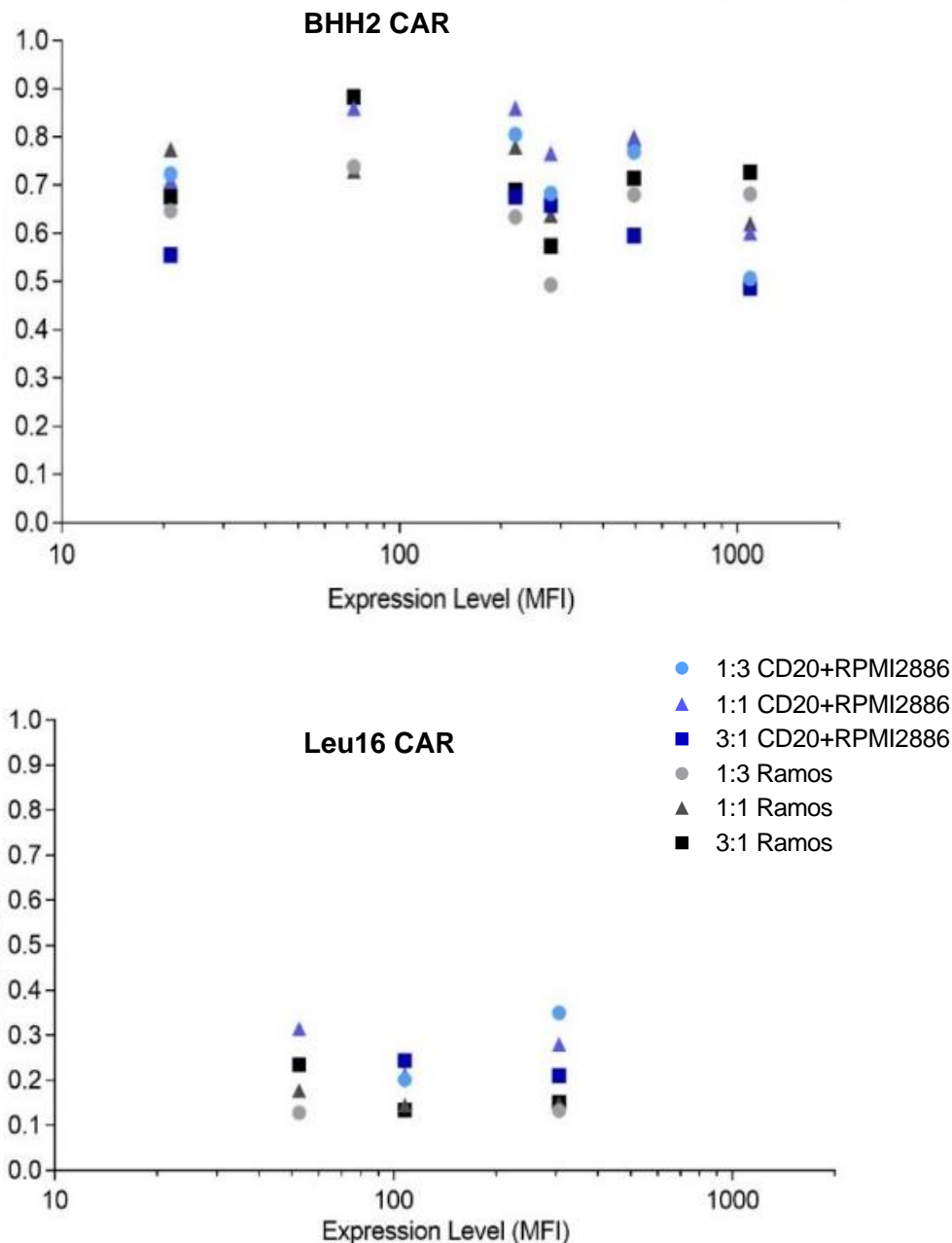


Figure 5.14: CPRG assays comparing the BWZ.36 activation responses of BHH2 CAR+ve and Leu16 CAR+ve cells at a range of expression levels.

CPRG assays were performed incorporating Leu16 or BHH2 CAR+ve BWZ.36 cells with varying levels of CAR expression. Expression levels (geometric MFI) of CARs were assessed immediately prior to the assay co-culture. Target cell type and effector:target ratios are shown in key. OD 595-655nm depicts assay absorbance readout. Each data point represents mean of duplicates. An F test was used to evaluate the existence of a correlation between MFI and OD and showed no significance for either CAR ($p > 0.2$ for all points).

5.3 Investigating the role of epitope distance from the membrane upon CAR function

The panel of constructs previously generated by Dr Kirstie Cleary [464] containing the cyclic epitope for rituximab, Rp3, were employed (**Figure 5.3**). The Ritux CAR+ve BWZ.36 cell line was used in CPRG assays with Rp3+ve target cells, to compare the T-cell activation responses.

Initially a stably-transfected A20 cell line, previously generated by Dr Kirstie Cleary, was used. Cells expressing Rp3 flush (Rp3 FD; epitope positioned directly at the cell surface) and 8 domain (8D; epitope held at a distance of 8 repeating CD137 domains) were selected first to investigate if the inclusion of the most proximal and distal epitopes altered the CAR+ve BWZ.36 activation. Expression of the Rp3 epitope on sub-cloned populations of the original nucleofection performed was assessed, and two with similar expression levels were selected (**Figure 5.15 A**). To ensure the Rp3 epitope was able to fold and be maintained correctly on the A20 cells, no β -mercaptoethanol was added the BWZ.36 cell media used in the CPRG assays. A CPRG assay was performed with BWZ.36 and Ritux CAR+ve BWZ.36 cells, and the FD and 8D Rp3 A20 cells as the target cell population (**Figure 5.15 C**). However, in this experiment there was no specific response to the Rp3+ve A20 cell compared with the untransfected A20 cells.

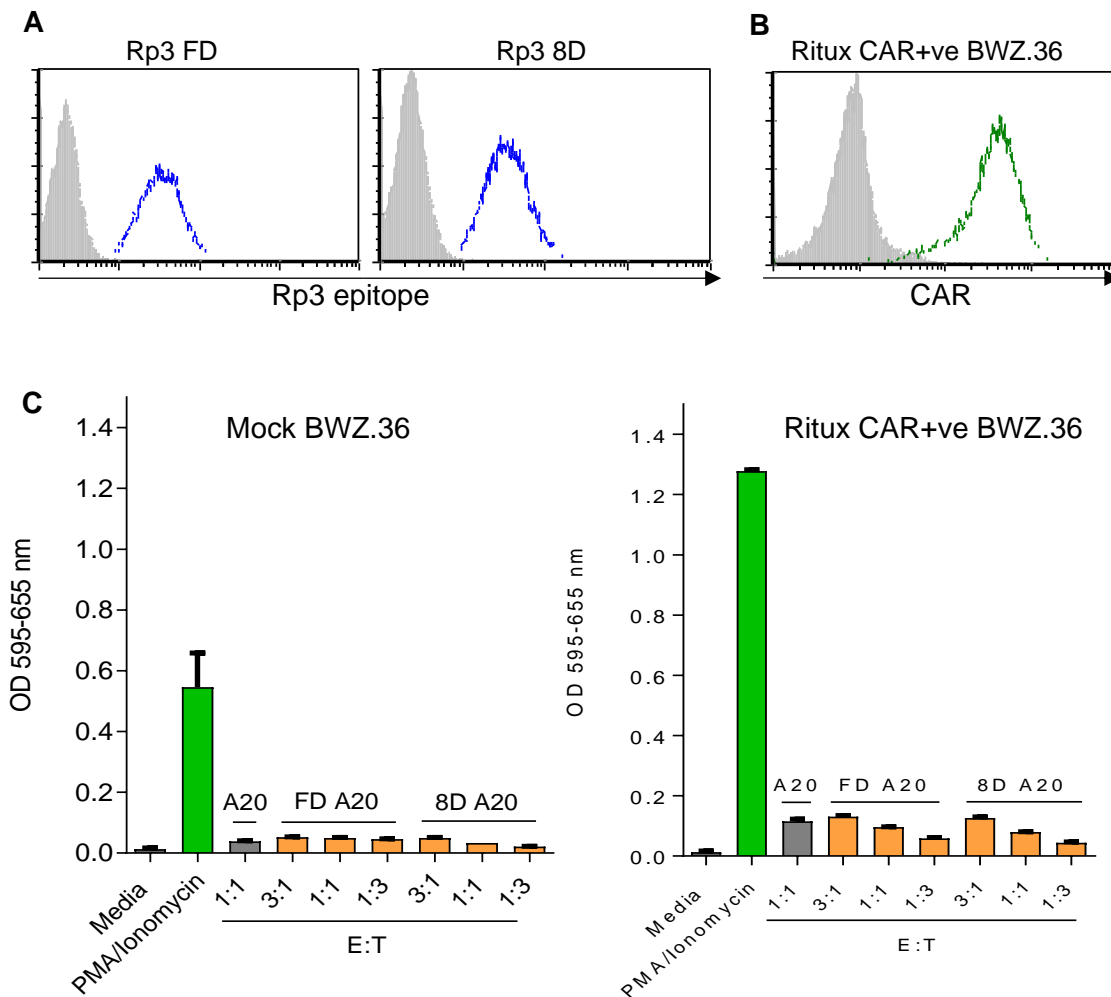


Figure 5.15: CPRG assay comprising A20 cells expressing Rp3 epitope constructs as the target population.

A: Expression of the flush-Rp3 (FD) and 8 domain-Rp3 (8D) constructs on nucleofected A20 cell populations. Cells were incubated with FITC-labelled rituximab and protein expression was assessed by flow cytometry. Isotype control (anti-CD52) staining is shown in grey, rituximab staining in blue.

B: Confirmation of Ritux CAR expression on the BWZ.36 cells prior to inclusion in the assay assessed using PE-anti-hlgG-Fc (green). Isotype control (PE-anti-mIgG-Fc), grey.

C: CPRG assay using mock transduced and Ritux CAR+ve BWZ.36 cells, co-cultured with A20 target cells expressing flush domain (FD) and 8 domain (8D) Rp3 epitope constructs (yellow). Media alone, and untransfected A20 cells were included as negative controls (grey). PMA/ionomycin was used as the positive control for T-cell activation (green). OD 595-655 nm depicts assay absorbance readout, representing BWZ.36 activation response. E:T, effector:target ratio. Mean+/- range of duplicates.

To determine if the A20 cells were inhibiting a CAR-specific T-cell response to the Rp3 epitopes, the experiment was repeated using HEK 293F cells. These were transiently transfected with each of the Rp3 constructs and expression was measured using FITC-rituximab labelling at 24 h post-transfection. As a positive control for use of a non-pure target population, CD20+ve RPMI8226 cells were selected that expressed CD20 in a similar heterogeneous expression profile to the transiently transfected HEK 293F (**Figure 5.16 A**).

A CPRG assay was performed including mock-transduced and Ritux CAR+ve BWZ.36 co-cultured with HEK 293F cells expressing Rp3 1 domain, 4 domain and 8 domain constructs (**Figure 5.16 B**). These were selected as the expression profiles from transfection were comparable. The flush Rp3 construct was not used in this assay due to its lower expression. The Ritux CAR+ve BWZ.36 were activated by CD20+ve RPMI8226 and Ramos cells as previously, demonstrating a CAR-specific response; the mock transfected cells showed no response. However, the response of the Ritux CAR+ve BWZ.36 to the Rp3 transfected HEK 293F cells was no higher than the mock-transfected cells, indicating no CAR-specific activation with these targets

CHO-S cells were transiently transfected with each Rp3 construct and the CPRG assay was repeated using these as the target population. All four Rp3 constructs were included in co-cultures with mock-transduced and Ritux CAR+ve BWZ.36 cells. No T-cell activation was observed for BWZ.36 cells with any of the Rp3 constructs, regardless of Ritux CAR expression. Ritux CAR+ve BWZ.36 again demonstrated a T-cell response to CD20+ve RPMI8226 cells but did not react to any of the Rp3+ve cells (**Figure 5.17**).

To ascertain whether the lower expression of a transient transfection was incapable of inducing BWZ.36 activation, CHO-S cells were transiently transfected with CD20 and 4D Rp3 (**Figure 5.18 A**). Whilst the transient expression of CD20 is overall higher than that of 4D Rp3, there is a similar heterogeneous expression profile, typical for transient protein expression. A low-expressing population of CD20+ve RPMI8226 cells was also selected. The CPRG assay was repeated, incorporating mock-transduced and Ritux CAR+ve BWZ.36 cells co-cultured with untransfected, CD20+ve and 4D Rp3+ve CHO-S cells (**Figure 5.18 B**).

Ritux CAR induced T-cell activation when co-cultured with CD20+ve RPMI8226 and CD20+ve CHO-S cell target populations. However, there was no response with 4D Rp3+ve CHO-S cells. It can therefore be concluded that Ritux CAR is not capable of sufficiently binding to the Rp3 epitope to allow a BWZ.36 activation response, despite this epitope being efficiently bound by rituximab.

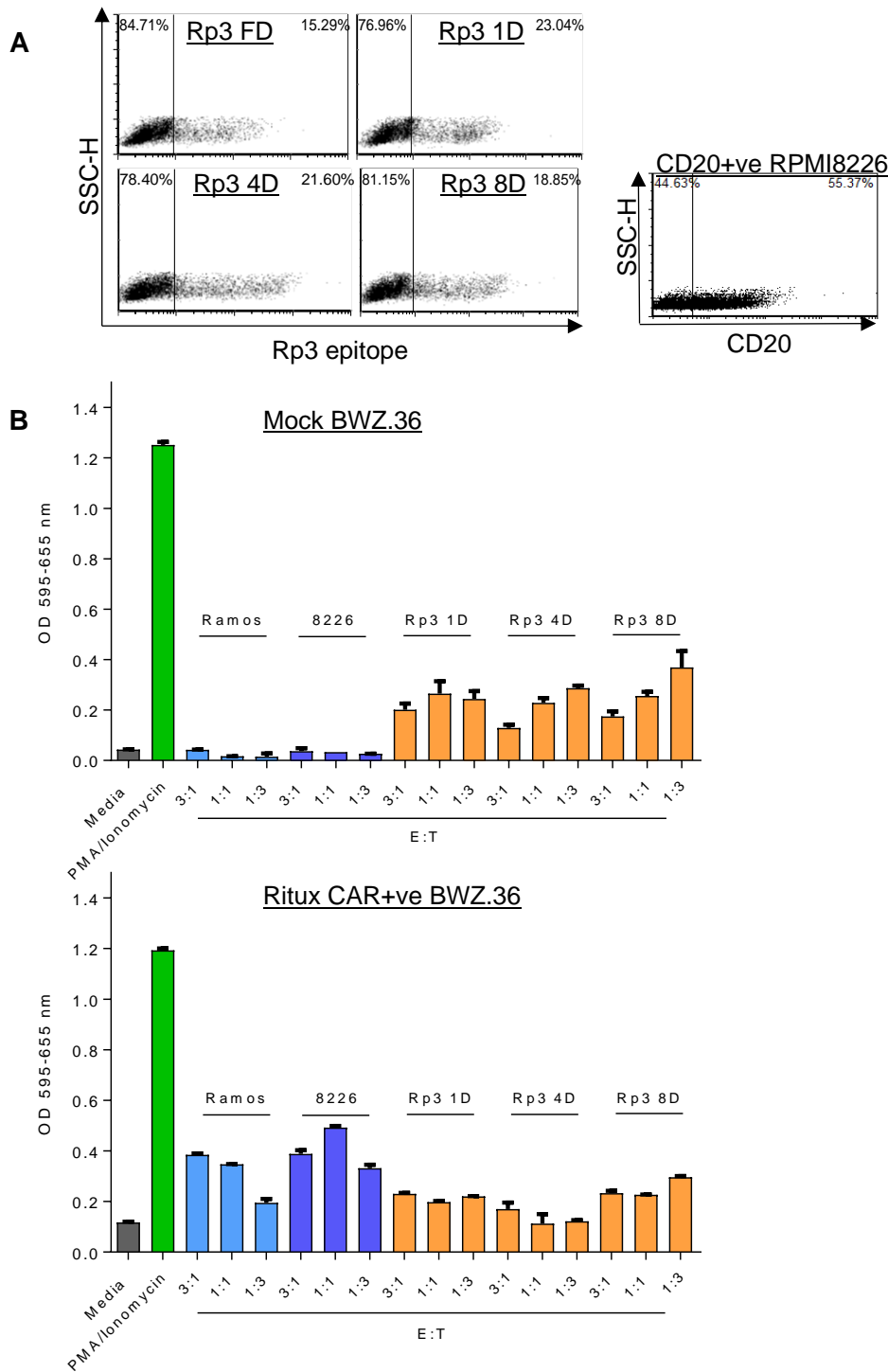


Figure 5.16: CPRG assay incorporating HEK 293F cells transfected with Rp3 epitope constructs as target cell population.

A: Transient expression of Rp3 epitope constructs on HEK 293F cells 24 h post-transfection, assessed using FITC-rituximab. Flush (FD), 1 domain (1D), 4 domain (4D) and 8 domain (8D) constructs are shown. CD20 expression on stably transfected RPMI2886 cells is also shown.

B: CPRG assay comprising mock-transduced and Ritux CAR+ve BWZ.36 cells with 1D, 4D and 8D Rp3+ve HEK 293F target cells (yellow). CD20+ve control populations are shown in blue (Ramos) and purple (CD20+ve RPMI8226). Addition of media alone was used to determine background activation levels (grey). Maximal T-cell activation response was induced using PMA/ionomycin (green). OD 595-655 nm depicts assay absorbance readout. E:T, effector:target ratio. Mean +/- range of duplicates, n=1.

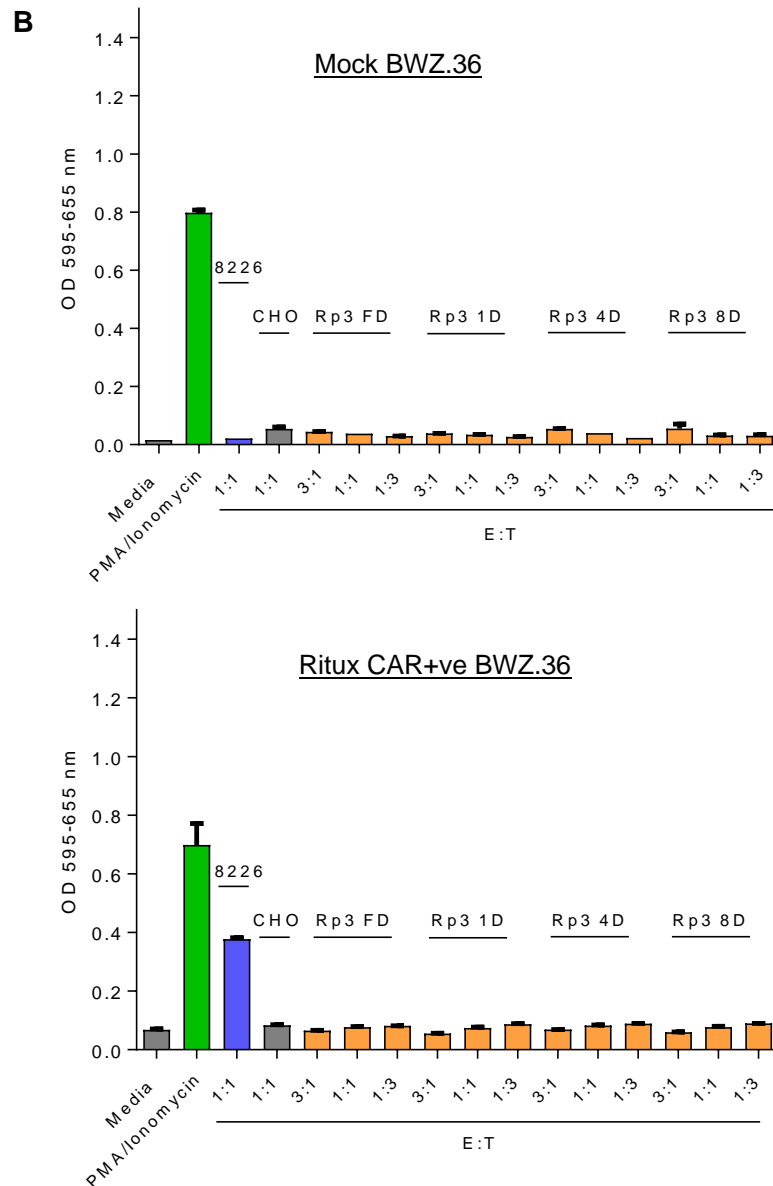
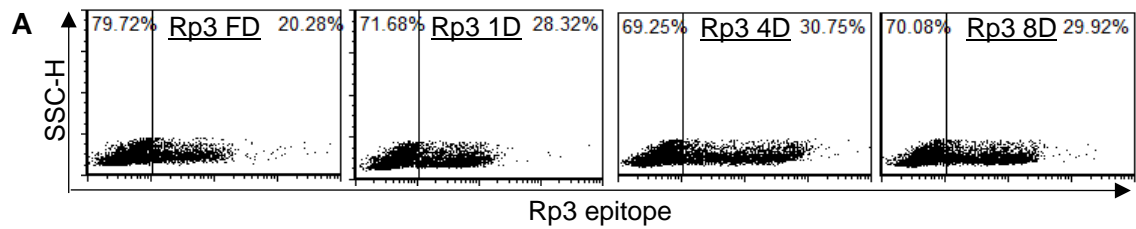


Figure 5.17: CPRG assay incorporating CHO-S cells transfected with RP3 epitope constructs as targets.

A: Transient expression of Rp3 epitope constructs on CHO-S cells 24 h post-transfection, assessed using FITC-rituximab. Flush (FD), 1 domain (1D), 4 domain (4D) and 8 domain (8D) constructs are shown.

B: CPRG assay comprising mock transduced and Ritux CAR+ve BWZ.36 cells with transfected CHO-S (CHO) target cells expressing Rp3 epitope constructs (yellow). CD20+ve RPMI8226 cells (8226, purple) were included as a positive control. PMA/ionomycin was used to induce maximal BWZ.36 response (green). Negative controls used were addition of media alone, and addition of untransfected CHO-S cells (grey). OD 595-655 nm depicts assay absorbance readout. E:T, effector:target ratio. Mean +/- range of duplicates, n=1.

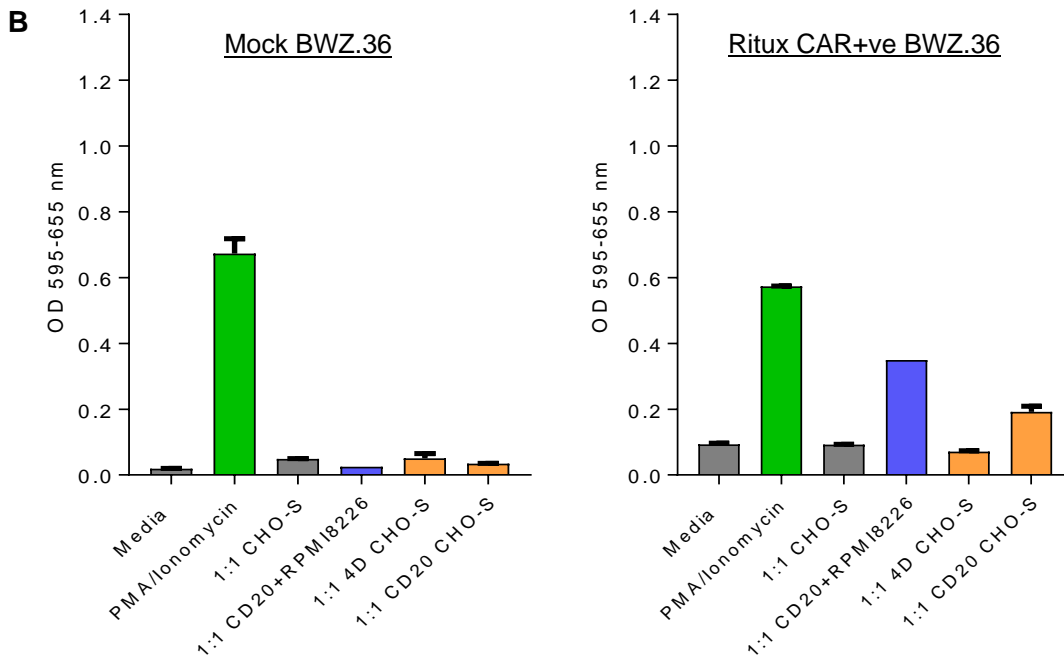
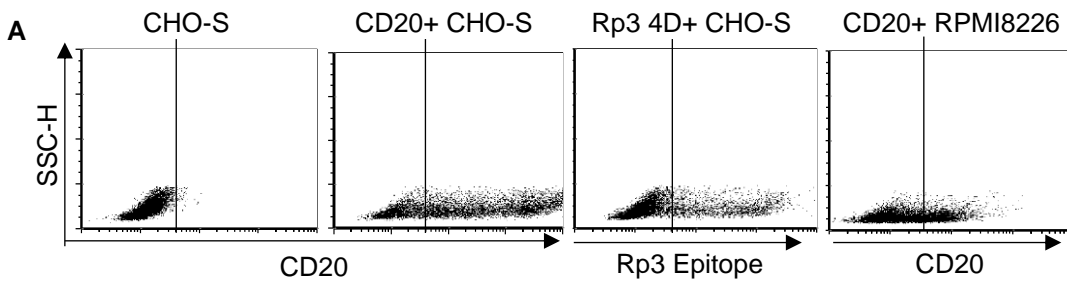


Figure 5.18: CPRG assay incorporating CD20+ve and Rp3+ve CHO-S cells as the target populations.

A: Transient expression of CD20 and 4D Rp3 epitope constructs on CHO-S cells 24 h post-transfection, assessed using FITC-rituximab. CD20 expression on stably transfected RPMI8226 cells is also shown.

B: CPRG assay comprising mock transduced and Ritux CAR+ve BWZ.36 cells with transfected CHO-S target cells expressing CD20 and the 4D Rp3 epitope construct (yellow). CD20+ve RPMI8226 cells (8226, purple) were included as a positive control. PMA/ionomycin was used to induce maximal T-cell response (green). Negative controls used were addition of media alone, and addition of untransfected CHO-S cells (grey). OD 595-655 nm depicts assay absorbance readout, representing T-cell activation response. Mean +/- range of duplicates.

It was hypothesised that Ritux CAR may need the full ¹⁷⁰ANPS¹⁷³ motif of the CD20 epitope to allow sufficiently stable binding for T-cell activation to occur. Whilst the Rp3 epitope, containing the 'SNPS' motif, is sufficient for rituximab binding, it was proposed that the nature of Ritux CAR binding may differ from the parental mAb. To investigate this, site directed mutagenesis was performed upon the 4D Rp3 construct to convert the first serine of the epitope to an alanine residue. The correct mutagenesis was confirmed using sequencing (**Figure 5.19**). This formed the previously described Rp15 cyclic rituximab epitope [481].

CHO-S cells were transiently transfected with the 4D Rp3 and 4D Rp15 constructs. Expression was assessed at 24 h post-transfection and the cells were used as target populations in a CPRG assay (**Figure 5.20**). Ritux CAR+ve BWZ.36 cells were activated by co-culture with CD20+ve RPMI8226 cells but failed to show any response to either Rp3+ve CHO-S or the new Rp15 epitope. Having confirmed (**Figure 5.18**) that CD20+ve CHO-S can induce antigen specific T-cell activation, it can be concluded that the CHO-S cells are not responsible for inhibiting a CAR-induced response. It must then be concluded that Ritux CAR cannot recognise or stably bind sufficiently to either Rp3 or Rp15, despite the parental mAb rituximab efficiently interacting with both epitopes. Whilst an interesting finding, this prohibited investigation into the role of epitope membrane proximity in the functional analysis of anti-CD20 CARs.

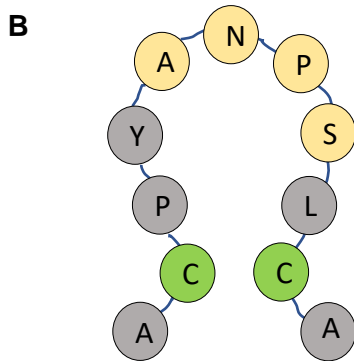
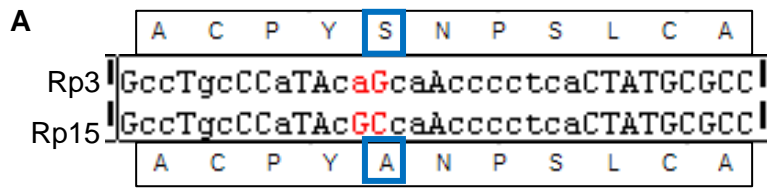


Figure 5.19: Mutagenesis of the 4D Rp3 construct to generate the Rp15 cyclic epitope.

A: DNA sequencing trace confirming the mutation of serine to an alanine residue in the Rp3 epitope of the 4D construct. This produced the Rp15 epitope incorporating the ¹⁷⁰ANPS¹⁷³ rituximab binding motif of CD20.

B: A schematic of the Rp15 rituximab epitope. The 'ANPS' motif is shown (yellow), along with the cysteine residues that form a disulphide bond to stabilise the cyclic epitope (green).

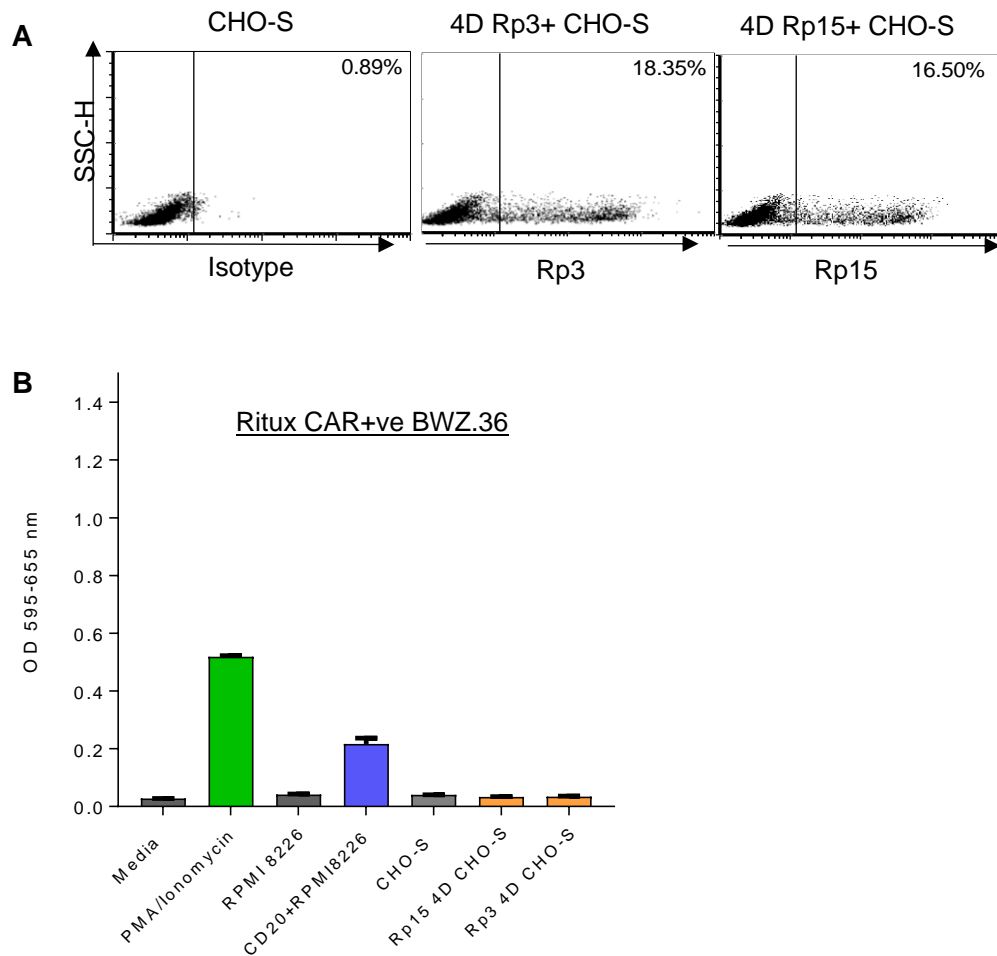


Figure 5.20: CPRG assay incorporating Rp3+ve and Rp15+ve CHO-S cells.

A: Transient expression of 4 domain (4D) Rp3 and Rp15 epitope constructs on CHO-S cells 24 h post-transfection, assessed using FITC-rituximab.

B: CPRG assay comprising Ritux CAR+ve BWZ.36 cells with transfected CHO-S target cells expressing 4D Rp3 and 4D Rp15 (yellow). CD20+ve RPMI8226 cells (8226, purple) were included as a positive control. PMA/ionomycin was used to induce maximal T-cell response (green). Negative controls used were addition of media alone, and addition of untransfected CHO-S and untransfected RPMI8226 (grey). OD 595-655 nm depicts assay absorbance readout, representing T-cell activation response. Mean \pm range of duplicates.

5.4 Generation of CAR+ve cytotoxic T-cell lines

5.4.1 CTLL-2 Characterisation

CTLL-2 cells were assessed for granzyme B expression, as a marker of potential cytotoxic function. Cells were unstimulated or stimulated for 16 h with 2 µg/ml each anti-CD3 (KT3) and anti-CD28 (37.51) antibodies. Intracellular staining was performed using a murine intracellular staining kit (eBioscience) and an anti-granzyme B mAb (Chapter 2.5.2). The unstimulated cells showed a background level of granzyme B expression, which increased after cell activation, suggesting cytotoxic potential (**Figure 5.21**).

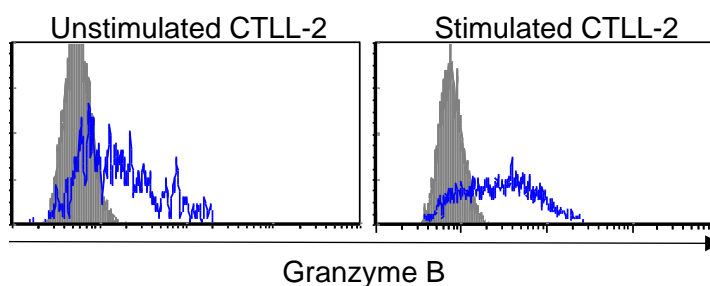


Figure 5.21: Granzyme B expression in CTLL-2 cells

CTLL-2 were left unstimulated or activated by the addition of 2 µg/ml each anti-CD3 (KT3) and anti-CD28 (37.51) for 16 h. Cells were harvested, stained intracellularly with anti-granzyme B using a murine T-cell intracellular staining kit (eBioscience) and analysed by flow cytometry. Grey, isotype control; blue, anti-granzyme B.

To investigate whether CTLL-2 cells would survive short-term *in vivo* and determine where in the body they track, cells were labelled with 5 µM CFSE. 1.5×10^7 labelled cells were injected intraperitoneally into two SCID mice (Chapter 2.9.1). Samples were taken at 24 h and 72 h post-injection. A peritoneal wash was performed to collect those cells remaining in the cavity, and blood, spleen, liver and lymph nodes harvested and stained for CD3 expression (Chapter 2.9.1). This was used along with the CFSE-labelling to ascertain cell population survival and where the CTLL-2 reside after 24 h and 72 h *in vivo* (**Figure 5.22 and 5.23**).

At 24 h post-injection, a large CFSE+ve CTLL-2 population was present in the peritoneal cavity, with a very small population detectable in the blood. (**Figure 5.22 A**). The cells from the peritoneal cavity were stained for CD3 expression, alongside *in vitro*-cultured CTLL-2 as a reference population to further confirm the identity of the CTLL-2 cells. The majority of the harvested cells that included the CFSE+ve population (**Figure 5.22 A**) were also CD3+ve confirming the identity of the CTLL-2 population (**Figure 5.22 B**).

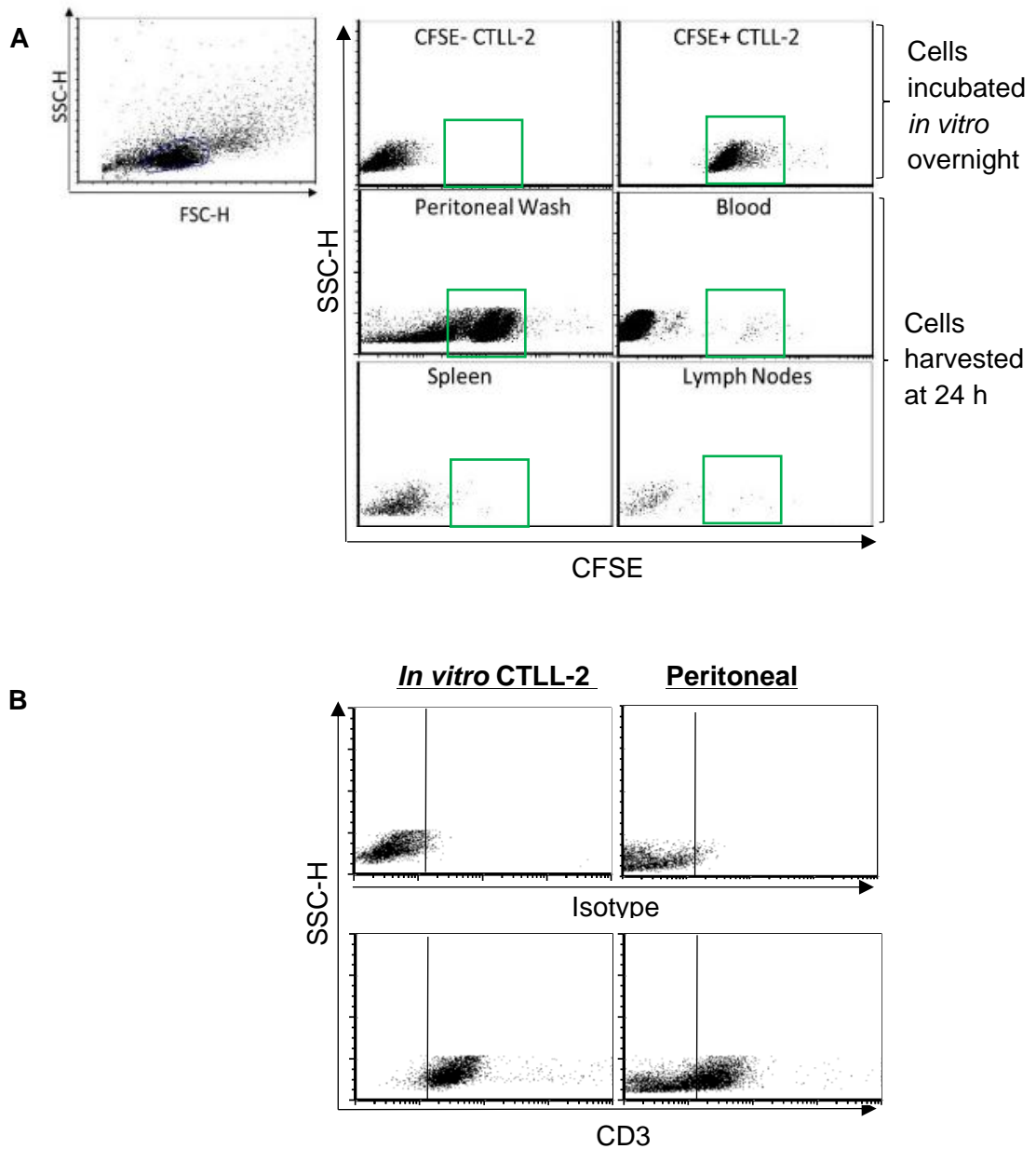


Figure 5.22: Evaluation of short-term *in vivo* survival and tracking of CTLL-2 cells

Untransfected CFSE-labelled CTLL-2 were given by IP injection to two SCID mice and cell survival and location were assessed at 24 h.

A: Gating to exclude debris using FSC-H/SSC-H is shown. Top panels show *in vitro*-cultured unlabelled and CFSE-labelled CTLL-2 cells as a reference population. Blood, spleen, axial and inguinal lymph nodes, and contents of the peritoneal cavity were collected, processed and assessed by flow cytometry for the presence of CFSE+ve CTLL-2 cells (green boxes).

B: *In vitro*-cultured CTLL-2 and the 24 h peritoneal wash harvested cells were stained for CD3 expression as additional marker of the population. N=1.

At 72 h the cells were stained for CD3 expression to locate the CTLL-2 cells (**Figure 5.23**). CFSE was not used as a marker at 72 h as the cells had divided and so lost fluorescence, making the population unclear. A significant population of the injected CTLL-2 cells were seen to have migrated from the peritoneal cavity into the blood, with a potential small subset observed in the lymph nodes. These findings confirmed that the CTLL-2 can survive short-term *in vivo* in SCID mice, and that at 24 h the cell population is retrievable from the peritoneal cavity. It would therefore be possible to use them in short-term *in vivo* assays.

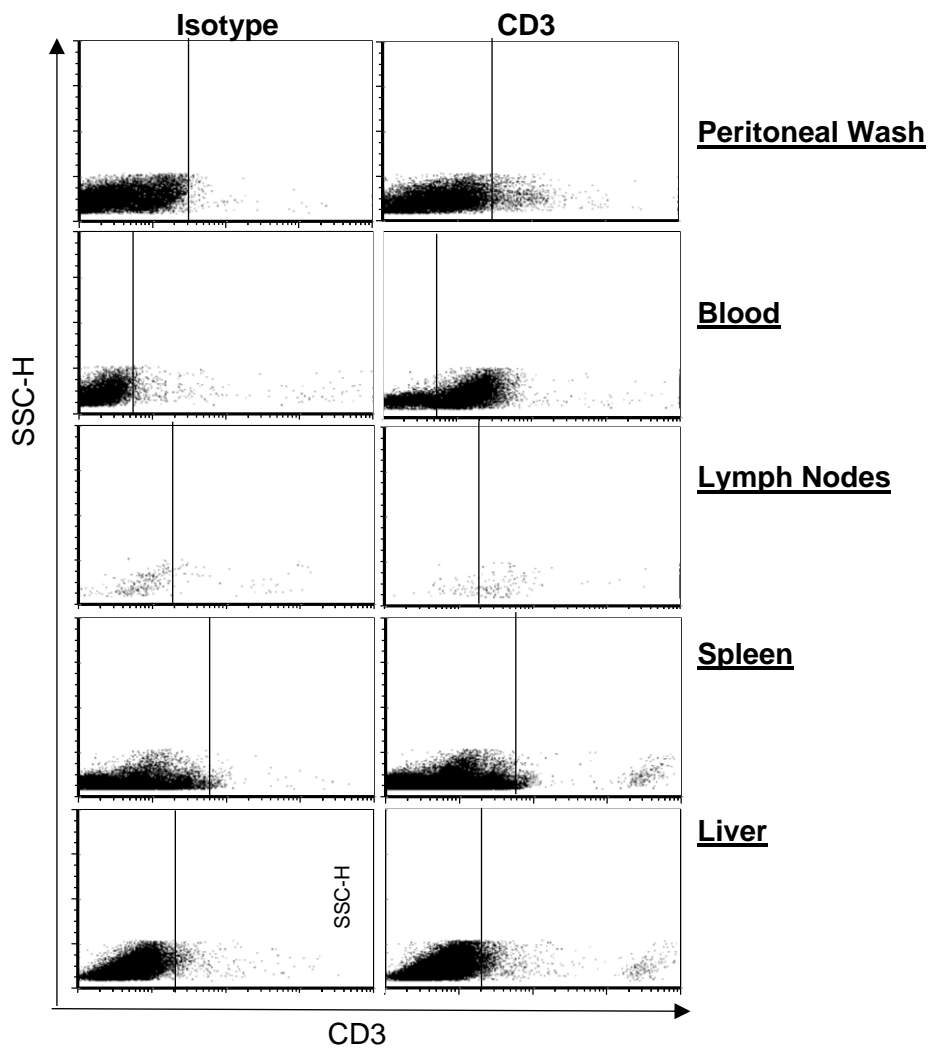


Figure 5.23: Evaluation of *in vivo* survival and tracking of CTLL-2 cells at 72 h
 The contents of the peritoneal cavity, blood, axial and inguinal lymph nodes, spleen and liver were collected, processed and stained for CD3 expression as a marker for the CTLL-2 population. Isotype control for each is also shown. N=1.

5.4.2 Establishing CAR-expressing CTLL-2 cell lines

To generate stably-expressing CAR+ve CTLL-2 populations, cells were nucleofected with BHH2 and Leu16 CAR constructs in pcDNA3.1(-) as detailed in Chapter 2.3.3. A GFP vector was also nucleofected into the cells as a positive control for the transfection. Leu16 and BHH2 CAR were chosen initially to test the nucleofection and CTLL-2 assays, as these were the two constructs that demonstrated the most difference in the BWZ.36 assays. A sample was taken at 24 h post-nucleofection and CTLL-2 were stained for CAR expression (**Figure 5.24**).

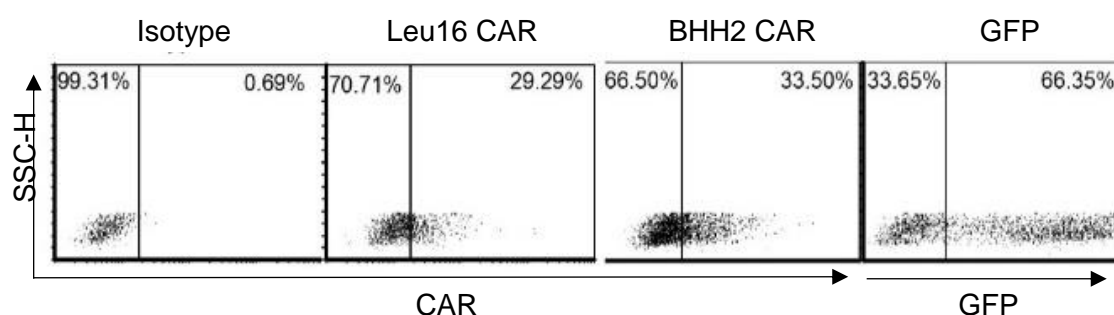


Figure 5.24: Nucleofection of CTLL-2 cells to generate CAR+ve CTL cell lines

5×10^6 CTLL-2 cells were transfected with 4 μg each of Leu16 CAR or BHH2 CAR in pcDNA3.1(-) using a mouse T-cell nucleofection kit (Lonza). A GFP plasmid was also transfected as a positive control for the nucleofection. At 24 h post-nucleofection, cells were stained with PE-anti-hlgG-Fc and screened for CAR expression by flow cytometry. Isotype, PE-anti-mIgG-Fc.

A trial cytotoxicity assay was performed on the transiently expressing cells (**Figure 5.25**). Briefly, Raji target cells were labelled with calcein-AM and co-cultured for 4 h with CAR-transfected CTLL-2 cells at a 40:1 effector:target ratio. Cells were pelleted, and the supernatants were analysed using excitation and emission wavelengths of 485 nm and 530 nm respectively as a readout for Raji cell lysis.

No cytotoxicity was observed from the Leu16 CAR or BHH2 CAR transfected CTLL-2 cells. As the CAR expression for both of these transiently-expressing populations was low in both percentage and expression level per cell, antibiotic selection was used to generate pure CAR-expressing populations. The nucleofected CTLL-2 (**Figure 5.24**) were sub-cloned over 96-well plates to generate pure CAR+ve populations for each (Chapter 2.3.4). These were selected using 0.3 $\mu\text{g}/\text{ml}$ G418 over 21 days, based on a G418 kill-curve performed on untransfected CTLL-2, and then cell viability and CAR expression were screened. Those wells with high percentage of CAR expression for

each construct were expanded and continued G418 selection was added to generate populations for use in assays (**Figure 5.26 A**).

The presence of granzyme B was re-assessed in these cells to ensure they had not lost expression during the nucleofection and expansion phases. Both CAR+ve cell lines showed continued granzyme B expression when unstimulated or stimulated by KT3/37.51 or PMA/ionomycin (Leu16 CAR+ve CTLL-2 shown in **Figure 5.26 B**). The levels observed were actually higher than previously seen in the untransfected CTLL-2, but as an alternative method of intracellular staining was used, this may explain the increase seen.

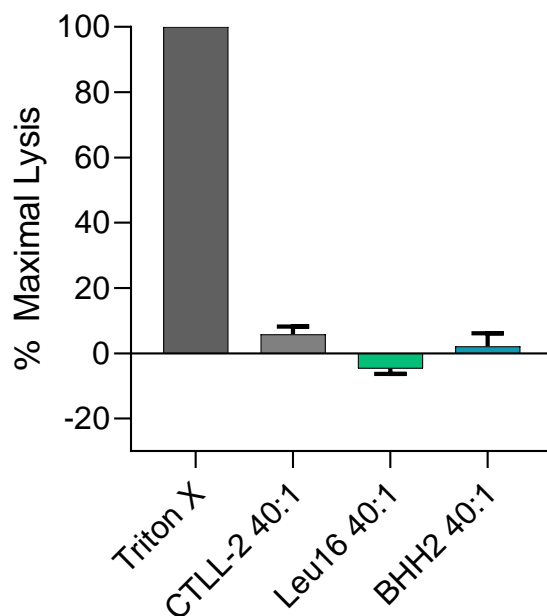


Figure 5.25: Calcein release cytotoxicity assay using transiently expressing Leu16 CAR and BHH2 CAR -transfected CTLL-2 cells

Raji target cells were labelled with calcein-AM for 30 min at 4 °C prior to co-culture with untransfected or CAR-transfected CTLL-2 cells at a 40:1 effector:target ratio. After 4 h, cells were pelleted by centrifugation and the supernatants transferred to an opaque 96-well plate. Calcein release was assessed on a Varioskan Flash plate reader (Thermo Scientific) using an excitation wavelength of 485 nm and an emission wavelength of 530 nm. Maximal lysis was induced in labelled target cells by the addition of 4 % Triton X. Baseline absorbance was measured for target cells alone and subtracted from all other data points. Data was analysed and expressed as a percentage of maximal lysis from inclusion of Triton X. Mean +/- SEM of triplicates. Representative of n=2.

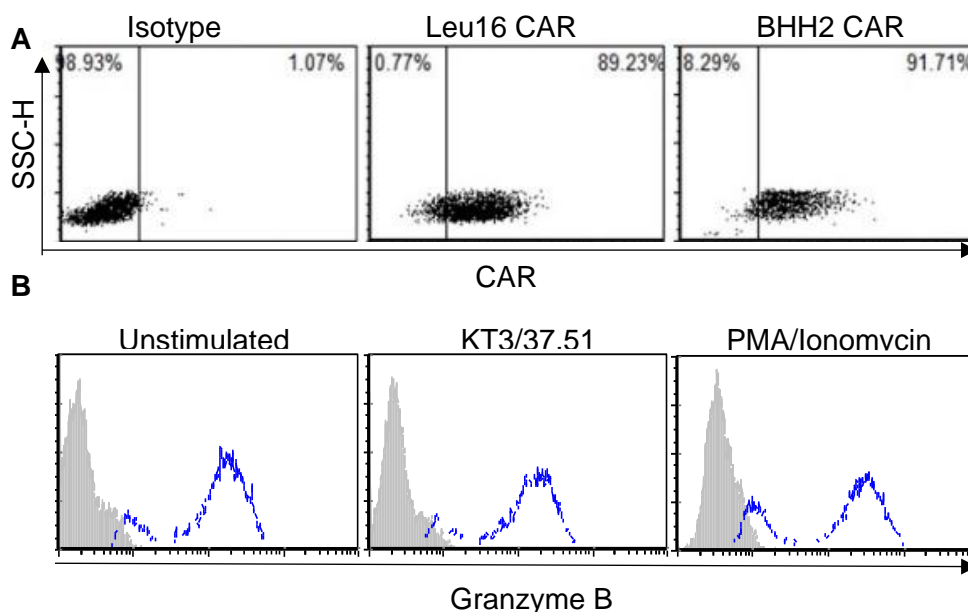


Figure 5.26: Subcloned and G418-selected Leu16 and BHH2 CAR+ve CTLL-2 populations

A: Successful nucleofections of 1×10^6 cells were subcloned across 2 96-well plates to give a low cell density per well, and 0.3 $\mu\text{g/ml}$ G418 was added to select for the pcDNA3.1(-) plasmid that contains the CAR constructs. At d 21, wells were screened for cell viability and CAR expression by staining with PE-anti-hIgG-Fc. Shown are one population each of Leu16 CAR+ve and BHH2 CAR+ve CTLL-2, compared to untransfected CTLL-2 cells.

B: Leu16 CAR+ve CTLL-2 were left unstimulated or stimulated by the addition of 2 $\mu\text{g/ml}$ each anti-CD3 (KT3) and anti-CD28 (37.51), or 50 ng/ml and 750 ng/ml of PMA and Ionomycin respectively for 16 h. Cells were harvested, stained intracellularly with anti-granzyme B using saponin, and analysed by flow cytometry. Grey, isotype control; blue, anti-granzyme B.

5.4.3 Functional assessment of CAR+ve CTLL-2 cell lines

The stably-expressing CAR+ve CTLL-2 cell lines were used in calcein-release cytotoxicity assays, described in Chapter 2.8.3. An assay was performed as described for the transiently expressing cells with CD20+ve target cells (Ramos) and CD20-ve non-targets (A20), labelled with calcein-AM and co-cultured with CTLL-2 cells for 4 h. Based upon the published CTLL-2 cytotoxicity assay [483], 10^4 labelled target cells per well were used at 40:1 and 10:1 effector:target ratios (**Figure 5.27 A**). Additionally, a plate was included with 10^5 target cells per well to ensure that the low target cell number did not mask a calcein release signal (**Figure 5.27 B**). Neither assay demonstrated any CTLL-2 cytotoxicity, irrespective of CAR expression and the presence of antigen. This assay was also repeated with the effector:target co-culture left for 16 h prior to the plate being read with equivalent results (not shown).

The CTLL-2 cell line was originally derived using splenocytes from a mouse inoculated with FLV-induced murine leukaemia cells. Thus, the resulting cytotoxic line exhibited antigenic-specific cytotoxicity to the murine tumour line FBL-3 [486]. To investigate the background cytotoxic ability of the CTLL-2 cells, a calcein release assay was performed including FBL-3 target cells (**Figure 5.28**). An absence of target cell lysis was consistently observed with the untransfected and CAR+ve CTLL-2 cells, against all target cells, suggesting an inability of the effector cells to kill regardless of the antigenic stimulation.

Kametaka *et al* [483] described depriving the CTLL-2 cells of the required T-stim IL-2 supplement for a period of 12 h prior to their inclusion in the cytotoxicity assay, at which time twice the usual concentration of T-stim was added for 2 h to re-stimulate the cells. CAR+ve CTLL-2 cells were treated overnight in this way and a subsequent calcein assay was performed using Raji target cells (**Figure 5.29**). Additionally, unlabelled target cells were co-cultured with each CTLL-2 population for the 16 h before inclusion in an assay, to investigate whether additional antigenic stimulation was required to permit cytotoxic activity (**Figure 5.30**). As previously, the CTLL-2 cells demonstrated no killing activity to any target cell.

Upon the discovery of a lack of cytotoxic activity from the CTLL-2 cells, they were examined further. A calcein-release assay was performed in which the target cells were the anti-CD3 ϵ antibody-producing hybridoma line 145-2C11 (**Figure 5.31**). The inclusion of these cells allowed a “reverse” killing assay to be performed, in which the anti-CD3 ϵ antibody-expressing cells would bind CD3 ϵ on the CTLL-2 cell surface and activate them in this manner. The activated CTLL-2 could then lyse the calcein-AM-labelled 145-2C11, if capable of cytotoxic activity. No significant cell lysis was observed, confirming the inability of the CTLL-2 cell line to lyse target cells.

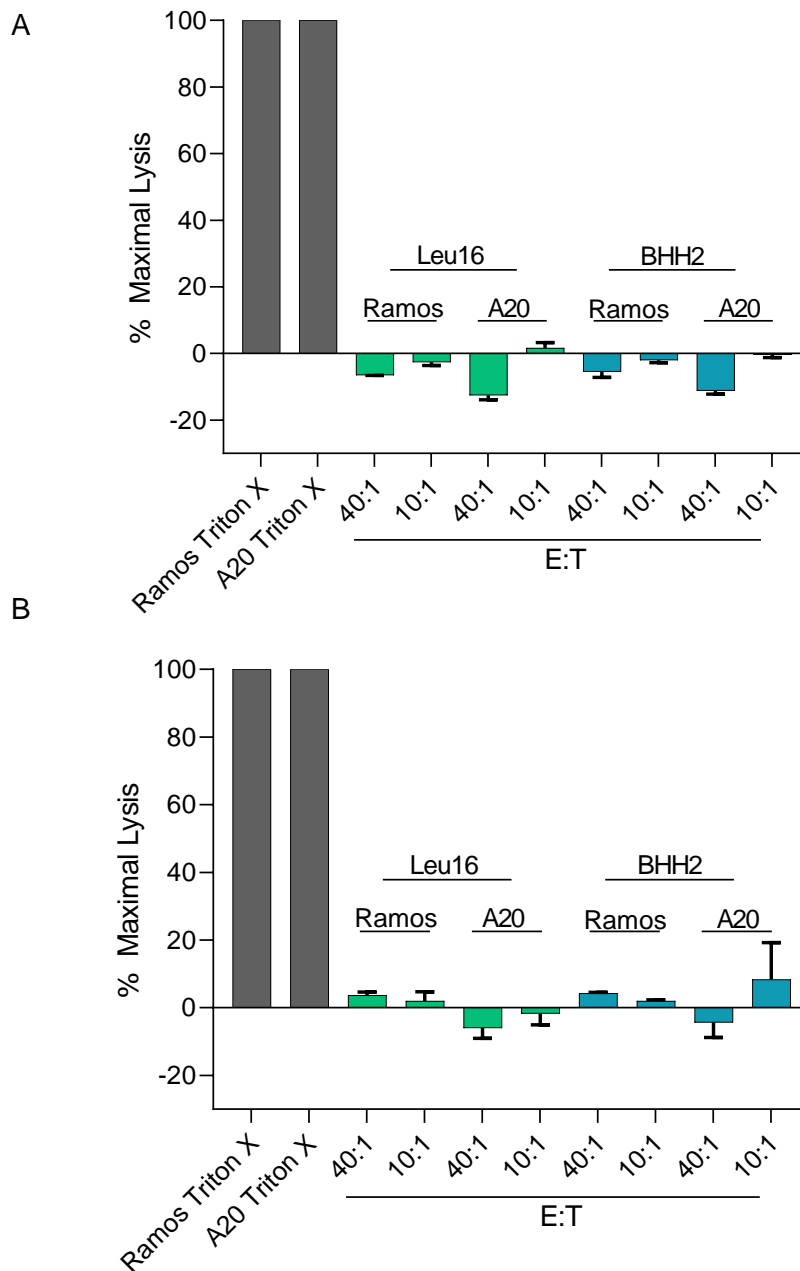


Figure 5.27: Calcein-release cytotoxicity assays incorporating stably-expressing CAR+ve CTLL-2 cell lines

Ramos and A20 target cells were labelled with calcein-AM for 30 min at 4 °C prior to co-culture with Leu16 CAR+ve and BHH2 CAR+ve CTLL-2 cells. E:T, effector:target ratio. Calcein release was assessed on a Varioskan Flash plate reader (Thermo Scientific) using an excitation wavelength of 485 nm and an emission wavelength of 530 nm at 4 h. Maximal lysis was induced in labelled target cells by the addition of 4 % Triton X. Baseline absorbance was measured for target cells alone and subtracted from all other data points. Data was analysed and expressed as a percentage of maximal lysis from inclusion of Triton X. Mean +/- range of duplicates.

A: 10⁴ labelled target cells per well. N=1.

B: 10⁵ labelled target cells per well. N=1.

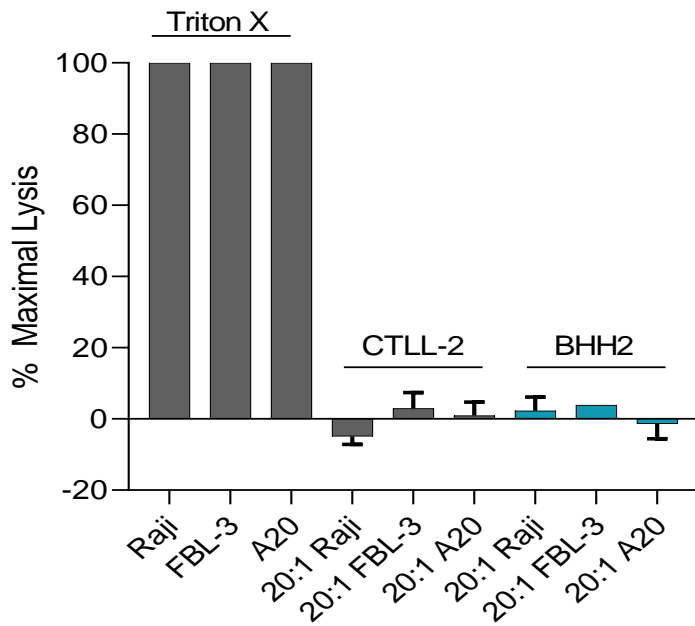


Figure 5.28: Calcein-release cytotoxicity assay incorporating FBL-3 target cells

Untransfected and BHH2 CAR+ve CTLL-2 cells were co-cultured with calcein-AM-labelled Raji, FBL-3 and A20 cells for 4 h. Calcein release was assessed using excitation and emission wavelengths of 485 nm and 530 nm respectively. Maximal lysis was induced in labelled target cells by the addition of 4 % Triton X. Baseline absorbance was measured for target cells alone, and subtracted from all other data points. Data was analysed and expressed as a percentage of maximal lysis from inclusion of Triton X. Mean +/- SD of triplicates. N=1.

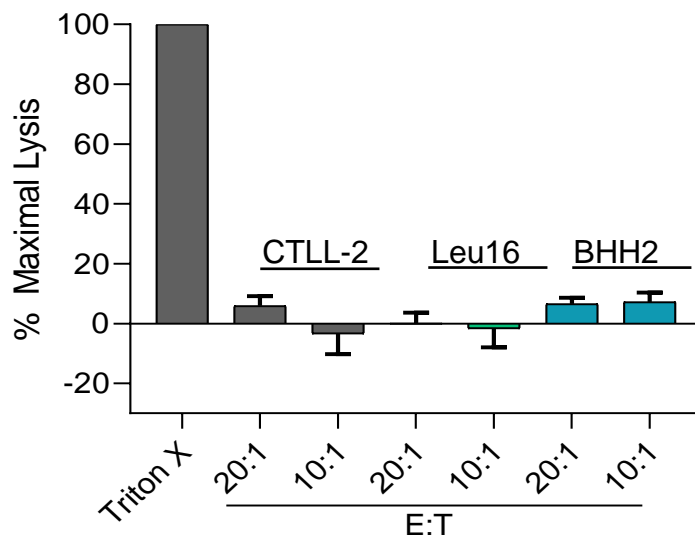


Figure 5.29: Calcein-release assay incorporating CTLL-2 cells deprived of T-stim IL-2 supplement for 12 h and re-stimulated prior to cytotoxic assessment

CTLL-2 cell populations were washed and resuspended in T-stim deficient media. After 12 h, 20 % T-stim was added and cells were left for 2 h. CTLL-2 cells were then co-cultured with calcein-AM-labelled Raji target cells. E:T, effector:target ratio. Calcein release was assessed using excitation and emission wavelengths of 485 nm and 530 nm respectively. Maximal lysis was induced in labelled target cells by the addition of 4% Triton X. Baseline absorbance was measured for target cells alone and subtracted from all other data points. Data was analysed and expressed as a percentage of maximal lysis from inclusion of Triton X. Mean +/- SD of triplicates. N=1.

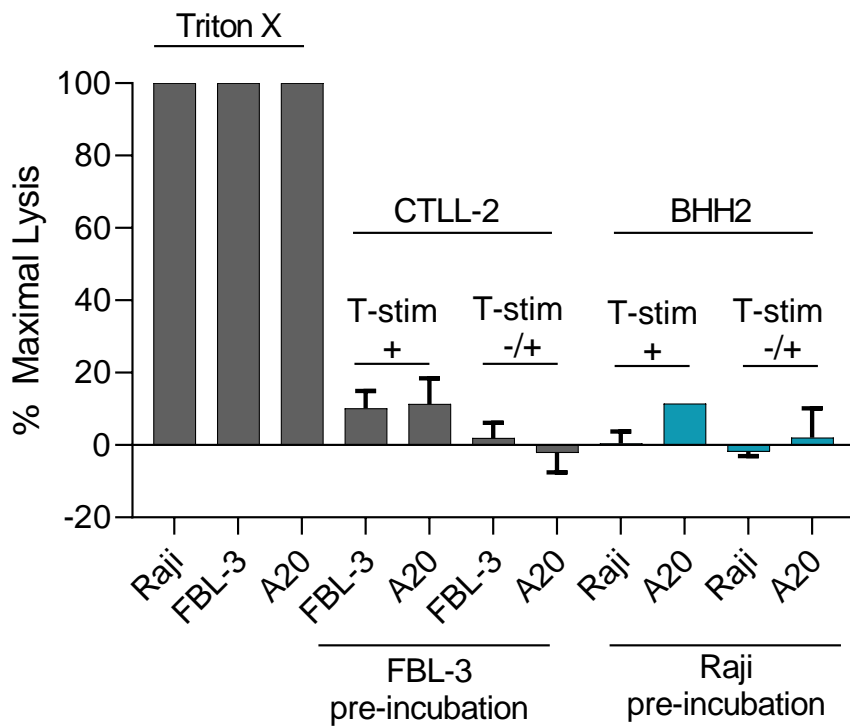


Figure 5.30: Calcein-release assay performed with pre-stimulated CTLL-2 cells
 CTLL-2 and BHH2 CAR+ve CTLL-2 were co-cultured for 12 h with unlabelled FBL-3 and Raji cells respectively. Half of each of these populations was also deprived of T-stim IL-2 supplement for 12 h, then subsequently had 20 % T-stim added for 2 h prior to inclusion in the assay (T-stim +/-). The remaining CTLL-2 were cultured with 10 % T-stim as previously (T-stim +). Untransfected CTLL-2 were then co-cultured with labelled A20 non-target or FBL-3 target cells. BHH2 CAR+ve CTLL-2 were co-cultured with labelled A20 non-target or Raji target cells. All supernatants were read using excitation and emission wavelengths of 485 nm and 530 nm respectively at 4 h. Maximal lysis was induced in labelled target cells by the addition of 4 % Triton X. Baseline absorbance was measured for target cells alone and subtracted from all other data points. Data was analysed and expressed as a percentage of maximal lysis from inclusion of Triton X. Mean +/- SD. N=1.

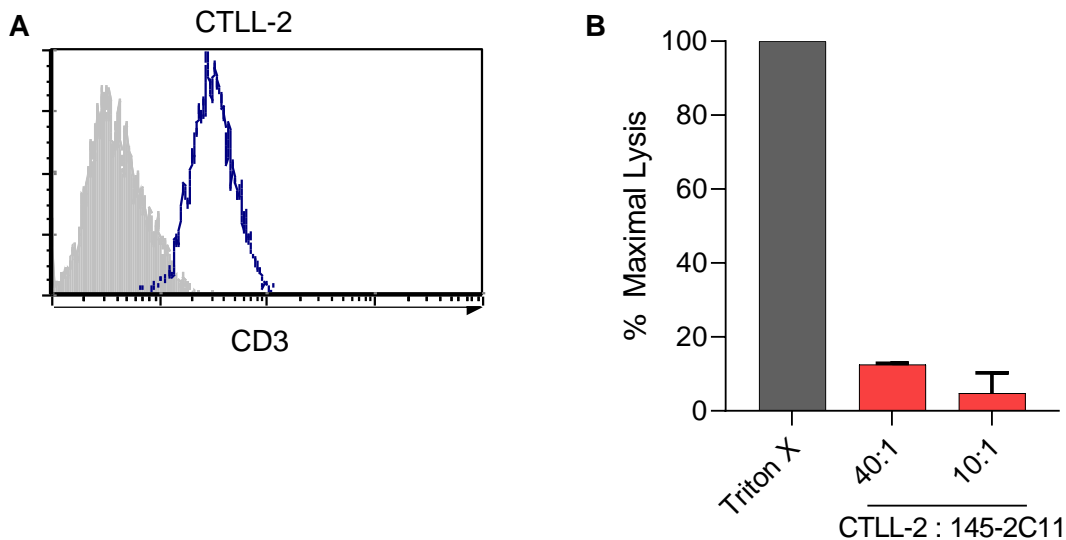


Figure 5.31: A calcein-release cytotoxicity assay incorporating 145-2C11 hybridoma cells

A: CD3 expression was confirmed on CTLL-2 cells by staining with FITC-KT3 (Blue). Isotype control, grey.

B: Untransfected CTLL-2 cells were co-cultured with calcein-AM-labelled 145-2C11 cells, an anti-CD3 ϵ antibody-producing hybridoma line. All supernatants were read using excitation and emission wavelengths of 485 nm and 530 nm respectively at 4 h. Maximal lysis was induced in labelled target cells by the addition of 4% Triton X. Baseline absorbance was measured for target cells alone and subtracted from all other data points. Data was analysed and expressed as a percentage of maximal lysis from inclusion of Triton X. Mean +/- range of duplicates. n=1.

Finally, an untransfected and minimally-cultured population of CTLL-2 cells were assessed for the cellular exhaustion markers PD-1, LAG3 and TIM-3. The presence of these cell surface molecules indicates CTL that have become exhausted due to prolonged antigenic exposure and no longer have cytotoxic functions. The CTLL-2 were confirmed to express LAG3, TIM3 and a sub-population also expressed PD-1. This provided an explanation for the lack of function observed and showed that this was not due to the nucleofection, sub-cloning and culturing process involved in generating the CAR+ve cell lines.

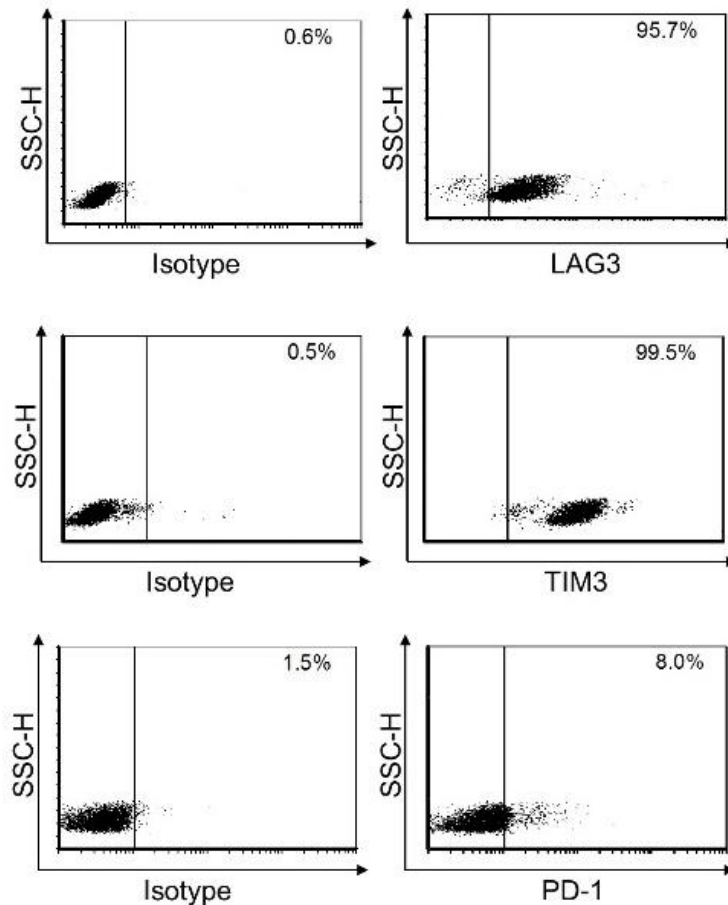


Figure 5.32: CTLL-2 cells stained for T-cell exhaustion markers

Untransfected, minimally-cultured CTLL-2 were stained with fluorescently labelled antibodies to the T-cell exhaustion markers TIM3, LAG3 and PD-1 and expression was assessed by flow cytometry. Isotype controls for each antibody are also shown. N=1.

To determine if an alternative readout of CAR+ve CTLL-2 function was possible, antigen-stimulated IFN γ production was assessed. CAR+ve and untransfected CTLL-2 cells were co-cultured with CD20+ve target cells and the supernatant was collected. Secretion of IFN γ was measured using a mouse IFN γ ELISA (Biolegend) for each CTLL-2 cell line (**Figure 5.33**) as described in Chapter 2.8.4. BHH2 CAR+ve CTLL-2 cells were observed to secrete high levels of IFN γ when co-cultured at a 25:1 effector:target ratio. Lower levels were also seen with BHH2 CAR at the E:T ratios of 5:1 and 1:1. Conversely, Leu16 CAR+ve CTLL-2 produced no IFN γ secretion above that of the untransfected CTLL-2 baseline at any E:T ratio. This superior cytokine production from BHH2 CAR+ve is similar to that seen from the BHH2 CAR+ve BWZ.36 IL-2 reporter cells, and also correlates with Leu16 CAR+ve BWZ.36 producing a very low IL-2 reporter cell response (**Figures 5.10 and 5.11**).

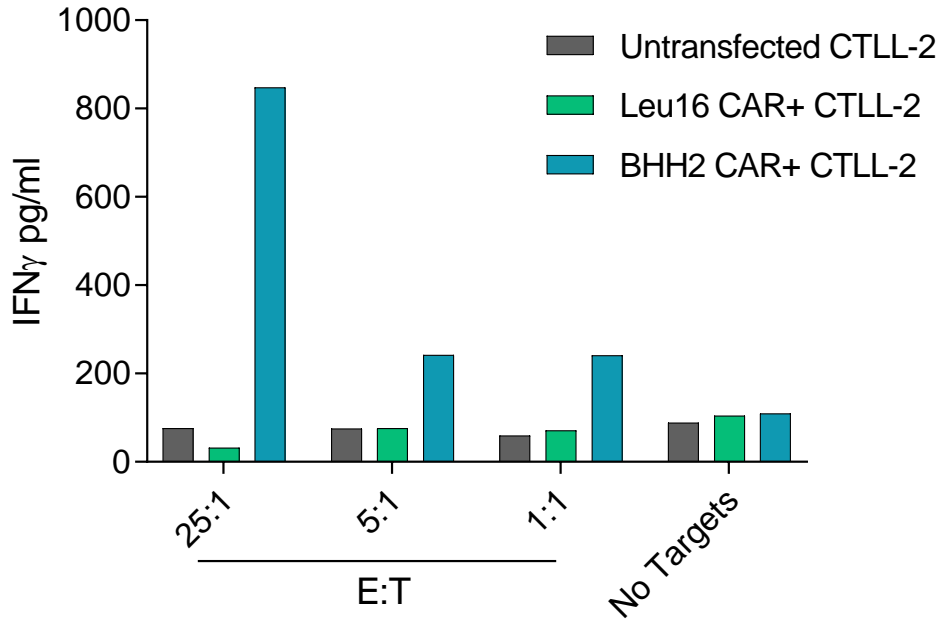


Figure 5.33: IFN γ ELISA performed on supernatants from CTLL-2 co-cultures with CD20+ve target cells

Untransfected and CAR+ve CTLL-2 cell lines were co-cultured with CD20+ve Ramos cells at the effector:target (E:T) ratios shown. Supernatants were collected and used in an IFN γ ELISA. Captured IFN γ was detected using a biotinylated antibody and avidin-HRP conjugate, and subsequent addition of HRP substrate. Plates were read at an absorbance wavelength of 495 nm on an Epoch reader. Analysis of data was performed using an IFN γ standard curve generated using known quantities of cytokine. Mean of duplicates. Representative of two independent experiments.

5.5 Discussion

In this chapter stably expressing CAR+ve cell lines were successfully generated, giving the opportunity to test the function of the constructs in a repeatable and comparable manner. Whilst the use of cell lines has limitations due to their potential deviation from the characteristics of the original primary cells from which they were derived, they still permit an insight into cell behaviours, and provide a robust system for stable protein expression. Unlike with the transient cell system employed in Chapter 2, comparisons between replicated experiments can be made more accurately using these stable populations that maintain construct expression in culture.

Each of the three CAR+ve BWZ.36 IL-2 reporter cell lines generated was observed to respond in an antigen-specific manner to CD20+ve target cells. IL-2 is vital for the proliferation of antigen-specific T cells, and in the differentiation of activated CD8+ve T cells into effector CTL [487]. In the case of T cells, including those expressing CARs,

cytokine production upon cell activation and consequent signalling provides the required “signal three” [488]. This is an essential part of expansion of the initial cell population to induce a full immune response and sufficient T-cell numbers and survival to permit a strong anti-tumour effect.

CAR+ve T-cell therapies are often comprised of a mixed pool of T cell subsets, as extracted from the PBMC pool of a patient (discussed in Chapter 1.8.6). Thus, it is important to consider the varied effects of this cytokine on all cell types. IL-2 can lead to the proliferation of a CAR+ve T cell population, promoting CTL expansion and supportive Th cell activation, depending on the other cytokines and factors present. The activation of multiple T-cell subsets in this way can help to promote a wider generalised immune response, which can in turn provide positive feedback for continued anti-tumour responses [477].

However, when the larger picture of an *in vivo* response is considered, the promotional effects of IL-2 on the Treg population must also be considered. As Tregs constitutively express the IL-2 α receptor subunit (CD25), the secretion of IL-2 from activated CAR+ve T cells will also enhance the expansion of this population [489, 490]. In CAR therapies, particularly in solid tumour targeting, this can be circumvented by pre-therapy lymphodepletion, but clearly provides another aspect to consider in CAR design [491]. Despite these considerations, a strong IL-2 response is still essential for CAR+ve T-cell activation and function. A suboptimal IL-2 signal has been linked to a significantly reduced CD8+ve T-cell expansion, whilst a stronger and prolonged level of IL-2 can induce efficient differentiation into effector CTL and rapid proliferation. [476].

The use of CAR+ve BWZ.36 cell lines in this chapter revealed a distinct difference in the IL-2 reporter activation response elicited by each CAR construct. BHH2 CAR consistently produced a significantly stronger IL-2- reporter readout than the other two constructs (**Figure 5.10**). This suggests that BHH2 CAR is capable of a much stronger activation of the T cells. Ritux CAR produced a lower activation readout, whilst Leu16 CAR elicited only a weak activation. When these results were adjusted to take into account the CAR expression it was shown that the differences seen were not due to CAR % positive or expression density. When the data from Chapter 2 is also considered, it can be concluded that the differences seen in T-cell activation are also not due to the CAR antigen binding abilities.

Ritux CAR was seen to have a higher BWZ.36 background activation response compared to both other constructs. This could be an artefact from the process of cell sorting due to the selection of a cell population that could exhibit some skewed characteristics. Alternatively, this construct may induce low level tonic signalling. Tonic

signalling from CAR constructs has been described and can be attributed to self-aggregation of CAR molecules [492]. It is unclear whether the scFv would influence these interactions, as the CAR dimerization known to happen has been shown to occur between the IgG spacer regions and between some transmembrane domains [368, 493].

Whilst the responses observed from Ritux CAR+ve and Leu16 CAR+ve BWZ.36 were consistently significantly lower than that for BHH2 CAR, they both showed an increased activation from CD20+ve RPMI8226 cells as targets compared with Ramos cells. No difference was seen with BHH2 CAR as the activation readouts were equivalent to maximal response with both target cell types. This is an interesting observation as the transfected RPMI8226 cells express CD20 at a much lower level than the Ramos cells (**Figure 5.10 A**). It is probable that other molecules expressed upon the cell surface were capable of interacting with the BWZ.36 cells to strengthen the interaction or activation.

The availability within the laboratory of previously generated constructs [464] containing the Rp3 cyclic rituximab epitope permitted the design of a side-by-side comparison of Ritux CAR+ve BWZ.36 activation upon binding to the same epitope at different membrane proximities (**Figure 5.3**). It was hypothesised that a closer distance between the interacting cells would elicit a higher CAR-induced T-cell response. The 4 domain construct holds the Rp3 epitope at approximately 8 nm from the cell surface [464]. A rough calculation can be performed, giving each residue 1.5-3.3 Å [494], the rituximab epitope of CD20 is held ~22.5-49.5 Å (2.25 nm- 4.95 nm) from the cell surface. The 1 domain construct (epitope held at ~1.5 nm) would bring the interactions into closer proximity, which previous studies suggest may enhance the CAR activation level [373-375, 495]. Conversely the 8 domain construct holds the epitope at approximately 16 nm from the target cell plasma membrane [464]. As the total optimal distance for an endogenous TCR-based IS is approximately 15 nm, the 8 domain construct would augment the IS distance significantly beyond this, especially when bound to a CAR construct [225]. An IgG mAb molecule length is sized between 10-15 nm, which provides an estimate of the extracellular CAR domain as being shorter by one Ig domain [496]. It was predicted that this greater distance would reduce the CAR ability to elicit a strong T-cell response [177, 464, 497].

Despite the use of several different cell lines to exclude the possibility of inadvertent signal inhibition, no response of Ritux CAR BWZ.36 was observed against any of the Rp3 constructs. It was confirmed that the CAR+ve cells were activated by CD20+ve transfected CHO-S cells, but in the same assay the equivalent Rp3 transfectants

elicited no response. The parental mAb rituximab binds to the Rp3 epitope [481], but the scFv portion of the Ritux CAR was seemingly unable to.

It was proposed that the exclusion of the full “ANPS” motif, shown to be a major component in rituximab binding to CD20, was leading to a weakened CAR interaction, and consequently no measurable T-cell activation. Mutagenesis was performed on the 4 domain Rp3 construct to alter the sequence to another previously described cyclic epitope, Rp15 [481]. This epitope contains the “ANPS” motif in place of the Rp3 “SNPS” sequence. Again, the Ritux CAR+ve BWZ.36 cells responded to the presence of CD20, but not to the cyclic epitope, despite successful rituximab staining of the transfected Rp15+ve cells.

Whilst this did not progress the investigation of the role of epitope distance on CAR activation, this was in itself an interesting observation. The conversion of a mAb or F(ab) into a scFv does not always retain target binding ability due to the nature of the fragment folding [498]. However, Ritux CAR has been shown to be capable of robustly binding CD20, and in a sustained manner allowing T-cell activation (**Figures 4.4 and 5.9**). The binding characteristics of a scFv, when able to bind target antigen, have been determined to be equivalent to that of the mAb or F(ab), thus Ritux CAR would be expected to bind both Rp3 and Rp15 [498].

It cannot be determined from the data presented in this chapter whether the Ritux CAR bound to Rp3 or Rp15, but in an insufficient manner to induce T-cell signalling, or whether no epitope recognition occurred. The nature of the linker in a scFv can affect the binding to a target antigen [499]. The Ritux scFv with the G/S linker may need a fuller epitope to stabilise antigenic binding, compared to the F(ab) or mAb constructs. A full “non-continuous” epitope within CD20 has been published for rituximab (**Figure 5.34**), whereby the antibody was shown to interact with a second region (¹⁸²YCYSI¹⁸⁶) of CD20 in combination with the established ¹⁷⁰ANPS¹⁷³ epitope. These epitopes are brought into proximity to allow rituximab interaction with both by the steric folding of CD20, stabilised by a disulphide bond between C¹⁶⁷ and C¹⁸³ [500]. It can be postulated that the Ritux scFv may require engagement with this longer epitope for optimal binding and thus CAR+ve T-cell activation, whereas the F(ab) and mAb can still stably interact with only the first motif.

The final part of this chapter involved the generation of CAR+ve CTLL-2 cell lines. The intention was to use these cells in *in vitro* calcein release cytotoxicity assays and short-term *in vivo* killing assays. The use of these cells was based upon published work that demonstrated a robust level of cytotoxicity from the CTLL-2 cells, and the successful transfection of these cells with fusion proteins [483]. CTLL-2 were assessed for

granzyme B expression, with and without pre-stimulation from anti-CD3/CD28 or PMA/ionomycin. Primary naïve CD8+ve T cells do not constitutively express granzyme B but upregulate it upon activation. Effector CTL can then store the granzyme in cytolytic granules within the cell, until ready to release them to kill an engaged target cell [501]. As granzyme B plays a key role in CTL cytotoxicity, its expression and secretion can be used as a marker for levels of target cell lysis [502]. Therefore, its presence in CTLL-2 cells was assessed- and shown to be positive -prior to transfection and after stable CAR+ve cell lines had been generated to determine cytotoxic potential.

Despite this, no CAR -dependent or –independent cytotoxic activity was observed from the CTLL-2 cells. When CTLL-2 were stained for common exhaustion markers, even the untransfected and minimally cultured cells were shown to be positive for LAG3, TIM3 and a subset expressed PD-1. T cells upregulate these molecules after sustained activation and they are involved in inhibition of T-cell signalling and suppression of activation [503]. Therefore, the presence of these on CTLL-2 cells is highly suggestive that this cell line has become exhausted and thus activation will be limited. This finding likely explained why the cells were non-cytotoxic and highlights the limitations of the use of cell lines, as they will have been cultured over a sustained period of time and can deviate from their original characteristics, and function in a manner different to that of the original primary cells.

As some non-cytotoxic cells can still secrete IFN γ [502] and this cytokine is essential in CTL function, the CAR+ve CTLL-2 were analysed for IFN γ production as an alternative activation readout. There is evidence that there is a strong relationship between IFN γ production and CAR efficacy [466]. IFN γ is a key pro-inflammatory cytokine in T-cell activation and function. It is known to enhance CD8+ve CTL cytotoxic function and motility, and skews CD4+ve cell differentiation towards a Th1 phenotype [504]. Correlatively to the IL-2 reporter cell line data, BHH2 CAR demonstrated the highest IFN γ response upon incubation with CD20+ve target cells. The Leu16 CAR did not produce IFN γ above background levels seen for CAR- cells. This again supports the BWZ.36 data, where Leu16 CAR produced a significantly reduced response compared to BHH2 CAR.

6 Assessment of CAR function in primary cells

6.1 Introduction

The previous chapter demonstrated clear functional differences between the CAR constructs, when expressed on cell lines. Cell line systems are beneficial for obtaining consistent, comparable data. However, after lengthy cell culture they can deviate from the characteristics of the original primary cells [505]. Thus, it was important to evaluate and compare CAR function in fresh primary cells. This would allow a more accurate insight into CAR+ve T-cell activity.

The induction of efficient target cell killing is the most essential aspect of a CAR. Having established the abilities of each of the CAR constructs regarding target antigen binding and cytokine production, it was next necessary to investigate whether these differences translated to a difference in cytotoxic activity.

The first half of this chapter involves the use of primary murine cells. As the BWZ.36 cells are a murine T-cell line, studies were proposed to evaluate if the differences observed translated to a primary system. Additionally, whilst *in vitro* data such as those shown in the previous chapters, give a useful insight into CAR function, analysis where only the cells in question are considered will always have limitations. Investigation of the interactions between CAR+ve T cells and target populations allows evaluation of the direct CAR functions but excludes other effects that may occur in an *in vivo* system. Evidence has shown that whilst *in vitro* assay CAR function often indicates the *in vivo* efficacy, other factors such as cytokine production can affect the overall *in vivo* response [384, 386]. A murine model provides a beneficial system to observe CAR effects *in vivo*.

Splenocytes were harvested from recipient mice, and the T cells present in the resulting cell suspension were activated using anti-CD3 and anti-CD28. The proliferating T cells were transduced with the CAR constructs in pMIGR1, using the same technique as that used for the BWZ.36 cell line. pMIGR1 has been previously used successfully to transduce primary murine T cells [480, 506]. The transduced cells can then be injected into recipient mice, with human CD20+ve target B cells, to evaluate the anti-CD20 CAR functions of target cell lysis assessed by B-cell depletion.

Murine bone marrow was also harvested and successfully transduced with CAR constructs in a similar manner. This was then used to reconstitute lethally-irradiated

recipients to generate bone marrow chimeras. It was proposed that this method may circumvent issues that arose surrounding T-cell CAR expression, as this technique avoids the additional activation required for splenocyte transduction [507].

The second half of the chapter addresses CAR cytotoxic function in human primary T cells. Due to the finding that the CTLL-2 cells described in the previous chapter were not capable of cytotoxic activity, an alternative method to perform *in vitro* cytotoxicity assays was sought. Human primary T cells are able to survive and proliferate in *ex vivo* culture. Once activated and proliferating, retroviral transduction is also possible. Human peripheral blood mononuclear cells (PBMCs), from National Blood Service blood cones from healthy donors, were used as the source for primary human T cells.

The work on human PBMCs in this chapter was greatly assisted by technical training at the Pule Lab at University College London, and the kind gifting of the pSFG, pEQPAM and RD114 vectors [439], a culture of HEK 293T cells and the relevant retroviral transduction protocol. All data shown was then generated in Southampton by the implementation these techniques.

Human PBMCs were activated using PHA-P and IL-2 and transduced using viral supernatants generated by transiently transfected HEK 293T cells. The CAR⁺ve T cells were then used in cytotoxicity assays and evaluated for cytokine production.

6.2 Retroviral transduction of murine splenocytes

Phoenix-ECO packaging cells were transfected initially with BHH2 CAR in the pMIGR1 viral vector, along with the additional viral packaging vector pCL-eco using effectene. Cells were transfected when approximately 60% confluent, in 6-well plates. Viral secretion commences at around 24 h post-transfection, so media was changed on the cells at 23 h. GFP levels were evaluated at 24 h using fluorescence microscopy (Chapter 2.6), to determine the success of the transfection (**Figure 6.1**).

At 48 h post-transfection, the BHH2 CAR viral supernatant was collected from the Phoenix-ECO cells and used in a trial transduction on NIH3T3 cells, a readily-transducible murine fibroblast cell line [508], as detailed in Chapter 2.4.1.2.1. Cells were spun at 800 xg at 32 °C for 1 h in the presence of the viral supernatant and 4 µg/ml polybrene. Media was changed after 24 h to remove the polybrene, and cells were assessed at 48 h post-transduction by flow cytometry to evaluate GFP and BHH2 CAR expression (**Figure 6.2**). Both GFP and BHH2 CAR were shown to be expressed on the NIH3T3 cells.

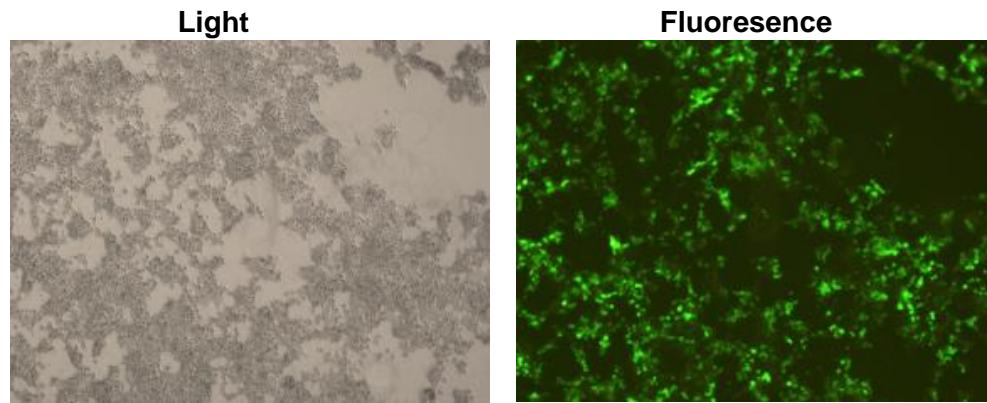


Figure 6.1: Phoenix-ECO cells transfected with BHH2 CAR in pMIGR1
 Phoenix-ECO cells were transfected using effectene with BHH2 CAR in pMIGR1 vector and pCL-eco packaging plasmid. As pMIGR1 contains an IRES-eGFP gene, successful transfection can be confirmed using fluorescence microscopy. GFP expression is shown at 24 h post-transfection (right), compared to Phoenix-ECO cell density as assessed by light microscopy (left). Images captured using 4x microscope magnification setting.

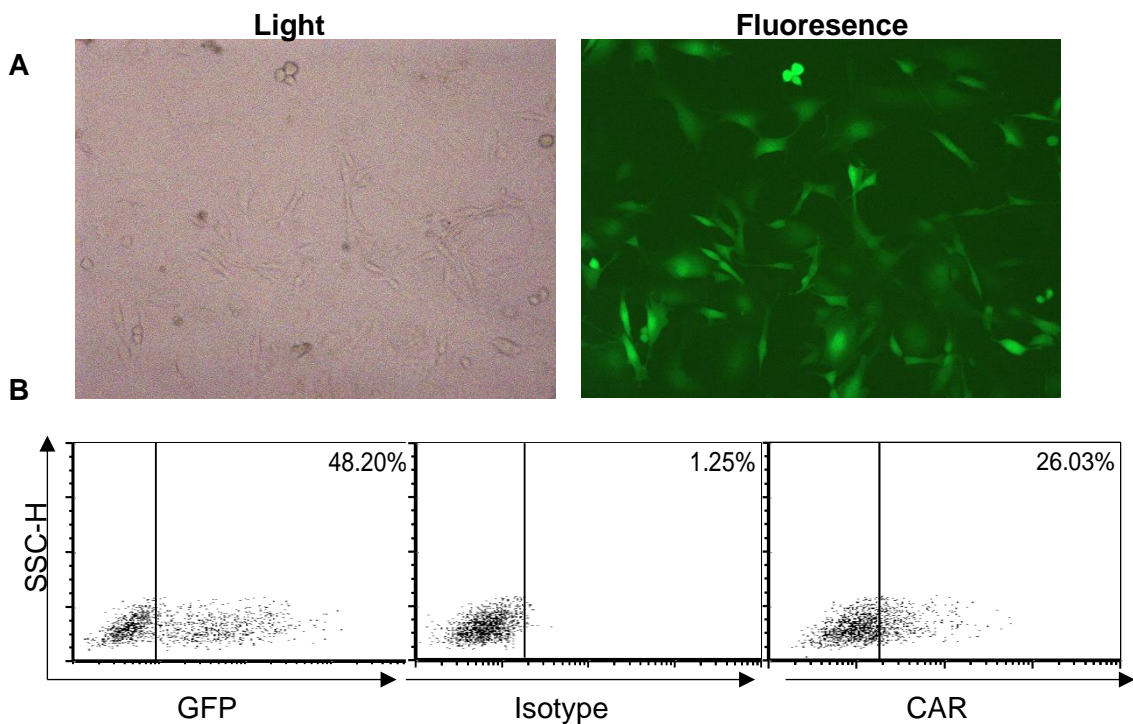


Figure 6.2: NIH3T3 cells transduced with BHH2 CAR viral supernatant
 NIH3T3 cells were spin transduced for 1 h at 800 xg, 32°C with 4 µg/ml polybrene and viral supernatant collected from transfected Phoenix-ECO cells (Figure 6.1). Images captured using 10x microscope magnification setting.
A: GFP expression was evaluated using fluorescence microscopy and compared with cell density by light microscopy at 48 h post-transduction.
B: GFP and BHH2 CAR expression (PE-anti-hlgG-Fc staining) was assessed by flow cytometry at 48 h post-transduction.

To repeat the transduction using murine T cells, splenocytes were harvested and a single cell suspension was produced (Chapter 2.1.3). Erythrocytes were lysed and cells were resuspended, plated and T-cell activation was induced by the addition of 2 µg/ml anti-CD3 (KT3) and 2.5 µg/ml anti-CD28 (37.51). The activation and proliferation of T cells required for transduction was confirmed using light microscopy after 48 hr (**Figure 6.3**).

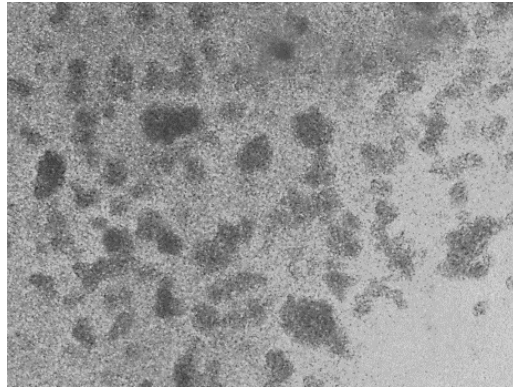


Figure 6.3: Activated murine splenocytes showing clustering after incubation with anti-CD3 and anti-CD28

Murine splenocytes were plated at 1.5×10^6 /ml. 2 µg/ml anti-CD3 (KT3) and 2.5 µg/ml anti-CD28 (37.51) were added and cells were incubated for 48 h. Cells were then examined using light microscopy for T-cell rosetting, as shown by the cell clusters above, which is characteristic of activated and proliferating T cells. Image captured using 4x microscope magnification setting.

The Phoenix-ECO cell system was once again used to produce viral supernatants. These were harvested at 48 h post-transfection and the activated murine T cells were transduced twice at an interval of 7 h. At 24 h, cells were washed and re-suspended in media containing 10 ng/ml IL-7. GFP and CAR expression were assessed by flow cytometry at 48 h post-transduction (**Figure 6.4**).

GFP expression was seen in both the empty pMIGR1 and CAR-pMIGR1 transductions, as compared with untransduced control cells. However, minimal CAR expression was present on the Leu16 CAR-transduced cells, as compared to both untransduced and empty vector-transduced cells. Whilst the IRES-eGFP of pMIGR1 has been observed previously (Chapter 3) to express at a higher level than the gene insert, this difference is more significant and suggests an issue with CAR expression or CAR+ve cell survival.

All vector and gene sequences were re-confirmed as correct and expression of the DNA preparations used were tested and proven able to be expressed by transiently transfected cells, as before.

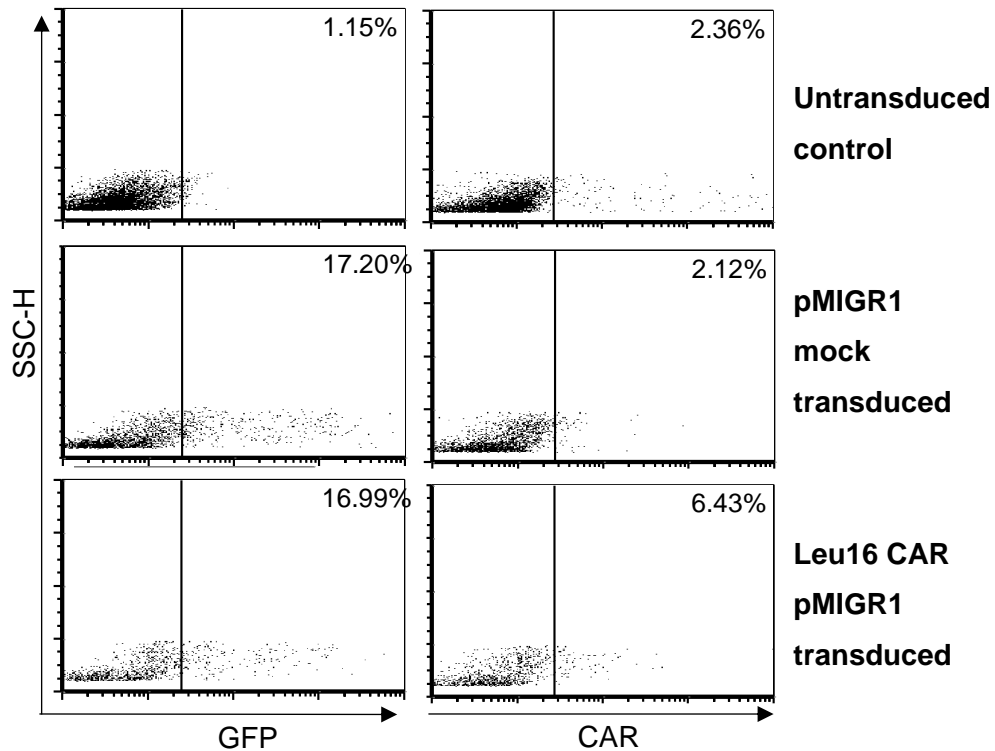


Figure 6.4: Murine splenocytes transduced with Leu16 CAR viral supernatant

Murine splenocytes were harvested, plated at $1.5 \times 10^6/\text{ml}$ in 24-well plates and activated using anti-CD3 and anti-CD28. Viral supernatant collected from Phoenix-ECO cells transfected with BHH2 CAR was used to transduce the activated T cells, in the presence of $4 \mu\text{g}/\text{ml}$ polybrene. GFP and CAR expression were evaluated at 48 h post-transduction using flow cytometry and PE-anti-hlgG-Fc.

To investigate whether the CAR expression levels could be increased on murine T cells, a longer viral-production period was introduced. Phoenix-ECO cells were incubated for 72 h post-transfection prior to the harvest of the viral supernatants. GFP levels of the same transfected well were observed at 48 and 72 h by fluorescence microscopy using identical settings (**Figure 6.5**). The intensity of GFP expression was seen to be increased at 72 h, suggesting that the plasmid expression of the CAR gene may also be improved. The 72 h supernatant was subsequently collected and used to transduce activated murine splenocytes (**Figure 6.6**). GFP was expressed by the T cells, but minimal CAR expression was seen.

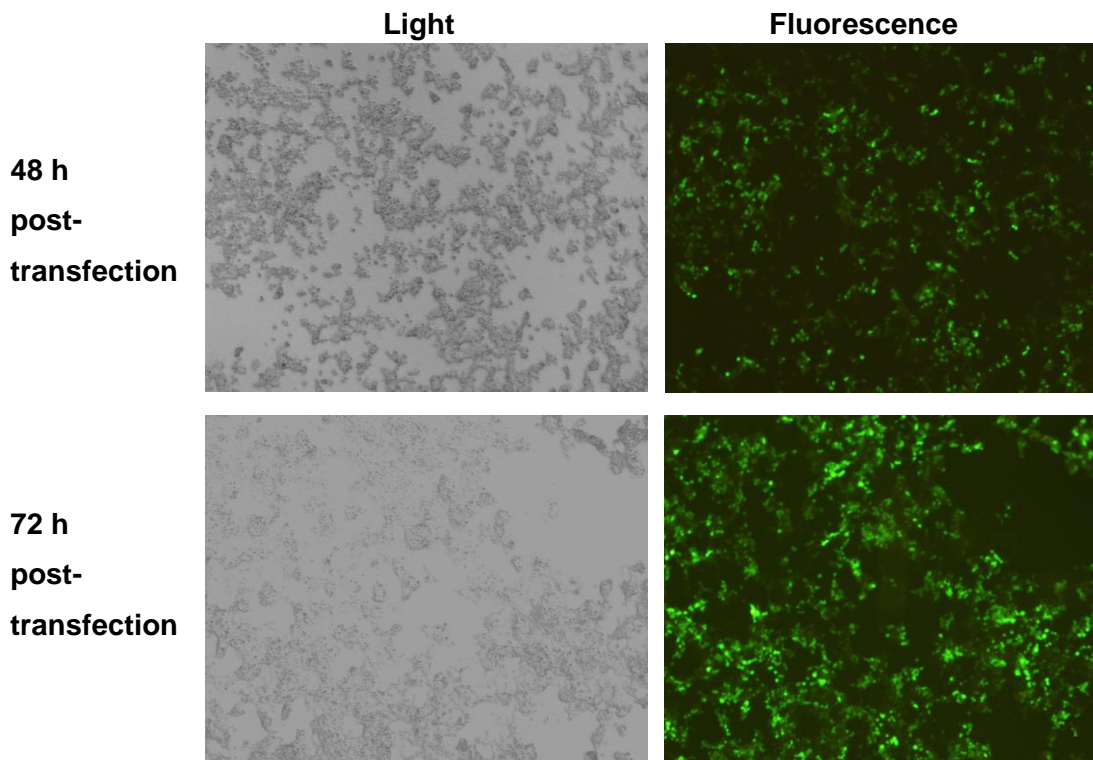


Figure 6.5: GFP expression in Phoenix-ECO cells at 48 and 72 h post-transfection

Fluorescence microscopy images were captured of the same BHH2 CAR-transfected well of Phoenix-ECO cells at 48 h and 72 h post-transfection to compare GFP expression levels. Several images of each were captured, using the same microscopy settings, and those shown are representative of the conditions. Light microscopy was also used to capture images to show total Phoenix-ECO cell densities. Images captured using 4x microscope magnification setting.

The transduction shown in **Figure 6.6** was repeated with both Leu16 and BHH2 CAR constructs, and with a reduced splenocyte activation period of 24 h, and the data shown are representative of each transduction. Cells consistently expressed GFP and displayed an absence of significant CAR expression. The lack of CAR expression suggests that either the cells are not successfully producing the construct despite GFP plasmid expression, or those cells that are CAR+ve are not able to survive. The CAR constructs were able to be expressed by murine cell lines, and as no issue was found with any sequences in the CAR gene or vector, it is unclear why the construct would not express.

It is unlikely that the issue is a technical one, as GFP is expressed well on the cells, both when transduced with empty pMIGR1 and the CAR-pMIGR1 plasmids. It is possible that CAR-expressing T cells are not surviving due to a feature of the construct. Previous work has found that the expression of human CD137 by primary murine cells

can be challenging, and it has been proposed that this is due to over activation of the cells, leading to cell death (personal communication from Dr Jane Willoughby). As T cells need to be robustly proliferating to allow successful retroviral transduction, it is not possible to limit the T-cell pre-activation.

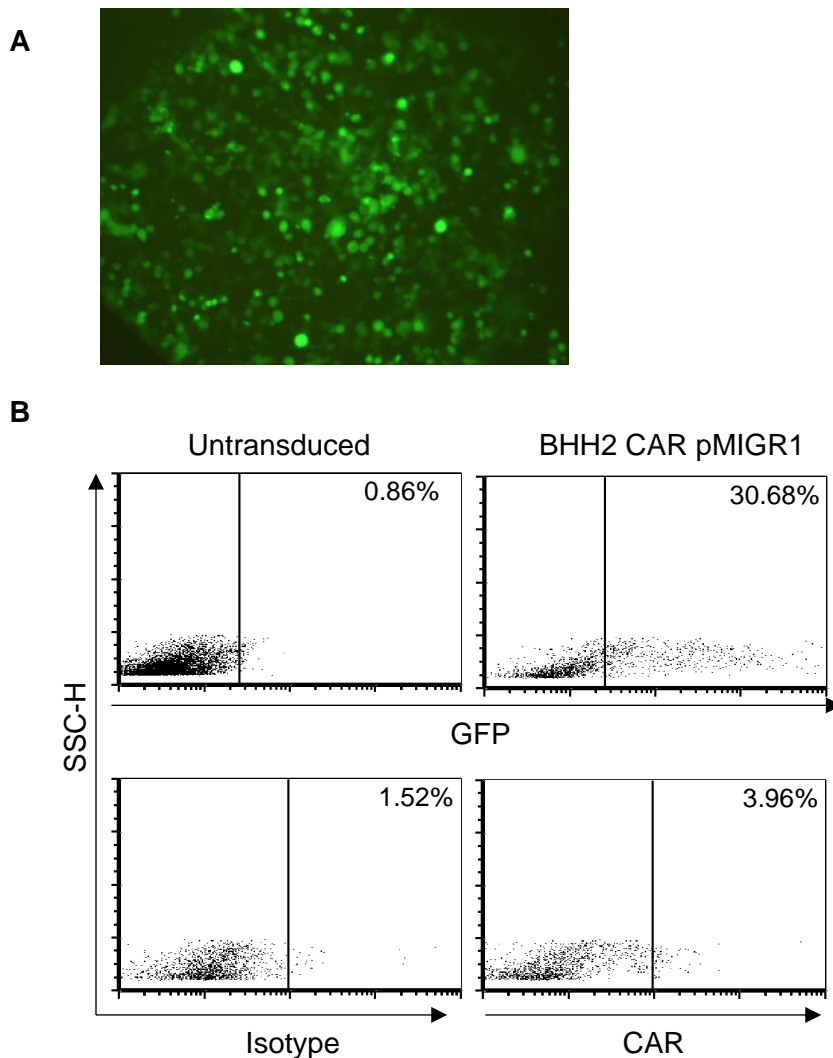


Figure 6.6: Murine splenocytes transduced with viral supernatant collected from Phoenix-ECO cells at 72 h post-transfection

Splenocytes were activated with 2 $\mu\text{g/ml}$ anti-CD3 (KT3) and 2.5 $\mu\text{g/ml}$ anti-CD28 (37.51) for 48 h. Spin transduction was performed twice in the presence of 4 $\mu\text{g/ml}$ polybrene, using viral supernatants collected from Phoenix-ECO cells at 72 h post-transfection. GFP and CAR expression were evaluated at 48 h post-transduction.

A: An area of the well containing CAR-transduced cells, showing high levels of GFP expression. Image captured using 4x microscope magnification setting.

B: GFP and BHH2 CAR expression were evaluated by flow cytometry. GFP expression is shown compared to untransduced control cells. CAR expression was assessed using PE-anti-hIgG-Fc. Isotype control, PE-anti-Syrian hamster (SH) IgG-Fc.

6.3 Generation of bone marrow chimeras

The generation of a bone marrow chimera murine model is a technique that allows the production of naïve T cells expressing the gene construct of choice. Thus, the potential issue of T-cell activation levels in the transduction and expression of CAR constructs would be circumvented. pMIGR1 has been successfully used to transduce murine bone marrow cells, and this method has also previously been employed for the production of several specific TCR+ve models [480, 507].

Donor mice received 150 mg/kg 5-Fluorouracil to ablate the proliferating cell populations prior to harvesting of the bone marrow. Erythrocytes were lysed, and the bone marrow cells were plated in media containing 50 ng/ml each murine IL-3, IL-6 and mSCF (Chapter 2.1.4). 48 h later cells were spun twice in retroviral supernatants at an interval of 6 h, detailed in Chapter 2.4.1.2.3. GFP and CAR expression was evaluated 48 h post-transduction by fluorescence microscopy and flow cytometry (**Figure 6.7**). The transduced donor cells all successfully expressed GFP to a high level. Both the Leu16 and BHH2 CAR transductions also achieved a high proportion of CAR+ve cells.

Strain- and sex- matched recipient mice were irradiated twice at an interval of 24 h, with 5.5 Gy each time (Chapter 2.9.2). After the second dose, each received $0.75-1.12 \times 10^6$ mock or CAR -transduced cells IV. At week 6 and week 10 post-injection the reconstituted mice were screened using flow cytometry for the presence of circulating GFP+ve and CAR+ve cells (**Figure 6.8**). Blood sample collection and flow cytometry screening was performed by Dr Kirstie Cleary and Dr Robert Oldham. Full analysis plots can be found in **Figures A4.1 and A4.2**, in the Appendix.

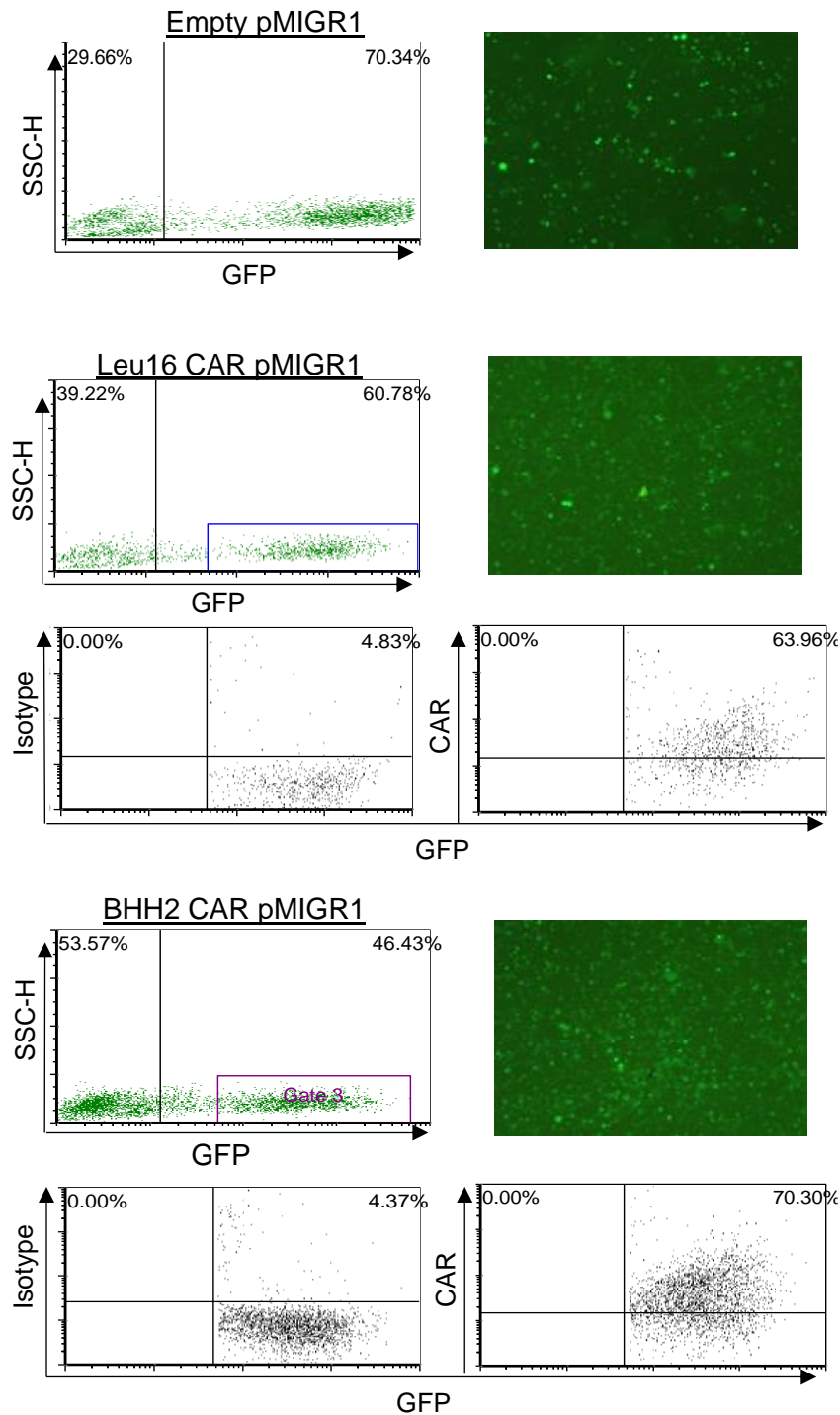


Figure 6.7: Murine bone marrow transduced with CAR constructs

Bone marrow was harvested from 5-Fluorouracil-treated mice and incubated with 50 ng/ml each IL-3, IL-6 and mSCF for 48 h. Cells were transduced twice at an interval of 6 h, for 1 h at 800 xg, 32 °C in the presence of 2 µg/ml polybrene. GFP and CAR expression was evaluated at 48 h post-transduction using fluorescence microscopy and flow cytometry. Shown are fluorescence microscopy images taken of empty pMIGR1, Leu16 and BHH2 CAR-transduced bone marrow cells expressing high levels of GFP. These expression levels were quantified using flow cytometry. For the CAR transduced cells, GFP+ve cells are shown gated upon in combination with staining using PE-anti-hlgG1-Fc to determine the % of GFP+ve CAR+ve cells. Isotype control used was PE-anti-SHlgG1-Fc. Images captured using 4x microscope magnification setting.

The gating strategies used to assess GFP and CAR expression in the bone marrow chimera blood samples are detailed in **Figure 6.8 A**. The lymphocyte gate based on FSC-H/SSC-H is shown, along with example plots of GFP and CAR expression in individual mice. The data were plotted graphically to compare reconstitution between mice (blood samples 1-4, empty vector-transduced donor cells; 5-7 Leu16 CAR-transduced donor cells; 8-10 BHH2 CAR-transduced donor cells), and between the two time points (**Figure 6.8 B and C**). Percentage GFP expression compared to a non-transduced control sample are shown at week 6 and 10 for each chimera (**Figure 6.8 B**). All four of the empty pMIGR1-reconstituted samples exhibited some level of GFP expression, whilst only one Leu16 CAR recipient and no BHH2 CAR recipients showed any.

The CAR expression data were analysed using gates based on isotype control stains for each sample. **Figure 6.8 C** shows the data for each CAR-transduced recipient, where the percentage positive for each isotype control stain has been subtracted from that detected using PE-anti-hlgG1-Fc. The GFP+ve Leu16 CAR sample was shown to also be CAR+ve, with a large increase in the percentage seen between week 6 and 10. No other CAR+ve staining was seen in the other samples.

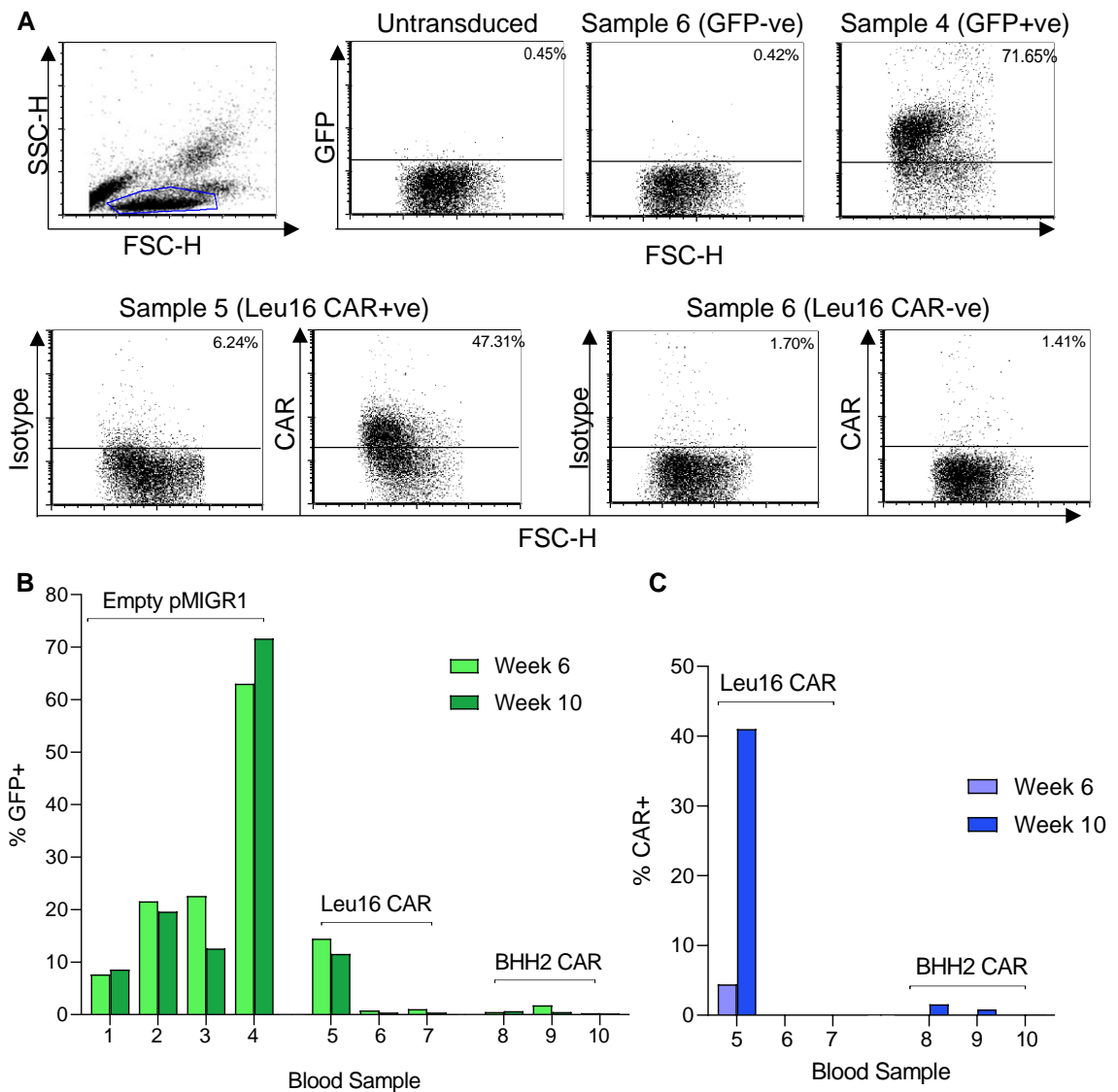


Figure 6.8: Assessment of GFP and CAR expression in the blood of reconstituted mice

Sex- and strain- matched recipients were lethally irradiated and given $0.75\text{-}1.2 \times 10^6$ empty pMIGR1 or CAR transduced bone marrow cells. Blood samples were collected at week 6 and week 10, and flow cytometry was used to screen for the presence of circulating GFP+ve and CAR+ve cells in the individual mice. Isotype control, PE-anti-SHlgG1-Fc; anti-CAR, PE-anti-hlgG1-Fc.

A: Gating strategies for sample analysis. A lymphocyte gate was used to screen this cell population, and to exclude cellular debris. Example plots from a GFP expressing (#4) and non-expressing (#6) mouse are shown, as compared to an untransduced control I. Isotype control staining for each sample was used to analyse percentage CAR+ve levels. Example plots are shown of a CAR+ve (#5) and a CAR-ve (#6) sample. Full analysis plots can be found in the Appendix.

B: Percentage GFP+ve at 6 and 10 w are shown graphically for each recipient sample.

C: Percentage CAR+ve at 6 and 10 w are shown graphically for each CAR transduced cell recipient. Each data point shows the CAR+ve expression percentage as assessed using PE-anti-hlgG1-Fc, minus the expression percentage observed using the isotype control. Where the isotype control percentage was higher than the anti-CAR stain, 0 % is shown.

Whilst the range of GFP+ve percentages for the empty vector-transduced cells is broad, all recipients showed GFP expression in circulating lymphocytes. It was expected that the CAR pMIGR1 transduced chimeras would also at least express GFP. However, only one of six successfully expressed any GFP. This recipient also demonstrated a robust positive CAR expression level, higher than the GFP expression level which is unusual. To confirm whether this expression staining was real, the spleen was harvested and analysed by flow cytometry compared to wild type untransduced control splenocytes (**Figure 6.9**). As the principle of bone marrow chimeras is to generate expressing cells in the initial recipient, and then to harvest these and use them to reconstitute additional mice to use in experimentation, the remaining spleen cells were frozen for possible future use.

Comparison of percentage CAR+ve cells between the chimera and untransduced samples revealed Leu16 CAR expression in the spleen of the recipient. Taken with the blood data, it can be concluded that this CAR expression is real, despite the low GFP expression and absence of any expression in the other recipients. The number of bone marrow donor cells transferred was similar between the three transduction categories, and each construct was robustly expressed in the bone marrow prior to injection. Likewise, all recipients received identical, simultaneous irradiation. Thus, it is difficult to conclude why the other recipients expressed neither GFP nor CAR. As only one Leu16 CAR chimera and no BHH2 CAR cells were positive, it was decided not to pursue this avenue within the confines of this project.

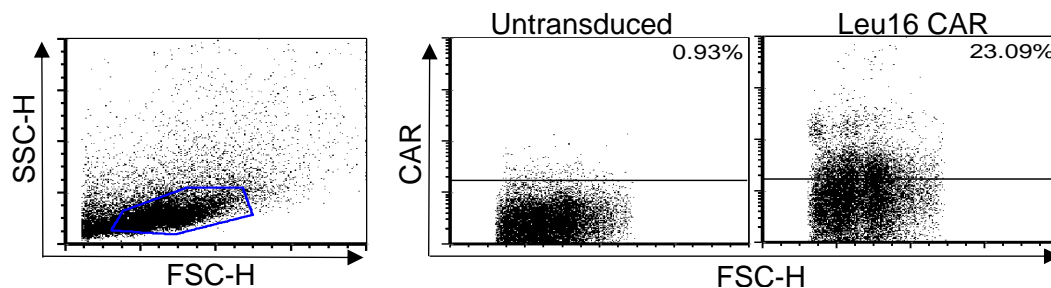


Figure 6.9: CAR expression in the spleen of a Leu16 CAR bone marrow chimera
 The Leu16 CAR+ve mouse (#5) from **Figure 6.8** was sacrificed and the spleen was harvested. CAR expression was evaluated on the splenocytes, as compared to untransduced wild type splenocytes using flow cytometry and PE-anti-hlgG1-Fc. The lymphocyte gate used to exclude other cells and cellular debris is shown. The chimera sample showed CAR+ve cells, correlating with the blood sample data.

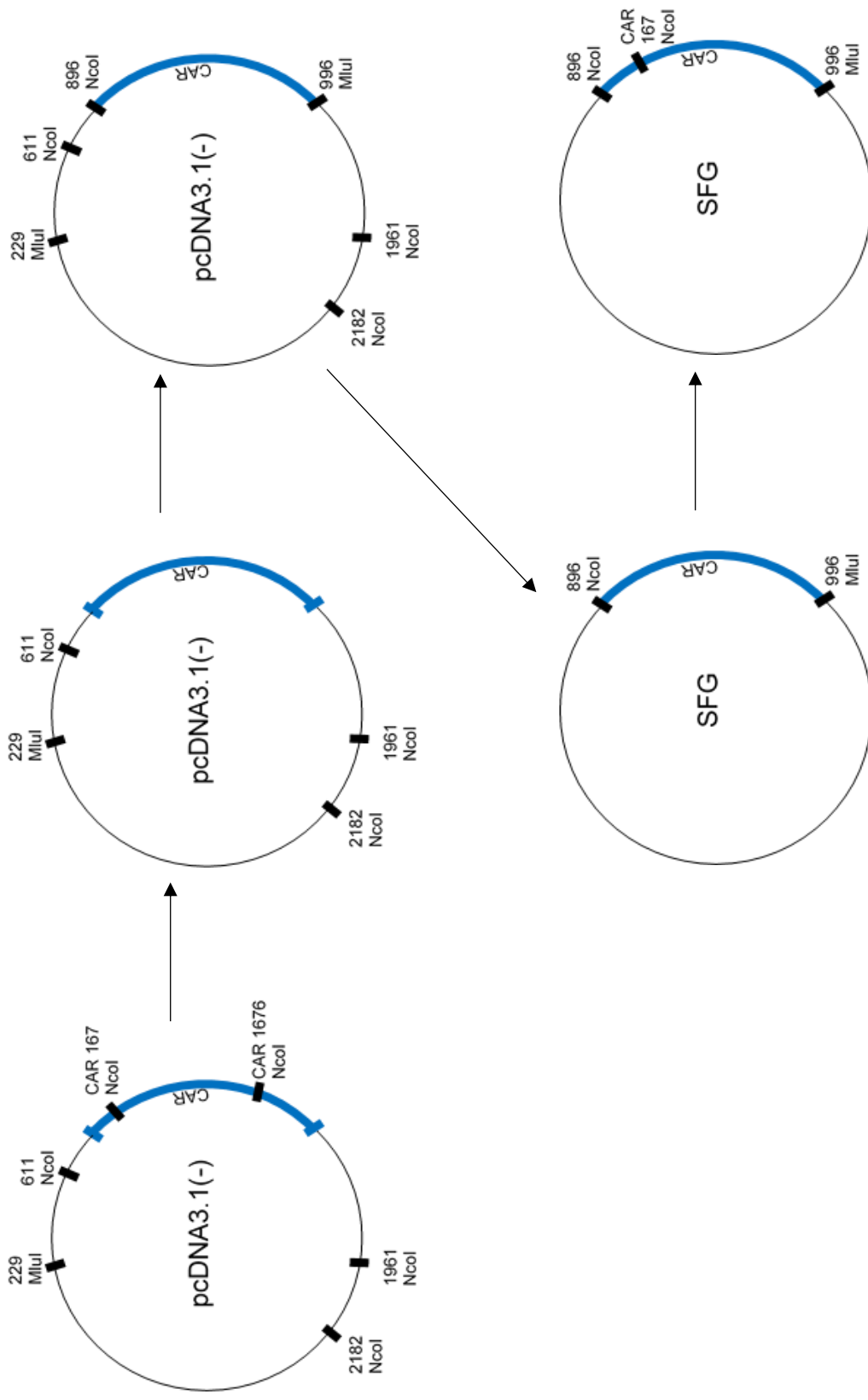
6.4 Transduction of human peripheral blood mononuclear cells

6.4.1 Molecular cloning of CAR constructs into pSFG

To optimise the transduction of human PBMCs, the CAR constructs were cloned into the retroviral vector pSFG (Chapter 2.2.6). This vector has been proven an efficient system for human T-cell transduction including using CAR constructs [389, 439, 509].

To allow cloning into the pSFG vector without altering the CAR sequence each CAR construct underwent several rounds of site-directed mutagenesis (**Figure 6.10**). Firstly, the intra-CAR NcoI restriction enzyme sites at CAR positions 167 and 1676 were removed (**Figure 6.10 B**). An NcoI site was then mutated in at the beginning of the construct, at pcDNA3.1(-) vector position 896 along with an MluI site at the end of the CAR at vector position 996 (**Figure 6.10 C**). This permitted each CAR to be removed from the pcDNA3.1(-) vector without internal CAR sites being engaged, and ligation into SFG via the existing NcoI and MluI sites present in the multiple cloning site of this vector (**Figure 6.10 D**). Finally, the intra-CAR ¹⁶⁷NcoI site mutagenesis was reversed in each, due to it altering the amino acid sequence within the leader sequence.

Each stage of mutagenesis was confirmed by restriction enzyme digests and sequencing. The CAR constructs were fully sequenced using vector and internal primers upon ligation into pSFG to ensure there has been no disruptions to the sequence. The final constructs were each transferred into JM109 chemically competent *E. coli* for replication and large bacterial cultures were grown. DNA was extracted and purified using a Qiagen MaxiPrep kit.



A

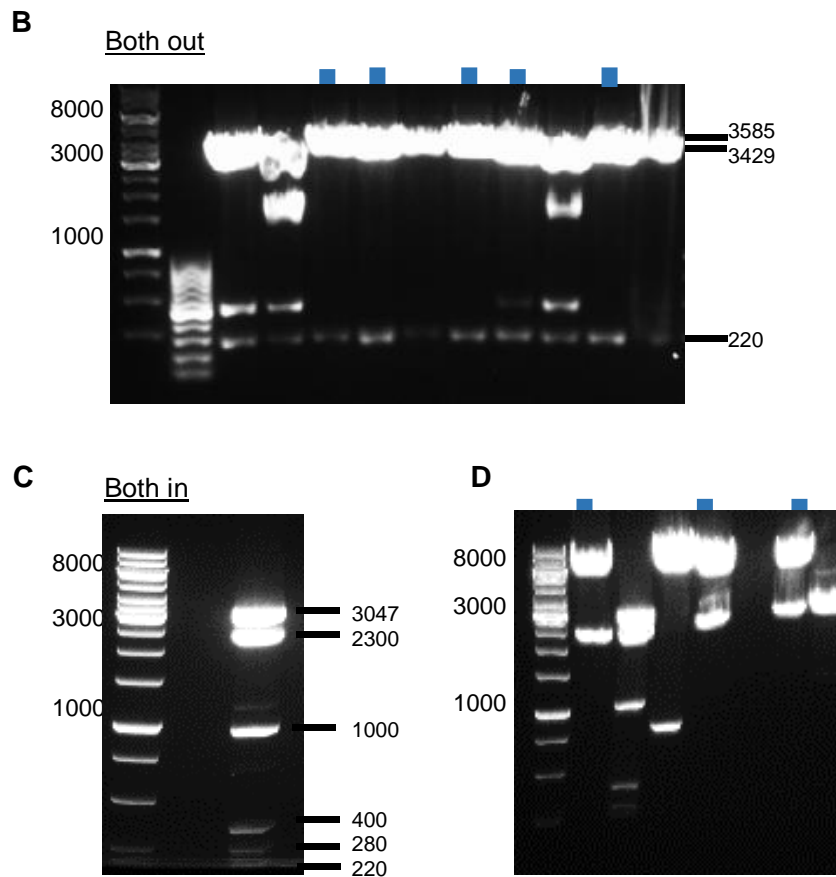


Figure 6.10: Molecular mutagenesis and cloning to transfer each CAR into pSFG

A: Each stage of mutagenesis and subsequent cloning is illustrated. The internal NcoI sites were removed from within the sequence of each CAR. A 5' NcoI and 3' MluI site were mutated in, and each CAR was excised by these sites from pcDNA3.1(-). The constructs were ligated into pSFG via NcoI and MluI restriction sites present in the vector multiple cloning site. Finally, the first intra-CAR NcoI sites were mutated back in, as performing this mutation to enable the cloning of each CAR altered the amino acid sequence.

B-D: Mutated DNA was transferred into XL-Gold chemically competent *E. coli*, cultured, and DNA was extracted and purified. Restriction enzyme digests were performed, and the products separated by gel electrophoresis to confirm the mutagenesis at each stage. Example gel electrophoresis images are shown to illustrate the steps. All ladders shown are 1 kb.

B: Removal of internal NcoI CAR sites. Blue squares indicate lanes containing successful full mutagenesis.

C: Insertion of 5' and 3' NcoI and MluI sites

D: Confirmation of CAR ligation into pSFG. Blue squares indicate lanes containing successful ligations.

6.4.2 Expression of CAR-SFG constructs

Initially, transient transfections were set up using HEK 293F cells to confirm that the constructs still expressed correctly in the new vector. A GFP vector was used as a control for the transfection, and each CAR-SFG construct was assessed for expression at 24 h post-transfection (**Figure 6.11**). All the constructs still were able to be expressed in SFG. As before Ritux CAR showed a lower expression density and percentage of CAR+ve cells.

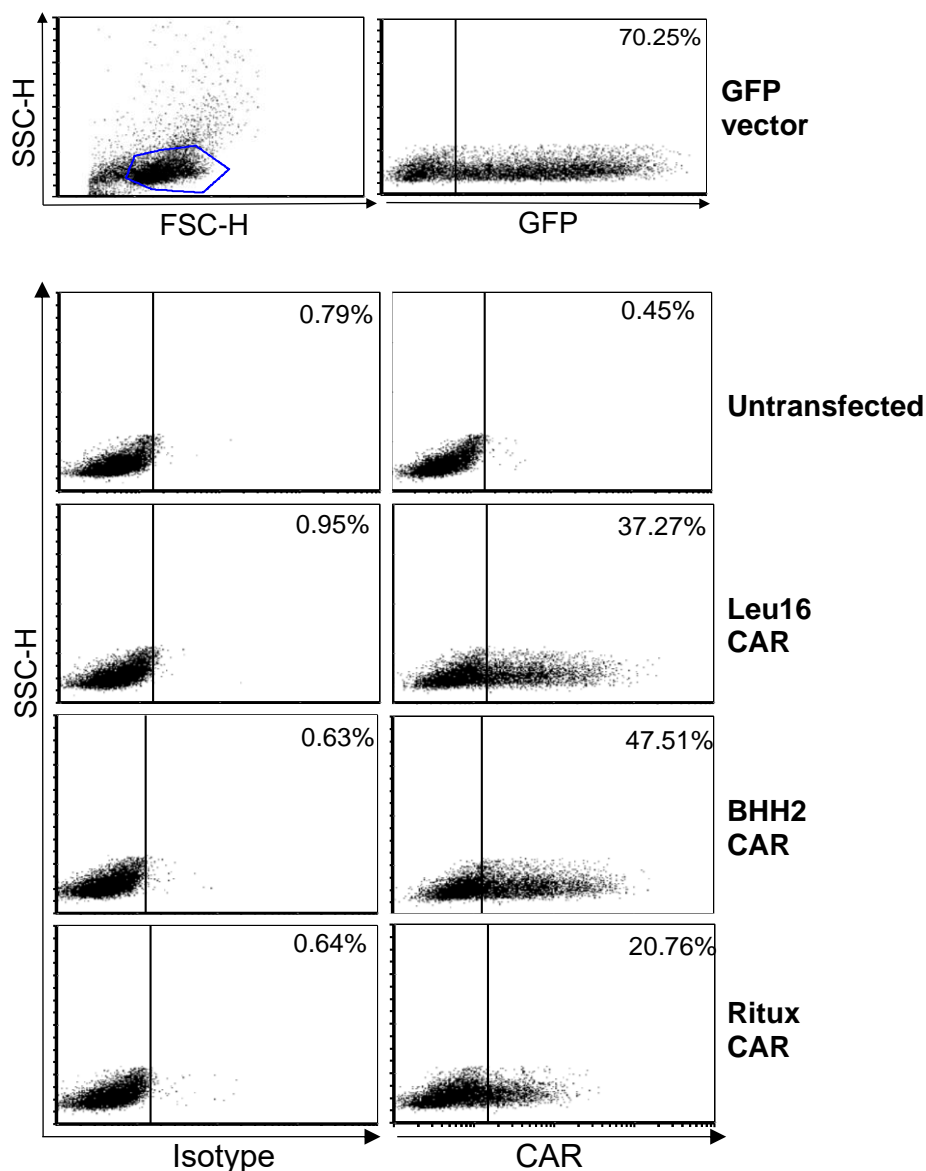


Figure 6.11: Expression of CAR constructs in the SFG vector in transiently transfected HEK 293F cells.

HEK 193F cells were transiently transfected with an empty GFP vector (top), or with each of the CAR constructs. Expression was assessed by flow cytometry at 24 h post-transfection. Gating to exclude cellular debris is shown. Isotype control: PE-anti-mIgG-Fc; anti-CAR: PE-anti-hIgG-Fc. N=1.

HEK 293T cells were cultured at a low density for use as a retroviral-producing cell line. These cells were transfected with the CAR-SFG constructs along with the RD114 envelope and pEQPAM gagpol amphotropic retroviral packaging plasmids (Chapter 2.4.2.1). The viral particle-containing supernatant was collected at 48 h post-transfection and media was replaced. Another harvest was performed at 72 h post-transfection, pooled with the equivalent supernatant from 48 h, and used to spin transduce cells, as described in Chapter 2.4.2.2. To confirm this as a viable method to express the CARs, HEK 293T cells were spin transduced with viral supernatant in the presence of polybrene and expression was assessed after 3 d (**Figure 6.12**). It was confirmed that the CAR-SFG constructs could all successfully be transduced and expressed on the HEK 293T cells. Pooled viral supernatants were either used fresh or were snap-frozen and stored at -80 °C for later use.

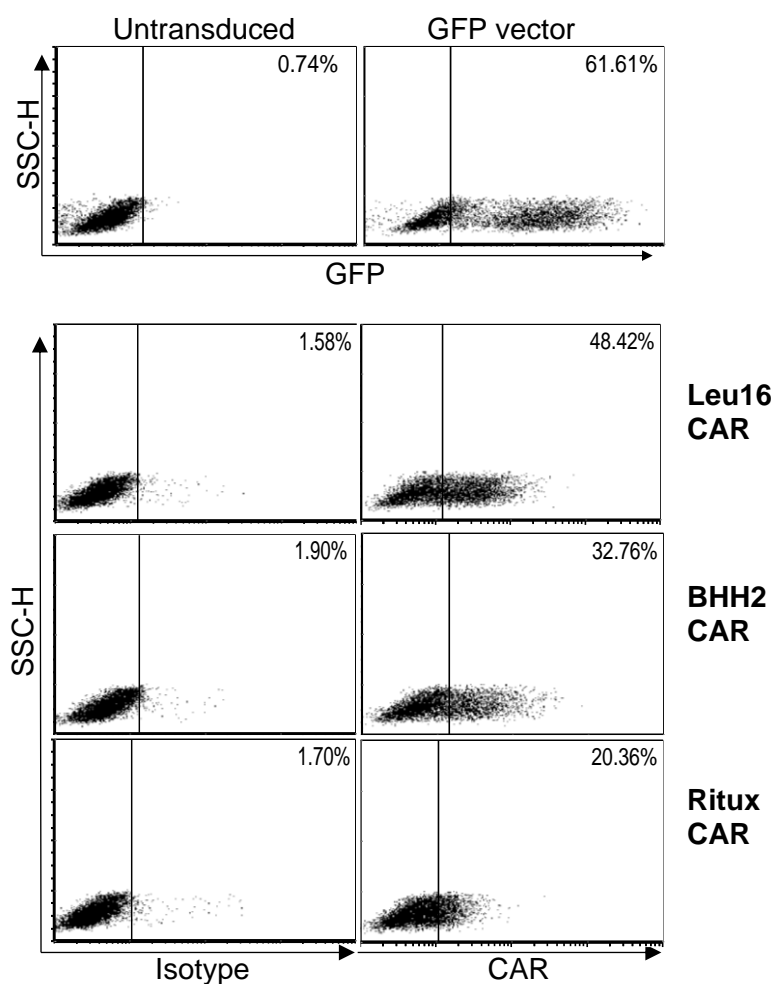


Figure 6.12: Expression of CAR constructs on transduced HEK 293T cells.

HEK 293T cells were spin transduced with viral media harvested from HEK 293T cells that has been transfected with the CAR-SFG constructs and retroviral co-plasmids. An empty GFP vector was also included as a positive control for the transduction (top). Expression was assessed by flow cytometry at d 3 using PE-anti-hlgG-Fc. Isotype control: PE-anti-mIgG-Fc. N=1.

Viral media can be filtered to remove cellular debris prior to spin transduction, but there is evidence that this may lower the viral titer and reduce transduction efficiency (personal communication from Dr John Ferdinand). This was tested using viral supernatant from GFP vector-transfected HEK 293T. A population of HEK 293T cells were identically transduced with either filtered or unfiltered viral supernatant from the same pool. The unfiltered supernatant was centrifuged as an alternative method to pellet the cellular debris. It was shown that the filtered supernatant had a reduced transduction efficiency leading to a 13 % reduction in GFP expression (**Figure 6.13**). The method of centrifuging all viral supernatant prior to use to remove cellular debris by pelleting was thus employed in all following transductions.

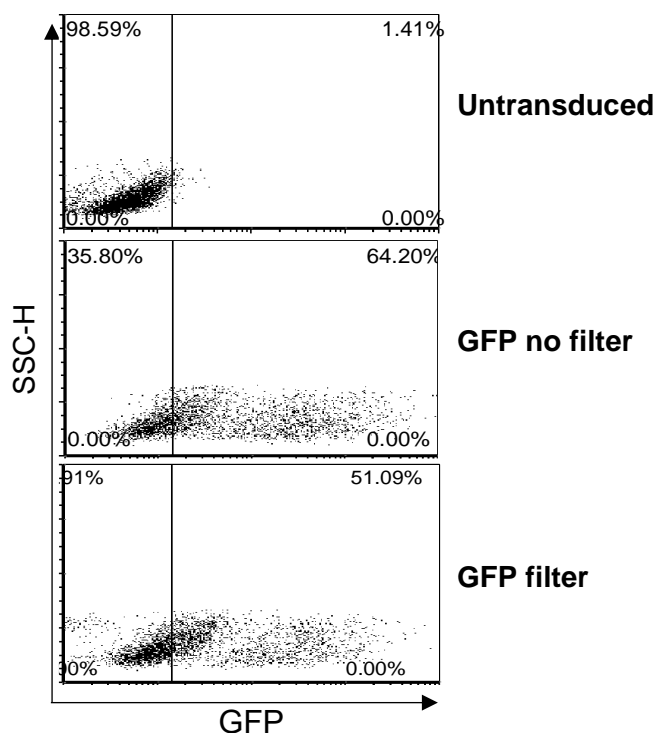


Figure 6.13: A comparison of HEK 293T transduction efficiency with filtered and unfiltered viral supernatant.

Viral supernatants produced from GFP-transfected HEK 293T cells were either filtered (GFP filter), or centrifuged (GFP no filter) to remove cellular debris prior to use. The supernatants were then used to spin transduce HEK 293T cells. GFP expression was compared using flow cytometry at d 3 post transduction between untransduced HEK 293T and those transduced with the two supernatants. N=1.

PBMCs were separated from blood cones from healthy donors using density gradient centrifugation, as described in Chapter 2.1.2. Cells were resuspended and plated in 24-well plates at a density of 2×10^6 / ml. To induce T-cell activation 5 μ g/ml PHA-P was added after 24 h. After a further 24 h, 100 IU/ml recombinant human IL-2 was added to

each well. T cells were examined 24 h later by light microscopy, to look for the large cell rosetting clumps that are characteristic of T-cell activation and the induction of proliferation (**Figure 6.14**). The actively cycling T cells were harvested and spin transduced with viral supernatants, detailed in Chapter 2.4.2.2. Briefly, non-coated 24-well plates were coated overnight with retronectin in PBS. Retronectin has been shown to be superior to polybrene in the transduction of human PBMCs with fusion protein constructs [510]. 2×10^5 PBMCs were plated to each well and freshly harvested or thawed snap-frozen viral supernatants were added with the addition of 100 IU/ml IL-2. Plates were spun at 1000 xg for 40 min, then re-incubated. T cells were harvested from the retronectin and plated in fresh media with IL-2 at 48 h post-transduction. Expression was measured on d 3-4 post-transduction.

An initial transduction trial was performed using Leu16 CAR viral supernatants. The T cells were assessed for CAR expression, and additionally for CD3, CD4 and CD8 expression (**Figure 6.15**). This allowed confirmation that the majority of surviving transduced cells- including the CAR+ve population- were T cells, and showed the proportions of CD4 and CD8 CAR+ve T cells present.

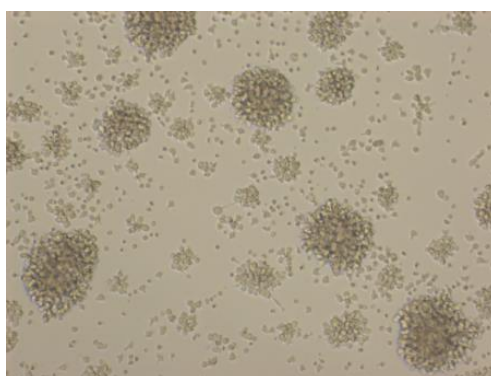


Figure 6.14: Human PBMCs treated with PHA-P and IL-2 to induce T-cell proliferation

Human PBMCs were plated at 2×10^6 /ml in 24-well plates and at 24 h 5 μ g/ml PHA-P was added to induce T-cell proliferation. After a further 24 h, 100 IU/ml IL-2 was added to further stimulate the T-cell populations. Prior to transduction, cells were visualised examined for rosetting and the formation of large cell clumps, a hallmark of T-cell activation and proliferation. Images captured using 4x microscope magnification setting.

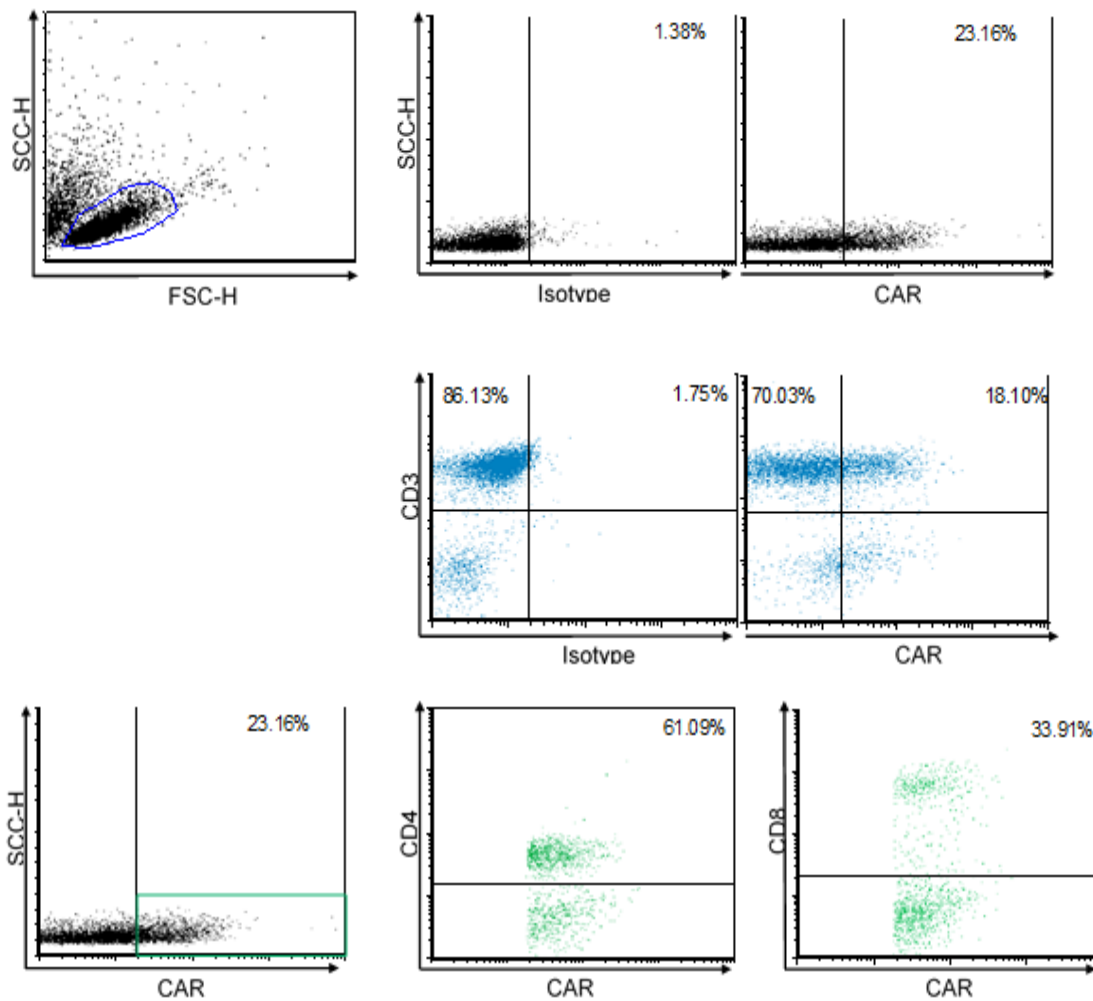


Figure 6.15: Assessment of T-cell populations present in Leu16 CAR-transduced human PBMCs

Human T cells were activated as shown in **Figure 6.14** and were subsequently spin-transduced with viral supernatant from Leu16 CAR-transfected HEK 293T cells. CAR expression and major T-cell populations present were assessed by flow cytometry at 4 d post-transduction. Cells were gated based on FSC-H/SSC-H to exclude debris and CAR expression was determined using PE-anti-hlgG-Fc (top row). Isotype control (PE-anti-mIgG-Fc) is also shown. Cells were additionally stained for CD3 (middle row), and CD4 and CD8 expression (bottom row) to determine the CAR+ve populations of these T-cell subsets. N=1.

Whilst the Leu16 CAR was successfully transduced and expressed on the T cells, a heterogenous population was produced with 23 % CAR positive. Cell sorting was attempted, by staining with PE-anti-hlgG-Fc and the use of a FACSAria (BD Bioscience) but this resulted in a high level of cell death. Therefore, cytotoxicity assays were performed with the mixed populations of transduced T cells.

6.5 Functional comparisons of CAR-mediated cytotoxicity in primary human T cells

PBMCs were activated as previously described and transduced with viral supernatants from HEK 293T cells transfected with each CAR construct, for comparison in cytotoxicity assays (Chapter 2.8.3) (**Figure 6.16 A**). Raji cells were selected as the target cell population due to their robust CD20 expression and being a superior target in antibody-dependent cellular cytotoxicity assays that also employ calcein-AM labelling and release (personal communication Dr Richard Stopforth). Throughout the assays, empty-vector mock-transduced T cells were used as a control population. These were treated in an equivalent manner to the other populations and were transduced with empty pSFG viral supernatant.

Due to the very low expression of Ritux CAR on the T cells, these cells were not included in the subsequent functional assay (**Figure 6.16 A**). The more substantial expression of BHH2 and Leu16 CARs allowed a primary cell comparison assay to be performed between the two CAR constructs that had exhibited the most significant difference in the cell line assays in the previous chapter. As the transduced populations were still mixed, with a substantial proportion of CAR-ve cells, the initial assay was performed over a 24 h period, to allow any more subtle differences to emerge. It was determined that both CAR-transduced populations were capable of cytotoxicity against CD20+ve target cells, above the level of the mock-transduced T cells. BHH2 CAR induced a very high level of cytotoxicity; near maximal at the highest effector:target ratio of 32:1 (**Figure 6.16 B**).

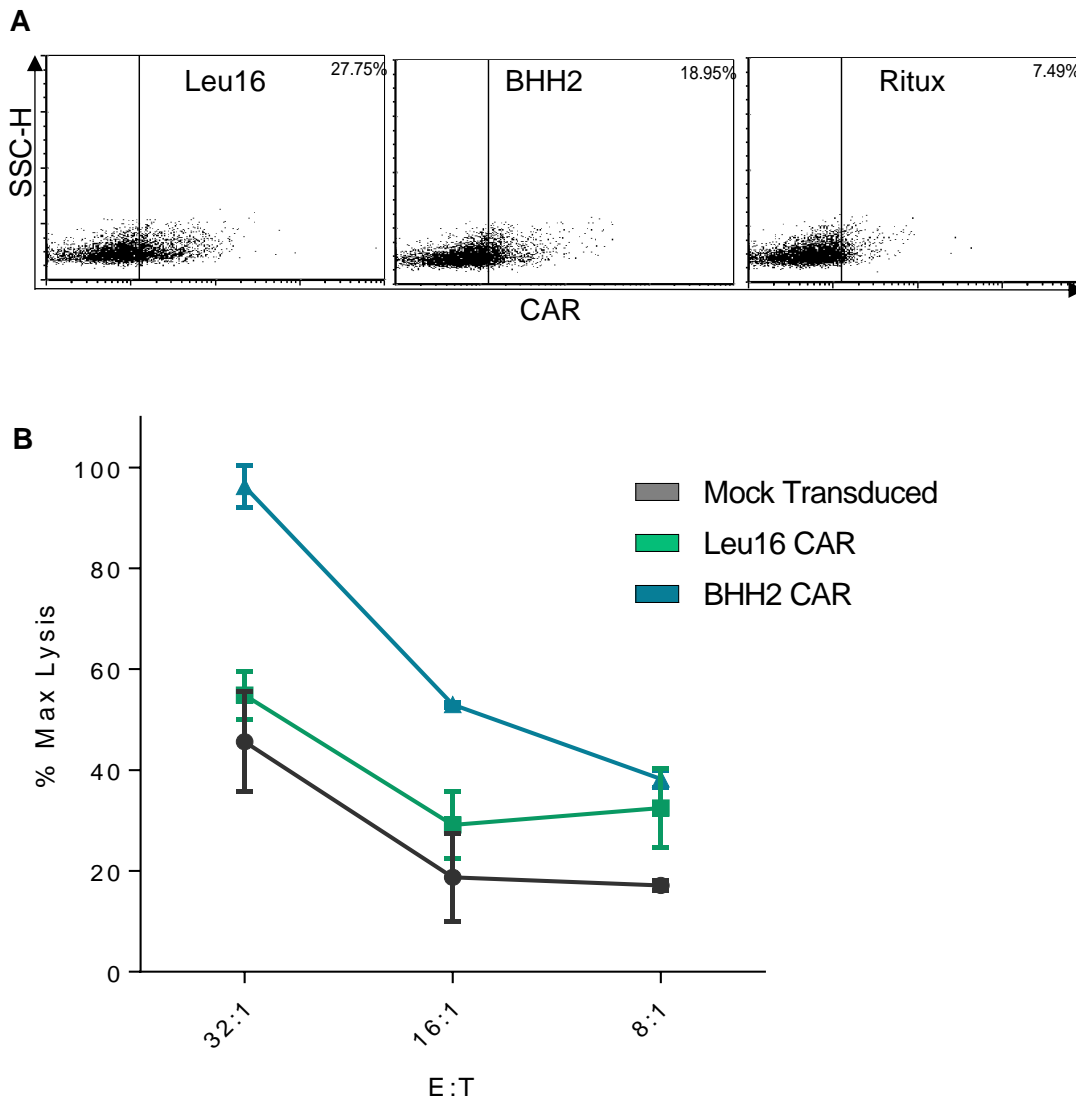


Figure 6.16: A calcein release assay to investigate CAR-mediated cytotoxicity of transduced primary human T cells

A: PBMCs were transduced with viral supernatants from HEK 293T cells transfected with each CAR construct. Expression was assessed at 4 d post-transduction using PE-anti-hlgG-Fc

B: A calcein release cytotoxicity assay was performed using the Leu16 CAR and BHH2 CAR transduced T cells, and with mock-transduced cells. Raji target cells were labelled with calcein-AM and incubated for 24 h with effector cells. The effector:target (E:T) ratios equal the number of CAR+ve cells included in each well, of the mixed transduced populations. Calcein release was assessed on a Varioskan Flash plate reader (Thermo Scientific) using an excitation wavelength of 485 nm and an emission wavelength of 530 nm. Maximal lysis was induced in labelled target cells by the addition of 4 % Triton X. Data was analysed and expressed as a percentage of maximal lysis minus baseline absorbance. Mean of duplicates +/- range, n=1.

The transductions of Leu16 and BHH2 CAR were repeated with fresh PBMCs, and the assay was repeated. Again, cytotoxicity was assessed at 24 h, and an additional 4 h co-culture was analysed (**Figure 6.17**). Whilst the overall levels of cytotoxicity were lower in this second assay, the results showed a similar hierarchy of killing to that shown previously (**Figure 6.16**). Leu16 CAR+ve T cells demonstrated a level of cytotoxicity above that of the mock-transduced T cells, whilst BHH2 CAR elicited a superior response. This was observed at both 24 h as before, and at 4 h (**Figure 6.17 B**).

However, for both these assays the effector:target ratios investigated describe the CAR+ve cell numbers. Thus, the total T cell count included in each population is different. As BHH2 CAR expressed at a lower percentage than Leu16 CAR a higher total number of the mixed population of transduced cells was added to produce the CAR+ve effector numbers required. As the mock-transduced T cells showed a background level of cytotoxicity, they may be providing an additive effect to the CAR-specific killing observed.

To overcome any effect of the different total T-cell numbers included in the assays, due to differing CAR expression levels, the total cell number was equalised using additional mock-transduced T cells. This allowed the total number of T cells per assay well to be constant, whilst maintaining the CAR+ve effector:target ratios. The cytotoxicity assay was repeated again using this adjustment, and CAR-specific killing was assessed at 4 h and 24 h (**Figure 6.18**).

At 4 h, BHH2 CAR was seen to elicit a superior cytotoxic response despite the other populations having equivalent total T-cell numbers. This demonstrates a true CAR-specific difference. However, by 24 h, the cytotoxicity with both the mock-transduced and the CAR+ve T cells was high and at a similar level, suggesting that the large quantity of extra T cells added to compensate for the low CAR expression levels result in a high background after a long incubation. Therefore, it was decided to further investigate short-term co-cultures of the CAR+ve T cells, using mock-transduced T cells to adjust the cell numbers to provide an accurate comparison.

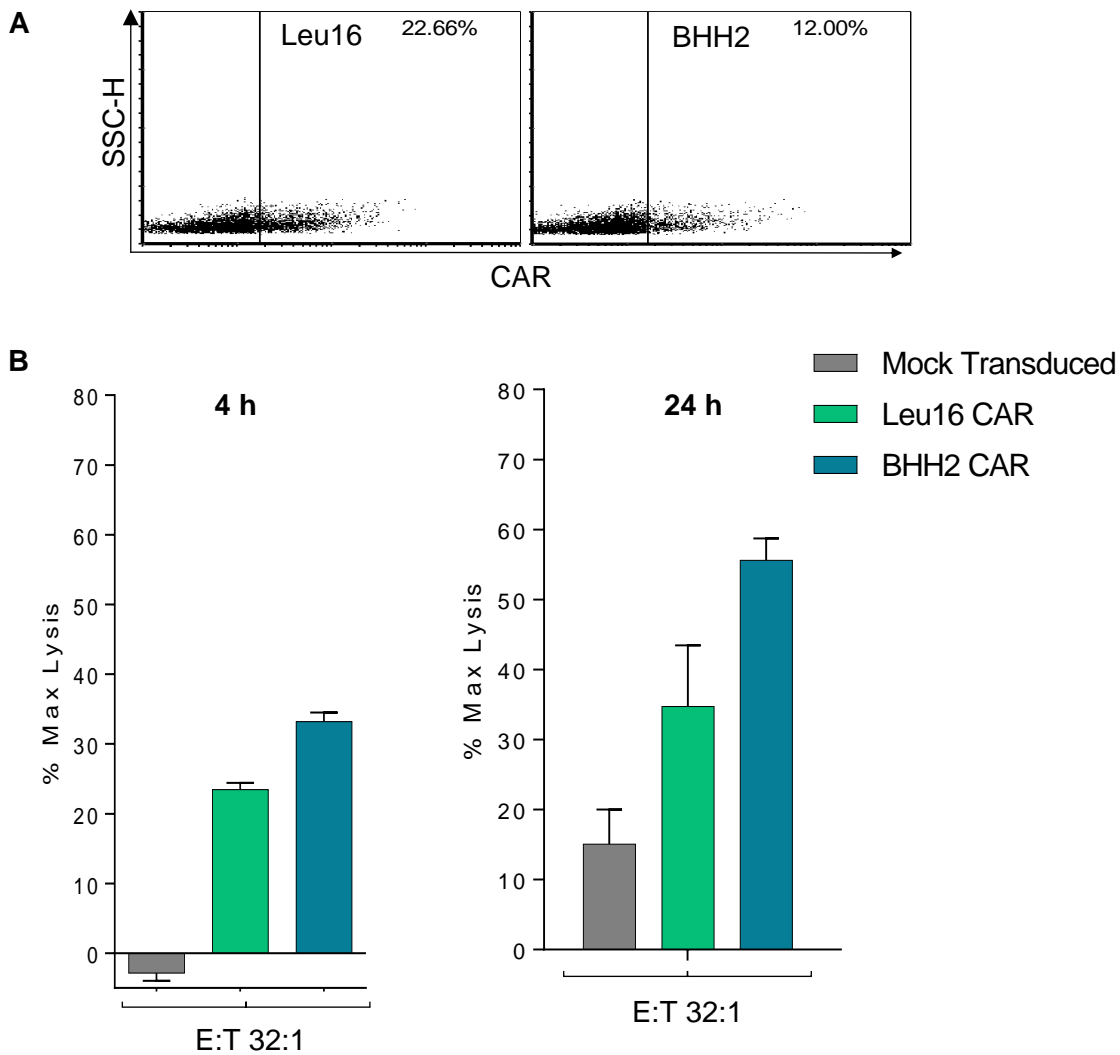


Figure 6.17: Calcein release assays to compare CAR-induced cytotoxicity in primary human T cells at 4 h and 24 h

A: PBMCs were transduced with viral supernatants from HEK 293T cells transfected with Leu16 and BHH2 CAR constructs, and with empty vector (control). Expression was assessed at 4 d post-transduction using PE-anti-hIgG-Fc

B: Calcein release cytotoxicity assays were performed using the Leu16 CAR and BHH2 CAR transduced T cells, and with mock-transduced cells. Raji target cells were labelled with calcein-AM and incubated for 4 h or 24 h with effector cells. The effector:target (E:T) ratios shown represent the number of CAR+ve cells present in the mixed transduced populations. Calcein release was assessed on a Varioskan Flash plate reader (Thermo Scientific) using an excitation wavelength of 485 nm and an emission wavelength of 530 nm. Maximal lysis was induced in labelled target cells by the addition of 4 % Triton X. Data was analysed and expressed as a percentage of maximal lysis minus baseline absorbance. Mean of duplicates +/- range, n=1.

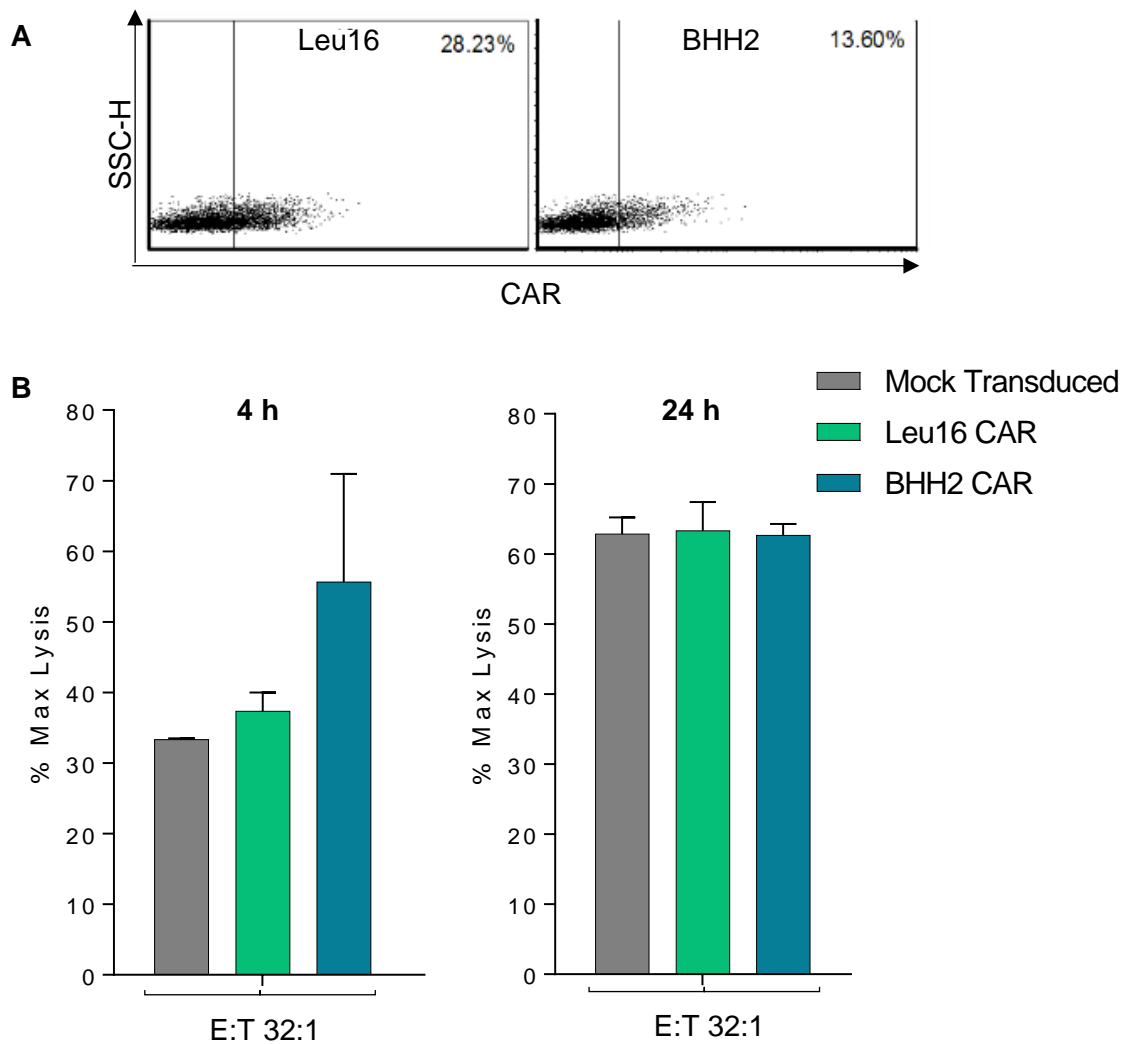


Figure 6.18: Calcein assays performed using Leu16 and BHH2 CAR+ve T cells with total cell numbers adjusted to be equivalent

A: PBMCs were transduced with viral supernatants from HEK 293T cells transfected with Leu16 and BHH2 CAR constructs, or empty vector (mock). Expression was assessed at 4 d post-transduction using PE-anti-hlgG-Fc

B: Calcein release cytotoxicity assays were performed using the Leu16 CAR and BHH2 CAR-transduced T cells, and with mock-transduced cells. Raji target cells were labelled with calcein-AM and incubated for 4 h or 24 h with effector cells. The effector:target (E:T) ratios shown equal the number of CAR+ve cells included in each well, of the mixed transduced populations. The total cell numbers in each comparable well were made equivalent by the addition of mock-transduced T cells. Calcein release was assessed on a Varioskan Flash plate reader (Thermo Scientific) using an excitation wavelength of 485 nm and an emission wavelength of 530 nm. Maximal lysis was induced in labelled target cells by the addition of 4 % Triton X. Data was analysed and expressed as a percentage of maximal lysis minus baseline absorbance. Mean of duplicates +/- range, n=1.

The 4 h cytotoxicity assay was repeated, using Leu16 and BHH2 CAR-transduced T cells (**Figure 6.19 C**). The transduction for this assay yielded higher expression for both CAR constructs (**Figure 6.19 A**), so fewer mock-transduced T cells were required to adjust total cell numbers, lowering background killing and providing a clearer assay. Additionally, a 2 h assay was included to determine any earlier differences in target cell lysis (**Figure 6.19 B**). At 2 h BHH2 CAR had clearly elicited a high level of cytotoxicity against the target cells, which increased by 4 h, whereas Leu16 CAR had no effect above background at 2 h. The Leu16 response increased by 4 h, however it still showed much lower cytotoxicity than the BHH2 CAR. A statistically significant difference ($p < 0.05$) was determined for all BHH2 CAR data points compared with Leu16 CAR and mock-transduced T cells. At 4 h, a statistically significant difference was seen for each Leu16 CAR ratio, when compared with mock-transduced T cells.

The two repeated assays (**Figure 6.18 B, 6.19 C**) comparing CAR+ve T-cell cytotoxicity at 4 h, using adjusted equivalent total T cell numbers are shown combined in **Figure 6.20**. Even allowing for variation in donor PBMCs and in the difference in CAR expression levels from each transduction, a clear difference exists between the mock-transduced T cells and the cytotoxicity stimulated by the CAR constructs. Furthermore, BHH2 CAR-induced killing is shown to be significantly higher than that of Leu16 CAR.

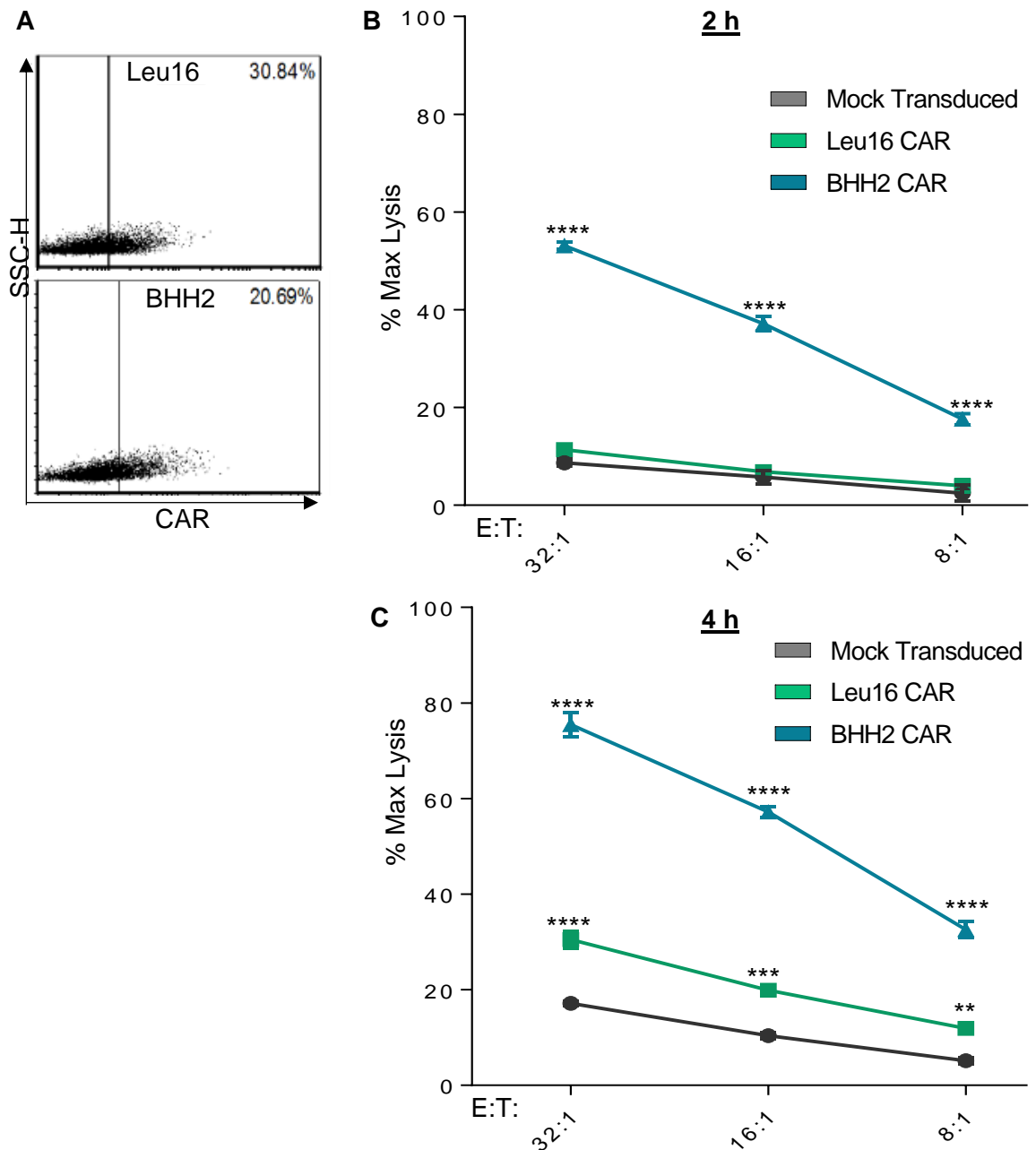


Figure 6.19: Calcein assays performed using total cell number-adjusted populations of Leu16 and BHH2 CAR-transduced T cells

A: Expression at 4 d post-transduction of CAR transduced PBMCs (PE-anti-hlgG-Fc). **B and C:** Calcein release assays were performed with mock, Leu16 and BHH2 CAR transduced T cells. Raji target cells were labelled with calcein-AM and incubated for 2 h (**B**) or 4 h (**C**) with effector cells. The effector:target (E:T) ratios shown equal the number of CAR+ve cells included in each well, of the mixed transduced populations. The total cell numbers in each comparable well were made equivalent by the addition of mock-transduced T cells. Calcein release was assessed on a Varioskan Flash plate reader (Thermo Scientific) using an excitation wavelength of 485 nm and an emission wavelength of 530 nm. Maximal lysis: 4 % Triton X. Data was analysed and expressed as a percentage of maximal lysis - baseline absorbance. Mean of triplicates +/- SEM. Statistical analysis was performed using 2-way ANOVA to compare the data points for each T-cell population to the equivalent populations for each effector:target ratio. Stars indicate statistical significance (* p<0.05; ** p<0.01; *** p<0.001; **** p<0.0001).

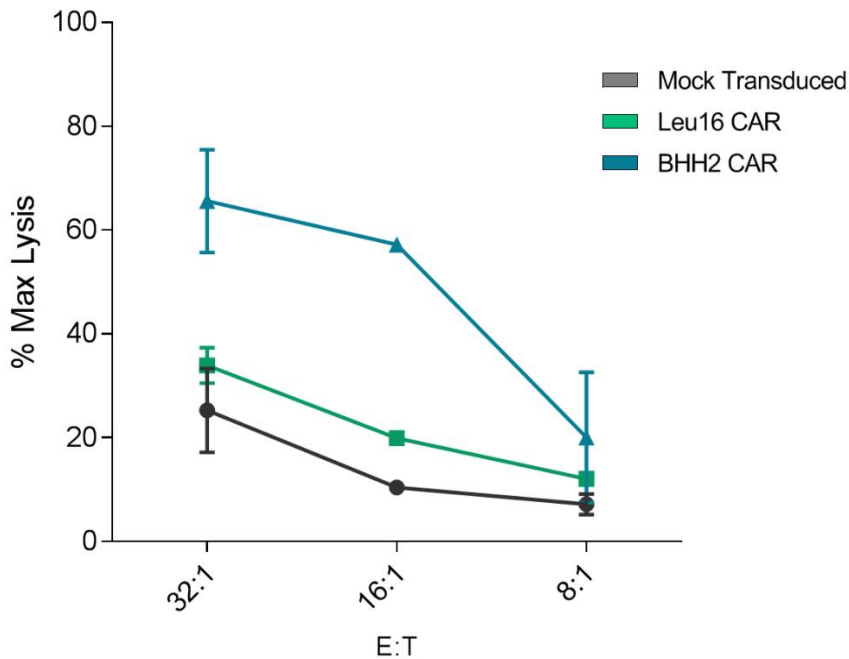


Figure 6.20: Combined data of calcein assays comparing Leu16 and BHH2 CAR-mediated cytotoxicity at 4 h

Data from **Figure 6.18 B** and **6.19 C** of 4 h calcein release are shown combined. Data points at 32:1 and 8:1 show mean +/- range of two independent experiments. Data points at 16:1 show means from a single experiment.

The inclusion of a target population of mock-transduced T cells in each assay has demonstrated that the cytotoxicity observed is CAR- and antigen- specific. To confirm this, a calcein release assay was performed using CD20+ve and CD20-ve RPMI8226 cells as the target populations (**Figure 6.21**). This assay benefited from robust CAR expression, with Leu16 and BHH2 CAR expressed at equivalent levels (**Figure 6.21 A**). The overall cytotoxicity levels seen using RPMI8226 cells were lower than when Raji cells were used as the target population. This may be explained by the lower CD20 expression on the RPMI2886 cells, compared with that of Raji. Another key factor in these assays is that of donor variation. As the PBMCs are harvested from individual donors and transduced separately for each assay, there will be a natural variance in response strengths between individuals.

Despite this, the antigen-specificity of the target cell lysis is clear. Whilst in the absence of CD20, the CAR T cells showed no cytotoxicity above background (**Figure 6.21 B**). In the presence of CD20, BHH2 CAR in particular shows a strong level of cytotoxicity compared to the mock-transduced T cells. Leu16 CAR demonstrates some CD20-specific cytotoxicity, although it is much lower than that seen with BHH2 CAR (**Figure 6.21 C**).

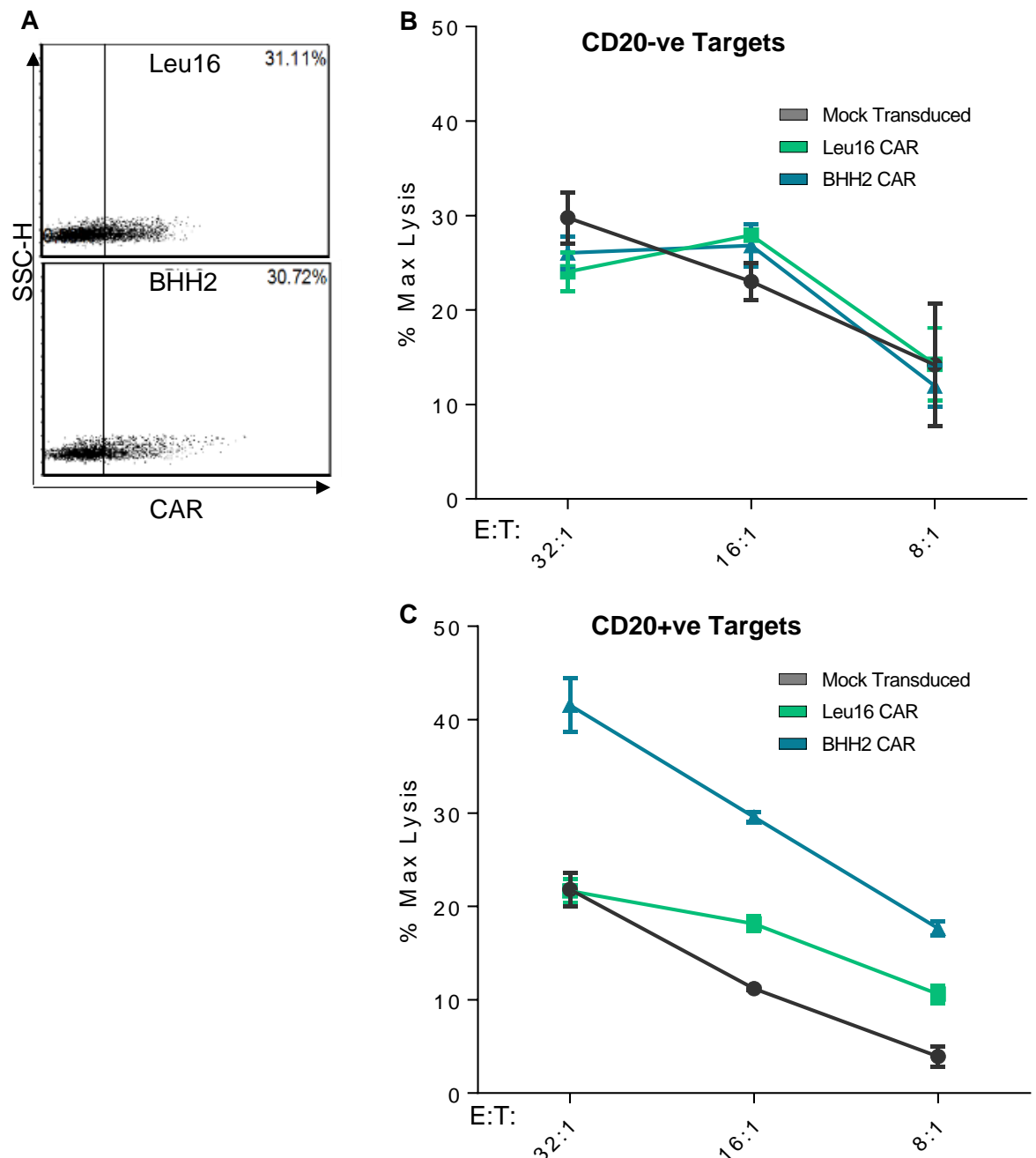


Figure 6.21: Calcein assay performed using Leu16 and BHH2 CAR+ve T cells and CD20+ve and CD20-ve RPMI8226 target cells

A: PBMCs were transduced with viral supernatants as before. Expression was assessed at 4 d post-transduction using PE-anti-hIgG-Fc.

B and C: Calcein release cytotoxicity assays were performed using the mock, Leu16 and BHH2 CAR transduced T cells. Untransfected and CD20-transfected RPMI8226 cells were labelled with calcein-AM and incubated with effector cells for 4 h. The effector:target (E:T) ratios shown equal the number of CAR+ve cells included in each well, of the mixed transduced populations (total numbers adjusted as before). Calcein release was assessed on a Varioskan Flash plate reader (Thermo Scientific) using an excitation wavelength of 485 nm and an emission wavelength of 530 nm. Maximal lysis was induced in labelled target cells by the addition of 4 % Triton X. Data was analysed and expressed as a percentage of maximal lysis minus baseline absorbance. Mean of triplicates +/- SEM, n=1.

To further interrogate the functional differences between Leu16 and BHH2 CAR, co-cultures of transduced human T cells with target cells were performed, and supernatants were harvested for cytokine analysis. The supernatants were used in ELISAs to measure IL-2 and IFN γ production (described in Chapter 2.8.4; performed by Dr Robert Oldham). Mock transduced and CAR+ve T cells (shown in **Figure 6.21 A**) were co-cultured 1:1 with unlabelled Raji cells, and mock and CAR+ve T cells (shown in **Figure 6.19 A**), were co-cultured 20:1 and 10:1 with unlabelled Raji cells. Both CAR+ve T-cell populations produced IFN γ after 24 h of antigenic stimulation, whilst the mock transduced cells produced minimal cytokine. (**Figure 6.22**). BHH2 CAR was shown to elicit higher levels of IFN γ than Leu16 CAR. At the lowest effector to target ratio of 1:1, the difference seen is particularly marked (**Figure 6.22 A**). At both 20:1 and 10:1 effector to target ratios BHH2 CAR induced a very high production of IFN γ , at an approximately two-fold higher level than Leu16 CAR (**Figure 6.22 B**).

1:1 co-cultures incorporating mock-transduced and CAR+ve T cells (shown in **Figure 6.21**) with Raji cells, and of CAR+ve T cells (shown in **Figure 6.18**) with Raji cells and the CD20-ve cell line K562 were also performed. Both CAR+ve T cell populations produced IL-2 upon antigenic stimulation, whilst mock-transduced T cells exhibited low levels of production (**Figure 6.23**). The CAR+ve T cells produced minimal IL-2 after co-culture with CD20-ve cells, confirming the antigen-specific nature of the response (**Figure 6.23 B**). Interestingly, converse to the BWZ.36 IL-2 reporter cell line data presented in Chapter 5, both CARs were shown to induce similar levels of IL-2 production in the primary human cells at the ratio of 1:1 at 24 h.

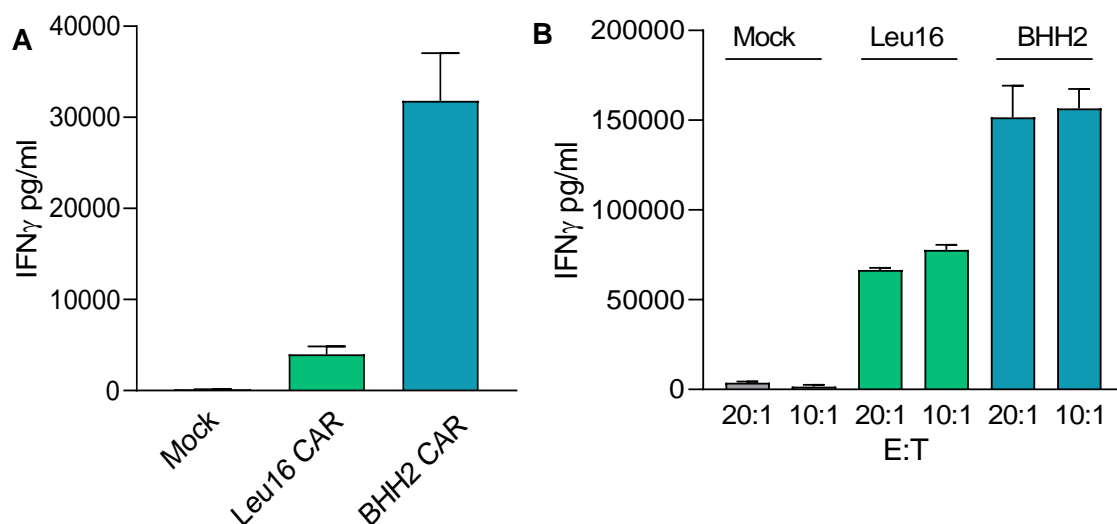


Figure 6.22: CAR-mediated IFN γ production by human primary T cells

Mock-transduced and CAR+ve human T cells were co-cultured with Raji target cells for 24 h. Supernatants were harvested and analysed by ELISA for IFN γ . Captured IFN γ was detected using a biotinylated antibody and avidin-HRP conjugate, and subsequent addition of TMB substrate. Plates were read at an absorbance wavelength of 440 nm - 570 nm on an Epoch plate reader. Analysis of data was performed using an IFN γ standard curve generated using known quantities of cytokine. Mean of co-culture experimental duplicates +/- range.

A: Mock and CAR+ve T cells shown in **Figure 6.21 A**, co-cultured 1:1 with Raji cells.

B: Mock and CAR+ve T cells shown in **Figure 6.19 A**, co-cultured 20:1 and 10:1 with Raji cells.

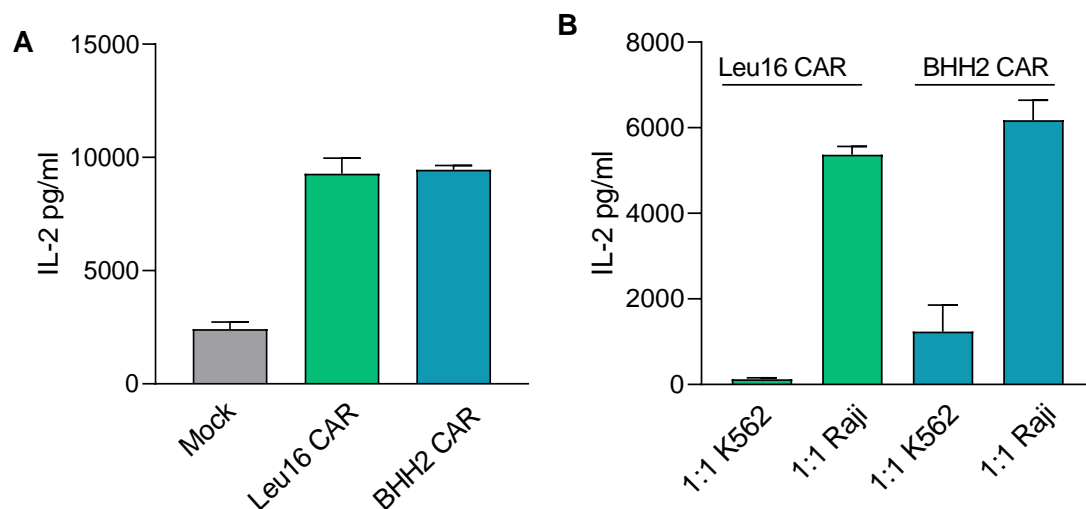


Figure 6.23: CAR-mediated IL-2 production by human primary T cells

Mock-transduced and CAR+ve human T cells were co-cultured with Raji or K562 target cells for 24 h. Supernatants were harvested and analysed by ELISA for IL-2. Captured IL-2 was detected using a biotinylated antibody and avidin-HRP conjugate, and subsequent addition of TMB substrate. Plates were read at an absorbance wavelength of 440 nm - 570 nm on an Epoch plate reader. Analysis of data was performed using an IL-2 standard curve generated using known quantities of cytokine. Mean of co-culture experimental duplicates +/- range.

A: Mock and CAR+ve T cells shown in **Figure 6.21 A**, co-cultured 1:1 with Raji cells.

B: Mock and CAR+ve T cells shown in **Figure 6.18 A**, co-cultured 1:1 with CD20-ve K562 cells or Raji cells.

6.6 Discussion

In the first half of this chapter several techniques were employed in an attempt to establish CAR expression in murine primary T cells. Despite robust GFP expression in both transduced splenocytes, and the pMIGR1 reconstituted circulating lymphocytes, the CAR constructs failed to express. The activated murine splenocytes demonstrated GFP expression when transduced with both the empty pMIGR1 vector, and with CAR constructs. A longer viral production time increased GFP expression in the transfected Phoenix-ECO cells and this translated to a higher percentage of GFP+ve T cells. However, CAR expression was still largely absent.

Similarly, GFP expression was achieved in all four of the bone marrow chimeras reconstituted with empty vector-transduced cells. However, unlike the spleen-derived T cells, all but one CAR-pMIGR1-transduced reconstituted mouse were both GFP-ve and CAR-ve, despite the high bone marrow transduction levels achieved. In the case of GFP+ve CAR-ve cells, an issue with CAR expression would be a likely explanation, but these cells were all double negative except in one case. Equally, in the case of an absence of GFP expression on cells from the empty vector-reconstituted mice, a failure of the bone marrow to graft due to a technical issue would be assumed resulting in no successful chimeras, but all showed GFP+ve cells. One Leu16 CAR-transduced recipient was observed to express both GFP and CAR, in circulating lymphocytes and in the spleen. This suggests that CAR expression is possible using this technique, however in a very inefficient manner.

High levels of CAR expression were observed in murine cell lines in Chapter 5, and expression was also seen in NIH3T3 cells (**Figure 6.2**). Furthermore, robust CAR expression was demonstrated in the primary murine bone marrow cells (**Figure 6.7**). Thus, the CAR constructs are able to be expressed to a high level in both primary murine cells and murine cell lines, but lack expression on primary murine T cells.

In the case of the murine splenocytes the explanation for this could be a technical problem, although the levels of GFP expression observed are indicative of successful transduction. It is possible that cells expressing both GFP and CAR are not capable of surviving. Previous work has encountered issues with over-activation leading to cell death in murine T cells activated for transduction and subsequently expressing signalling components of human CD137 using the pMIGR1 vector (personal communication from Dr Jane Willoughby). Additionally, it has been reported that high expression of a CAR construct comprising CD137 signalling components resulted in CAR+ve T-cell death due to CD137-induced tonic signalling [511].

It can thus be hypothesised that the splenic T cells are activated by anti-CD3 and anti-CD28 to a level permissive of transduction. The upregulation of Fas and FasL on an activated T cell provides the physiological control of an expanding T cell population via activation induced cell death (AICD). In the case of GFP-expressing cells, it can be proposed that the cells do not become over-activated and thus survive. The presence of the CAR may provide sufficient tonic signalling to lead to over-activation of the cells, higher upregulation of Fas and FasL, and subsequent cell death [512].

Alternatively, there may be an issue with murine T-cell expression of the CAR protein, either in transcription or translation control, or in the successful folding of the molecule to allow stable surface expression. This is less likely due to the high expression levels of CAR achieved on other murine primary cells and on murine T-cell lines. Other techniques could be employed, such as the use of codon optimisation to enhance expression specifically in murine cells by increasing the efficiency of transcription [513], although this technique is not without potential complications [514]. Alternatively, the use of a lentiviral vector system may enhance expression and avoid T-cell over-activation [515].

The issue of potential T-cell over-activation was addressed by use of the bone marrow chimera methodology. The transduction of bone marrow cells that are then used to reconstitute lethally-irradiated mice allows the production of circulating immune cells expressing the desired gene, without prior activation. Whilst the CAR constructs were expressed strongly in the transduced murine bone marrow cells, this did not translate to expression on circulating T cells. The absence of both GFP and CAR on circulating cells from these recipients strongly implies cell deletion or death.

CAR+ve T cells may have been deleted when in circulation due to their expressing a foreign protein construct, or the presence of the IgG1-Fc spacer region. Constructs incorporating IgG1-Fc and IgG4-Fc spacer regions have been reported to interact with FcR-expressing immune cells. This has led to instances of both immune clearance of CAR+ve T cells, and of activation of CAR+ve T cells via this region, resulting in AICD [368-371]. It has also been shown that CAR+ve T cells are highly susceptible to Fas-mediated AICD in a mouse model, irrespective of antigenic stimulation [512]. Whilst this study employed transduced splenocytes given by IV injection, it demonstrates a strong correlation between the presence of a CAR construct on circulating lymphocytes, and an increased level of AICD. These explanations do not however clarify why one Leu16 CAR recipient did express both low level GFP and CAR. It would be possible to ascertain if immune interaction was to blame by the use

of an immunocompromised mouse model such as SCID, in combination with the Fc gamma chain knock out [516, 517].

The second half of this chapter involved the use of human primary T cells to assess *in vitro* CAR cytotoxic functions. Human PBMCs were successfully transduced with Leu16 and BHH2 CARs. Ritux CAR consistently expressed at a reduced level, as seen previously, and so was excluded from these investigations. The use of Leu16 and BHH2 CARs provided a comparison between a type I and a type II scFv-based CAR, and also continued the evaluation of those constructs shown to exhibit the most differences in the cell line studies of Chapter 5.

The constructs were evaluated in an *in vitro* system and both were shown to be capable of target cell lysis. The total cell numbers were adjusted using mock-transduced T cells, to account for variation in transduction efficiency. This allowed the real difference in CAR-mediated cytotoxicity to be revealed. BHH2 CAR was shown to be superior to Leu16 CAR at killing CD20+ve target cells in all circumstances. Antigen-specific killing was confirmed by the inclusion of mock-transduced T cells, and the use of untransfected CD20-ve RPMI8226 target cells.

When compared to the data presented in the previous chapters, a clear correlation is shown between the ability of BHH2 CAR to induce a T-cell activation response and the cytotoxic ability demonstrated. Equally, Leu16 CAR was observed to elicit both a lower activation level in the cell lines, and cytotoxic efficacy in the primary T cells. As Leu16 CAR has consistently expressed at a higher level than BHH2 CAR on the primary human T cells, the difference in target cell lysis cannot be attributed to percentage CAR+ve cells, nor to the CAR density per cell.

When the cytokine production of human primary transduced T cells was evaluated, IFN γ production was shown to be induced by both CARs, whilst mock transduced cells showed minimal levels. Correlative to the previous CTLL-2 murine IFN γ ELISA data (**Figure 5.33**), BHH2 CAR elicited a much higher production of human IFN γ than Leu16 CAR. This also correlates with the higher cytotoxicity seen with the same BHH2 CAR+ve cells as compared to both mock and Leu16 CAR+ve T cells.

Surprisingly, both the CAR+ve human T-cell populations were shown to produce similar levels of human IL-2 after 24 h co-culture with CD20+ve target cells. Both BHH2 and Leu16 CAR were able to induce production of high levels of IL-2 in the presence of antigenic stimulation. This is contrary to the data discussed in Chapter 5, whereby Leu16 CAR+ve BWZ.36 IL-2 reporter cells were activated to a much lower level than BHH2 CAR+ve cells. Whilst the reporter cell line data was demonstrated to be consistent it is clear that in a different, more physiologically relevant context, Leu16

CAR has an increased T-cell activation ability. The BWZ.36 cells are a murine fusion cell line that has been manipulated to perform a reporter function. In this cell context BHH2 CAR can elicit an increased activation level compared to Leu16 CAR.

Transduced human T cells from PBMCs present a different, less manipulated primary cell type. This finding highlights the need for evaluation of CARs in primary cells, and the limitations of cell lines.

Additionally, further investigation using a range of effector:target ratios and different co-culture times would reveal if the CAR-mediated IL-2 production is consistent in other conditions. A higher effector:target ratio may result in overall increased production of IL-2, as seen with IFN γ , and levels of secreted IL-2 induced by the two CARs may differ. As autocrine IL-2 signalling in cytotoxic T cells leads to upregulation of IFN γ production [477], further time points would reveal if temporal differences in the activation response are present between BHH2 and Leu16 CARs. Despite the similar human IL-2 levels produced, it can be concluded overall that the inclusion of BHH2 scFv in the CAR construct provides a superior T-cell effector response than incorporation of Leu16 scFv.

In the published work using the Leu16 CAR construct by Oliver Press' group [466], a chromium release assay was employed, similar to the calcein-AM assay. Levels of target cell lysis of approximately 55 % were observed when Daudi cells ([518] a Burkitt's lymphoma cell line, of similar origin to Raji cells) were the target population. Cytotoxicity levels of between ~25 % and ~60 % were reported with use of patient samples. IFN γ production mediated by this CAR were low (~100 pg/ml), however this was measured on d 7 of a 14 d re-stimulation experiment so is not comparable to a 24 h co-culture. Whilst this study used a similar CAR construct to that used in this thesis, expressing on primary human T cells, there are several differences between the studies that inhibit direct comparison.

The published Leu16 CAR sequence is identical in the scFv domain to the construct used in this thesis; and the spacer, transmembrane and signalling domains are equivalent. However, the sequences for these domains were acquired from The Universal Protein Resource database [519], and did not undergo any further change or optimisation except for the alteration of the dileucine motif in the signalling domain of CD28 to a diglycine motif [466, 520]. Thus, there may be differences between the two final construct sequences. Additionally, the techniques used are not comparable with regards to T-cell activation, vector systems, DNA introduction, and cell cloning. The assays presented in the published work used pure CD8+ve CAR+ve CTL clones, following the use of electroporation and sub-cloning, whilst the data presented in this

thesis were generated using heterogeneous populations of retrovirally-transduced PBMCs. Despite this, the published Leu16 scFv has been proven to be inferior to BHH2 scFv when compared in this thesis using equivalent methodology.

A 1F5-based CAR study [521]- in which human primary T cells were retrovirally-transduced with the construct and similar short-term cytotoxicity assays using Raji cells to those in this thesis were performed- demonstrated a target cell lysis level of ~60 % and ~50% at effector:target ratios of 40:1 and 20:1 respectively. Whilst this cannot be directly compared to the data presented in this chapter, it would be interesting to investigate whether BHH2 CAR demonstrates a true higher level of cytotoxic function when analysed side-by-side with this 1F5 CAR. Interestingly, when the 1F5 CAR was assessed for cytokine production after 24 h in a co-culture with Raji cells, as performed in this chapter with BHH2 and Leu16 CARs, the IL-2 levels seen were comparable. However, when compared to BHH2 CAR, much lower (~600 pg/ml) IFN γ levels were measured, similar to that seen for Leu16 CAR at 1:1. Again, it would be interesting to design a direct comparison study with this published construct and the CARs generated in this thesis.

A key issue with some of the human T-cell data presented in this chapter is that of a high background cytotoxic response, seen in the absence of CAR or CD20 expression. This can be explained by the use of heterogeneous T-cell populations due to differences in CAR expression levels. It is likely that the high number of CAR-ve cells added to equalise the total cell number is increasing the background cytotoxicity. Fluorescence-activated cell sorting (FACS) using the anti-CAR spacer antibody was attempted to produce a purer population of CAR+ve cells. However, this resulted in high levels of CAR+ve T-cell death and was not a viable option. An expression marker such as GFP could be inserted into the vector and used for detection and FACS without the need for use of an anti-CAR antibody that may lead to inadvertent activation and contribute to cell death.

Alternatively, a retroviral vector with an antibiotic selection gene could be used to allow selection and sub-cloning of the transduced cells. This would however require longer-term cell culture which may also affect T-cell function. With a higher percentage of CAR+ve T cells, fewer total cells would need to be added to the assays to produce the required ratios, and background levels of target cell death would be reduced. This would also allow the inclusion of the lower-expressing Ritux CAR+ve T cells. Additionally, NK cells present in the culture will be capable of influencing background cytotoxicity levels. These can be depleted using anti-CD56 prior to T-cell activation and transduction to eliminate any background cytotoxicity.

The properties of the scFv in terms of their parental mAb type, antigen binding angle and binding strength may all contribute to the differences seen in cytotoxic function between Leu16 and BHH2 CAR. To achieve efficient cytotoxic lysis of a target cell an IS must be formed and sustained for T-cell activation signalling, and to allow actin and microfilament reorganisation for lytic granule transport. These mechanisms are dependent on both the width of the IS, and strength and duration of interaction [177, 497]. Whilst the CAR synapse has been shown to differ from the conventional TCR-MHC synapse in being less ordered and structured, a strong interaction is still vital to elicit an effector response [358]. Equally, the synaptic distance for effective cytotoxicity by lytic granule release has been proven in both CTLs -and NK cells acting via FcRs- to be critical for optimal lysis [177, 377, 464, 497] . A CAR synapse that is of similar distance to the endogenous IS, bringing the cells into close contact, will therefore induce more effective killing. The binding angle of BHH2 CAR is hypothesised to hold the T cell-target cells in closer proximity, facilitating both a superior T-cell response and a more effective synapse for lytic granule release and function.

Whilst these differences are very interesting, it must be noted that *in vitro* assays always have limitations. The cytotoxicity levels seen provide a clear insight into CAR functional ability and efficacy, however this does only take into account the cells present in the assay system. *In vitro* assays to evaluate CAR function often translate to efficacy seen *in vivo*, but some aspects can be altered. For example, a study comparing anti-ROR1 CAR comprising scFv with varying affinities showed similar lysis levels *in vitro* between the CAR constructs, but the higher affinity scFv lead to overall higher anti-tumour effects in an *in vivo* model due to enhance proliferation and cytokine production [386]. The binding, cytokine and cytotoxicity data presented in this thesis provides the hypothesis that BHH2 CAR+ve T cells would be activated, proliferate and function to a higher level than the other constructs *in vivo*. However, there are complicated cellular interactions and effects of a cytokine milieu *in vivo* that an *in vitro* system cannot always predict. Therefore, it would be essential to use these CAR+ve T cells in an *in vivo* model to determine if the differences in CAR function translate.

7 Final discussion and future directions

This thesis aimed to design and produce a panel of anti-CD20 CAR constructs and investigate their function and characteristics with the purpose of comparing the role of the scFv domain. Previous studies have demonstrated that the targeted epitope position and scFv binding affinity can both strongly influence CAR efficacy. Whilst this has been investigated for several antigens, [373, 374, 379-381, 384-386, 388, 389] no published data present an interrogation of the role of the scFv in anti-CD20 CAR.

CD20 is a favoured target antigen for many B-cell targeted immunotherapies due to its expression on >95 % of B cells, at all stages of development. Whilst internalisation is observed upon binding by type I mAb, CD20 typically maintains stable cell surface expression [187, 195]. Importantly, CD20 also has restricted expression to B cells only, reducing potentially harmful off-target effects seen with antigens with wider tissue expression profiles. Whilst anti-CD20 therapies lead to the depletion of the healthy B-cell population alongside malignant cells, often resulting in hypogammaglobulinemia, the effects of this can be counteracted with the administration of intravenous immunoglobulin (IVIg) [522, 523].

In addition to multiple anti-CD20 mAb, anti-CD20 CAR have also been developed and have progressed to early clinical trials [524, 525]. The major CAR successes seen in the clinic however have been those targeting CD19, and multiple anti-CD19 CAR have been developed. These early successes, and consequent focus on CD19 as a target, may explain why relatively few anti-CD20 CAR have been developed to date, despite the positive aspects of CD20 as a target antigen and the availability of effective anti-CD20 mAb. Additionally, CAR therapy is used currently only for patients with relapsed, otherwise untreatable disease. The frontline immunotherapies for B-cell malignancies are anti-CD20 mAb, and relapsed disease is often refractory to these treatments.

Whilst this resistance can be due to mAb-specific mechanisms such as the upregulation of complement defence molecules, it can also be attributed to reduced CD20 surface expression as a consequence of internalisation or shaving [526]. Thus, anti-CD19 CAR can provide a way to target CD20-ve relapsed disease. The design of dual-targeting and trivalent CAR+ve T cells, as discussed in Chapter 1.8.4, has recently brought anti-CD20 CAR into further clinical evaluation [527] [528].

However, the optimal design for an anti-CD20 CAR has not been thoroughly investigated with regard to the antigen binding domain. The published constructs incorporate the murine-derived scFv Leu16 or 1F5, or a humanised scFv, 1.5.3, for use

in clinical evaluation. With the exception of the comparison between the murine and the humanised scFv [529], the role of the binding domain has not previously been demonstrated. As discussed in Chapter 1.8.4, a published conference abstract [495] reports the *in vitro* evaluation of different anti-CD20 scFv included in a CAR construct. They report that a CAR incorporating an ofatumumab scFv demonstrated superior IFN γ production and target cell lysis, compared to those incorporating scFv from rituximab, Leu16 and obinutuzumab. The authors attribute this to the binding of ofatumumab to the smaller extracellular loop of CD20, at a membrane proximal epitope, and to the markedly slow off-rate of ofatumumab. However, no data is as yet published, and the authors mis-categorise the parental mAb used (obinutuzumab as type I, ofatumumab as type II) making the conclusions unclear. They conclude that inclusion of type II scFv in a CAR gives superior function, despite ofatumumab being a type I mAb. It is also unclear from the abstract whether the other constructs, including obinutuzumab, presented similar functional abilities, or if a hierarchy existed.

The type II mAb BHH2, a non-glycoengineered clone of obinutuzumab, has been shown to outperform type I mAb [197], thus the question of whether this would translate to CAR incorporating each scFv was raised. The CAR constructs designed and generated in this thesis comprise identical intracellular, transmembrane and spacer domains, and differed only in the scFv included. Additionally, identical enhancer and leader sequences were included, and constructs were expressed in the same vectors containing the same promoters. Of the five constructs generated, three expressed stably on the cell surface; Ritux, Leu16 and BHH2 CARs. A successfully expressing ofatumumab (2F2) scFv CAR has been described [495], but no data or sequence is currently available of the construct, and so the differences between this construct and the 2F2 CAR described in this thesis are not known. It is possible that slight alteration of the construct would allow the expression and interrogation of a 2F2 CAR.

The comparison of the different anti-CD20 CAR in cell line systems revealed successful, specific antigen binding of all three surface-expressed constructs. BHH2 and Leu16 CAR were shown to bind at an equivalent level, whilst the Ritux CAR consistently exhibited reduced binding. Throughout the study, the Ritux CAR was expressed at a lower level (% and MFI) on all cell types. This suggests a component of this scFv is less efficiently generated by mammalian cells or that it is less stable.

When T-cell activation was evaluated using the BWZ.36 IL-2 reporter cell line, the BHH2 CAR consistently elicited the highest response. The Ritux CAR demonstrated an intermediate activation, whilst the Leu16 CAR induced a low response. These data are further supported by the IFN γ production seen from CAR-expressing CTLL-2 cells.

Again, when the two were compared, the BHH2 CAR produced a high level of cytokine, whilst the Leu16 CAR+ve cells did not secrete any above background levels.

Furthermore, these data correlate with the primary human T-cell cytotoxicity assays performed in which the BHH2 CAR was repeatedly shown to be superior to the Leu16 CAR at specific target cell lysis.

Evaluation of IFN γ production from the primary human T cells revealed a correlative finding. BHH2 CAR was shown to induce much higher IFN γ production upon antigenic stimulation than Leu16 CAR. IFN γ is a marker for CTL cytotoxicity, and the BHH2 CAR+ve cells shown to produce higher IFN γ were those that also demonstrated superior target cell lysis in the calcein release assays, as compared with Leu16 CAR+ve T cells.

Despite Leu16 CAR repeatedly inducing a significantly lower activation response in the IL-2 T-cell reporter assays, the levels of IL-2 produced by the primary human T cells was similar for BHH2 and Leu16 CAR. This can most likely be attributed to the differences in cells used. The murine cell line could not be as effectively activated by Leu16 CAR, whilst BHH2 CAR was capable of a near-maximal reporter read-out. However, in the more physiologically relevant primary human T cells, both CARs were able to induce high IL-2 production. Differences in signalling sensitivity between the murine reporter cells and human primary T cells are proposed to be responsible for the differences seen.

IFN γ and IL-2 have complex and often over-lapping roles in a cytotoxic T-cell response. IL-2 plays a key role in the proliferation of activated T cells and triggers signalling pathways via JAK 1/3 and STAT 5, increasing glucose uptake and metabolism and the phosphorylation of mTOR, driving the cell into the cell cycle [477] [487]. A study on the phosphoproteome of IL-2 signalling revealed phosphorylation and activation of multiple proteins involved in transcription, translation, cytoskeletal organisation, and vesicle trafficking [530]. Again, this demonstrates the role of IL-2 in the upregulation of protein production to allow cell division, and also in the polarisation of a T cell towards an IS. Transcription of perforin, granzyme and IFN γ genes are known to be upregulated via IL-2 signalling. Production of Bcl-2, CD25 and cyclins have also been demonstrated to be induced via IL-2 signalling pathways, promoting cell survival, further IL-2-mediated activation and cell cycle entry respectively [531, 532].

IFN γ signals via JAK1/2 and STAT1, mediating activation of the transcription factor T-bet in effector T cells. T-bet increases the expression of granzyme B, perforin and IFN γ genes, promoting cytotoxicity and initiating a positive feedback loop [533]. This autocrine function of IFN γ has been shown essential in maintaining CTL function. IFN γ

is known to act upon target cells, upregulating MHC expression to enhance antigen presentation in the context of a viral response [534]. It can also induce Fas expression on target cells, allowing FasL directed killing [535]. Additionally, IFN γ directly promotes the cytotoxicity of CTLs, demonstrated by pre-incubation of effector cells prior to cytotoxicity assays. When CTLs alone were exposed to IFN γ , which was then removed before the addition of target cells, levels of cytotoxicity were found to be much higher than in the absence of cytokine [534]. Whilst IFN γ signalling and its downstream consequences are complex, the cytokine is strongly correlated with cytotoxicity in T cells, and can be used as a marker for cytotoxic function in the place of cell lysis assays [536].

Together, this supports the findings of this thesis that higher IFN γ production by the BHH2 CAR+ve cells correlates with significantly increased cytotoxic function. It would be interesting to determine whether the Leu16 and BHH2 CAR+ve T cells have comparative levels of proliferation and cell cycle progression due to the similar IL-2 production levels seen with the human T cells, or whether the differences suggested by the BWZ.36 data transpire. This could be examined using a flow cytometry-based proliferation assay, in which CAR+ve T cells are CFSE-labelled and cell division can be visualised by the halving of fluorescence intensity over time [537]. Alternatively, Ki67 can be used to determine cell cycle progression. This nuclear protein is expressed in T cells during all active cell cycle phases but is absent in the G0 phase. Expression can be quantified over a time-course, providing a read-out of active cell proliferation rates [538].

The ELISA analysis of cytokines produced by the human T cells were all performed on supernatants from 24 h co-cultures. It would be interesting to investigate other time-points to compare speed and duration of the cytokine production between the CARs. Additionally, the IL-2 analysis was only performed on supernatants from co-cultures with effector:target ratios of 1:1. This analysis could be expanded to include higher ratios to determine if the production of IL-2 remains equivalent between the constructs, or whether differences emerge.

The use of individual donor PBMCs for CAR expression also results in natural donor variation between assays. Different individuals' T cells will display a range of activation response strengths, which will influence the results seen. A high number of repeated assays can compensate for this variation, allowing mean responses to be evaluated. Additionally, more robust, reproducible CAR transduction levels would improve these assays, lowering background T-cell cytokine production. This would allow assays to be more comparable, and so true differences between CAR efficacy to be clearer.

CAR and BiTE function, and ADCC levels from mAb, targeting a variety of antigens have all been shown to be strongly influenced by epitope position and the consequent distance of the IS [373-375, 377, 464]. It can therefore be hypothesised that the differences seen between the anti-CD20 CAR in this work are due to the nature of the different scFv binding properties resulting in altered IS distances. It is known that BHH2 binds a different epitope within CD20 to the other two mAb. Whilst Leu16 and rituximab bind to an overlapping epitope located within the large extracellular loop of CD20, it has been determined that BHH2 binds further around this loop (**Figure 7.1**). This would alter the immunological synapse formed and the proximity that the cells are held together and could influence the CAR efficacy [187, 500].

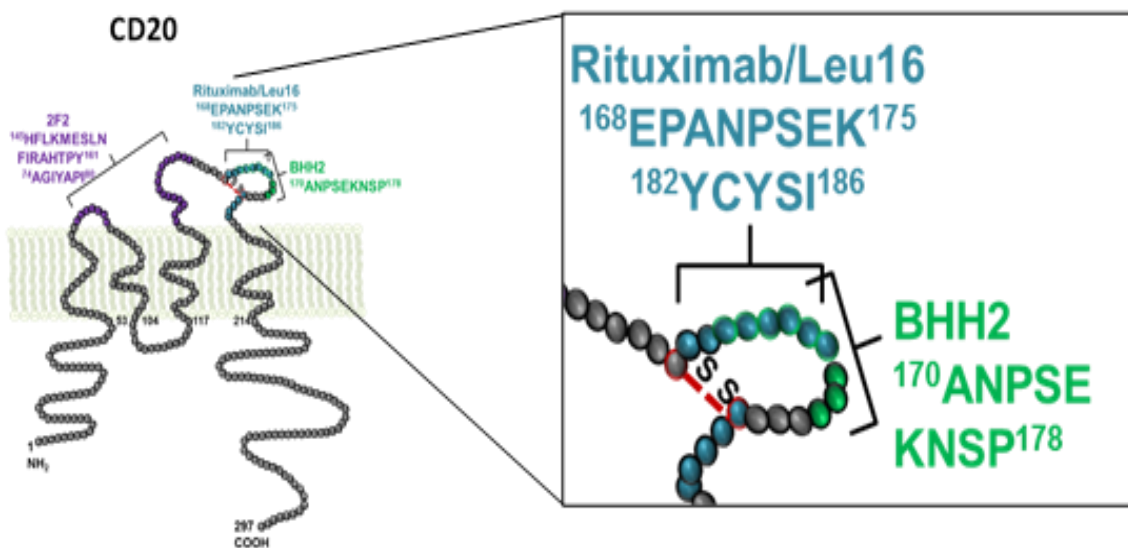


Figure 7.1: An illustration of the CD20 binding epitopes of rituximab, Leu16 and BHH2 mAb

The CD20 molecule is shown, with the binding regions of the mAbs discussed in more detail in the box. Rituximab and Leu16 bind a main epitope on the large extracellular loop of CD20, shown in blue. There is evidence that rituximab also can interact with a secondary non-continuous part of the epitope, positioned across from the other epitope section by the disulphide interaction that stabilises this loop, shown in red. BHH2 also binds to the extracellular loop but to an alternative, partially overlapping epitope (green) positioned further round the loop, towards the carboxy terminal.

BHH2 CAR is hypothesised to hold the effector and target cells in closer proximity, providing a more optimal synaptic distance that permits more efficient clustering of Lck and LFA-1, and exclusion of CD45 [539, 540] (**Figure 7.2**). Thus, higher levels of T-cell

activation are induced, leading to enhanced signalling and remodelling of actin and microtubules. In turn this results in increased lytic granule trafficking and release into the synaptic cleft, evoking superior target cell lysis [541].

As discussed in Chapter 1.8.4 and above, a published conference abstract [495] claims to demonstrate a successfully expressed 2F2 CAR construct that elicits a higher T-cell response than other anti-CD20 CARs. The authors suggest that this would be due to the alternative binding domain of this scFv on the small loop of CD20, leading to a closer interaction between the immunological synapse.

In addition to the different epitope bound by BHH2, the type II mAb are known to bind the CD20 tetramer in a different manner to type I mAb. As previously described in Chapter 1.6, one molecule of a type II mAb is thought to span a CD20 tetramer diagonally, whilst two type I mAb molecules bind in parallel across the tetramer, or between tetramers. This difference has been attributed to both the increased elbow angle present in BHH2, and to the epitope bound [186]. As CAR constructs are proposed to dimerise via the IgG Fc spacer [368, 500], it can be proposed that a CAR dimer may mimic the parental mAb binding, with type I and type II scFv-containing CAR binding straight across and diagonally across the tetramer, respectively. This alternative binding could additionally alter the width of the immunological synapse formed, impacting CAR function.

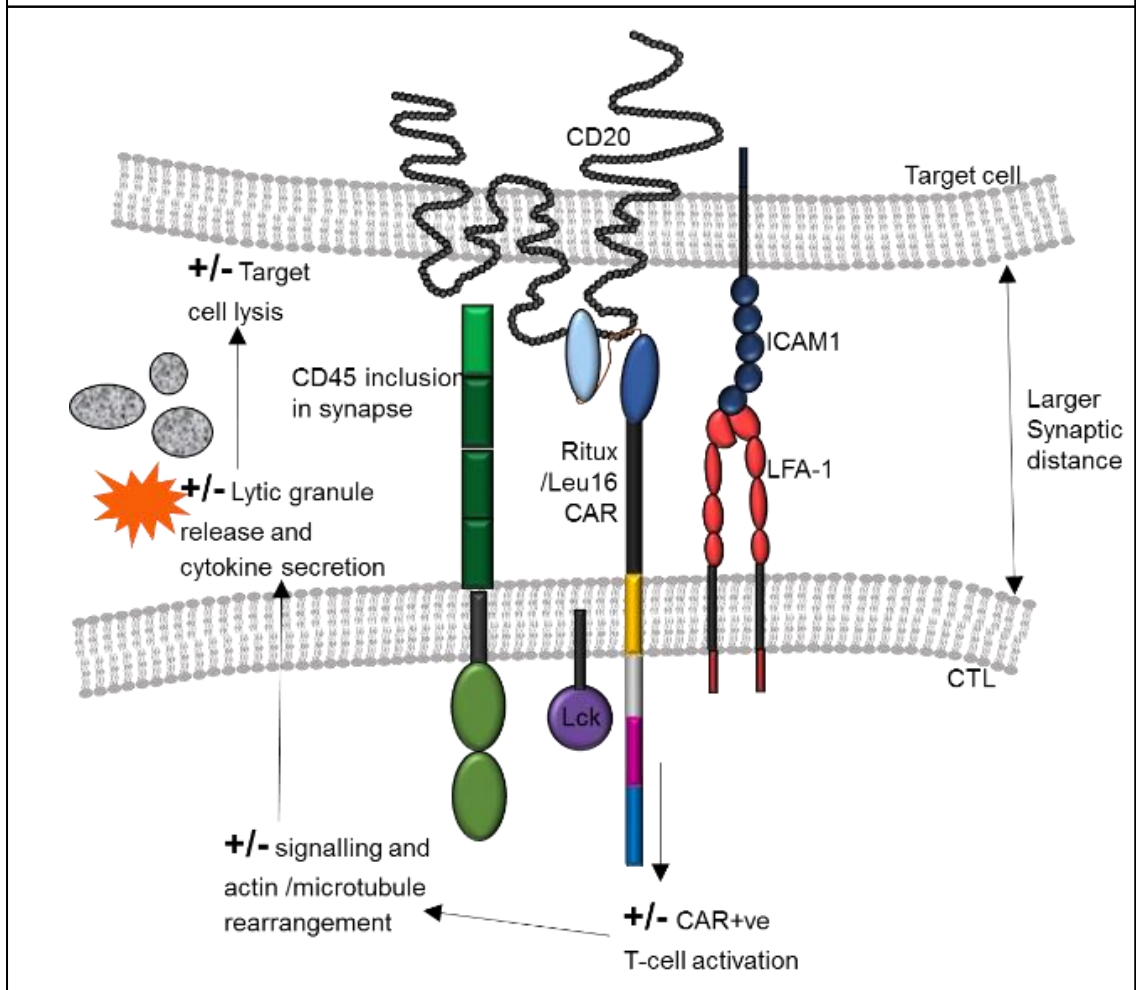
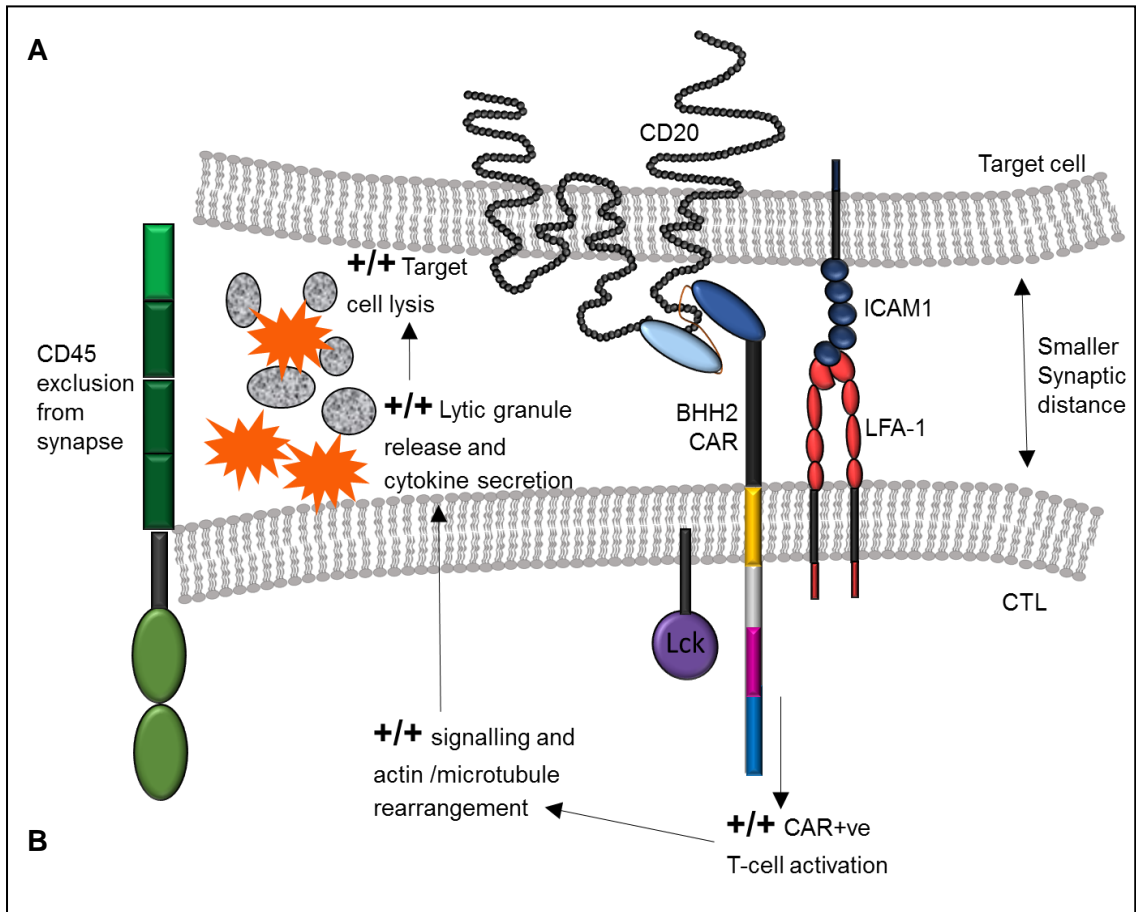


Figure 7.2: Proposed hypothesis for enhanced BHH2 CAR activity

It is hypothesised that the known difference in epitope and binding angle of the type II scFv BHH2 (**A**) results in a decreased immunological synapse distance, closer to that of the endogenous TCR-MHC IS. This would result in clustering of Lck and LFA-1 as observed previously at the CAR IS [358], and exclusion of large phosphatase molecules such as CD45 from the synapse as described by the kinetic-segregation model of T-cell IS formation [225]. Consequently, a higher level of T-cell activation signalling via the CAR intracellular domains would lead to an increased level of cytokine production alongside actin polarisation towards the IS, and lytic granule transport to the cleft. The result of this would be a higher level of target cell lysis and cytokine secretion, as observed predominantly with BHH2 CAR. Conversely, a type I scFv (**B**), binding more towards the N-terminal side of the large extracellular loop, would produce a larger synaptic gap, allowing CD45 to remain in the synapse with the CAR, LFA-1 and Lck and would reduce the T-cell activation signalling resulting in a decreased level of target cell lysis and cytokine production, as seen for Ritux and Leu16 CAR.

It is important to again acknowledge that the short flexible linker domain connecting the V_H and V_K chains of the Leu16 and BHH2 scFvs does differ. The Leu16 scFv contains an 18-residue linker (GSTSGGGSGGGSGGGSS), whilst the in-house generated scFvs including BHH2 incorporate a 15-residue sequence (GGGGSIEGRSGGGGS). Whilst both being glycine and serine-rich peptides that provide the same role of allowing the scFv to correctly fold to allow antigen binding, the linkers can themselves influence scFv function [499, 542]. These previous studies have evaluated the effects seen between linker peptides with much larger size differences and reported variance in antigen target binding. As the linker peptides used in the work presented here are more similar it is unlikely that this would entirely explain the functional differences observed. However, it would be interesting to confirm if the alternative linker peptide enhances -or diminishes- BHH2 CAR function alongside the antigen binding domain itself, by replacing the linker with the GS18 peptide.

To interrogate the IS distance hypothesis, BHH2 scFv could be incorporated into CAR constructs with varied-length spacer domains, altering the IS distance to discover the impact on CAR function. Alternatively, the epitope position could be changed. This was attempted in Chapter 5, however an unexpected finding in this study was the failure of Ritux CAR to bind either of the rituximab cyclic epitopes, RP3 and Rp15. Whilst the Ritux CAR recognises the full CD20 molecule, no interaction with either cyclic epitope was seen despite their strong interaction with rituximab. An explanation for this could be the requirement of extra stability from the extended epitope for scFv binding compared to mAb. It has been reported that rituximab binds a non-continuous epitope

within CD20 comprising the ¹⁶⁸(EP)ANPS(EK)¹⁷⁵ motif and an additional ¹⁸²YCYSI¹⁸⁵ motif, brought together sterically by a disulphide bond between C¹⁶⁷ and C¹⁸³ (**Figure 7.3**) [500]. Whilst the mAb is able to bind to the shorter cyclic mimetopes RP3 (PYSNPSL) and RP15 (PYANPSL), it can be hypothesised that the scFv requires the full epitope comprising both motifs to allow stable binding.

Niederfellner *et al* [186] demonstrated that the affinity of rituximab for an alternative cyclic epitope (¹⁶³NIYNCEPANPSEKNSPSTQYCYSIQ¹⁸⁷ [543]) was significantly reduced than compared to the interaction with native CD20. Whilst they observed an affinity of ~5 nM for the full molecule, an affinity of 27.7 μM at 15 °C was determined for rituximab binding to a cyclic epitope. They were unable to take affinity measurements at higher temperatures than this, due to the weak interaction. This demonstrates affinity of the parental mAb was considerably lower when interacting with a cyclic epitope, even when the fuller non-continuous epitope was included. Whilst some of this decrease may be attributed to loss of avidity it is a considerable reduction, suggesting that the nature of the epitope is also involved. It would therefore be expected that the rituximab scFv would also have lower affinity for a cyclic epitope than to native CD20, which may contribute to Ritux CAR being unable to bind Rp3/Rp15.

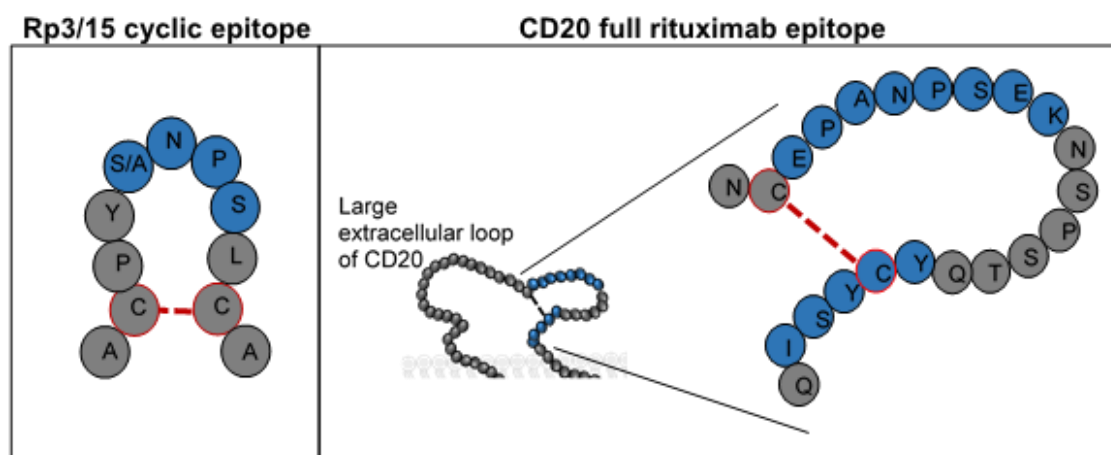


Figure 7.3: The cyclic Rp3/15 CD20 mimetope constructs compared to the full rituximab epitope of CD20

The cyclic epitope of the Rp3 (SNPS) and Rp15 (ANPS) constructs is shown (left) as compared to the full CD20 extracellular loop comprising the non-continuous long rituximab epitope. Stabilising disulphide bonds are shown in red.

This finding prohibited the use of the RP3/15 fusion proteins to probe the role of epitope-membrane proximity on CAR function. The cyclic epitopes could be extended

to incorporate the longer EPANPSEK motif to evaluate if the Ritux CAR could bind this in a sufficiently stable manner. Alternatively, other epitopes could be generated that incorporate the longer rituximab motifs, or that interact with BHH2 CAR. A cyclic epitope that is bound by BHH2 has been described [186] and could be generated and attached to the CD137 fusion proteins [464], thus positioning the epitope at a variety of membrane distances to investigate its impact on BHH2 CAR function if the CAR is able to bind it.

Further to the binding angle of the scFv, affinity may also play a role in the differences seen in CAR function. Overall affinity is described by the K_D value, which represents the dissociation equilibrium constant between a mAb, F(ab) or scFv with the target antigen. This K_D value is a ratio of the K_{ON} and K_{OFF} values, which are the on- and off-rate of the interaction. Thus, constructs can have the same overall affinity, but distinct on- and off-rates, which can have strong impact on function. The on-rate describes the speed of binding of the antibody binding site to the antigen, whilst off-rate is the speed of dissociation of that interaction, representing the strength of interaction.

As discussed in Chapter 1.8.4, the role of affinity in CAR function is unclear, and depends upon the target antigen and the context. CAR targeting CD22, CEA, Tryp1 and CD123 were not influenced by scFv affinity, whilst anti-Her2 CAR were not affected when affinity was above threshold. Affinity was found to impact anti-MAGE-A1 CAR activity, but again, the potential threshold affinity was relevant in this work as the difference in affinities was distinct. A strong influence was observed in the context of anti-ROR1 CARs [386]. The higher affinity anti-ROR1 construct was shown to have higher functional efficacy than the lower, despite both being above the proposed threshold from other studies (detailed in Chapter 1.8.4). Interestingly, the anti-ROR1 CAR differed in their off-rates, whilst the anti-CD123 CAR had similar off-rates despite possessing a much larger range of overall affinities. It may be that the dissociation rate, and so binding strength and duration of interaction, plays a key role in CAR function more than overall affinity.

As discussed in Chapter 1.8.4, *in vitro* anti-CD20 CAR function has been reported to be influenced by antigen binding affinity [388]. The cytokine production and target cell lysis levels were stated to positively correlate with increased affinity, to a point, above which the highest affinity scFv was described as detrimental to function due to increased AICD of the CAR+ve T cells. Thus, the effect of binding strength appears to vary between constructs and antigenic targets and its importance remains unclear, although may be influential in the context of anti-CD20 CAR.

BHH2 mAb has a higher affinity for CD20 than rituximab [544], whilst that of Leu16 is not known. The relative affinity is usually preserved when a mAb is converted to a scFv [498, 545], thus BHH2 CAR would likely have a stronger binding to CD20 than Ritux CAR. As described above, the duration of binding may also impact the efficacy. Due to the lack of a stably expressed soluble CD20 molecule, the use of SPR to determine affinity of the CAR would have to be restricted to a soluble recombinant CD20 large extracellular loop, as described [546]. It is not known if this technique would be successful using this recombinant molecule, nor if the CAR constructs would bind sufficiently. The immobilisation of each scFv-Fc via an anti-IgG mAb may allow the assessment of binding affinity by the flow of this soluble CD20 epitope over the sensor chip. As this loop contains the epitopes of BHH2, Ritux and Leu16 CAR, these could all be compared using the same antigen, if binding function is retained in the recombinant protein.

Alternatively, to evaluate the comparative binding affinities for each CAR, either a flow cytometry or ELISA -based technique could be used. An ELISA allows the calculation of antibody dissociation constants, using linearization plots [547]. This could be performed using the recombinant CD20 peptide described above, as the authors confirm success using it in ELISA. Alternatively, a cell-based ELISA could be used, as described for rituximab titrations using a CD20+ve cell line [548]. To allow detection of the scFv, they could be expressed adjoined to the spacer domain to produce a soluble scFv-Fc fragment, or with an HA or HIS tag.

A flow cytometry assay could also be developed, to determine binding off-rates of the scFv by using a titration of soluble scFv-Fc and plotting the MFI of the anti-spacer detection antibody [549]. Additionally, a flow cytometry-based competition assay would provide the hierarchy of binding strength of each scFv. Similar to the binding assay described in Chapter 4, rituximab could be used to block scFv binding. If this was performed in a titration with each scFv-Fc, the ability to outcompete anti-CD20 mAb binding would be determined. As discussed previously, a high yield of scFv-Fc would be required to perform this assay, as higher concentrations would be needed to outcompete the bivalent mAb binding.

As shown in Chapter 3, the scFvs could be expressed as soluble protein and purified using a peptide tag. However, the low yield of scFv was an obstacle to further evaluation of the fragments. Now that a difference between CAR function has been determined, the investigation into the reasons for this are a priority. The pFUSE vector used in Chapter 3 would allow the soluble scFv-Fc to be produced and purified for affinity experiments. To achieve sufficient yield of the peptides, large-scale HEK 293F

cultures could be used, and the resultant supernatants purified and concentrated. Alternatively, *E. coli* cultures could be employed as they are well suited for the expression of small soluble proteins and can rapidly produce high yields. However stable protein folding, particularly in proteins requiring disulphide bonds, can be an issue due to the reducing nature of the *E. coli* cytoplasm. As an alternative, the fusion of scFv to another protein-stabilising domain could be assessed, such as the maltose-binding protein (MBP). This approach has been shown to allow the accumulation of soluble, correctly folded scFv, and other recombinant proteins. MBP is proposed to act as a chaperone to binding, and to prevent misfolding and consequent degradation of the desired protein [550, 551].

As discussed in Chapter 1.8.4, the effect of affinity on CAR efficacy is not completely understood. Compared to native TCRs, CARs constructed with scFvs demonstrate much higher affinities to target antigens (KD values in the pico- or nano- molar range, compared to TCR values in the μ M range). Despite this, one target antigen molecule per target cell is sufficient to trigger a TCR-induced response, whilst CARs require >100 antigen molecules per cell. TCR molecules do not achieve this via high affinity binding, rather by serial binding of many TCRs to one antigen molecule. This is possible due to the fast off-rate of TCRs and allows sufficient TCR signalling to reach the threshold for T-cell activation [552].

CARs are known to bind with higher affinity to target antigens, to form more disorganised ISs and to induce faster signalling and cytotoxicity than TCRs (Chapter 1.8.2.2) [553]. Despite these differences, there is evidence that CAR+ve T cells can perform serial killing, as seen with native TCR+ve cells [383, 554]. The levels of CAR-induced serial killing were observed to be equivalent to TCR-induced events in short term assays using cells expressing and co-expressing an anti-Her2 CAR and the OT-I TCR [383]. CAR down-regulation reduced all CAR-induced cytotoxicity at longer time points (>20 h). CAR+ve T cells were again observed to form more rapid ISs, induce cytotoxicity faster and detach more quickly from target cells than the TCR+ve cells. This fast synaptic interaction and detachment may allow CAR+ve T cells to serially kill many targets in the manner of the native TCR+ve cells, despite their increased binding affinities [555].

One of the major obstacles in this work was the failure of the CARs to be expressed in murine primary T cells, both from splenocyte transductions and from bone marrow chimeras. As discussed in Chapter 6, the issue with splenocyte expression following transduction may be addressed by codon optimisation. This would help circumvent any issues with the expression caused by the inherent nature of the construct sequence.

Additionally, the activation state of the cells could be addressed by the use of a lentiviral vector system. Proliferation of the T cells was observed after activation with anti-CD3 and anti-CD28, as characterised by the development of large cell clusters in culture, and an increase in total cell numbers. This suggests that the issues encountered with transduction was not due to lack of proliferation. As discussed in Chapter 6, a probable explanation was over-activation resulting in AICD. A reduced period of activation prior to transduction (24 h instead of 48 h) did not produce more successful results. As GFP was expressed in the surviving cells, but very minimal CAR expression was seen, it was concluded that the nature of the CAR molecule was the cause. Tonic signalling has been described in CAR+ve T cells [511, 512], resulting in AICD. Unlike retroviral vectors, lentiviral vectors can transduce proliferating and non-proliferating cells so pre-activation of the T cells would not be required [515]. This may allow the activation state of the cells expressing CAR constructs to remain below the threshold of AICD, resulting in surviving CAR+ve T cells.

Another aspect to consider is that of Treg depletion prior to T-cell transduction. As discussed in Chapter 5.5, it has been shown that Treg depletion *in vivo*, prior to the administration of CAR+ve T cells improves both the survival of the infused T cells, and the anti-tumour response seen [556]. The production of cytokines and other factors by Tregs, as discussed in Chapter 1.7.4.2, can act to suppress the CAR+ve T cells, and a general anti-tumour immune response. Both CAR-transduced and native Tregs can impact the anti-tumour response in CAR therapy. CAR+ve Tregs can become activated at the site of the target cells, upon antigen interaction. Consequently, their activity will occur at the tumour location, generating an immune-suppressive micro-environment that will inhibit the CAR+ve anti-tumour response [557]. Tregs can be removed from the PBMC pool using anti-CD25 prior to T-cell activation and transduction, removing this inhibitory subset [558].

To address the obstacles in the generation of bone marrow chimeras, alternative mouse strains could be investigated. If the issue was with host immune activity against CAR+ve T cells leading to immune-mediated deletion, employing an immunodeficient and FcR γ -chain knockout as the recipient may allow successful grafting and CAR+ve T-cell circulation. The lack of lymphocytes present in SCID or Rag mutant mice [517] would provide an immunodeficient niche for the grafting of the bone marrow cells and subsequent production and expansion of circulating cells, which persists after recovery from irradiation. The FcR γ -chain KO lacks functional activatory Fc γ R which would prevent any potential interaction with the IgG Fc spacer domain of the CAR, which has been shown to lead to CAR+ve T-cell deletion via the host innate immune system [368-370]. Alternatively, mutagenesis could be performed on the IgG Fc spacer to remove

the FcR binding motifs, as discussed in Chapter 6 [368-371]. The previous *in vitro* experiments shown in this work would need to be repeated using these mutated CAR Fc constructs, to determine if their functions remain equivalent with these mutations present.

As an alternative to murine T cells, human T cells from PBMCs were assessed and shown to be successfully transduced with CAR constructs. Therefore, these could be used for further *in vivo* investigation. Whilst BHH2 CAR has been proven to have a higher level of *in vitro* function, as discussed in Chapters 5 and 6, these assays always have limitations. *In vivo* analysis would allow the interrogation of target cells lysis to determine if the cytotoxicity data shown in Chapter 6 translates. It would also provide an insight into the effect of the differential cytokine production seen on CAR+ve T-cell function. As Leu16 CAR was found to produce similar IL-2 levels to BHH2 CAR in the human T cells, it would be interesting to see if this or the IFN γ levels -much higher for BHH2 CAR- were more important for *in vivo* T-cell proliferation, survival and cytotoxicity over time.

Transduced PBMCs could be used as effector cells in an immunodeficient mouse model, such as SCID. An initial study using short-term peritoneal cavity *in vivo* assays, as described in Chapter 5.4.1, would allow simple evaluation of CAR cytotoxic efficacy in an *in vivo* setting. Further, a model system such as that described previously [359, 529, 559] could be employed. In these studies of anti-CD20 and anti-CD19 CAR+ve T cells, Raji cells were given IV to non-obese diabetic/severe combined immunodeficiency/IL-2R γ -chain KO mice (NOD/SCID/ γ -/-) [560]. 2-7 d later, 10 x CAR+ve human T cells were administered also IV, and tumour burden and survival were monitored. Collection of peripheral blood samples and staining for CD20/CD19 target cells and CAR+ve T cells is possible to track CAR+ve T-cell expansion and reduction of target cell numbers. Alternatively, in these studies, the Raji cells were positive for firefly luciferase (Raji-FFLuc cells), allowing *in vivo* bioluminescent imaging of the target cells to assess tumour burden.

Another potential way to assess human CAR+ve T-cell function *in vivo* would be the use of a human transgenic (Tg) CD20 mouse tumour model. The E μ -Tcl-1 x hCD20 was previously generated [561] and could be established in SCID mice. CAR+ve T cells could be administered IV once the tumour was established; monitored by the presence of circulating tumour cells in the blood. This would provide a way to analyse the different CAR+ve T-cell abilities to respond to an established tumour, regarding both anti-tumour cytotoxicity and CAR+ve T-cell expansion and survival. It would be interesting to determine whether cells expressing the BHH2 CAR have higher

cytotoxicity in an *in vivo* setting, and whether this could be attributed to enhanced T-cell survival and/or higher initial activation due to direct binding differences.

These experiments using human CAR+ve T cells would be performed in immunocompromised hosts, and so other potential immune system effects would not be considered. With successful murine T-cell expression, for instance using lentiviral transduction as described above, immunocompetent models could be used. A method similar to that used in anti-CD19 CAR studies [562, 563] could be adopted. A20-tumour bearing Balb/c mice were lymphodepleted with 5 Gy TBI or 200 mg/kg cyclophosphamide to allow CAR+ve T-cell expansion and persistence. CAR+ve murine T cells were administered IV 24 h after lymphodepletion. The mice were monitored for the tumour burden as the depleted cell counts returned, and CAR+ve T-cell persistence.

In preparation for the *in vivo* work planned in this thesis, a similar lymphodepletion test was performed (see Appendix, **Figures A5.1 and A5.2**). Two C57/BL6 mice were given 5 Gy TBI. The return of circulating lymphocyte levels was monitored by flow cytometry analysis of peripheral blood samples, taken at d 0 (pre-irradiation), 2, 5, 9, 15, 21 and 42. If performed in an hCD20 Tg mouse, CAR+ve T cells could be given and allowed to expand prior to the full recovery of the host T-cell populations, including Tregs. The return of B-cell numbers in the periphery could be monitored for hCD20+ve cell clearance by the CAR+ve T cells. Alternatively, hCD20+ve target cells could be administered IV in the lymphodepleted hosts, prior to CAR+ve T cell injection to analyse clearance of a more established target population.

A more recent study by the same group demonstrated a method of CAR+ve T-cell tumour clearance in lymphoreplete hosts, where the host immune system was shown to play a role [564]. Balb/c mice were treated with 100 mg/kg cyclophosphamide 24 h prior to the administration of A20 tumour cells. Blood counts were monitored, and when they had returned to normal levels and systemic A20 leukaemia was successfully established, anti-CD19 CAR+ve T cells -also expressing IL-12- were again given IV. Tumour burden and CAR+ve T-cell persistence were monitored, and it was shown that the host immune system cells were recruited by the IL-12-expressing CAR+ve T cells to mount an anti-tumour response, and that immune memory was formed. This would be interesting to replicate with the anti-CD20 CAR in this thesis, to determine not only the CAR+ve T-cell abilities to clear tumour cells in an *in vivo* model, but to also investigate the interaction of CAR+ve T cells with the host immune system and consequent wider effects that may be seen. An IL-12 transgene would be required,

inserted downstream of the CAR constructs to enhance the T-cell persistence, as in the published study.

Techniques now exist that can be used to generate mice with a fully human immune system [565]. As the CAR constructs analysed in this thesis incorporate human protein domains and target a human antigen, a fully humanised system would potentially allow a more physiologically relevant comparison of efficacy. Moreover, the effects of the cytokine milieu produced from the CAR+ve T-cell immune response on other human immune cells could be evaluated, giving a greater insight into all aspects of CAR function. The interplay between immune cells can result in enhanced or diminished CAR+ve T-cell immune responses and so short- and long-term anti-tumour effects, which would be more easily dissected by use of such a technique.

Whilst the expression levels achieved from the PBMC transductions in this work were sufficient to evaluate functional CAR differences, they could be improved. Again, codon optimisation may have an impact on expression, and could be implemented for human cells. Otherwise, a GFP transgene could be included into the CAR vectors, allowing a method of cell sorting to generate purer CAR+ve populations that would not involve use of the anti-CAR antibody and may therefore cause less cell death. Similarly, a co-expressed tEGFR joined by a self-cleaving linker sequence has been successfully used as a method to sort CAR+ve T cells, using anti-EGFR mAb [437]. This could be inserted downstream of the CAR transgene and used to purify the CAR+ve population, whilst avoiding interaction with the CAR construct itself.

In addition to *in vivo* evaluation of the CAR constructs, further *in vitro* investigation could be performed. Longer-term *in vitro* assays can provide information on CAR function that is not seen in the usual 4 h cytotoxicity assays [359]. CAR+ve T cells can be co-cultured with target cells and analysed at intervals over a week by flow cytometry. Using this method, the decrease in target cell numbers, apoptosis levels, and the expansion of CAR+ve T cell populations could be tracked and compared between constructs over an extended time period. Temporal cytokine analysis could also be performed, to monitor and compare secretion levels over a longer exposure to antigen.

Another interesting aspect to investigate, initially *in vitro*, would be the targeting of CD20+ve tumour samples that have reduced antigen expression. Target antigen density has been observed to effect anti-CD20 CAR efficacy [566]. Whilst an anti-CD20 CAR was proven able to lyse target cells expressing ~200 CD20 molecules, the threshold for true T-cell activation signalling and expansion was shown to be ~10 fold higher. It would be interesting to determine if there was a difference between BHH2

CAR and the other constructs in the threshold for target lysis and for T-cell activation and cytokine production, or whether the antigen density dictates this regardless of the scFv included.

The different CARs could also be explored further with regards any potential for auto-activation or off-target effects. As described in Chapter 1.8.7, on-target, off-organ consequences of CAR therapies can be severe [372]. As CD20 is very specifically expressed -only on B cells- on-target off-organ damage is extremely unlikely. The side-effect of hypogammaglobulinemia, mentioned previously, is common in the use of anti-CD20 therapies including CAR+ve T cells where healthy B cells are also depleted. Whilst this increases infection risks and can be serious, treatment is available in the form of IVIg.

Whilst recognition of a non-target antigen lead to unforeseen fatal consequences in a trial of an engineered TCR to MAGE-A3 [58], off target effects are unlikely when a scFv is used to direct a CAR as the specificity for the TAA is known, particularly if the mAb is clinically approved. However, it is always essential to confirm that no other recognition apart from the intended antigen occurs. This can be performed using *in vitro* tissue screening, by exposing tissues presenting a wide variety of antigens to CAR+ve T cells [567]. General associated toxicities, such as cytokine release syndrome, can be analysed in *in vivo* toxicity models by giving increasing CAR+ve T-cell doses and monitoring serum cytokine levels and overall animal health [568].

In summary, the data presented in this thesis has demonstrated a clear difference in *in vitro* anti-CD20 CAR function between constructs comprising different scFv. The CAR incorporating the type II BHH2 scFv has been shown to elicit the overall highest T-cell activation response and superior levels of specific target cell lysis. *In vivo* investigations would be a vital next step to determine if these differences translate in a more physiological setting. The work presented here further highlights what has been shown by many other studies; how the subtleties of CAR design are often crucial to function. The factors influencing CAR efficacy are complex, and often vary depending on the properties of the target antigen. Whilst clinical CAR therapeutic success grows, it is essential to continue investigation into the optimal designs and mechanisms of function of constructs targeting a range of antigens.

This thesis has discussed the field of CAR development and current progress in the context of T cells. CAR+ve T cells are now a well-established area of research, with many promising developments ongoing. Another avenue of CAR research not covered in this thesis involves the modification of NK cells. This area is less well studied than that of CAR+ve T cells, but recently there have been positive advances reported. NK

cells, defined as CD3^{-ve} CD56^{+ve}, form a cytotoxic branch of the innate immune system. As described in Chapter 1.4, they are able to recognise and clear transformed cells during early oncogenesis [569]. NK cells have spontaneous cytotoxicity, meaning they do not require the antigenic priming that T cells need. They are proficient at “serial killing”, like CTLs, where several tumour cells can be sequentially lysed by one cytotoxic cell [570]. NK cells recognise other cells based on the expression of self/non-self ligands, which interact with inhibitory and activatory receptors on the NK cell. The balance of these signals determines if a cell is then targeted for lysis [571]. Additionally, active NK cells produce IFN- γ , IL-3 and GM-CSF, rather than the inflammatory cytokines typical of activated T cells which can result in cytokine release syndrome [572]. The chance of side effects due to ongoing on-target off-tumour targeting, such as long-term B-cell dysplasia seen with anti-CD19 CAR^{+ve} T cells, is also reduced with NK cells [573] as they do not undergo clonal expansion the way T cells do, and they are short lived.

These characteristics have made NK cells an appealing target for CAR modification. Furthermore, unlike T-cell adoptive therapies, NK cells do not require HLA pairing, meaning allogeneic donor cells can be used. This has potential benefits in allowing healthy donor cells to be used for modification, rather than patient T cells which may be skewed to an exhausted phenotype after chronic antigen exposure. Moreover, this may permit the development of universal off-the-shelf CAR therapies without the need for further genetic manipulation of the TCR in CAR^{+ve} T cells (Chapter 1.8.8) [574].

There are logistical obstacles to successful NK CAR development, explaining why successes have only been very recently reported. Primary NK cells have proven difficult to maintain and manipulate in culture. Resistance to transduction has been widely reported [575]. Optimisation of transduction and of other genetic techniques including electroporation has improved NK CAR expression levels [576, 577]. Several of the more successful studies reported have employed the NK cell line NK-92 [578] rather than primary NK cells. This cell line has maintained its cytotoxic function robustly in culture but due to its origin as a malignant non-Hodgkin's lymphoma cells must be irradiated prior to infusion, removing their ability to proliferate [579]. Phase I/II trials of NK-92 cells modified with CARs including those targeting CD19, GD2, CD22, Her2 and BCMA are ongoing [574].

Two small-scale trials of CAR NK therapy have been published of three patients each. The first involved primary NK cells modified with an NKG2D CAR given to colorectal patients [580]. A reduction in tumour cells in ascites was reported, and a decrease in liver metastases in one patient. The second trial utilized the NK-92 cell line, expressing

an anti-CD33 CAR to target AML [581]. The results reported were mixed, with some short-term responses but no lasting positive outcomes. However, the authors report that no adverse side effects were seen even with infusion of very high numbers of CAR+ve NK cells. The first larger-scale trial, of anti-CD19 CAR+ve NK cells reported more positive clinical results. Of 11 patients with relapsed/refractory CLL or non-Hodgkin's lymphoma, 7 achieved complete remission, and 1 a partial response. Importantly no cytokine release syndrome or neurotoxicity, often seen with CAR+ve T cell therapies, were reported and the NK cells expanded and persisted at a low level *in vivo* for ≥ 12 months [582].

The appeal of NK cells as a potential "universal" CAR therapy has been expanded by the development of a reported "UniCAR" [583]. This technique uses the NK-92 cell line, which is a source of off-the-shelf cells rather than harvesting patient cells, modified with a CAR directed to a specific peptide moiety. A tumour-specific target module (TM) incorporating the targeted peptide, and a tumour antigen-specific scFv are infused alongside the CAR modified NK cells. The CAR recognises and binds the peptide of the TM, which also contains a full mAb or scFv. This antibody is able to recognise the scFv which itself is targeted to the tumour antigen on the target cells. This four-part system allows any tumour-targeting scFv to be used with the CAR-modified NK-92 cells and the TM, providing a truly universal CAR therapy. The effect of these additional components on cell synapse distances and consequent impact on efficacy have not yet been investigated.

Another essential aspect of CAR+ve NK development to consider is the impact of the tumour microenvironment, particularly in solid tumours. NK cells are strongly suppressed by the tumour microenvironment, so methods to overcome this must be established [584]. The inclusion of the IL-15 gene in the CAR construct has been investigated in the context of anti-CD19, CD123 and BCMA CAR+ve NK cells [585, 586]. A study using anti-GD2 CAR+ve NKT cells -a subset of T cells expressing the $\alpha\beta$ TCR and NK cell markers which recognise lipid antigens in the context of CD1d- has also been reported [587]. The inclusion of the IL-15 inducible gene increased the persistence of the cells in *in vivo* models in all cases. An increased anti-tumour response was also seen, as the NK and NKT cells overcame the immune suppression.

These very recent studies suggest that CAR modification of NK cells may provide an alternative avenue for CAR therapy development. As discussed, a particular advantage may be the less complicated development of "universal" CAR treatments, and the ability to use allogeneic donor cells which would help to streamline the production of CAR therapies.

CAR+ve cell manufacturing is a long and complex process. Cells must be harvested from each patient and transported to a central manufacturing centre where they are modified, before being returned to the clinic. Patients may undergo conditioning chemotherapy, and often require treatment for side-effects from the CAR therapy. The costs of the two approved anti-CD19 CAR+ve T-cell therapies, axi-cel and tisagenlecleucel (described in Chapter 1.8.9) have been costed at \$373,000 and \$475,000 respectively per patient, excluding other complementary care [588]. The cost per quality adjusted life year achieved with axi-cel treatment has been estimated at \$58,146 [589]. These huge expenses are an obstacle to the introduction of CAR therapy as a mainstream or first-line clinical option.

To overcome this, there are several logistical possibilities. Firstly, the optimisation of CAR design to avoid disease relapse (discussed in Chapter 1.8.4) would increase the likelihood of the treatment being a lasting success from a singular dose. This would improve the cost-benefit ratio of CAR therapy, when compared to long-term repeated treatments with chemotherapy or other drugs [588]. The manufacturing process may be economised by the modification of CAR cells in a non-centralised location, and by the use of automated processes to cut labour costs. The use of allogeneic cells would also be economically beneficial, as therapies for several patients could be produced together, in a scaled-up process. A modelling study estimated that the production of a pool of CAR+ve T cells would cost \$95,780/dose when using autologous cells. This cost was estimated to decrease to \$4,460/dose if using scaled-up production of CAR+ve allogeneic cells [588, 590].

As discussed in detail in Chapter 1.8.8, several attempts are ongoing to develop universal off-the-shelf CAR therapies. Genetic editing of the TCR genes to remove function can allow the use of allogeneic donor T cells [415, 445, 446], whilst NK cells may provide an alternative option as discussed above. The development of CAR-expressing induced pluripotent stem cells (described in Chapter 1.8.8) is an exciting potential source of a renewing pool of universal CAR+ve T cells [448]. The targeting of “universal antigens” such as FITC or biotin in conjunction with labelled anti-tumour mAb is another technique under investigation to produce off-the-shelf CARs (Chapter 1.8.8) [449-452].

An interesting study using CD3-targeted DNA nanocarriers reported the potential for *in vivo* CAR production [591]. This technology allows the CAR genes to be transported into T cells *in vivo* where they are expressed, providing an “on-demand” CAR therapy. The authors report the DNA nanocarriers as easy to produce, stable in storage, and capable of inducing CAR expression *in vivo* resulting in tumour clearance in a

leukaemia model. If translatable in clinical trials, the removal of the leukapheresis, transport, transduction and re-infusion steps in the CAR manufacturing process would significantly reduce the associated costs. These advancements towards universal CAR systems that would allow an off-the-shelf therapy option, alongside the economisation of the CAR+ve cell manufacturing processes, provide an opportunity to bring CAR therapy into the foreground for widespread application in the clinic.

8 References

1. UK, C.R. <http://www.cancerresearchuk.org/about-cancer/what-is-cancer>. 2016 [cited 2016].
2. Hanahan, D. and R.A. Weinberg, *The hallmarks of cancer*. Cell, 2000. **100**(1): p. 57-70.
3. Hanahan, D. and R.A. Weinberg, *Hallmarks of cancer: the next generation*. Cell, 2011. **144**(5): p. 646-74.
4. Delaval, B. and D. Birnbaum, *A cell cycle hypothesis of cooperative oncogenesis (Review)*. Int J Oncol, 2007. **30**(5): p. 1051-8.
5. Malumbres, M. and A. Carnero, *Cell cycle deregulation: a common motif in cancer*. Prog Cell Cycle Res, 2003. **5**: p. 5-18.
6. Lodish H, B.A., Zipursky SL, et al, *Molecular Cell Biology*. Proto-Oncogenes and Tumor-Suppressor Genes. Vol. 4th edition. 2000, New York: W. H. Freeman.
7. Narayanan, D.L., R.N. Saladi, and J.L. Fox, *Ultraviolet radiation and skin cancer*. Int J Dermatol, 2010. **49**(9): p. 978-86.
8. Furrukh, M., *Tobacco Smoking and Lung Cancer: Perception-changing facts*. Sultan Qaboos Univ Med J, 2013. **13**(3): p. 345-58.
9. Uguen, M., et al., *Asbestos-related lung cancers: A retrospective clinical and pathological study*. Mol Clin Oncol, 2017. **7**(1): p. 135-139.
10. Zámbořszky, J., et al., *Loss of BRCA1 or BRCA2 markedly increases the rate of base substitution mutagenesis and has distinct effects on genomic deletions*. Oncogene, 2016. **36**: p. 746.
11. Antoniou, A., et al., *Average risks of breast and ovarian cancer associated with BRCA1 or BRCA2 mutations detected in case Series unselected for family history: a combined analysis of 22 studies*. Am J Hum Genet, 2003. **72**(5): p. 1117-30.
12. Kang, Z.J., et al., *The Philadelphia chromosome in leukemogenesis*. Chin J Cancer, 2016. **35**: p. 48.
13. Correia, C., et al., *BCL2 mutations are associated with increased risk of transformation and shortened survival in follicular lymphoma*. Blood, 2015. **125**(4): p. 658-67.
14. Burd, E.M., *Human papillomavirus and cervical cancer*. Clin Microbiol Rev, 2003. **16**(1): p. 1-17.
15. Raab-Traub, N., *Novel mechanisms of EBV-induced oncogenesis*. Curr Opin Virol, 2012. **2**(4): p. 453-8.
16. Krock, B.L., N. Skuli, and M.C. Simon, *Hypoxia-induced angiogenesis: good and evil*. Genes Cancer, 2011. **2**(12): p. 1117-33.
17. Liberti, M.V. and J.W. Locasale, *The Warburg Effect: How Does it Benefit Cancer Cells?* Trends Biochem Sci, 2016. **41**(3): p. 211-218.
18. Colegio, O.R., et al., *Functional polarization of tumour-associated macrophages by tumour-derived lactic acid*. Nature, 2014. **513**(7519): p. 559-63.
19. Campo, E., et al., *The 2008 WHO classification of lymphoid neoplasms and beyond: evolving concepts and practical applications*. Blood, 2011. **117**(19): p. 5019-32.

20. Harris, N.L., et al., *The World Health Organization classification of neoplastic diseases of the haematopoietic and lymphoid tissues: Report of the Clinical Advisory Committee Meeting, Airlie House, Virginia, November 1997*. *Histopathology*, 2000. **36**(1): p. 69-86.
21. Wisnivesky, J.P., et al., *Effectiveness of radiation therapy for elderly patients with unresected stage I and II non-small cell lung cancer*. *Am J Respir Crit Care Med*, 2010. **181**(3): p. 264-9.
22. Sterzing, F., et al., *Image-guided radiotherapy: a new dimension in radiation oncology*. *Dtsch Arztebl Int*, 2011. **108**(16): p. 274-80.
23. Hengstler, J.G., et al., *Induction of DNA crosslinks and DNA strand lesions by cyclophosphamide after activation by cytochrome P450 2B1*. *Mutat Res*, 1997. **373**(2): p. 215-23.
24. Jordan, M.A., D. Thrower, and L. Wilson, *Mechanism of inhibition of cell proliferation by Vinca alkaloids*. *Cancer Res*, 1991. **51**(8): p. 2212-22.
25. Tewey, K.M., et al., *Adriamycin-induced DNA damage mediated by mammalian DNA topoisomerase II*. *Science*, 1984. **226**(4673): p. 466-8.
26. Gatti, L. and F. Zunino, *Overview of tumor cell chemoresistance mechanisms*. *Methods Mol Med*, 2005. **111**: p. 127-48.
27. Hallek, M., et al., *Addition of rituximab to fludarabine and cyclophosphamide in patients with chronic lymphocytic leukaemia: a randomised, open-label, phase 3 trial*. *Lancet*, 2010. **376**(9747): p. 1164-74.
28. Hiddemann, W., et al., *Frontline therapy with rituximab added to the combination of cyclophosphamide, doxorubicin, vincristine, and prednisone (CHOP) significantly improves the outcome for patients with advanced-stage follicular lymphoma compared with therapy with CHOP alone: results of a prospective randomized study of the German Low-Grade Lymphoma Study Group*. *Blood*, 2005. **106**(12): p. 3725-32.
29. Ehrlich, P., *Über den jetzigen stand der karzinomforschung*. *Ned. Tijdschr. Geneesk.*, 1909. **5**: p. 273–290
30. Old, L.J. and E.A. Boyse, *Immunology of Experimental Tumors*. *Annu Rev Med*, 1964. **15**: p. 167-86.
31. Burnet, F.M., *The concept of immunological surveillance*. *Prog Exp Tumor Res*, 1970. **13**: p. 1-27.
32. Kim, R., M. Emi, and K. Tanabe, *Cancer immunoediting from immune surveillance to immune escape*. *Immunology*, 2007. **121**(1): p. 1-14.
33. Smyth, M.J., et al., *Differential tumor surveillance by natural killer (NK) and NKT cells*. *J Exp Med*, 2000. **191**(4): p. 661-8.
34. Dunn, G.P., L.J. Old, and R.D. Schreiber, *The three Es of cancer immunoediting*. *Annu Rev Immunol*, 2004. **22**: p. 329-60.
35. Girardi, M., et al., *Regulation of cutaneous malignancy by gammadelta T cells*. *Science*, 2001. **294**(5542): p. 605-9.
36. Shankaran, V., et al., *IFN γ and lymphocytes prevent primary tumour development and shape tumour immunogenicity*. *Nature*, 2001. **410**(6832): p. 1107-11.
37. Haanen, J.B., et al., *Melanoma-specific tumor-infiltrating lymphocytes but not circulating melanoma-specific T cells may predict survival in resected advanced-stage melanoma patients*. *Cancer Immunol Immunother*, 2006. **55**(4): p. 451-8.

38. Sato, E., et al., *Intraepithelial CD8+ tumor-infiltrating lymphocytes and a high CD8+/regulatory T cell ratio are associated with favorable prognosis in ovarian cancer*. Proc Natl Acad Sci U S A, 2005. **102**(51): p. 18538-43.
39. Naito, Y., et al., *CD8+ T cells infiltrated within cancer cell nests as a prognostic factor in human colorectal cancer*. Cancer Res, 1998. **58**(16): p. 3491-4.
40. DuPage, M., et al., *Expression of tumour-specific antigens underlies cancer immunoediting*. Nature, 2012. **482**(7385): p. 405-9.
41. Gruber, I.V., et al., *Down-regulation of CD28, TCR-zeta (zeta) and up-regulation of FAS in peripheral cytotoxic T-cells of primary breast cancer patients*. Anticancer Res, 2008. **28**(2A): p. 779-84.
42. Uyttenhove, C., et al., *Evidence for a tumoral immune resistance mechanism based on tryptophan degradation by indoleamine 2,3-dioxygenase*. Nat Med, 2003. **9**(10): p. 1269-74.
43. Sojka, D.K., Y.H. Huang, and D.J. Fowell, *Mechanisms of regulatory T-cell suppression - a diverse arsenal for a moving target*. Immunology, 2008. **124**(1): p. 13-22.
44. Kim, R., et al., *Tumor-driven evolution of immunosuppressive networks during malignant progression*. Cancer Res, 2006. **66**(11): p. 5527-36.
45. Ahmadzadeh, M., et al., *Tumor antigen-specific CD8 T cells infiltrating the tumor express high levels of PD-1 and are functionally impaired*. Blood, 2009. **114**(8): p. 1537-44.
46. Peggs, K.S., S.A. Quezada, and J.P. Allison, *Cancer immunotherapy: co-stimulatory agonists and co-inhibitory antagonists*. Clin Exp Immunol, 2009. **157**(1): p. 9-19.
47. Coley, W.B., *The treatment of inoperable sarcoma with the mixed toxins of erysipelas and bacillus prodigiosus ± immediate and final results in one hundred and forty cases*. JAMA, 1898. **31**: p. 389-421.
48. Coley, W.B., *The treatment of malignant tumors by repeated inoculations of erysipelas with a report of ten original cases*. Am J Med Sci, 1891. **105**: p. 487-511.
49. Hollingsworth, R.E. and K. Jansen, *Turning the corner on therapeutic cancer vaccines*. npj Vaccines, 2019. **4**(1): p. 7.
50. Dranoff, G., et al., *Vaccination with irradiated tumor cells engineered to secrete murine granulocyte-macrophage colony-stimulating factor stimulates potent, specific, and long-lasting anti-tumor immunity*. Proc Natl Acad Sci U S A, 1993. **90**(8): p. 3539-43.
51. Jinushi, M., F.S. Hodi, and G. Dranoff, *Enhancing the clinical activity of granulocyte-macrophage colony-stimulating factor-secreting tumor cell vaccines*. Immunol Rev, 2008. **222**: p. 287-98.
52. Kircheis, R., et al., *Interleukin-2 gene-modified allogeneic melanoma cell vaccines can induce cross-protection against syngeneic tumors in mice*. Cancer Gene Ther, 2000. **7**(6): p. 870-8.
53. Hsueh, E.C. and D.L. Morton, *Antigen-based immunotherapy of melanoma: Canvaxin therapeutic polyvalent cancer vaccine*. Semin Cancer Biol, 2003. **13**(6): p. 401-7.
54. Bonifaz, L., et al., *Efficient targeting of protein antigen to the dendritic cell receptor DEC-205 in the steady state leads to antigen presentation on major histocompatibility complex class I products and peripheral CD8+ T cell tolerance*. J Exp Med, 2002. **196**(12): p. 1627-38.

55. Anassi, E. and U.A. Ndefo, *Sipuleucel-T (provenge) injection: the first immunotherapy agent (vaccine) for hormone-refractory prostate cancer*. P T, 2011. **36**(4): p. 197-202.
56. Pol, J., et al., *Trial Watch: Peptide-based anticancer vaccines*. Oncoimmunology, 2015. **4**(4): p. e974411.
57. Kircheis, R., et al., *Immunization of Rhesus monkeys with the conjugate vaccine IGN402 induces an IgG immune response against carbohydrate and protein antigens, and cancer cells*. Vaccine, 2006. **24**(13): p. 2349-57.
58. Linette, G.P., et al., *Cardiovascular toxicity and titin cross-reactivity of affinity-enhanced T cells in myeloma and melanoma*. Blood, 2013. **122**(6): p. 863-71.
59. Koutsky, L.A., et al., *A controlled trial of a human papillomavirus type 16 vaccine*. N Engl J Med, 2002. **347**(21): p. 1645-51.
60. Lowy, D.R. and J.T. Schiller, *Prophylactic human papillomavirus vaccines*. J Clin Invest, 2006. **116**(5): p. 1167-73.
61. Joura, E.A., et al., *Effect of the human papillomavirus (HPV) quadrivalent vaccine in a subgroup of women with cervical and vulvar disease: retrospective pooled analysis of trial data*. BMJ, 2012. **344**: p. e1401.
62. McClung, N.M., et al., *Trends in Human Papillomavirus Vaccine Types 16 and 18 in Cervical Precancers, 2008-2014*. Cancer Epidemiol Biomarkers Prev, 2019. **28**(3): p. 602-609.
63. Lopes, A., G. Vandermeulen, and V. Pr eat, *Cancer DNA vaccines: current preclinical and clinical developments and future perspectives*. Journal of Experimental & Clinical Cancer Research, 2019. **38**(1): p. 146.
64. Jorritsma, S.H.T., et al., *Delivery methods to increase cellular uptake and immunogenicity of DNA vaccines*. Vaccine, 2016. **34**(46): p. 5488-5494.
65. McNamara, M.A., S.K. Nair, and E.K. Holl, *RNA-Based Vaccines in Cancer Immunotherapy*. J Immunol Res, 2015. **2015**: p. 794528.
66. Kranz, L.M., et al., *Systemic RNA delivery to dendritic cells exploits antiviral defence for cancer immunotherapy*. Nature, 2016. **534**(7607): p. 396-401.
67. Kantoff, P.W., J.L. Gulley, and C. Pico-Navarro, *Revised Overall Survival Analysis of a Phase II, Randomized, Double-Blind, Controlled Study of PROSTVAC in Men With Metastatic Castration-Resistant Prostate Cancer*. J Clin Oncol, 2017. **35**(1): p. 124-125.
68. Gulley, J.L., et al., *Phase III Trial of PROSTVAC in Asymptomatic or Minimally Symptomatic Metastatic Castration-Resistant Prostate Cancer*. Journal of Clinical Oncology, 2019. **37**(13): p. 1051-1061.
69. Ali, O.A., et al., *Vaccines Combined with Immune Checkpoint Antibodies Promote Cytotoxic T-cell Activity and Tumor Eradication*. Cancer Immunol Res, 2016. **4**(2): p. 95-100.
70. Massarelli, E., et al., *Combining Immune Checkpoint Blockade and Tumor-Specific Vaccine for Patients With Incurable Human Papillomavirus 16-Related Cancer: A Phase 2 Clinical Trial*. JAMA Oncol, 2019. **5**(1): p. 67-73.
71. Belardelli, F., et al., *Interferon-alpha in tumor immunity and immunotherapy*. Cytokine Growth Factor Rev, 2002. **13**(2): p. 119-34.
72. Lee, S. and K. Margolin, *Cytokines in cancer immunotherapy*. Cancers (Basel), 2011. **3**(4): p. 3856-93.
73. Conlon, K.C., M.D. Miljkovic, and T.A. Waldmann, *Cytokines in the Treatment of Cancer*. J Interferon Cytokine Res, 2019. **39**(1): p. 6-21.

74. Kalaaji, A.N., et al., *Combination cytokine therapy inhibits tumor growth by generation of tumor-specific T-cell responses in a murine melanoma model*. Cytokine, 2010. **49**(3): p. 287-93.
75. Wigginton, J.M. and R.H. Wiltout, *IL-12/IL-2 combination cytokine therapy for solid tumours: translation from bench to bedside*. Expert Opin Biol Ther, 2002. **2**(5): p. 513-24.
76. Wen, Q., et al., *Fusion cytokine IL-2-GMCSF enhances anticancer immune responses through promoting cell-cell interactions*. J Transl Med, 2016. **14**(1): p. 41.
77. Chen, W.-Y., et al., *Prognostic significance of tumor-infiltrating lymphocytes in patients with operable tongue cancer*. Radiation Oncology, 2018. **13**(1): p. 157.
78. Kurozumi, S., et al., *Prognostic significance of tumour-infiltrating lymphocytes for oestrogen receptor-negative breast cancer without lymph node metastasis*. Oncol Lett, 2019. **17**(3): p. 2647-2656.
79. Zhang, D., et al., *Scoring System for Tumor-Infiltrating Lymphocytes and Its Prognostic Value for Gastric Cancer*. Front Immunol, 2019. **10**: p. 71.
80. Fefer, A., *Immunotherapy and chemotherapy of Moloney sarcoma virus-induced tumors in mice*. Cancer Res, 1969. **29**(12): p. 2177-83.
81. Rosenberg, S.A., et al., *Use of tumor-infiltrating lymphocytes and interleukin-2 in the immunotherapy of patients with metastatic melanoma. A preliminary report*. N Engl J Med, 1988. **319**(25): p. 1676-80.
82. Rosenberg, S.A., et al., *Adoptive cell transfer: a clinical path to effective cancer immunotherapy*. Nat Rev Cancer, 2008. **8**(4): p. 299-308.
83. Besser, M.J., et al., *Clinical responses in a phase II study using adoptive transfer of short-term cultured tumor infiltration lymphocytes in metastatic melanoma patients*. Clin Cancer Res, 2010. **16**(9): p. 2646-55.
84. Chapuis, A.G., et al., *Transferred melanoma-specific CD8+ T cells persist, mediate tumor regression, and acquire central memory phenotype*. Proc Natl Acad Sci U S A, 2012. **109**(12): p. 4592-7.
85. Doubrovina, E., et al., *Adoptive immunotherapy with unselected or EBV-specific T cells for biopsy-proven EBV+ lymphomas after allogeneic hematopoietic cell transplantation*. Blood, 2012. **119**(11): p. 2644-56.
86. Zha, X., et al., *Generation of V alpha13/beta21+T cell specific target CML cells by TCR gene transfer*. Oncotarget, 2016. **7**(51): p. 84246-84257.
87. Ali, M., et al., *Induction of neoantigen-reactive T cells from healthy donors*. Nat Protoc, 2019. **14**(6): p. 1926-1943.
88. Ping, Y., C. Liu, and Y. Zhang, *T-cell receptor-engineered T cells for cancer treatment: current status and future directions*. Protein Cell, 2018. **9**(3): p. 254-266.
89. Stauss, H.J., E.C. Morris, and H. Abken, *Cancer gene therapy with T cell receptors and chimeric antigen receptors*. Curr Opin Pharmacol, 2015. **24**: p. 113-8.
90. Ahmadi, M., et al., *CD3 limits the efficacy of TCR gene therapy in vivo*. Blood, 2011. **118**(13): p. 3528-37.
91. Garrido, F., et al., *Implications for immunosurveillance of altered HLA class I phenotypes in human tumours*. Immunol Today, 1997. **18**(2): p. 89-95.
92. Bendle, G.M., et al., *Lethal graft-versus-host disease in mouse models of T cell receptor gene therapy*. Nat Med, 2010. **16**(5): p. 565-70, 1p following 570.

93. Provasi, E., et al., *Editing T cell specificity towards leukemia by zinc finger nucleases and lentiviral gene transfer*. Nature Medicine, 2012. **18**: p. 807.
94. Legut, M., et al., *CRISPR-mediated TCR replacement generates superior anticancer transgenic T cells*. Blood, 2018. **131**(3): p. 311-322.
95. Brenner, M.K. and H.E. Heslop, *Adoptive T cell therapy of cancer*. Curr Opin Immunol, 2010. **22**(2): p. 251-7.
96. Kuball, J., et al., *Facilitating matched pairing and expression of TCR chains introduced into human T cells*. Blood, 2007. **109**(6): p. 2331-8.
97. Morgan, R.A., et al., *Cancer regression in patients after transfer of genetically engineered lymphocytes*. Science, 2006. **314**(5796): p. 126-9.
98. Sandri, S., et al., *Effective control of acute myeloid leukaemia and acute lymphoblastic leukaemia progression by telomerase specific adoptive T-cell therapy*. Oncotarget, 2017. **8**(50): p. 86987-87001.
99. Tawara, I., et al., *Safety and persistence of WT1-specific T-cell receptor gene-transduced lymphocytes in patients with AML and MDS*. Blood, 2017. **130**(18): p. 1985-1994.
100. Rapoport, A.P., et al., *NY-ESO-1-specific TCR-engineered T cells mediate sustained antigen-specific antitumor effects in myeloma*. Nat Med, 2015. **21**(8): p. 914-921.
101. Robbins, P.F., et al., *A pilot trial using lymphocytes genetically engineered with an NY-ESO-1-reactive T-cell receptor: long-term follow-up and correlates with response*. Clin Cancer Res, 2015. **21**(5): p. 1019-27.
102. Robbins, P.F., et al., *Tumor regression in patients with metastatic synovial cell sarcoma and melanoma using genetically engineered lymphocytes reactive with NY-ESO-1*. J Clin Oncol, 2011. **29**(7): p. 917-24.
103. Thomas, R., et al., *NY-ESO-1 Based Immunotherapy of Cancer: Current Perspectives*. Front Immunol, 2018. **9**: p. 947.
104. Morgan, R.A., et al., *Cancer regression and neurological toxicity following anti-MAGE-A3 TCR gene therapy*. J Immunother, 2013. **36**(2): p. 133-51.
105. Blankenstein, T., et al., *Targeting cancer-specific mutations by T cell receptor gene therapy*. Curr Opin Immunol, 2015. **33**: p. 112-9.
106. Kato, T., et al., *Effective screening of T cells recognizing neoantigens and construction of T-cell receptor-engineered T cells*. Oncotarget, 2018. **9**(13): p. 11009-11019.
107. Ren, L., et al., *Identification of neoantigen-specific T cells and their targets: implications for immunotherapy of head and neck squamous cell carcinoma*. Oncoimmunology, 2019. **8**(4): p. e1568813.
108. Matsuda, T., et al., *Induction of Neoantigen-Specific Cytotoxic T Cells and Construction of T-cell Receptor-Engineered T Cells for Ovarian Cancer*. Clin Cancer Res, 2018. **24**(21): p. 5357-5367.
109. Tran, E., et al., *Cancer immunotherapy based on mutation-specific CD4+ T cells in a patient with epithelial cancer*. Science, 2014. **344**(6184): p. 641-5.
110. Tubb, V.M., et al., *Isolation of T cell receptors targeting recurrent neoantigens in hematological malignancies*. Journal for ImmunoTherapy of Cancer, 2018. **6**(1): p. 70.
111. Thomas, S., et al., *Human T cells expressing affinity-matured TCR display accelerated responses but fail to recognize low density of MHC-peptide antigen*. Blood, 2011. **118**(2): p. 319-29.

112. Parkhurst, M.R., et al., *Characterization of genetically modified T-cell receptors that recognize the CEA:691-699 peptide in the context of HLA-A2.1 on human colorectal cancer cells*. Clin Cancer Res, 2009. **15**(1): p. 169-80.
113. Parkhurst, M.R., et al., *T cells targeting carcinoembryonic antigen can mediate regression of metastatic colorectal cancer but induce severe transient colitis*. Mol Ther, 2011. **19**(3): p. 620-6.
114. Robbins, P.F., et al., *Single and dual amino acid substitutions in TCR CDRs can enhance antigen-specific T cell functions*. J Immunol, 2008. **180**(9): p. 6116-31.
115. Robbins, P.F., et al., *Tumor Regression in Patients With Metastatic Synovial Cell Sarcoma and Melanoma Using Genetically Engineered Lymphocytes Reactive With NY-ESO-1*. Journal of Clinical Oncology, 2011. **29**(7): p. 917-924.
116. Cartellieri, M., et al., *Chimeric antigen receptor-engineered T cells for immunotherapy of cancer*. J Biomed Biotechnol, 2010. **2010**: p. 956304.
117. Ryman, J.T. and B. Meibohm, *Pharmacokinetics of Monoclonal Antibodies*. CPT Pharmacometrics Syst Pharmacol, 2017. **6**(9): p. 576-588.
118. Schroeder, H.W., Jr. and L. Cavacini, *Structure and function of immunoglobulins*. J Allergy Clin Immunol, 2010. **125**(2 Suppl 2): p. S41-52.
119. Bassing, C.H., W. Swat, and F.W. Alt, *The mechanism and regulation of chromosomal V(D)J recombination*. Cell, 2002. **109 Suppl**: p. S45-55.
120. Dudley, D.D., et al., *Mechanism and control of V(D)J recombination versus class switch recombination: similarities and differences*. Adv Immunol, 2005. **86**: p. 43-112.
121. Köhler, G. and C. Milstein, *Continuous cultures of fused cells secreting antibody of predefined specificity*. Nature, 1975. **256**(5517): p. 495-497.
122. Tjandra, J.J., L. Ramadi, and I.F. McKenzie, *Development of human anti-murine antibody (HAMA) response in patients*. Immunol Cell Biol, 1990. **68 (Pt 6)**: p. 367-76.
123. Laffleur, B., et al., *Production of human or humanized antibodies in mice*. Methods Mol Biol, 2012. **901**: p. 149-59.
124. Yamashita, M., Y. Katakura, and S. Shirahata, *Recent advances in the generation of human monoclonal antibody*. Cytotechnology, 2007. **55**(2-3): p. 55-60.
125. Bradbury, A.R. and J.D. Marks, *Antibodies from phage antibody libraries*. J Immunol Methods, 2004. **290**(1-2): p. 29-49.
126. Marks, J.D., et al., *By-passing immunization. Human antibodies from V-gene libraries displayed on phage*. J Mol Biol, 1991. **222**(3): p. 581-97.
127. Clynes, R.A., et al., *Inhibitory Fc receptors modulate in vivo cytotoxicity against tumor targets*. Nat Med, 2000. **6**(4): p. 443-6.
128. Beers, S.A., M.J. Glennie, and A.L. White, *Influence of immunoglobulin isotype on therapeutic antibody function*. Blood, 2016. **127**(9): p. 1097-101.
129. Li, F. and J.V. Ravetch, *Apoptotic and antitumor activity of death receptor antibodies require inhibitory Fcγ receptor engagement*. Proc Natl Acad Sci U S A, 2012. **109**(27): p. 10966-71.
130. Qi, X., et al., *Optimization of 4-1BB antibody for cancer immunotherapy by balancing agonistic strength with FcγR affinity*. Nature Communications, 2019. **10**(1): p. 2141.

131. White, A.L., et al., *Conformation of the human immunoglobulin G2 hinge imparts superagonistic properties to immunostimulatory anticancer antibodies*. *Cancer Cell*, 2015. **27**(1): p. 138-48.
132. Hodi, F.S., et al., *Improved survival with ipilimumab in patients with metastatic melanoma*. *N Engl J Med*, 2010. **363**(8): p. 711-23.
133. Farolfi, A., et al., *Ipilimumab in advanced melanoma: reports of long-lasting responses*. *Melanoma Res*, 2012. **22**(3): p. 263-70.
134. Romano, E., et al., *Ipilimumab-dependent cell-mediated cytotoxicity of regulatory T cells ex vivo by nonclassical monocytes in melanoma patients*. *Proc Natl Acad Sci U S A*, 2015. **112**(19): p. 6140-5.
135. Tarhini, A., E. Lo, and D.R. Minor, *Releasing the brake on the immune system: ipilimumab in melanoma and other tumors*. *Cancer Biother Radiopharm*, 2010. **25**(6): p. 601-13.
136. Vanpouille-Box, C., et al., *Trial watch: Immune checkpoint blockers for cancer therapy*. *Oncoimmunology*, 2017. **6**(11): p. e1373237.
137. Markham, A. and S. Duggan, *Cemiplimab: First Global Approval*. *Drugs*, 2018. **78**(17): p. 1841-1846.
138. Larkin, J., et al., *Combined Nivolumab and Ipilimumab or Monotherapy in Untreated Melanoma*. *N Engl J Med*, 2015. **373**(1): p. 23-34.
139. Rotte, A., *Combination of CTLA-4 and PD-1 blockers for treatment of cancer*. *J Exp Clin Cancer Res*, 2019. **38**(1): p. 255.
140. Pilon-Thomas, S., et al., *Blockade of programmed death ligand 1 enhances the therapeutic efficacy of combination immunotherapy against melanoma*. *J Immunol*, 2010. **184**(7): p. 3442-9.
141. von Pawel, J., et al., *Long-term survival in patients with advanced non-small-cell lung cancer treated with atezolizumab versus docetaxel: Results from the randomised phase III OAK study*. *Eur J Cancer*, 2019. **107**: p. 124-132.
142. Chaudhri, A., et al., *PD-L1 Binds to B7-1 Only In Cis on the Same Cell Surface*. *Cancer Immunol Res*, 2018. **6**(8): p. 921-929.
143. Han, X. and M.D. Vesely, *Stimulating T Cells Against Cancer With Agonist Immunostimulatory Monoclonal Antibodies*. *Int Rev Cell Mol Biol*, 2019. **342**: p. 1-25.
144. Ju, S.A., et al., *Eradication of established renal cell carcinoma by a combination of 5-fluorouracil and anti-4-1BB monoclonal antibody in mice*. *Int J Cancer*, 2008. **122**(12): p. 2784-90.
145. Shi, W. and D.W. Siemann, *Augmented antitumor effects of radiation therapy by 4-1BB antibody (BMS-469492) treatment*. *Anticancer Res*, 2006. **26**(5A): p. 3445-53.
146. Segal, N.H., et al., *Results from an Integrated Safety Analysis of Urelumab, an Agonist Anti-CD137 Monoclonal Antibody*. *Clin Cancer Res*, 2017. **23**(8): p. 1929-1936.
147. Bansal-Pakala, P., A.G. Jember, and M. Croft, *Signaling through OX40 (CD134) breaks peripheral T-cell tolerance*. *Nat Med*, 2001. **7**(8): p. 907-12.
148. So, T. and M. Croft, *Cutting edge: OX40 inhibits TGF-beta- and antigen-driven conversion of naive CD4 T cells into CD25+Foxp3+ T cells*. *J Immunol*, 2007. **179**(3): p. 1427-30.
149. Vu, M.D., et al., *OX40 costimulation turns off Foxp3+ Tregs*. *Blood*, 2007. **110**(7): p. 2501-10.

150. Bulliard, Y., et al., *OX40 engagement depletes intratumoral Tregs via activating Fcγ₁Rs, leading to antitumor efficacy*. Immunol Cell Biol, 2014. **92**(6): p. 475-80.
151. Guo, Z., et al., *PD-1 blockade and OX40 triggering synergistically protects against tumor growth in a murine model of ovarian cancer*. PLoS One, 2014. **9**(2): p. e89350.
152. Marabelle, A., et al., *Depleting tumor-specific Tregs at a single site eradicates disseminated tumors*. J Clin Invest, 2013. **123**(6): p. 2447-63.
153. Aranda, F., et al., *Trial Watch: Immunostimulatory monoclonal antibodies in cancer therapy*. Oncoimmunology, 2014. **3**(1): p. e27297.
154. Cabo, M., et al., *Trial Watch: Immunostimulatory monoclonal antibodies for oncological indications*. Oncoimmunology, 2017. **6**(12): p. e1371896.
155. Glade-Bender, J., J.J. Kandel, and D.J. Yamashiro, *VEGF blocking therapy in the treatment of cancer*. Expert Opin Biol Ther, 2003. **3**(2): p. 263-76.
156. Gajria, D. and S. Chandralapaty, *HER2-amplified breast cancer: mechanisms of trastuzumab resistance and novel targeted therapies*. Expert Rev Anticancer Ther, 2011. **11**(2): p. 263-75.
157. Honeychurch, J., et al., *Antibody-induced nonapoptotic cell death in human lymphoma and leukemia cells is mediated through a novel reactive oxygen species-dependent pathway*. Blood, 2012. **119**(15): p. 3523-33.
158. Weiner, G.J., *Monoclonal antibody mechanisms of action in cancer*. Immunol Res, 2007. **39**(1-3): p. 271-8.
159. Weiner, L.M., Surana, R. and Wang, S., *Monoclonal antibodies: versatile platforms for cancer immunotherapy*. Nature Reviews Immunology, 2010. **10**: p. 317-327.
160. Bowles, J.A., et al., *Anti-CD20 monoclonal antibody with enhanced affinity for CD16 activates NK cells at lower concentrations and more effectively than rituximab*. Blood, 2006. **108**(8): p. 2648-54.
161. Mellor, J.D., et al., *A critical review of the role of Fc gamma receptor polymorphisms in the response to monoclonal antibodies in cancer*. J Hematol Oncol, 2013. **6**: p. 1.
162. Cartron, G., et al., *Therapeutic activity of humanized anti-CD20 monoclonal antibody and polymorphism in IgG Fc receptor Fcγ₁R11a gene*. Blood, 2002. **99**(3): p. 754-8.
163. Noris, M. and G. Remuzzi, *Overview of complement activation and regulation*. Semin Nephrol, 2013. **33**(6): p. 479-92.
164. Guo, R.F. and P.A. Ward, *Role of C5a in inflammatory responses*. Annu Rev Immunol, 2005. **23**: p. 821-52.
165. Keyel, M.E. and C.P. Reynolds, *Spotlight on dinutuximab in the treatment of high-risk neuroblastoma: development and place in therapy*. Biologics, 2019. **13**: p. 1-12.
166. McKeage, K. and C.M. Perry, *Trastuzumab: a review of its use in the treatment of metastatic breast cancer overexpressing HER2*. Drugs, 2002. **62**(1): p. 209-43.
167. Robak, T., *GA-101, a third-generation, humanized and glyco-engineered anti-CD20 mAb for the treatment of B-cell lymphoid malignancies*. Curr Opin Investig Drugs, 2009. **10**(6): p. 588-96.
168. Mossner, E., et al., *Increasing the efficacy of CD20 antibody therapy through the engineering of a new type II anti-CD20 antibody with enhanced direct and*

- immune effector cell-mediated B-cell cytotoxicity*. Blood, 2010. **115**(22): p. 4393-402.
169. Kawashima, H., *Radioimmunotherapy: a specific treatment protocol for cancer by cytotoxic radioisotopes conjugated to antibodies*. ScientificWorldJournal, 2014. **2014**: p. 492061.
 170. Kufer, P., R. Lutterbuse, and P.A. Baeuerle, *A revival of bispecific antibodies*. Trends Biotechnol, 2004. **22**(5): p. 238-44.
 171. Glennie, M.J., et al., *Preparation and performance of bispecific F(ab' gamma)2 antibody containing thioether-linked Fab' gamma fragments*. J Immunol, 1987. **139**(7): p. 2367-75.
 172. Spiess, C., Q. Zhai, and P.J. Carter, *Alternative molecular formats and therapeutic applications for bispecific antibodies*. Mol Immunol, 2015. **67**(2 Pt A): p. 95-106.
 173. Walsh, G., *Biopharmaceutical benchmarks 2010*. Nat Biotechnol, 2010. **28**(9): p. 917-24.
 174. Bargou, R., et al., *Tumor regression in cancer patients by very low doses of a T cell-engaging antibody*. Science, 2008. **321**(5891): p. 974-7.
 175. Wu, J., et al., *Blinatumomab: a bispecific T cell engager (BiTE) antibody against CD19/CD3 for refractory acute lymphoid leukemia*. J Hematol Oncol, 2015. **8**: p. 104.
 176. Huehls, A.M., T.A. Coupet, and C.L. Sentman, *Bispecific T-cell engagers for cancer immunotherapy*. Immunol Cell Biol, 2015. **93**(3): p. 290-6.
 177. Dustin, M.L., A.K. Chakraborty, and A.S. Shaw, *Understanding the structure and function of the immunological synapse*. Cold Spring Harb Perspect Biol, 2010. **2**(10): p. a002311.
 178. Sedykh, S.E., et al., *Bispecific antibodies: design, therapy, perspectives*. Drug Des Devel Ther, 2018. **12**: p. 195-208.
 179. Yuraszcek, T., S. Kasichayanula, and J.E. Benjamin, *Translation and Clinical Development of Bispecific T-cell Engaging Antibodies for Cancer Treatment*. Clin Pharmacol Ther, 2017. **101**(5): p. 634-645.
 180. Stashenko, P., et al., *Expression of cell surface markers after human B lymphocyte activation*. Proc Natl Acad Sci U S A, 1981. **78**(6): p. 3848-52.
 181. Walshe, C.A., et al., *Induction of cytosolic calcium flux by CD20 is dependent upon B Cell antigen receptor signaling*. J Biol Chem, 2008. **283**(25): p. 16971-84.
 182. Robak, T. and E. Robak, *New anti-CD20 monoclonal antibodies for the treatment of B-cell lymphoid malignancies*. BioDrugs, 2011. **25**(1): p. 13-25.
 183. Oldham, R.J., K.L.S. Cleary, and M.S. Cragg, *CD20 and Its Antibodies: Past, Present, and Future*. 2014. **5**(1-2): p. 7-23.
 184. Lim, S.H., et al., *Anti-CD20 monoclonal antibodies: historical and future perspectives*. Haematologica, 2010. **95**(1): p. 135-43.
 185. Stern, M. and R. Herrmann, *Overview of monoclonal antibodies in cancer therapy: present and promise*. Crit Rev Oncol Hematol, 2005. **54**(1): p. 11-29.
 186. Niederfellner, G., et al., *Epitope characterization and crystal structure of GA101 provide insights into the molecular basis for type I/II distinction of CD20 antibodies*. Blood, 2011. **118**(2): p. 358-67.
 187. Klein, C., et al., *Epitope interactions of monoclonal antibodies targeting CD20 and their relationship to functional properties*. MAbs, 2013. **5**(1): p. 22-33.

188. Singh, V., D. Gupta, and A. Almasan, *Development of Novel Anti-Cd20 Monoclonal Antibodies and Modulation in Cd20 Levels on Cell Surface: Looking to Improve Immunotherapy Response*. J Cancer Sci Ther, 2015. **7**(11): p. 347-358.
189. Jazirehi, A.R. and B. Bonavida, *Cellular and molecular signal transduction pathways modulated by rituximab (rituxan, anti-CD20 mAb) in non-Hodgkin's lymphoma: implications in chemosensitization and therapeutic intervention*. Oncogene, 2005. **24**(13): p. 2121-2143.
190. Marshall, M.J.E., R.J. Stopforth, and M.S. Cragg, *Therapeutic Antibodies: What Have We Learnt from Targeting CD20 and Where Are We Going?* Frontiers in Immunology, 2017. **8**(1245).
191. Beers, S.A., et al., *Type II (tositumomab) anti-CD20 monoclonal antibody out performs type I (rituximab-like) reagents in B-cell depletion regardless of complement activation*. Blood, 2008. **112**(10): p. 4170-7.
192. Cragg, M.S., et al., *Complement-mediated lysis by anti-CD20 mAb correlates with segregation into lipid rafts*. Blood, 2003. **101**(3): p. 1045-52.
193. Cragg, M.S., *CD20 antibodies: doing the time warp*. Blood, 2011. **118**(2): p. 219-20.
194. Marshall, M.J.E., R.J. Stopforth, and M.S. Cragg, *Therapeutic Antibodies: What Have We Learnt from Targeting CD20 and Where Are We Going?* Front Immunol, 2017. **8**: p. 1245.
195. Lim, S.H., et al., *Fc gamma receptor IIb on target B cells promotes rituximab internalization and reduces clinical efficacy*. Blood, 2011. **118**(9): p. 2530-40.
196. Vaughan, A.T., et al., *Inhibitory Fc gamma RIIb (CD32b) becomes activated by therapeutic mAb in both cis and trans and drives internalization according to antibody specificity*. Blood, 2014. **123**(5): p. 669-77.
197. Marcus, R., et al., *Obinutuzumab for the First-Line Treatment of Follicular Lymphoma*. N Engl J Med, 2017. **377**(14): p. 1331-1344.
198. Goede, V., et al., *Obinutuzumab plus chlorambucil in patients with CLL and coexisting conditions*. N Engl J Med, 2014. **370**(12): p. 1101-10.
199. Goede, V., et al., *Obinutuzumab as frontline treatment of chronic lymphocytic leukemia: updated results of the CLL11 study*. Leukemia, 2015. **29**(7): p. 1602-4.
200. Orkin, S.H. and L.I. Zon, *Hematopoiesis: an evolving paradigm for stem cell biology*. Cell, 2008. **132**(4): p. 631-44.
201. Akashi, K., et al., *A clonogenic common myeloid progenitor that gives rise to all myeloid lineages*. Nature, 2000. **404**(6774): p. 193-7.
202. Kondo, M., I.L. Weissman, and K. Akashi, *Identification of clonogenic common lymphoid progenitors in mouse bone marrow*. Cell, 1997. **91**(5): p. 661-72.
203. Adolfsson, J., et al., *Identification of Flt3+ lympho-myeloid stem cells lacking erythro-megakaryocytic potential a revised road map for adult blood lineage commitment*. Cell, 2005. **121**(2): p. 295-306.
204. Serwold, T., L.I. Ehrlich, and I.L. Weissman, *Reductive isolation from bone marrow and blood implicates common lymphoid progenitors as the major source of thymopoiesis*. Blood, 2009. **113**(4): p. 807-15.
205. Porritt, H.E., K. Gordon, and H.T. Petrie, *Kinetics of steady-state differentiation and mapping of intrathymic-signaling environments by stem cell transplantation in nonirradiated mice*. J Exp Med, 2003. **198**(6): p. 957-62.

206. Radtke, F., et al., *Deficient T cell fate specification in mice with an induced inactivation of Notch1*. *Immunity*, 1999. **10**(5): p. 547-58.
207. Masuda, K., et al., *T cell lineage determination precedes the initiation of TCR beta gene rearrangement*. *J Immunol*, 2007. **179**(6): p. 3699-706.
208. Kang, J., A. Volkman, and D.H. Raulet, *Evidence that gammadelta versus alphabeta T cell fate determination is initiated independently of T cell receptor signaling*. *J Exp Med*, 2001. **193**(6): p. 689-98.
209. Godfrey, D.I., et al., *Onset of TCR-beta gene rearrangement and role of TCR-beta expression during CD3-CD4-CD8- thymocyte differentiation*. *J Immunol*, 1994. **152**(10): p. 4783-92.
210. Capone, M., R.D. Hockett, Jr., and A. Zlotnik, *Kinetics of T cell receptor beta, gamma, and delta rearrangements during adult thymic development: T cell receptor rearrangements are present in CD44(+)CD25(+) Pro-T thymocytes*. *Proc Natl Acad Sci U S A*, 1998. **95**(21): p. 12522-7.
211. Fugmann, S.D., *RAG1 and RAG2 in V(D)J recombination and transposition*. *Immunol Res*, 2001. **23**(1): p. 23-39.
212. Maillard, I., et al., *The requirement for Notch signaling at the beta-selection checkpoint in vivo is absolute and independent of the pre-T cell receptor*. *J Exp Med*, 2006. **203**(10): p. 2239-45.
213. Allman, D., et al., *Separation of Notch1 promoted lineage commitment and expansion/transformation in developing T cells*. *J Exp Med*, 2001. **194**(1): p. 99-106.
214. Muro, R., H. Takayanagi, and T. Nitta, *T cell receptor signaling for $\gamma\delta$ T cell development*. *Inflammation and Regeneration*, 2019. **39**(1): p. 6.
215. Koch, U. and F. Radtke, *Mechanisms of T cell development and transformation*. *Annu Rev Cell Dev Biol*, 2011. **27**: p. 539-62.
216. Starr, T.K., S.C. Jameson, and K.A. Hogquist, *Positive and negative selection of T cells*. *Annu Rev Immunol*, 2003. **21**: p. 139-76.
217. Hogquist, K.A., et al., *T Cell Adolescence: Maturation Events Beyond Positive Selection*. *J Immunol*, 2015. **195**(4): p. 1351-7.
218. Xing, Y. and K.A. Hogquist, *T-cell tolerance: central and peripheral*. *Cold Spring Harb Perspect Biol*, 2012. **4**(6).
219. Hsieh, C.S., H.M. Lee, and C.W. Lio, *Selection of regulatory T cells in the thymus*. *Nat Rev Immunol*, 2012. **12**(3): p. 157-67.
220. Matloubian, M., et al., *Lymphocyte egress from thymus and peripheral lymphoid organs is dependent on S1P receptor 1*. *Nature*, 2004. **427**(6972): p. 355-60.
221. Gunn, M.D., et al., *A chemokine expressed in lymphoid high endothelial venules promotes the adhesion and chemotaxis of naive T lymphocytes*. *Proc Natl Acad Sci U S A*, 1998. **95**(1): p. 258-63.
222. Weninger, W., et al., *Migratory properties of naive, effector, and memory CD8(+) T cells*. *J Exp Med*, 2001. **194**(7): p. 953-66.
223. Sprent, J. and C.D. Surh, *Generation and maintenance of memory T cells*. *Curr Opin Immunol*, 2001. **13**(2): p. 248-54.
224. Daniels, M. and E. Teixeiro, *TCR signaling in T cell memory*. *Frontiers in Immunology*, 2015. **6**.
225. Davis, S.J. and P.A. van der Merwe, *The kinetic-segregation model: TCR triggering and beyond*. *Nat Immunol*, 2006. **7**(8): p. 803-9.
226. Guy, C.S. and D.A. Vignali, *Organization of proximal signal initiation at the TCR:CD3 complex*. *Immunol Rev*, 2009. **232**(1): p. 7-21.

227. Smith-Garvin, J.E., G.A. Koretzky, and M.S. Jordan, *T cell activation*. Annu Rev Immunol, 2009. **27**: p. 591-619.
228. Saito, T., T. Yokosuka, and A. Hashimoto-Tane, *Dynamic regulation of T cell activation and co-stimulation through TCR-microclusters*. FEBS Lett, 2010. **584**(24): p. 4865-71.
229. Bromley, S.K., et al., *The immunological synapse*. Annu Rev Immunol, 2001. **19**: p. 375-96.
230. Grakoui, A., et al., *The immunological synapse: a molecular machine controlling T cell activation*. Science, 1999. **285**(5425): p. 221-7.
231. Zamoyska, R., *Why is there so much CD45 on T cells?* Immunity, 2007. **27**(3): p. 421-3.
232. Rossy, J., D.J. Williamson, and K. Gaus, *How does the kinase Lck phosphorylate the T cell receptor? Spatial organization as a regulatory mechanism*. Front Immunol, 2012. **3**: p. 167.
233. Love, P.E. and S.M. Hayes, *ITAM-mediated signaling by the T-cell antigen receptor*. Cold Spring Harb Perspect Biol, 2010. **2**(6): p. a002485.
234. Wang, H., et al., *ZAP-70: an essential kinase in T-cell signaling*. Cold Spring Harb Perspect Biol, 2010. **2**(5): p. a002279.
235. Balagopalan, L., et al., *The linker for activation of T cells (LAT) signaling hub: from signaling complexes to microclusters*. J Biol Chem, 2015. **290**(44): p. 26422-9.
236. Pollitt, A.Y. and R.H. Insall, *WASP and SCAR/WAVE proteins: the drivers of actin assembly*. Journal of Cell Science, 2009. **122**(15): p. 2575-2578.
237. Wu, C.-J. and J.D. Ashwell, *NEMO recognition of ubiquitinated Bcl10 is required for T cell receptor-mediated NF- κ B activation*. Proceedings of the National Academy of Sciences, 2008. **105**(8): p. 3023-3028.
238. Huse, M., *The T-cell-receptor signaling network*. Journal of Cell Science, 2009. **122**(9): p. 1269-1273.
239. Karin, M., Z. Liu, and E. Zandi, *AP-1 function and regulation*. Curr Opin Cell Biol, 1997. **9**(2): p. 240-6.
240. Martin-Cofreces, N.B., B. Alarcon, and F. Sanchez-Madrid, *Tubulin and actin interplay at the T cell and antigen-presenting cell interface*. Front Immunol, 2011. **2**: p. 24.
241. de la Roche, M., et al., *Hedgehog signaling controls T cell killing at the immunological synapse*. Science, 2013. **342**(6163): p. 1247-50.
242. Mueller, D.L., M.K. Jenkins, and R.H. Schwartz, *Clonal expansion versus functional clonal inactivation: a costimulatory signalling pathway determines the outcome of T cell antigen receptor occupancy*. Annu Rev Immunol, 1989. **7**: p. 445-80.
243. Aggarwal, B.B., *Signalling pathways of the TNF superfamily: a double-edged sword*. Nat Rev Immunol, 2003. **3**(9): p. 745-56.
244. Hehlhans, T. and K. Pfeffer, *The intriguing biology of the tumour necrosis factor/tumour necrosis factor receptor superfamily: players, rules and the games*. Immunology, 2005. **115**(1): p. 1-20.
245. Dempsey, P.W., et al., *The signaling adaptors and pathways activated by TNF superfamily*. Cytokine Growth Factor Rev, 2003. **14**(3-4): p. 193-209.
246. Chen, L. and D.B. Flies, *Molecular mechanisms of T cell co-stimulation and co-inhibition*. Nat Rev Immunol, 2013. **13**(4): p. 227-42.

247. Zhu, Y., S. Yao, and L. Chen, *Cell surface signaling molecules in the control of immune responses: a tide model*. *Immunity*, 2011. **34**(4): p. 466-78.
248. Boomer, J.S. and J.M. Green, *An enigmatic tail of CD28 signaling*. *Cold Spring Harb Perspect Biol*, 2010. **2**(8): p. a002436.
249. Sanchez-Lockhart, M., M. Kim, and J. Miller, *Cutting edge: A role for inside-out signaling in TCR regulation of CD28 ligand binding*. *J Immunol*, 2011. **187**(11): p. 5515-9.
250. van der Merwe, P.A., et al., *CD80 (B7-1) binds both CD28 and CTLA-4 with a low affinity and very fast kinetics*. *J Exp Med*, 1997. **185**(3): p. 393-403.
251. Qureshi, O.S., et al., *Trans-endocytosis of CD80 and CD86: a molecular basis for the cell-extrinsic function of CTLA-4*. *Science*, 2011. **332**(6029): p. 600-3.
252. Lindstein, T., et al., *Regulation of lymphokine messenger RNA stability by a surface-mediated T cell activation pathway*. *Science*, 1989. **244**(4902): p. 339-43.
253. Pages, F., et al., *Binding of phosphatidylinositol-3-OH kinase to CD28 is required for T-cell signalling*. *Nature*, 1994. **369**(6478): p. 327-9.
254. Prasad, K.V., et al., *T-cell antigen CD28 interacts with the lipid kinase phosphatidylinositol 3-kinase by a cytoplasmic Tyr(P)-Met-Xaa-Met motif*. *Proc Natl Acad Sci U S A*, 1994. **91**(7): p. 2834-8.
255. Srivastava, N., R. Sudan, and W.G. Kerr, *Role of inositol poly-phosphatases and their targets in T cell biology*. *Front Immunol*, 2013. **4**: p. 288.
256. Riha, P. and C.E. Rudd, *CD28 co-signaling in the adaptive immune response*. *Self Nonself*, 2010. **1**(3): p. 231-240.
257. Thaker, Y.R., H. Schneider, and C.E. Rudd, *TCR and CD28 activate the transcription factor NF-kappaB in T-cells via distinct adaptor signaling complexes*. *Immunol Lett*, 2015. **163**(1): p. 113-9.
258. Fos, C., et al., *ICOS ligation recruits the p50alpha PI3K regulatory subunit to the immunological synapse*. *J Immunol*, 2008. **181**(3): p. 1969-77.
259. Simpson, T.R., S.A. Quezada, and J.P. Allison, *Regulation of CD4 T cell activation and effector function by inducible costimulator (ICOS)*. *Curr Opin Immunol*, 2010. **22**(3): p. 326-32.
260. Valk, E., et al., *T cell receptor-interacting molecule acts as a chaperone to modulate surface expression of the CTLA-4 coreceptor*. *Immunity*, 2006. **25**(5): p. 807-21.
261. Schneider, H. and C.E. Rudd, *Diverse mechanisms regulate the surface expression of immunotherapeutic target *ctla-4**. *Front Immunol*, 2014. **5**: p. 619.
262. Nirschl, C.J. and C.G. Drake, *Molecular pathways: coexpression of immune checkpoint molecules: signaling pathways and implications for cancer immunotherapy*. *Clin Cancer Res*, 2013. **19**(18): p. 4917-24.
263. Riley, J.L., *PD-1 signaling in primary T cells*. *Immunol Rev*, 2009. **229**(1): p. 114-25.
264. Sheppard, K.A., et al., *PD-1 inhibits T-cell receptor induced phosphorylation of the ZAP70/CD3zeta signalosome and downstream signaling to PKCtheta*. *FEBS Lett*, 2004. **574**(1-3): p. 37-41.
265. Bally, A.P., J.W. Austin, and J.M. Boss, *Genetic and Epigenetic Regulation of PD-1 Expression*. *J Immunol*, 2016. **196**(6): p. 2431-7.
266. Du, W., et al., *TIM-3 as a Target for Cancer Immunotherapy and Mechanisms of Action*. *Int J Mol Sci*, 2017. **18**(3).

267. Lichtenegger, F.S., et al., *Targeting LAG-3 and PD-1 to Enhance T Cell Activation by Antigen-Presenting Cells*. *Front Immunol*, 2018. **9**: p. 385.
268. Croft, M., *Costimulation of T cells by OX40, 4-1BB, and CD27*. *Cytokine Growth Factor Rev*, 2003. **14**(3-4): p. 265-73.
269. Kim, J.-O., et al., *NF- κ B and AP-1 regulate activation-dependent CD137 (4-1BB) expression in T cells*. *FEBS Letters*, 2003. **541**(1-3): p. 163-170.
270. Arch, R.H. and C.B. Thompson, *4-1BB and Ox40 are members of a tumor necrosis factor (TNF)-nerve growth factor receptor subfamily that bind TNF receptor-associated factors and activate nuclear factor kappaB*. *Mol Cell Biol*, 1998. **18**(1): p. 558-65.
271. Chen, Z.J., *Ubiquitination in signaling to and activation of IKK*. *Immunol Rev*, 2012. **246**(1): p. 95-106.
272. Vallabhapurapu, S. and M. Karin, *Regulation and function of NF-kappaB transcription factors in the immune system*. *Annu Rev Immunol*, 2009. **27**: p. 693-733.
273. Sun, S.C., *Non-canonical NF-kappaB signaling pathway*. *Cell Res*, 2011. **21**(1): p. 71-85.
274. McPherson, A.J., et al., *Opposing roles for TRAF1 in the alternative versus classical NF-kappaB pathway in T cells*. *J Biol Chem*, 2012. **287**(27): p. 23010-9.
275. Sun, S.C., *The noncanonical NF-kappaB pathway*. *Immunol Rev*, 2012. **246**(1): p. 125-40.
276. Sabbagh, L., et al., *ERK-dependent Bim modulation downstream of the 4-1BB-TRAF1 signaling axis is a critical mediator of CD8 T cell survival in vivo*. *J Immunol*, 2008. **180**(12): p. 8093-101.
277. Wang, C., et al., *Immune regulation by 4-1BB and 4-1BBL: complexities and challenges*. *Immunol Rev*, 2009. **229**(1): p. 192-215.
278. Watts, T.H., *TNF/TNFR family members in costimulation of T cell responses*. *Annu Rev Immunol*, 2005. **23**: p. 23-68.
279. Cannons, J.L., et al., *4-1BB ligand induces cell division, sustains survival, and enhances effector function of CD4 and CD8 T cells with similar efficacy*. *J Immunol*, 2001. **167**(3): p. 1313-24.
280. Lee do, Y., et al., *4-1BB signaling activates the t cell factor 1 effector/beta-catenin pathway with delayed kinetics via ERK signaling and delayed PI3K/AKT activation to promote the proliferation of CD8+ T Cells*. *PLoS One*, 2013. **8**(7): p. e69677.
281. Hendriks, J., et al., *CD27 is required for generation and long-term maintenance of T cell immunity*. *Nat Immunol*, 2000. **1**(5): p. 433-40.
282. Borst, J., J. Hendriks, and Y. Xiao, *CD27 and CD70 in T cell and B cell activation*. *Curr Opin Immunol*, 2005. **17**(3): p. 275-81.
283. Claus, C., et al., *CD27 signaling increases the frequency of regulatory T cells and promotes tumor growth*. *Cancer Res*, 2012. **72**(14): p. 3664-76.
284. Croft, M., *Control of immunity by the TNFR-related molecule OX40 (CD134)*. *Annu Rev Immunol*, 2010. **28**: p. 57-78.
285. Rogers, P.R., et al., *OX40 promotes Bcl-xL and Bcl-2 expression and is essential for long-term survival of CD4 T cells*. *Immunity*, 2001. **15**(3): p. 445-55.
286. Croft, M., et al., *The significance of OX40 and OX40L to T-cell biology and immune disease*. *Immunol Rev*, 2009. **229**(1): p. 173-91.

287. Mosmann, T.R., et al., *Two types of murine helper T cell clone. I. Definition according to profiles of lymphokine activities and secreted proteins.* J Immunol, 1986. **136**(7): p. 2348-57.
288. Szabo, S.J., et al., *Regulation of the interleukin (IL)-12R beta 2 subunit expression in developing T helper 1 (Th1) and Th2 cells.* J Exp Med, 1997. **185**(5): p. 817-24.
289. Szabo, S.J., et al., *A novel transcription factor, T-bet, directs Th1 lineage commitment.* Cell, 2000. **100**(6): p. 655-69.
290. Romagnani, S., *Th1/Th2 cells.* Inflamm Bowel Dis, 1999. **5**(4): p. 285-94.
291. Swain, S.L., et al., *IL-4 directs the development of Th2-like helper effectors.* J Immunol, 1990. **145**(11): p. 3796-806.
292. Zhu, J. and W.E. Paul, *CD4 T cells: fates, functions, and faults.* Blood, 2008. **112**(5): p. 1557-69.
293. Kaplan, M.H., et al., *Stat6 is required for mediating responses to IL-4 and for development of Th2 cells.* Immunity, 1996. **4**(3): p. 313-9.
294. Zhang, D.H., et al., *Transcription factor GATA-3 is differentially expressed in murine Th1 and Th2 cells and controls Th2-specific expression of the interleukin-5 gene.* J Biol Chem, 1997. **272**(34): p. 21597-603.
295. Deo, S.S., et al., *Role played by Th2 type cytokines in IgE mediated allergy and asthma.* Lung India, 2010. **27**(2): p. 66-71.
296. Hegazy, A.N., et al., *Interferons direct Th2 cell reprogramming to generate a stable GATA-3(+)T-bet(+) cell subset with combined Th2 and Th1 cell functions.* Immunity, 2010. **32**(1): p. 116-28.
297. Peine, M., et al., *Stable T-bet(+)GATA-3(+) Th1/Th2 hybrid cells arise in vivo, can develop directly from naive precursors, and limit immunopathologic inflammation.* PLoS Biol, 2013. **11**(8): p. e1001633.
298. Jabeen, R. and M.H. Kaplan, *The symphony of the ninth: the development and function of Th9 cells.* Curr Opin Immunol, 2012. **24**(3): p. 303-7.
299. Korn, T., et al., *IL-17 and Th17 Cells.* Annu Rev Immunol, 2009. **27**: p. 485-517.
300. Eyerich, S., et al., *Th22 cells represent a distinct human T cell subset involved in epidermal immunity and remodeling.* J Clin Invest, 2009. **119**(12): p. 3573-85.
301. Crotty, S., *Follicular helper CD4 T cells (TFH).* Annu Rev Immunol, 2011. **29**: p. 621-63.
302. O'Shea, J.J. and W.E. Paul, *Mechanisms underlying lineage commitment and plasticity of helper CD4+ T cells.* Science, 2010. **327**(5969): p. 1098-102.
303. Gershon, R.K., *A disquisition on suppressor T cells.* Transplant Rev, 1975. **26**: p. 170-85.
304. Sakaguchi, S., et al., *Immunologic self-tolerance maintained by activated T cells expressing IL-2 receptor alpha-chains (CD25). Breakdown of a single mechanism of self-tolerance causes various autoimmune diseases.* J Immunol, 1995. **155**(3): p. 1151-64.
305. Dhamne, C., et al., *Peripheral and thymic foxp3(+) regulatory T cells in search of origin, distinction, and function.* Front Immunol, 2013. **4**: p. 253.
306. Burocchi, A., M.P. Colombo, and S. Piconese, *Convergences and divergences of thymus- and peripherally derived regulatory T cells in cancer.* Front Immunol, 2013. **4**: p. 247.
307. Thornton, A.M. and E.M. Shevach, *CD4+CD25+ immunoregulatory T cells suppress polyclonal T cell activation in vitro by inhibiting interleukin 2 production.* J Exp Med, 1998. **188**(2): p. 287-96.

308. Schmidt, A., N. Oberle, and P.H. Krammer, *Molecular mechanisms of treg-mediated T cell suppression*. Front Immunol, 2012. **3**: p. 51.
309. Romano, M., et al., *Past, Present, and Future of Regulatory T Cell Therapy in Transplantation and Autoimmunity*. Front Immunol, 2019. **10**: p. 43.
310. Mittrucker, H.W., A. Visekruna, and M. Huber, *Heterogeneity in the differentiation and function of CD8(+) T cells*. Arch Immunol Ther Exp (Warsz), 2014. **62**(6): p. 449-58.
311. Zhang, N. and M.J. Bevan, *CD8(+) T cells: foot soldiers of the immune system*. Immunity, 2011. **35**(2): p. 161-8.
312. Kaech, S.M. and W. Cui, *Transcriptional control of effector and memory CD8+ T cell differentiation*. Nat Rev Immunol, 2012. **12**(11): p. 749-61.
313. Visekruna, A., et al., *Tc9 cells, a new subset of CD8(+) T cells, support Th2-mediated airway inflammation*. Eur J Immunol, 2013. **43**(3): p. 606-18.
314. Liang, Y., H.F. Pan, and D.Q. Ye, *Tc17 Cells in Immunity and Systemic Autoimmunity*. Int Rev Immunol, 2015. **34**(4): p. 318-31.
315. Elmore, S., *Apoptosis: a review of programmed cell death*. Toxicol Pathol, 2007. **35**(4): p. 495-516.
316. Kagi, D., et al., *Cytotoxicity mediated by T cells and natural killer cells is greatly impaired in perforin-deficient mice*. Nature, 1994. **369**(6475): p. 31-7.
317. Young, J.D., et al., *Purification and characterization of a cytolytic pore-forming protein from granules of cloned lymphocytes with natural killer activity*. Cell, 1986. **44**(6): p. 849-59.
318. Motyka, B., et al., *Mannose 6-phosphate/insulin-like growth factor II receptor is a death receptor for granzyme B during cytotoxic T cell-induced apoptosis*. Cell, 2000. **103**(3): p. 491-500.
319. Keefe, D., et al., *Perforin triggers a plasma membrane-repair response that facilitates CTL induction of apoptosis*. Immunity, 2005. **23**(3): p. 249-62.
320. Thiery, J., et al., *Perforin activates clathrin- and dynamin-dependent endocytosis, which is required for plasma membrane repair and delivery of granzyme B for granzyme-mediated apoptosis*. Blood, 2010. **115**(8): p. 1582-93.
321. Bird, C.H., et al., *Selective regulation of apoptosis: the cytotoxic lymphocyte serpin proteinase inhibitor 9 protects against granzyme B-mediated apoptosis without perturbing the Fas cell death pathway*. Mol Cell Biol, 1998. **18**(11): p. 6387-98.
322. Balaji, K.N., et al., *Surface cathepsin B protects cytotoxic lymphocytes from self-destruction after degranulation*. J Exp Med, 2002. **196**(4): p. 493-503.
323. Clayberger, C. and A.M. Krensky, *Granulysin*. Curr Opin Immunol, 2003. **15**(5): p. 560-5.
324. Lieberman, J. and Z. Fan, *Nuclear war: the granzyme A-bomb*. Curr Opin Immunol, 2003. **15**(5): p. 553-9.
325. Ricci, J.E., et al., *Disruption of mitochondrial function during apoptosis is mediated by caspase cleavage of the p75 subunit of complex I of the electron transport chain*. Cell, 2004. **117**(6): p. 773-86.
326. Martinvalet, D., et al., *Granzyme A cleaves a mitochondrial complex I protein to initiate caspase-independent cell death*. Cell, 2008. **133**(4): p. 681-92.
327. Heibein, J.A., et al., *Granzyme B-mediated cytochrome c release is regulated by the Bcl-2 family members bid and Bax*. J Exp Med, 2000. **192**(10): p. 1391-402.

328. Heibein, J.A., et al., *Granzyme B-induced loss of mitochondrial inner membrane potential ($\Delta\psi_m$) and cytochrome c release are caspase independent*. J Immunol, 1999. **163**(9): p. 4683-93.
329. Thomas, D.A., et al., *DFF45/ICAD can be directly processed by granzyme B during the induction of apoptosis*. Immunity, 2000. **12**(6): p. 621-32.
330. Goping, I.S., et al., *Granzyme B-induced apoptosis requires both direct caspase activation and relief of caspase inhibition*. Immunity, 2003. **18**(3): p. 355-65.
331. Kojima, Y., et al., *Localization of Fas ligand in cytoplasmic granules of CD8+ cytotoxic T lymphocytes and natural killer cells: participation of Fas ligand in granule exocytosis model of cytotoxicity*. Biochem Biophys Res Commun, 2002. **296**(2): p. 328-36.
332. Bossi, G. and G.M. Griffiths, *Degranulation plays an essential part in regulating cell surface expression of Fas ligand in T cells and natural killer cells*. Nat Med, 1999. **5**(1): p. 90-6.
333. Hao, Z. and T.W. Mak, *Type I and type II pathways of Fas-mediated apoptosis are differentially controlled by XIAP*. J Mol Cell Biol, 2010. **2**(2): p. 63-4.
334. Yamada, A., et al., *Dual Role of Fas/FasL-Mediated Signal in Peripheral Immune Tolerance*. Front Immunol, 2017. **8**: p. 403.
335. Chang, Y.H., et al., *A Chimeric Receptor with NKG2D Specificity Enhances Natural Killer Cell Activation and Killing of Tumor Cells*. Cancer Res, 2013.
336. Zhang, T., M.R. Wu, and C.L. Sentman, *An NKp30-based chimeric antigen receptor promotes T cell effector functions and antitumor efficacy in vivo*. J Immunol, 2012. **189**(5): p. 2290-9.
337. Gross, G., T. Waks, and Z. Eshhar, *Expression of immunoglobulin-T-cell receptor chimeric molecules as functional receptors with antibody-type specificity*. Proc Natl Acad Sci U S A, 1989. **86**(24): p. 10024-8.
338. Eshhar, Z., et al., *Specific activation and targeting of cytotoxic lymphocytes through chimeric single chains consisting of antibody-binding domains and the gamma or zeta subunits of the immunoglobulin and T-cell receptors*. Proc Natl Acad Sci U S A, 1993. **90**(2): p. 720-4.
339. Jensen, M., et al., *CD20 is a molecular target for scFvFc:zeta receptor redirected T cells: implications for cellular immunotherapy of CD20+ malignancy*. Biol Blood Marrow Transplant, 1998. **4**(2): p. 75-83.
340. Xu, D., et al., *The development of CAR design for tumor CAR-T cell therapy*. Oncotarget, 2018. **9**(17): p. 13991-14004.
341. Kolb, H.J., et al., *Graft-versus-leukemia reactions in allogeneic chimeras*. Blood, 2004. **103**(3): p. 767-76.
342. Maeda, T., et al., *Up-regulation of costimulatory/adhesion molecules by histone deacetylase inhibitors in acute myeloid leukemia cells*. Blood, 2000. **96**(12): p. 3847-56.
343. Pule, M.A., et al., *A chimeric T cell antigen receptor that augments cytokine release and supports clonal expansion of primary human T cells*. Mol Ther, 2005. **12**(5): p. 933-41.
344. Kowolik, C.M., et al., *CD28 costimulation provided through a CD19-specific chimeric antigen receptor enhances in vivo persistence and antitumor efficacy of adoptively transferred T cells*. Cancer Res, 2006. **66**(22): p. 10995-1004.
345. Vera, J., et al., *T lymphocytes redirected against the kappa light chain of human immunoglobulin efficiently kill mature B lymphocyte-derived malignant cells*. Blood, 2006. **108**(12): p. 3890-7.

346. Savoldo, B., et al., *CD28 costimulation improves expansion and persistence of chimeric antigen receptor-modified T cells in lymphoma patients*. J Clin Invest, 2011. **121**(5): p. 1822-6.
347. Song, D.G., et al., *In vivo persistence, tumor localization, and antitumor activity of CAR-engineered T cells is enhanced by costimulatory signaling through CD137 (4-1BB)*. Cancer Res, 2011. **71**(13): p. 4617-27.
348. Imai, C., et al., *Chimeric receptors with 4-1BB signaling capacity provoke potent cytotoxicity against acute lymphoblastic leukemia*. Leukemia, 2004. **18**(4): p. 676-84.
349. Kawalekar, O.U., et al., *Distinct Signaling of Coreceptors Regulates Specific Metabolism Pathways and Impacts Memory Development in CAR T Cells*. Immunity, 2016. **44**(2): p. 380-90.
350. Zhong, X.S., et al., *Chimeric antigen receptors combining 4-1BB and CD28 signaling domains augment PI3kinase/AKT/Bcl-XL activation and CD8+ T cell-mediated tumor eradication*. Mol Ther, 2010. **18**(2): p. 413-20.
351. Ramos, C.A., et al., *In Vivo Fate and Activity of Second- versus Third-Generation CD19-Specific CAR-T Cells in B Cell Non-Hodgkin's Lymphomas*. Mol Ther, 2018. **26**(12): p. 2727-2737.
352. Quintarelli, C., et al., *Choice of costimulatory domains and of cytokines determines CAR T-cell activity in neuroblastoma*. Oncoimmunology, 2018. **7**(6): p. e1433518.
353. Guedan, S., et al., *ICOS-based chimeric antigen receptors program bipolar TH17/TH1 cells*. Blood, 2014. **124**(7): p. 1070-80.
354. Guedan, S., et al., *Enhancing CAR T cell persistence through ICOS and 4-1BB costimulation*. JCI Insight, 2018. **3**(1).
355. Curran, K.J., et al., *Enhancing antitumor efficacy of chimeric antigen receptor T cells through constitutive CD40L expression*. Mol Ther, 2015. **23**(4): p. 769-78.
356. Collinson-Pautz, M.R., et al., *Constitutively active MyD88/CD40 costimulation enhances expansion and efficacy of chimeric antigen receptor T cells targeting hematological malignancies*. Leukemia, 2019.
357. Mata, M., et al., *Inducible Activation of MyD88 and CD40 in CAR T Cells Results in Controllable and Potent Antitumor Activity in Preclinical Solid Tumor Models*. Cancer Discov, 2017. **7**(11): p. 1306-1319.
358. Davenport, A.J., et al., *Chimeric antigen receptor T cells form nonclassical and potent immune synapses driving rapid cytotoxicity*. Proc Natl Acad Sci U S A, 2018. **115**(9): p. E2068-E2076.
359. Xiong, W., et al., *Immunological Synapse Predicts Effectiveness of Chimeric Antigen Receptor Cells*. Mol Ther, 2018. **26**(4): p. 963-975.
360. James, J.R. and R.D. Vale, *Biophysical mechanism of T-cell receptor triggering in a reconstituted system*. Nature, 2012. **487**: p. 64.
361. Karlsson, H., et al., *Evaluation of Intracellular Signaling Downstream Chimeric Antigen Receptors*. PLoS One, 2015. **10**(12): p. e0144787.
362. Milone, M.C., et al., *Chimeric receptors containing CD137 signal transduction domains mediate enhanced survival of T cells and increased antileukemic efficacy in vivo*. Mol Ther, 2009. **17**(8): p. 1453-64.
363. Casucci, M., et al., *Extracellular NGFR Spacers Allow Efficient Tracking and Enrichment of Fully Functional CAR-T Cells Co-Expressing a Suicide Gene*. Front Immunol, 2018. **9**: p. 507.

364. Moritz, D. and B. Groner, *A spacer region between the single chain antibody- and the CD3 zeta-chain domain of chimeric T cell receptor components is required for efficient ligand binding and signaling activity*. *Gene Ther*, 1995. **2**(8): p. 539-46.
365. Weijtens, M.E., et al., *A retroviral vector system 'STITCH' in combination with an optimized single chain antibody chimeric receptor gene structure allows efficient gene transduction and expression in human T lymphocytes*. *Gene Ther*, 1998. **5**(9): p. 1195-203.
366. Patel, S.D., et al., *Impact of chimeric immune receptor extracellular protein domains on T cell function*. *Gene Ther*, 1999. **6**(3): p. 412-9.
367. Guest, R.D., et al., *The role of extracellular spacer regions in the optimal design of chimeric immune receptors: evaluation of four different scFvs and antigens*. *J Immunother*, 2005. **28**(3): p. 203-11.
368. Hombach, A., A.A. Hombach, and H. Abken, *Adoptive immunotherapy with genetically engineered T cells: modification of the IgG1 Fc 'spacer' domain in the extracellular moiety of chimeric antigen receptors avoids 'off-target' activation and unintended initiation of an innate immune response*. *Gene Ther*, 2010. **17**(10): p. 1206-13.
369. Hudecek, M., et al., *The nonsignaling extracellular spacer domain of chimeric antigen receptors is decisive for in vivo antitumor activity*. *Cancer Immunol Res*, 2015. **3**(2): p. 125-35.
370. Jonnalagadda, M., et al., *Chimeric antigen receptors with mutated IgG4 Fc spacer avoid fc receptor binding and improve T cell persistence and antitumor efficacy*. *Mol Ther*, 2015. **23**(4): p. 757-68.
371. Watanabe, N., et al., *Fine-tuning the CAR spacer improves T-cell potency*. *Oncoimmunology*, 2016. **5**(12): p. e1253656.
372. Morgan, R.A., et al., *Case report of a serious adverse event following the administration of T cells transduced with a chimeric antigen receptor recognizing ERBB2*. *Mol Ther*, 2010. **18**(4): p. 843-51.
373. Hombach, A.A., et al., *T cell activation by antibody-like immunoreceptors: The position of the binding epitope within the target molecule determines the efficiency of activation of redirected T cells*. *Journal of Immunology*, 2007. **178**(7): p. 4650-4657.
374. Haso, W., et al., *Anti-CD22-chimeric antigen receptors targeting B-cell precursor acute lymphoblastic leukemia*. *Blood*, 2013. **121**(7): p. 1165-74.
375. James, S.E., et al., *Antigen sensitivity of CD22-specific chimeric TCR is modulated by target epitope distance from the cell membrane*. *J Immunol*, 2008. **180**(10): p. 7028-38.
376. Zhang, Z., et al., *Modified CAR T cells targeting membrane-proximal epitope of mesothelin enhances the antitumor function against large solid tumor*. *Cell Death & Disease*, 2019. **10**(7): p. 476.
377. Bluemel, C., et al., *Epitope distance to the target cell membrane and antigen size determine the potency of T cell-mediated lysis by BiTE antibodies specific for a large melanoma surface antigen*. *Cancer Immunology Immunotherapy*, 2010. **59**(8): p. 1197-1209.
378. Bang, S., et al., *HA22 (R490A) is a recombinant immunotoxin with increased antitumor activity without an increase in animal toxicity*. *Clin Cancer Res*, 2005. **11**(4): p. 1545-50.

379. Chmielewski, M., et al., *T cell activation by antibody-like immunoreceptors: increase in affinity of the single-chain fragment domain above threshold does not increase T cell activation against antigen-positive target cells but decreases selectivity.* J Immunol, 2004. **173**(12): p. 7647-53.
380. Turatti, F., et al., *Redirected activity of human antitumor chimeric immune receptors is governed by antigen and receptor expression levels and affinity of interaction.* J Immunother, 2007. **30**(7): p. 684-93.
381. Chames, P., et al., *TCR-like human antibodies expressed on human CTLs mediate antibody affinity-dependent cytolytic activity.* J Immunol, 2002. **169**(2): p. 1110-8.
382. Davenport, A.J. and M.R. Jenkins, *Programming a serial killer: CAR T cells form non-classical immune synapses.* Oncoscience, 2018. **5**(3-4): p. 69-70.
383. Davenport, A.J., et al., *CAR-T Cells Inflict Sequential Killing of Multiple Tumor Target Cells.* Cancer Immunol Res, 2015. **3**(5): p. 483-94.
384. Arcangeli, S., et al., *Balance of Anti-CD123 Chimeric Antigen Receptor Binding Affinity and Density for the Targeting of Acute Myeloid Leukemia.* Mol Ther, 2017. **25**(8): p. 1933-1945.
385. Kokalaki, E., *Affinity Gradient of Chimeric Antigen Receptor T-Cells Against Low-Antigen Density Target, in UCL Cancer Institute, Haematology Department.* 2017, UCL.
386. Hudecek, M., et al., *Receptor affinity and extracellular domain modifications affect tumor recognition by ROR1-specific chimeric antigen receptor T cells.* Clin Cancer Res, 2013. **19**(12): p. 3153-64.
387. Baskar, S., et al., *Targeting malignant B cells with an immunotoxin against ROR1.* MAbs, 2012. **4**(3): p. 349-61.
388. Watanabe, K., et al., *Excessively High-Affinity Single-Chain Fragment Variable Region in a Chimeric Antigen Receptor Can Counteract T-Cell Proliferation.* Blood, 2014. **124**(21): p. 4799-4799.
389. Drent, E., et al., *A Rational Strategy for Reducing On-Target Off-Tumor Effects of CD38-Chimeric Antigen Receptors by Affinity Optimization.* Mol Ther, 2017. **25**(8): p. 1946-1958.
390. Majzner, R.G. and C.L. Mackall, *Tumor Antigen Escape from CAR T-cell Therapy.* Cancer Discov, 2018. **8**(10): p. 1219-1226.
391. Shah, N.N., et al., *Multi Targeted CAR-T Cell Therapies for B-Cell Malignancies.* Front Oncol, 2019. **9**: p. 146.
392. Evans, A.G., et al., *Evolution to plasmablastic lymphoma evades CD19-directed chimeric antigen receptor T cells.* Br J Haematol, 2015. **171**(2): p. 205-209.
393. Schneider, D., et al., *A tandem CD19/CD20 CAR lentiviral vector drives on-target and off-target antigen modulation in leukemia cell lines.* J Immunother Cancer, 2017. **5**: p. 42.
394. Zah, E., et al., *T Cells Expressing CD19/CD20 Bispecific Chimeric Antigen Receptors Prevent Antigen Escape by Malignant B Cells.* Cancer Immunol Res, 2016. **4**(6): p. 498-508.
395. Shah, N., et al., *A Phase 1 Study with Point-of-Care Manufacturing of Dual Targeted, Tandem Anti-CD19, Anti-CD20 Chimeric Antigen Receptor Modified T (CAR-T) Cells for Relapsed, Refractory, Non-Hodgkin Lymphoma.* Blood, 2018. **132**: p. 4193-4193.
396. Qin, H., et al., *Preclinical Development of Bivalent Chimeric Antigen Receptors Targeting Both CD19 and CD22.* Mol Ther Oncolytics, 2018. **11**: p. 127-137.

397. ClinicalTrials.gov. *A Feasibility and Safety Study of Dual Specificity CD19 and CD22 CAR-T Cell Immunotherapy for CD19+CD22+ Leukemia* <https://clinicaltrials.gov/ct2/show/NCT03330691> 2019 [cited 2019].
398. Yang, J., et al., *A Feasibility and Safety Study of CD19 and CD22 Chimeric Antigen Receptors-Modified T Cell Cocktail for Therapy of B Cell Acute Lymphoblastic Leukemia*. *Blood*, 2018. **132**(Supplement 1): p. 277-277.
399. Fousek, K., et al., *Targeting CD19-negative relapsed B-acute lymphoblastic leukemia using trivalent CAR T cells*. *Journal of Clinical Oncology*, 2018. **36**(5_suppl): p. 121-121.
400. Hegde, M., et al., *Combinational targeting offsets antigen escape and enhances effector functions of adoptively transferred T cells in glioblastoma*. *Mol Ther*, 2013. **21**(11): p. 2087-101.
401. Bielamowicz, K., et al., *Trivalent CAR T cells overcome interpatient antigenic variability in glioblastoma*. *Neuro-Oncology*, 2017. **20**(4): p. 506-518.
402. Kerkar, S.P., et al., *Tumor-specific CD8+ T cells expressing interleukin-12 eradicate established cancers in lymphodepleted hosts*. *Cancer Res*, 2010. **70**(17): p. 6725-34.
403. Adachi, K., et al., *IL-7 and CCL19 expression in CAR-T cells improves immune cell infiltration and CAR-T cell survival in the tumor*. *Nature Biotechnology*, 2018. **36**: p. 346.
404. Perna, S.K., et al., *Interleukin-7 mediates selective expansion of tumor-redirected cytotoxic T lymphocytes (CTLs) without enhancement of regulatory T-cell inhibition*. *Clin Cancer Res*, 2014. **20**(1): p. 131-9.
405. Craddock, J.A., et al., *Enhanced tumor trafficking of GD2 chimeric antigen receptor T cells by expression of the chemokine receptor CCR2b*. *J Immunother*, 2010. **33**(8): p. 780-8.
406. Moon, E.K., et al., *Expression of a functional CCR2 receptor enhances tumor localization and tumor eradication by retargeted human T cells expressing a mesothelin-specific chimeric antibody receptor*. *Clin Cancer Res*, 2011. **17**(14): p. 4719-30.
407. Yoon, D.H., et al., *Incorporation of Immune Checkpoint Blockade into Chimeric Antigen Receptor T Cells (CAR-Ts): Combination or Built-In CAR-T*. *Int J Mol Sci*, 2018. **19**(2).
408. John, L.B., et al., *Anti-PD-1 antibody therapy potently enhances the eradication of established tumors by gene-modified T cells*. *Clin Cancer Res*, 2013. **19**(20): p. 5636-46.
409. ClinicalTrials.gov. *CD19 Chimeric Receptor Expressing T Lymphocytes In B-Cell Non Hodgkin's Lymphoma, ALL & CLL (CRETI-NH)* <https://clinicaltrials.gov/ct2/show/NCT00586391>. 2019 [cited 2019].
410. ClinicalTrials.gov. *Phase I/II Study of Pembrolizumab in Patients Failing to Respond to or Relapsing After Anti-CD19 Chimeric Antigen Receptor Modified T Cell Therapy for Relapsed or Refractory CD19+ Lymphomas* <https://clinicaltrials.gov/ct2/show/NCT02650999>. 2019 [cited 2019].
411. ClinicalTrials.gov. *Safety and Efficacy of KTE-C19 in Combination With Atezolizumab in Adults With Refractory Diffuse Large B-Cell Lymphoma (DLBCL) (ZUMA-6)* <https://clinicaltrials.gov/ct2/show/NCT02926833>. 2019 [cited 2019].
412. Rafiq, S., et al., *Targeted delivery of a PD-1-blocking scFv by CAR-T cells enhances anti-tumor efficacy in vivo*. *Nature Biotechnology*, 2018. **36**: p. 847.

413. Liu, X., et al., *A Chimeric Switch-Receptor Targeting PD1 Augments the Efficacy of Second-Generation CAR T Cells in Advanced Solid Tumors*. *Cancer Res*, 2016. **76**(6): p. 1578-90.
414. Bajgain, P., et al., *CAR T cell therapy for breast cancer: harnessing the tumor milieu to drive T cell activation*. *J Immunother Cancer*, 2018. **6**(1): p. 34.
415. Ren, J., et al., *Multiplex Genome Editing to Generate Universal CAR T Cells Resistant to PD1 Inhibition*. *Clin Cancer Res*, 2017. **23**(9): p. 2255-2266.
416. ClinicalTrials.gov. *CD19 CAR and PD-1 Knockout Engineered T Cells for CD19 Positive Malignant B-cell Derived Leukemia and Lymphoma* <https://clinicaltrials.gov/ct2/show/NCT03298828> 2017 [cited 2019].
417. Benmebarek, M.R., et al., *Killing Mechanisms of Chimeric Antigen Receptor (CAR) T Cells*. *Int J Mol Sci*, 2019. **20**(6).
418. Kalos, M., et al., *T Cells with Chimeric Antigen Receptors Have Potent Antitumor Effects and Can Establish Memory in Patients with Advanced Leukemia*. *Science Translational Medicine*, 2011. **3**(95): p. 95ra73-95ra73.
419. Inoo, K., et al., *Immunological quality and performance of tumor vessel-targeting CAR-T cells prepared by mRNA-EP for clinical research*. *Mol Ther Oncolytics*, 2016. **3**: p. 16024.
420. McLellan, A.D. and S.M. Ali Hosseini Rad, *Chimeric antigen receptor T cell persistence and memory cell formation*. *Immunol Cell Biol*, 2019. **97**(7): p. 664-674.
421. Tay, R.E., E.K. Richardson, and H.C. Toh, *Revisiting the role of CD4+ T cells in cancer immunotherapy—new insights into old paradigms*. *Cancer Gene Therapy*, 2020.
422. Wang, D., et al., *Glioblastoma-targeted CD4+ CAR T cells mediate superior antitumor activity*. *JCI Insight*, 2018. **3**(10).
423. Gacerez, A.T. and C.L. Sentman, *T-bet promotes potent antitumor activity of CD4+ CAR T cells*. *Cancer Gene Therapy*, 2018. **25**(5): p. 117-128.
424. Quezada, S.A., et al., *Tumor-reactive CD4(+) T cells develop cytotoxic activity and eradicate large established melanoma after transfer into lymphopenic hosts*. *J Exp Med*, 2010. **207**(3): p. 637-50.
425. Sledzinska, A., et al., *Regulatory T Cells Restrain Interleukin-2- and Blimp-1-Dependent Acquisition of Cytotoxic Function by CD4(+) T Cells*. *Immunity*, 2020. **52**(1): p. 151-166 e6.
426. Yang, Y., et al., *CD4 CAR T Cells Mediate CD8-like Cytotoxic Anti-Leukemic Effects Resulting in Leukemic Clearance and Are Less Susceptible to Attenuation By Endogenous TCR Activation Than CD8 CAR T Cells*. *Blood*, 2015. **126**(23): p. 100-100.
427. Moeller, M., et al., *Adoptive transfer of gene-engineered CD4+ helper T cells induces potent primary and secondary tumor rejection*. *Blood*, 2005. **106**(9): p. 2995-3003.
428. Sommermeyer, D., et al., *Chimeric antigen receptor-modified T cells derived from defined CD8+ and CD4+ subsets confer superior antitumor reactivity in vivo*. *Leukemia*, 2016. **30**(2): p. 492-500.
429. Turtle, C.J., et al., *CD19 CAR-T cells of defined CD4+:CD8+ composition in adult B cell ALL patients*. *The Journal of Clinical Investigation*, 2016. **126**(6): p. 2123-2138.
430. Cohen, A.D., et al., *B cell maturation antigen-specific CAR T cells are clinically active in multiple myeloma*. *J Clin Invest*, 2019. **129**(6): p. 2210-2221.

431. Ponce, R., *Adverse consequences of immunostimulation*. J Immunotoxicol, 2008. **5**(1): p. 33-41.
432. Casucci, M., et al., *Co-Expression of a Suicide Gene in CAR-Redirected T Cells Enables the Safe Targeting of CD44v6 for Leukemia and Myeloma Eradication*. Blood, 2012. **120**(21): p. 949-949.
433. Bonini, C., et al., *HSV-TK gene transfer into donor lymphocytes for control of allogeneic graft-versus-leukemia*. Science, 1997. **276**(5319): p. 1719-24.
434. Di Stasi, A., et al., *Inducible apoptosis as a safety switch for adoptive cell therapy*. N Engl J Med, 2011. **365**(18): p. 1673-83.
435. Thomis, D.C., et al., *A Fas-based suicide switch in human T cells for the treatment of graft-versus-host disease*. Blood, 2001. **97**(5): p. 1249-57.
436. Stavrou, M., et al., *A Rapamycin-Activated Caspase 9-Based Suicide Gene*. Mol Ther, 2018. **26**(5): p. 1266-1276.
437. Wang, X., et al., *A transgene-encoded cell surface polypeptide for selection, in vivo tracking, and ablation of engineered cells*. Blood, 2011. **118**(5): p. 1255-63.
438. Griffioen, M., et al., *Retroviral transfer of human CD20 as a suicide gene for adoptive T-cell therapy*. Haematologica, 2009. **94**(9): p. 1316-20.
439. Philip, B., et al., *A highly compact epitope-based marker/suicide gene for easier and safer T-cell therapy*. Blood, 2014. **124**(8): p. 1277-87.
440. Kloss, C.C., et al., *Combinatorial antigen recognition with balanced signaling promotes selective tumor eradication by engineered T cells*. Nat Biotechnol, 2013. **31**(1): p. 71-5.
441. Roybal, K.T., et al., *Precision Tumor Recognition by T Cells With Combinatorial Antigen-Sensing Circuits*. Cell, 2016. **164**(4): p. 770-9.
442. Roybal, K.T., et al., *Engineering T Cells with Customized Therapeutic Response Programs Using Synthetic Notch Receptors*. Cell, 2016. **167**(2): p. 419-432 e16.
443. Fedorov, V.D., M. Themeli, and M. Sadelain, *PD-1- and CTLA-4-Based Inhibitory Chimeric Antigen Receptors (iCARs) Divert Off-Target Immunotherapy Responses*. Sci Transl Med, 2013. **5**(215): p. 215ra172.
444. Torikai, H., et al., *A foundation for universal T-cell based immunotherapy: T cells engineered to express a CD19-specific chimeric-antigen-receptor and eliminate expression of endogenous TCR*. Blood, 2012. **119**(24): p. 5697-705.
445. Joung, J.K. and J.D. Sander, *TALENs: a widely applicable technology for targeted genome editing*. Nat Rev Mol Cell Biol, 2013. **14**(1): p. 49-55.
446. Qasim, W., et al., *Molecular remission of infant B-ALL after infusion of universal TALEN gene-edited CAR T cells*. Sci Transl Med, 2017. **9**(374).
447. Ran, F.A., et al., *Genome engineering using the CRISPR-Cas9 system*. Nature Protocols, 2013. **8**: p. 2281.
448. Clarke, R.L., et al., *Abstract LB-108: Generation of off-the-shelf TCR-less CAR-targeted cytotoxic T cells from renewable pluripotent cells for cancer immunotherapy*. Cancer Research, 2018. **78**(13 Supplement): p. LB-108-LB-108.
449. Tamada, K., et al., *Redirecting gene-modified T cells toward various cancer types using tagged antibodies*. Clin Cancer Res, 2012. **18**(23): p. 6436-45.
450. Kim, M.S., et al., *Redirection of genetically engineered CAR-T cells using bifunctional small molecules*. J Am Chem Soc, 2015. **137**(8): p. 2832-5.

451. Urbanska, K., et al., *A Universal Strategy for Adoptive Immunotherapy of Cancer through Use of a Novel T-cell Antigen Receptor*. *Cancer Research*, 2012. **72**(7): p. 1844-1852.
452. Lohmueller, J.J., et al., *mSA2 affinity-enhanced biotin-binding CAR T cells for universal tumor targeting*. *Oncoimmunology*, 2017. **7**(1): p. e1368604.
453. Kalos, M., et al., *T cells with chimeric antigen receptors have potent antitumor effects and can establish memory in patients with advanced leukemia*. *Sci Transl Med*, 2011. **3**(95): p. 95ra73.
454. <https://www.fda.gov/biologicsbloodvaccines/cellulargenetherapyproducts/approvedproducts/ucm573706.htm>, U.F.a.D.A. KYMRIA[®] (*tisagenlecleucel*) 2017 [cited 2019].
455. <https://www.fda.gov/BiologicsBloodVaccines/CellularGeneTherapyProducts/ApprovedProducts/ucm581222.htm>, U.F.a.D.A. YESCARTA (*axicabtagene ciloleucel*). 2017 [cited 2019].
456. Salmikangas, P., N. Kinsella, and P. Chamberlain, *Chimeric Antigen Receptor T-Cells (CAR T-Cells) for Cancer Immunotherapy - Moving Target for Industry?* *Pharm Res*, 2018. **35**(8): p. 152.
457. Yu, W.L. and Z.C. Hua, *Chimeric Antigen Receptor T-cell (CAR T) Therapy for Hematologic and Solid Malignancies: Efficacy and Safety-A Systematic Review with Meta-Analysis*. *Cancers (Basel)*, 2019. **11**(1).
458. Fry, T.J., et al., *CD22-targeted CAR T cells induce remission in B-ALL that is naive or resistant to CD19-targeted CAR immunotherapy*. *Nat Med*, 2018. **24**(1): p. 20-28.
459. Ramos, C.A., et al., *Clinical and immunological responses after CD30-specific chimeric antigen receptor-redirected lymphocytes*. *J Clin Invest*, 2017. **127**(9): p. 3462-3471.
460. Wang, Y., et al., *Effective response and delayed toxicities of refractory advanced diffuse large B-cell lymphoma treated by CD20-directed chimeric antigen receptor-modified T cells*. *Clin Immunol*, 2014. **155**(2): p. 160-75.
461. ClinicalTrials.gov. *Dose Escalation Study of UCART19 in Adult Patients With Relapsed / Refractory B-cell Acute Lymphoblastic Leukaemia (CALM)* <https://clinicaltrials.gov/ct2/show/NCT02746952>. 2019 [cited 2019].
462. ClinicalTrials.gov. *A Study to Evaluate the Long-term Safety of Patients With Advanced Lymphoid Malignancies Who Have Been Previously Administered With UCART19/ALLO-501* <https://clinicaltrials.gov/ct2/show/NCT02735083>. 2019 [cited 2019].
463. Martinez, M. and E.K. Moon, *CAR T Cells for Solid Tumors: New Strategies for Finding, Infiltrating, and Surviving in the Tumor Microenvironment*. *Front Immunol*, 2019. **10**: p. 128.
464. Cleary, K.L.S., et al., *Antibody Distance from the Cell Membrane Regulates Antibody Effector Mechanisms*. *The Journal of Immunology*, 2017. **198**(10): p. 3999-4011.
465. Till, B.G., et al., *CD20-specific adoptive immunotherapy for lymphoma using a chimeric antigen receptor with both CD28 and 4-1BB domains: pilot clinical trial results*. *Blood*, 2012. **119**(17): p. 3940-50.

466. Wang, J., et al., *Optimizing adoptive polyclonal T cell immunotherapy of lymphomas, using a chimeric T cell receptor possessing CD28 and CD137 costimulatory domains*. Hum Gene Ther, 2007. **18**(8): p. 712-25.
467. Lim, S.H., et al., *Fc gamma receptor IIb on target B cells promotes rituximab internalization and reduces clinical efficacy*. Blood, 2011: p. blood-2011-01-330357.
468. Nguyen, P., I. Moisini, and T.L. Geiger, *Identification of a murine CD28 dileucine motif that suppresses single-chain chimeric T-cell receptor expression and function*. Blood, 2003. **102**(13): p. 4320-4325.
469. Database, E.B.I.C. <https://www.ebi.ac.uk/chembl/compound/inspect/CHEMBL1201576>. 2019.
470. Database, E.B.I.C. <https://www.ebi.ac.uk/chembl/compound/inspect/CHEMBL1743048>. 2019.
471. Houck, S.A., S. Singh, and D.M. Cyr, *Cellular responses to misfolded proteins and protein aggregates*. Methods Mol Biol, 2012. **832**: p. 455-61.
472. Banfield, D.K., *Mechanisms of protein retention in the Golgi*. Cold Spring Harb Perspect Biol, 2011. **3**(8): p. a005264.
473. Proteins, T.E.L.M.r.f.F.S.i. <http://elm.eu.org/search.html>. 2019.
474. Hombach, A., A.A. Hombach, and H. Abken, *Adoptive immunotherapy with genetically engineered T cells: modification of the IgG1 Fc 'spacer' domain in the extracellular moiety of chimeric antigen receptors avoids 'off-target' activation and unintended initiation of an innate immune response*. Gene Therapy, 2010. **17**: p. 1206.
475. Sun, S., et al., *Immunotherapy with CAR-Modified T Cells: Toxicities and Overcoming Strategies*. J Immunol Res, 2018. **2018**: p. 2386187.
476. Boyman, O. and J. Sprent, *The role of interleukin-2 during homeostasis and activation of the immune system*. Nat Rev Immunol, 2012. **12**(3): p. 180-90.
477. Ross, S.H. and D.A. Cantrell, *Signaling and Function of Interleukin-2 in T Lymphocytes*. Annu Rev Immunol, 2018. **36**: p. 411-433.
478. Sanderson, S. and N. Shastri, *LacZ inducible, antigen/MHC-specific T cell hybrids*. Int Immunol, 1994. **6**(3): p. 369-76.
479. Chen, T.T., et al., *TIM-2 is expressed on B cells and in liver and kidney and is a receptor for H-ferritin endocytosis*. J Exp Med, 2005. **202**(7): p. 955-65.
480. Pear, W.S., et al., *Efficient and rapid induction of a chronic myelogenous leukemia-like myeloproliferative disease in mice receiving P210 bcr/abl-transduced bone marrow*. Blood, 1998. **92**(10): p. 3780-92.
481. Perosa, F., et al., *Generation of biologically active linear and cyclic peptides has revealed a unique fine specificity of rituximab and its possible cross-reactivity with acid sphingomyelinase-like phosphodiesterase 3b precursor*. Blood, 2006. **107**(3): p. 1070-1077.
482. Gillis, S. and K.A. Smith, *Long term culture of tumour-specific cytotoxic T cells*. Nature, 1977. **268**(5616): p. 154-6.
483. Kametaka, M., et al., *Reduction of CTLL-2 cytotoxicity by induction of apoptosis with a Fas-estrogen receptor chimera*. Cancer Sci, 2003. **94**(7): p. 639-43.
484. Durward, M., J. Harms, and G. Splitter, *Antigen specific killing assay using CFSE labeled target cells*. J Vis Exp, 2010(45).
485. Collection, A.T.C., *RPMI 8226 (ATCC® CCL-155™)*. https://www.lgcstandards-atcc.org/products/all/CCL-155.aspx?geo_country=gb#characteristics, 2019.

486. Baker, P.E., S. Gillis, and K.A. Smith, *Monoclonal cytolytic T-cell lines*. J Exp Med, 1979. **149**(1): p. 273-8.
487. Liao, W., J.X. Lin, and W.J. Leonard, *Interleukin-2 at the crossroads of effector responses, tolerance, and immunotherapy*. Immunity, 2013. **38**(1): p. 13-25.
488. DeRenzo, C. and S. Gottschalk, *Genetic Modification Strategies to Enhance CAR T Cell Persistence for Patients With Solid Tumors*. Front Immunol, 2019. **10**: p. 218.
489. Moon, B.I., T.H. Kim, and J.Y. Seoh, *Functional Modulation of Regulatory T Cells by IL-2*. PLoS One, 2015. **10**(11): p. e0141864.
490. Xu, X.J., et al., *Multiparameter comparative analysis reveals differential impacts of various cytokines on CART cell phenotype and function ex vivo and in vivo*. Oncotarget, 2016. **7**(50): p. 82354-82368.
491. Suryadevara, C.M., et al., *Preventing Lck Activation in CAR T Cells Confers Treg Resistance but Requires 4-1BB Signaling for Them to Persist and Treat Solid Tumors in Nonlymphodepleted Hosts*. Clin Cancer Res, 2019. **25**(1): p. 358-368.
492. Gomes-Silva, D., et al., *Tonic 4-1BB Costimulation in Chimeric Antigen Receptors Impedes T Cell Survival and Is Vector-Dependent*. Cell Rep, 2017. **21**(1): p. 17-26.
493. Bridgeman, J.S., et al., *The optimal antigen response of chimeric antigen receptors harboring the CD3zeta transmembrane domain is dependent upon incorporation of the receptor into the endogenous TCR/CD3 complex*. J Immunol, 2010. **184**(12): p. 6938-49.
494. Springer, T.A., *Adhesion receptors of the immune system*. Nature, 1990. **346**(6283): p. 425-434.
495. Yihong Yao, X.Y., Shigui Zhu, Wei Zhu, Zhiyuan Li, Qingxia Wang, Lin Zhu, Anyun Ma, Yanfeng Li, Yutian Wei, Chengxiang Dai, Li Zhang, Jiaqi Huang, Bizuo Liu *Target cell killing effects of CD20 targeting chimeric antigen receptor T cells derived from the type II anti-CD20 antibody*. Journal of Clinical Oncology 2017. **35**(no. 15_suppl).
496. Pleiner, T., M. Bates, and D. Gorlich, *A toolbox of anti-mouse and anti-rabbit IgG secondary nanobodies*. J Cell Biol, 2018. **217**(3): p. 1143-1154.
497. Choudhuri, K., et al., *T-cell receptor triggering is critically dependent on the dimensions of its peptide-MHC ligand*. Nature, 2005. **436**(7050): p. 578-582.
498. Gacerez, A.T., B. Arellano, and C.L. Sentman, *How Chimeric Antigen Receptor Design Affects Adoptive T Cell Therapy*. J Cell Physiol, 2016. **231**(12): p. 2590-8.
499. Shan, D., et al., *Characterization of scFv-Ig constructs generated from the anti-CD20 mAb 1F5 using linker peptides of varying lengths*. J Immunol, 1999. **162**(11): p. 6589-95.
500. Binder, M., et al., *The epitope recognized by rituximab*. Blood, 2006. **108**(6): p. 1975-8.
501. Nowacki, T.M., et al., *Granzyme B production distinguishes recently activated CD8(+) memory cells from resting memory cells*. Cell Immunol, 2007. **247**(1): p. 36-48.
502. Shafer-Weaver, K.A., et al., *Evaluating the cytotoxicity of innate immune effector cells using the GrB ELISPOT assay*. J Transl Med, 2004. **2**(1): p. 31.
503. Wherry, E.J. and M. Kurachi, *Molecular and cellular insights into T cell exhaustion*. Nat Rev Immunol, 2015. **15**(8): p. 486-99.

504. Bhat, P., et al., *Interferon- γ derived from cytotoxic lymphocytes directly enhances their motility and cytotoxicity*. *Cell Death & Disease*, 2017. **8**: p. e2836.
505. Hughes, P., et al., *The costs of using unauthenticated, over-passaged cell lines: how much more data do we need?* *Biotechniques*, 2007. **43**(5): p. 575, 577-8, 581-2 passim.
506. Wang, L.C., et al., *Targeting fibroblast activation protein in tumor stroma with chimeric antigen receptor T cells can inhibit tumor growth and augment host immunity without severe toxicity*. *Cancer Immunol Res*, 2014. **2**(2): p. 154-66.
507. Bettini, M.L., M. Bettini, and D.A. Vignali, *T-cell receptor retrogenic mice: a rapid, flexible alternative to T-cell receptor transgenic mice*. *Immunology*, 2012. **136**(3): p. 265-72.
508. Collection, A.T.C., *NIH/3T3 (ATCC® CRL-1658™)*. https://www.lgcstandards-atcc.org/products/all/CRL-1658.aspx?geo_country=gb, 2019.
509. Lee, L., et al., *An APRIL-based chimeric antigen receptor for dual targeting of BCMA and TACI in multiple myeloma*. *Blood*, 2018. **131**(7): p. 746-758.
510. Lamers, C., et al., *Lamers CH, Willemsen RA, Luider BA, Debets R, Bolhuis RL Protocol for gene transduction and expansion of human T lymphocytes for clinical immunogene therapy of cancer*. *Cancer Gene Ther* 9: 613-623. Vol. 9. 2002. 613-23.
511. Mamonkin, M., et al., *Tonic 4-1BB signaling from chimeric antigen receptors (CARs) impairs expansion of T cells due to Fas-mediated apoptosis*. *The Journal of Immunology*, 2016. **196**(1 Supplement): p. 143.7-143.7.
512. Tschumi, B.O., et al., *CART cells are prone to Fas- and DR5-mediated cell death*. *J Immunother Cancer*, 2018. **6**(1): p. 71.
513. Zhou, Z., et al., *Codon usage is an important determinant of gene expression levels largely through its effects on transcription*. *Proc Natl Acad Sci U S A*, 2016. **113**(41): p. E6117-E6125.
514. Mauro, V.P. and S.A. Chappell, *A critical analysis of codon optimization in human therapeutics*. *Trends Mol Med*, 2014. **20**(11): p. 604-13.
515. Cooray, S., S.J. Howe, and A.J. Thrasher, *Retrovirus and lentivirus vector design and methods of cell conditioning*. *Methods Enzymol*, 2012. **507**: p. 29-57.
516. Laboratory, T.J., <https://www.jax.org/strain/002847>. The Jackson Laboratory MOUSE STRAIN DATASHEET - 002847, 2019.
517. River, C., <https://www.criver.com/products-services/research-models-services/animal-models/immunodeficient-mice-rats/scid-mice?region=3671>. Charles River Laboratory Website, 2019.
518. Collection, A.T.C., *Daudi (ATCC® CCL-213™)*. <https://www.atcc.org/products/all/CCL-213.aspx>, 2019.
519. Resource, T.U.P., <https://www.uniprot.org/>. UniProt, 2019.
520. Nguyen, P., I. Moisini, and T.L. Geiger, *Identification of a murine CD28 dileucine motif that suppresses single-chain chimeric T-cell receptor expression and function*. *Blood*, 2003. **102**(13): p. 4320-5.
521. Yu, K., et al., *Immunotherapy of lymphomas with T cells modified by anti-CD20 scFv/CD28/CD3zeta recombinant gene*. *Leuk Lymphoma*, 2008. **49**(7): p. 1368-73.
522. Doan, A. and M.A. Pulsipher, *Hypogammaglobulinemia due to CAR T-cell therapy*. *Pediatr Blood Cancer*, 2018. **65**(4).

523. Roberts, D.M., et al., *Rituximab-associated hypogammaglobulinemia: incidence, predictors and outcomes in patients with multi-system autoimmune disease*. *J Autoimmun*, 2015. **57**: p. 60-5.
524. ClinicalTrials.gov. *The Clinical Research of Anti-CD20 CAR-T Cells in Patients With Refractory or Relapsed B Lymphocyte Lymphoma* <https://clinicaltrials.gov/ct2/show/NCT03576807>. 2018 [cited 2019].
525. ClinicalTrials.gov. *Modified Immune Cells (CD19/CD20 CAR-T Cells) in Treating Patients With Recurrent or Refractory B-Cell Lymphoma or Chronic Lymphocytic Leukemia* <https://clinicaltrials.gov/ct2/show/NCT04007029>. 2019 [cited 2019].
526. Rezvani, A.R. and D.G. Maloney, *Rituximab resistance*. *Best Pract Res Clin Haematol*, 2011. **24**(2): p. 203-16.
527. Fousek, K., et al., *Targeting Primary Pre-B Cell Acute Lymphoblastic Leukemia and CD19-Negative Relapses Using Trivalent CAR T Cells*. *Blood*, 2017. **130**(Suppl 1): p. 4614-4614.
528. Shah, N.N., et al., *A Phase 1 Study with Point-of-Care Manufacturing of Dual Targeted, Tandem Anti-CD19, Anti-CD20 Chimeric Antigen Receptor Modified T (CAR-T) Cells for Relapsed, Refractory, Non-Hodgkin Lymphoma*. *Blood*, 2018. **132**(Suppl 1): p. 4193-4193.
529. Lee, S.Y., et al., *Preclinical Optimization of a CD20-specific Chimeric Antigen Receptor Vector and Culture Conditions*. *J Immunother*, 2018. **41**(1): p. 19-31.
530. Ross, S.H., et al., *Phosphoproteomic Analyses of Interleukin 2 Signaling Reveal Integrated JAK Kinase-Dependent and -Independent Networks in CD8(+) T Cells*. *Immunity*, 2016. **45**(3): p. 685-700.
531. Janas, M.L., et al., *IL-2 regulates perforin and granzyme gene expression in CD8+ T cells independently of its effects on survival and proliferation*. *J Immunol*, 2005. **175**(12): p. 8003-10.
532. Kovanen, P.E., et al., *Global analysis of IL-2 target genes: identification of chromosomal clusters of expressed genes*. *International Immunology*, 2005. **17**(8): p. 1009-1021.
533. Glimcher, L.H., et al., *Recent developments in the transcriptional regulation of cytolytic effector cells*. *Nat Rev Immunol*, 2004. **4**(11): p. 900-11.
534. Bhat, P., et al., *Interferon-gamma derived from cytotoxic lymphocytes directly enhances their motility and cytotoxicity*. *Cell Death Dis*, 2017. **8**(6): p. e2836.
535. Mullbacher, A., et al., *Antigen-dependent release of IFN-gamma by cytotoxic T cells up-regulates Fas on target cells and facilitates exocytosis-independent specific target cell lysis*. *J Immunol*, 2002. **169**(1): p. 145-50.
536. Horton, H., et al., *Correlation between Interferon- γ Secretion and Cytotoxicity, in Virus-Specific Memory T Cells*. *The Journal of Infectious Diseases*, 2004. **190**(9): p. 1692-1696.
537. Quah, B.J. and C.R. Parish, *The use of carboxyfluorescein diacetate succinimidyl ester (CFSE) to monitor lymphocyte proliferation*. *J Vis Exp*, 2010(44).
538. Soares, A., et al., *Novel application of Ki67 to quantify antigen-specific in vitro lymphoproliferation*. *J Immunol Methods*, 2010. **362**(1-2): p. 43-50.
539. Graf, B., T. Bushnell, and J. Miller, *LFA-1-mediated T cell costimulation through increased localization of TCR/class II complexes to the central supramolecular activation cluster and exclusion of CD45 from the immunological synapse*. *J Immunol*, 2007. **179**(3): p. 1616-24.

540. Leupin, O., et al., *Exclusion of CD45 from the T-cell receptor signaling area in antigen-stimulated T lymphocytes*. *Curr Biol*, 2000. **10**(5): p. 277-80.
541. Kabanova, A., V. Zurli, and C.T. Baldari, *Signals Controlling Lytic Granule Polarization at the Cytotoxic Immune Synapse*. *Front Immunol*, 2018. **9**: p. 307.
542. Le Gall, F., et al., *Effect of linker sequences between the antibody variable domains on the formation, stability and biological activity of a bispecific tandem diabody*. *Protein Engineering, Design and Selection*, 2004. **17**(4): p. 357-366.
543. Du, J., et al., *Structural basis for recognition of CD20 by therapeutic antibody Rituximab*. *J Biol Chem*, 2007. **282**(20): p. 15073-80.
544. Shah, A., *New developments in the treatment of chronic lymphocytic leukemia: role of obinutuzumab*. *Ther Clin Risk Manag*, 2015. **11**: p. 1113-22.
545. Bird, R.E., et al., *Single-chain antigen-binding proteins*. *Science*, 1988. **242**(4877): p. 423-6.
546. Habibi Anbouhi, M., et al., *Functional recombinant extra membrane loop of human CD20, an alternative of the full length CD20 antigen*. *Iran Biomed J*, 2012. **16**(3): p. 121-6.
547. Orosz, F. and J. Ovadi, *A simple method for the determination of dissociation constants by displacement ELISA*. *J Immunol Methods*, 2002. **270**(2): p. 155-62.
548. Hong, K., et al., *Simple quantitative live cell and anti-idiotypic antibody based ELISA for humanized antibody directed to cell surface protein CD20*. *J Immunol Methods*, 2004. **294**(1-2): p. 189-97.
549. Geuijen, C.A., et al., *Affinity ranking of antibodies using flow cytometry: application in antibody phage display-based target discovery*. *J Immunol Methods*, 2005. **302**(1-2): p. 68-77.
550. Pennati, A., J. Deng, and J. Galipeau, *Maltose-binding protein fusion allows for high level bacterial expression and purification of bioactive mammalian cytokine derivatives*. *PLoS One*, 2014. **9**(9): p. e106724.
551. Vaks L., B.I., *Production of Stabilized scFv Antibody Fragments in the E. coli Bacterial Cytoplasm*. . *Human Monoclonal Antibodies. Methods in Molecular Biology*, ed. S. M. Vol. 1060. 2014, Totowa, NJ: Humana Press,
- .
552. Harris, D.T. and D.M. Kranz, *Adoptive T Cell Therapies: A Comparison of T Cell Receptors and Chimeric Antigen Receptors*. *Trends Pharmacol Sci*, 2016. **37**(3): p. 220-230.
553. Davenport, A.J., et al., *Chimeric antigen receptor T cells form nonclassical and potent immune synapses driving rapid cytotoxicity*. *Proceedings of the National Academy of Sciences*, 2018. **115**(9): p. E2068-E2076.
554. Liadi, I., et al., *Individual Motile CD4(+) T Cells Can Participate in Efficient Multikilling through Conjugation to Multiple Tumor Cells*. *Cancer Immunol Res*, 2015. **3**(5): p. 473-82.
555. Davenport, A.J., et al., *CAR-T cells are serial killers*. *Oncoimmunology*, 2015. **4**(12): p. e1053684.
556. Han, S., et al., *Turning the Tide Against Regulatory T Cells*. *Front Oncol*, 2019. **9**: p. 279.
557. Golubovskaya, V. and L. Wu, *Different Subsets of T Cells, Memory, Effector Functions, and CAR-T Immunotherapy*. *Cancers (Basel)*, 2016. **8**(3).

558. Stock, S., M. Schmitt, and L. Sellner, *Optimizing Manufacturing Protocols of Chimeric Antigen Receptor T Cells for Improved Anticancer Immunotherapy*. Int J Mol Sci, 2019. **20**(24).
559. Budde, L.E., et al., *Combining a CD20 chimeric antigen receptor and an inducible caspase 9 suicide switch to improve the efficacy and safety of T cell adoptive immunotherapy for lymphoma*. PLoS One, 2013. **8**(12): p. e82742.
560. Ito, M., et al., *NOD/SCID/gamma(c)(null) mouse: an excellent recipient mouse model for engraftment of human cells*. Blood, 2002. **100**(9): p. 3175-82.
561. Tipton, T.R., et al., *Antigenic modulation limits the effector cell mechanisms employed by type I anti-CD20 monoclonal antibodies*. Blood, 2015. **125**(12): p. 1901-9.
562. Cheadle, E.J., et al., *Differential role of Th1 and Th2 cytokines in autotoxicity driven by CD19-specific second-generation chimeric antigen receptor T cells in a mouse model*. J Immunol, 2014. **192**(8): p. 3654-65.
563. Cheadle, E.J., et al., *Natural expression of the CD19 antigen impacts the long-term engraftment but not antitumor activity of CD19-specific engineered T cells*. J Immunol, 2010. **184**(4): p. 1885-96.
564. Kueberuwa, G., et al., *CD19 CAR T Cells Expressing IL-12 Eradicate Lymphoma in Fully Lymphoreplete Mice through Induction of Host Immunity*. Mol Ther Oncolytics, 2018. **8**: p. 41-51.
565. Huey, D.D. and S. Niewiesk, *Production of Humanized Mice through Stem Cell Transfer*. Curr Protoc Mouse Biol, 2018. **8**(1): p. 17-27.
566. Watanabe, K., et al., *Target antigen density governs the efficacy of anti-CD20-CD28-CD3 zeta chimeric antigen receptor-modified effector CD8+ T cells*. J Immunol, 2015. **194**(3): p. 911-20.
567. River, C. <https://www.criver.com/products-services/safety-assessment/pathology-services/specialty-endpoints/tissue-cross-reactivity?region=3696>. Tissue cross-reactivity studies 2019 [cited 2019].
568. Sharpe, M.E., *T-cell Immunotherapies and the Role of Nonclinical Assessment: The Balance between Efficacy and Pathology*. Toxicol Pathol, 2018. **46**(2): p. 131-146.
569. Grossenbacher, S.K., E.G. Aguilar, and W.J. Murphy, *Leveraging natural killer cells for cancer immunotherapy*. Immunotherapy, 2017. **9**(6): p. 487-497.
570. Bhat, R. and C. Watzl, *Serial killing of tumor cells by human natural killer cells--enhancement by therapeutic antibodies*. PLoS One, 2007. **2**(3): p. e326.
571. Lanier, L.L., *NK CELL RECEPTORS*. Annual Review of Immunology, 1998. **16**(1): p. 359-393.
572. Habib, S., S.M. Tariq, and M. Tariq, *Chimeric Antigen Receptor-Natural Killer Cells: The Future of Cancer Immunotherapy*. Ochsner J, 2019. **19**(3): p. 186-187.
573. Kalos, M., et al., *Long-Term Functional Persistence, B Cell Aplasia and Anti-Leukemia Efficacy In Refractory B Cell Malignancies Following T Cell Immunotherapy Using CAR-Redirected T Cells Targeting CD19*. Blood, 2013. **122**(21): p. 163-163.
574. Pfefferle, A. and N.D. Huntington, *You Have Got a Fast CAR: Chimeric Antigen Receptor NK Cells in Cancer Therapy*. Cancers (Basel), 2020. **12**(3).
575. Carlsten, M. and R.W. Childs, *Genetic Manipulation of NK Cells for Cancer Immunotherapy: Techniques and Clinical Implications*. Front Immunol, 2015. **6**: p. 266.

576. Boissel, L., et al., *Comparison of mRNA and lentiviral based transfection of natural killer cells with chimeric antigen receptors recognizing lymphoid antigens*. *Leuk Lymphoma*, 2012. **53**(5): p. 958-65.
577. Li, L., et al., *Expression of chimeric antigen receptors in natural killer cells with a regulatory-compliant non-viral method*. *Cancer Gene Ther*, 2010. **17**(3): p. 147-54.
578. Collection, A.T.C., *NK-92® (ATCC® CRL-2407™)*. <https://www.atcc.org/products/all/CRL-2407.aspx>, 2019.
579. Klingemann, H., L. Boissel, and F. Toneguzzo, *Natural Killer Cells for Immunotherapy - Advantages of the NK-92 Cell Line over Blood NK Cells*. *Front Immunol*, 2016. **7**: p. 91.
580. Xiao, L., et al., *Adoptive Transfer of NKG2D CAR mRNA-Engineered Natural Killer Cells in Colorectal Cancer Patients*. *Mol Ther*, 2019. **27**(6): p. 1114-1125.
581. Tang, X., et al., *First-in-man clinical trial of CAR NK-92 cells: safety test of CD33-CAR NK-92 cells in patients with relapsed and refractory acute myeloid leukemia*. *Am J Cancer Res*, 2018. **8**(6): p. 1083-1089.
582. Liu, E., et al., *Use of CAR-Transduced Natural Killer Cells in CD19-Positive Lymphoid Tumors*. *N Engl J Med*, 2020. **382**(6): p. 545-553.
583. Mitwasi, N., et al., *"UniCAR"-modified off-the-shelf NK-92 cells for targeting of GD2-expressing tumour cells*. *Sci Rep*, 2020. **10**(1): p. 2141.
584. Melaiu, O., et al., *Influence of the Tumor Microenvironment on NK Cell Function in Solid Tumors*. *Frontiers in Immunology*, 2020. **10**(3038).
585. Liu, E., et al., *Cord blood NK cells engineered to express IL-15 and a CD19-targeted CAR show long-term persistence and potent antitumor activity*. *Leukemia*, 2018. **32**(2): p. 520-531.
586. Wang, X., et al., *Inducible MyD88/CD40 synergizes with IL-15 to enhance antitumor efficacy of CAR-NK cells*. *Blood Advances*, 2020. **4**(9): p. 1950-1964.
587. Xu, X., et al., *NKT Cells Coexpressing a GD2-Specific Chimeric Antigen Receptor and IL15 Show Enhanced In Vivo Persistence and Antitumor Activity against Neuroblastoma*. *Clin Cancer Res*, 2019. **25**(23): p. 7126-7138.
588. Hay, A.E. and M.C. Cheung, *CAR T-cells: costs, comparisons, and commentary*. *J Med Econ*, 2019. **22**(7): p. 613-615.
589. Roth, J.A., et al., *Cost-effectiveness of axicabtagene ciloleucel for adult patients with relapsed or refractory large B-cell lymphoma in the United States*. *J Med Econ*, 2018. **21**(12): p. 1238-1245.
590. Harrison, R.P., et al., *Chimeric antigen receptor-T cell therapy manufacturing: modelling the effect of offshore production on aggregate cost of goods*. *Cytotherapy*, 2019. **21**(2): p. 224-233.
591. Smith, T.T., et al., *In situ programming of leukaemia-specific T cells using synthetic DNA nanocarriers*. *Nat Nanotechnol*, 2017. **12**(8): p. 813-820.

9 Appendix

Appendix A1: Parental mAb

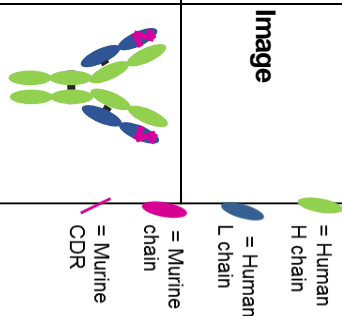
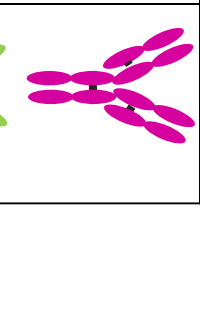
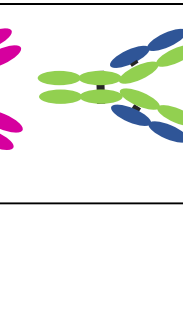
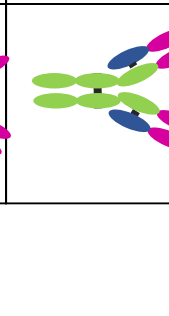
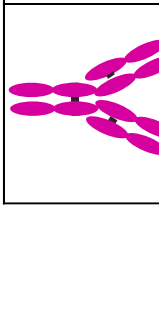
Name (alt. names)	Source and type	Mechanisms of action	Use in this thesis	Image
BHH2 (obintuzumab; GA101)	Humanised; generated from mouse hybridoma. Type II; IgG1.	Strong ADCC, strong direct cell death	BHH2 used in this project is equivalent to non-afucosylated obintuzumab. Sequence used in this project was previously generated commercially from published obintuzumab sequence.	
B1-WG (B1;tositumomab)	Murine; generated from mouse hybridoma. Type II; mIgG2a.	Strong ADCC, strong direct cell death	B1-WG used in this project is related to the clinical mAb tositumomab. The B1-WG sequence was determined previously using a combination of mass spectrometry and mutagenesis.	
2F2 (ofatumomab; HuMax-CD20)	Fully human; generated against CD20+ transfected cells in humanised mice. Type I; IgG1.	Strong CDC, ADCC	2F2 is an alternative name for ofatumomab. The sequence for this project was generated commercially from the published sequence.	
Rituximab	Chimeric; generated from mouse hybridoma. Type I; IgG1.	CDC, ADCC	The sequence for this project was previously generated commercially from the published sequence.	
Leu16	Murine; generated from mouse hybridoma. Type I; mIgG2a.	CDC, ADCC	The sequence for this project was generated commercially from the published sequence.	

Table A1.1: Information on parental antibodies used as scFv in this thesis
m, murine; CDC, complement-dependent cytotoxicity; ADCC, antibody-dependent cellular cytotoxicity.

Appendix A2: Primers

Primer Name	Use	Sequence 5'-3'
B1-WG scFv Vk-F	Generating Vk fragment of B1-WG scFv with 5' KpnI site	AAGGTACCACAGCTGGTGC TGACCCAGTCCTCC
B1-WG scFv Vk-R	Generating Vk fragment of B1-WG scFv with 3' BglII site	AGATCTGCCCTCGATGCTG CCTCCGCCGCCGCCAGCA CGGTCAC
B1-WG scFv Vh-F	Generating Vh fragment of B1-WG scFv with 5' BamHI site	CGGATCCGGCGGAGGCGG ATCTCAGATCCAGCTGGTG CAGTC
B1-WG scFv Vh-R	Generating Vh fragment of B1-WG scFv with 3' XbaI site	TCTAGATCAAGCTGCAGAG ACTAGTGTGCCCTG
BHH2 scFv Vk-F	Generating Vk fragment of BHH2 scFv with 5' KpnI site	AAGGTACCAGATATCGTGA TGACCCAGACTCCA
BHH2 scFv Vk-R	Generating Vk fragment of BHH2 scFv with 3' BglII site	CCAGATCTGCCCTCGATGC TGCCTCCGCCGCCTTTGAT CTCCACC
BHH2 scFv Vh-F	Generating Vh fragment of BHH2 scFv with 5' BamHI site	GCGGATCCGGCGGSGGCG GSTCTCAGCTGCAATTGGT GCAGT
BHH2 scFv Vh-R	Generating Vh fragment of BHH2 scFv with 3' XbaI site	TCTAGATCATGAGGAGACG GRGACCAGGGTTCC
Ritux scFv Vk-F	Generating Vk fragment of Ritux scFv with 5' KpnI site	AAGGTACCACAAATTGTTCT CTCCCAGTCTCCA
Ritux scFv Vk-R	Generating Vk fragment of Ritux scFv with 3' BglII site	CCAGATCTGCCCTCGATGC TGCCTCCGCCGCCTTTGAT TTCCAGC
Ritux scFv Vh-F	Generating Vh fragment of Ritux scFv with 5' BamHI site	GCGGATCCGGCGGAGGCG GATCTCAGGTACAAGTCA GCAGGCCTG

Ritux scFv Vh-R	Generating Vh fragment of Ritux scFv with 3' XbaI site	TCTAGATCAAGCTGCAGAG ACTAGTACCGTGGT
hIgG1 hinge-F-XhoI	Generating CAR spacer of hIgG1 Hinge-CH2-CH3 from human IgG1 template DNA with 5' XhoI site	ACTCGAGCCCAAATCTTGT GACAAAACCTCA
hIgG1 CH3-R-BamHI	Generating CAR spacer of hIgG1 Hinge-CH2-CH3 from human IgG1 template DNA with 3' BamHI site	ATGGATCCTTTACCCGGAG ACAGGGAGAGG
Sp163-start- F	For overlap PCR to generate enhancer-leader-scFv constructs to clone into the CAR in place of Leu16 scFv with 5' NheI site	ATGCTAGCGCAGAGGCTTG GGGCACCCGAG
Sp163 R-60	For overlap PCR to generate enhancer-leader-scFv constructs to clone into the CAR in place of Leu16 scFv	CGCCTTGGCGGGCTCCTCT CCCTTCTGGAA
Sp163 F-58	For overlap PCR to generate enhancer-leader-scFv constructs to clone into the CAR in place of Leu16 scFv	GGAGAGAACAATTTGAGAG AGGACACCTGC
BHH2 CAR leader R-211	For overlap PCR to generate enhancer-leader-B-HH2 construct to clone into the CAR in place of Leu16 scFv	GGTCATCACGATATCAGAG AGGACACCTGC
BHH2 CAR leader F-211	For overlap PCR to generate enhancer-leader-B-HH2 construct to clone into the CAR in place of Leu16 scFv	GCAGGTGTCCTCTCTGATA TCGTGATGACC

BHH2 CAR R-951 Sall	For overlap PCR to generate enhancer-leader-B-HH2 construct to clone into the CAR in place of Leu16 scFv with a 3' Sall site (complementary to XhoI)	GGGTCGACTGAGGAGACG GTGACCAGGGTT
Ritux CAR leader R-211	For overlap PCR to generate enhancer-leader-Ritux construct to clone into the CAR in place of Leu16 scFv	GGAGAGAACAATTTGAGAG AGGACACCTGC
Ritux CAR leader F-209	For overlap PCR to generate enhancer-leader-Ritux construct to clone into the CAR in place of Leu16 scFv	CTGCAGGTGTCCTCTCTCA AATTGTTCTCTCCAGTCTC
Ritux CAR R-942 XhoI	For overlap PCR to generate enhancer-leader-Ritux construct to clone into the CAR in place of Leu16 scFv with a 3' XhoI site	GGCTCGAGAGCTGCAGAGA CTAGTACCGTG
B1-WG CAR leader R-211	For overlap PCR to generate enhancer-leader-B1-WG construct to clone into the CAR in place of Leu16 scFv	GGTCAGCACCAGCTGAGAG AGGACACCTGC
B1-WG CAR F- 211	For overlap PCR to generate enhancer-leader-B1-WG construct to clone into the CAR in place of Leu16 scFv	GCAGGTGTCCTCTCTCAGC TGGTGCTGACC
B1-WG CAR R- XhoI	For overlap PCR to generate enhancer-leader-B1-WG construct to clone into the CAR in place of Leu16 scFv with a 3' XhoI site	GGCTCGAGAGCTGCAGAGA CTAGTGTGCC

ScFv-pFUSE-F	To add recombination sequences to BHH2 scFv	GTCTTGCACTTGTCACGAAT TCGAAGGTACCAGATATCG TGATG
ScFv-pFUSE-R	To add recombination sequences to BHH2 scFv	GTAGTCTGGGACGTCGTAT GGGTATGAGGAGACGGTGA CCAGG

Table A2.1: PCR primers used in this project

Primer Name	Use	Sequence 5'-3'
Bhh2 scFv XbaI-296 mut	To remove extra restriction sites within the scFv	TACTGCGCTCAGAATCTG GAACTTCCTTACACC
Bhh2 scFv BglII mut	To remove extra restriction sites within the scFv	GAGCTGAGCAGCCTGAGG TCTGAGGACACGGCC
Bhh2 scFv KpnI-130 mut	To remove extra restriction sites within the scFv	TCACTTATTTGTATTGGTAT CTGCAAAGCCAG
B1-WG scFv BglII mut	To remove extra restriction sites within the scFv	GCATCGAGGGCAGGTCTGG CGGAGGCGG
CAR EcoRI mut	Generating an EcoRI site at the 3' end of the CAR constructs to allow cloning into pMIGR1	CTGCCCCCTCGCTAGAATTC TAAGTTTAAACCG
CAR BglII mut	Generating a BglII site at the 5' end of the CAR constructs to allow cloning into pMIGR1	ATAGGGAGACCCAAGATCTC TAGCGCAGAGCCTTGGGGC
Bhh2 NheI mut	To remove extra restriction sites within the scFv	GTGAAGGTGTCCTGCAAGG CCAGCGGCTACGCCTTCAGC
B1-WG cys/ser mut	To remove extra cysteine in the svFv	CCGTGACCACCGCCTCCCT GCAGATCAACAACC

Leader KpnI mut	To insert a KpnI site into the leader sequence of a CAR construct to allow insertion of 2F2 scFv	CTCTTTCTCCTGTCAGGTA CCGCAGGTGTCCTCTCT
Leu16 scFv EcoRI mut	To mutate an EcoRI site between the Leu16 scFv and the leader sequence to allow cloning into pcDNA4 as a scfv	GGAAGTGCAGGTGTCGAATT CGACATCGTTCTGACC
Rp3-15	To convert the Rp3 motif to the Rp15 motif	CAGCCTGCCCATACGCCA ACCCCTCAC
NcoI remove 1	To remove an NcoI restriction site in the CAR constructs	TCC GAA ACG ATG GGA TGG AGC TGG ATC
NcoI remove 2	To remove a second NcoI restriction site in the CAR constructs	TCT CCG GGT AAA GGA TCG ATG GCC CTG ATT GTG CTG GGG
NcoI 5' mut	To add a 5' NcoI site to the CAR constructs to facilitate cloning into SFG	TAG GGA GAC CCA CCA TGG CTA GCG CAG AGG CTT GG
MluI 3' mut	To add a 3' MluI site to the CAR constructs to facilitate cloning into SFG	CTG CCC CCT CGC TAG ACG CGT AAG TTT CCC CCG CTG
NcoI revert 1	To revert the first NcoI site in the CAR constructs after cloning into SFG	TCC GAA ACC ATG GGA TGG AGC TGG ATC

Table A2.2: Mutagenesis primers used in this project

Primer Name	Use	Sequence 5'-3'
Leu16 Seq 483	Internal sequencing primer for Leu16 CAR construct	CTGCCAGCAGTGGAGCTT CAACCCACCCAC
Leu16 Seq 1560	Internal sequencing primer for Leu16 CAR construct	CAAGAGCAGGTGGCAGCA GGGGAACGTCTT
2F2 scFv F	Sequencing of 2F2 scFv	CCATGGCGTCCACAGGAGA GAC
2F2 scFv R	Sequencing of 2F2 scFv	CTCGAGAGCAGCAGACACC AGGG
SP6	Sequencing primer for pCR-Blunt II-TOPO	ATTTAGGTGACACTATAG
T7	Sequencing primer for pCR-Blunt II-TOPO, pcDNA3.1(-) and pcDNA4 HisMax B	TAATACGACTCACTATAGGG
BGH Reverse	Sequencing primer for pcDNA3.1(-) and pcDNA4 HisMax B	TAGAAGGCACAGTCGAGG
MSCV	Sequencing primer for retroviral vector	CCCTTGAACCTCCTCGTTCCG ACC
SFG F	Sequencing primer for retroviral vector	CTAAGAACCTAGAACCTCGC
SFG R	Sequencing primer for retroviral vector	TCACATTGCCAAAAGACGGC

Table A2.3: Sequencing primers used in this project

Appendix A3: Antibodies

Specificity	Clone	Isotype	Labelled	Source	Use
hIgG-Fc	Polyclonal	Goat F(ab)2	PE	Jackson Immuno Research	CAR detection
mIgG-Fc	Polyclonal	Goat F(ab)2	PE	Jackson Immuno Research	Isotype control for CAR detection
SHIgG-Fc	Polyclonal	Goat F(ab)2	PE	Jackson Immuno Research	Isotype control for CAR detection
hCD20	Rituximab	hIgG1	Unlabelled /FITC	Southampton General Hospital Pharmacy, labelled in house	Blocking assay/ CD20 detection
hCD52	CAMPATH	hIgG1	FITC	Prof. G Hale, labelled in house	Isotype control for CD20 detection
Rituximab	MB2A4	Rat IgG2a	Unlabelled /FITC	In house	Blocking assay /detection of Ritux CAR expression
B1-WG	AT148	Rat IgG2b	FITC	In house	Detection of B1-WG CAR expression
hCD32	AT10	mIgG1	APC	In house	Binding assay target labelling
Granzyme B	GB11	mIgG1	FITC	Biologend	Granzyme B expression check
Isotype control	MOPC-21	mIgG1	FITC	Biologend	Isotype control for GB11/ RPAT-T4 and SK1
mCD3	KT3	mIgG2a	Unlabelled /APC /FITC	In house	Activation of murine T cells/ CTLL-2 tracking

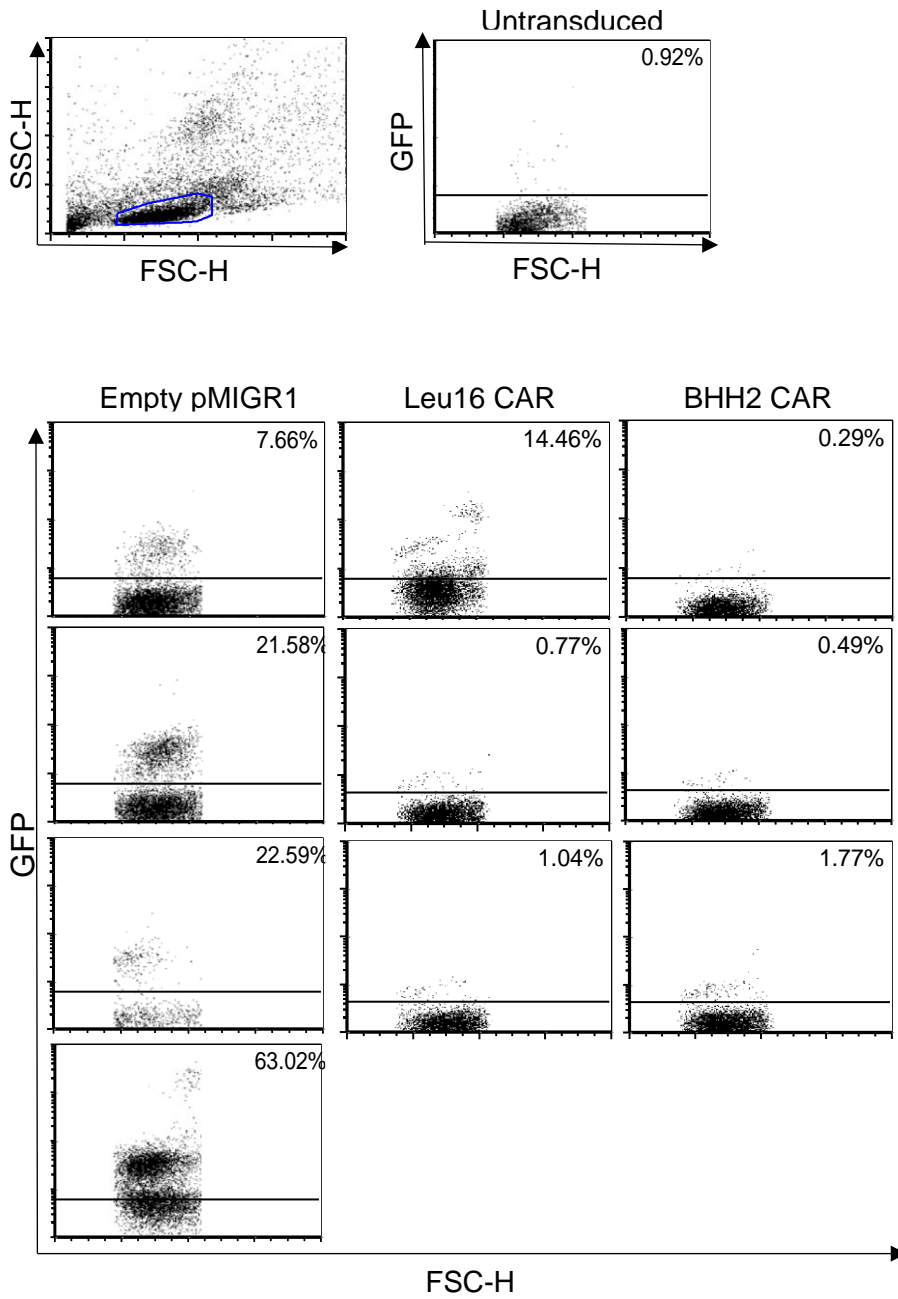
					/isotype control for OKT3
mCD28	37.51	SHIgG1	Unlabelled	In house	Activation of murine T cells
hCD3	OKT3	mIgG2a	FITC	In house	Labelling of transduced PBMCs
hCD4	RPA-T4	mIgG1	FITC	Biolegend	Labelling of transduced PBMCs
hCD8	SK1	mIgG1	FITC	Biolegend	Labelling of transduced PBMCs
His Tag	HIS.H8	mIgG2b	Unlabelled	Abcam	Western blot
HA Tag	HA7	mIgG1	Unlabelled	Sigma Aldrich	Western blot
mIgG1	Polyclonal	Rabbit	HRP	In house	Western blot detection

Table A3.1: Antibodies used in this thesis for fluorescent labelling of cells, assays and Western blots

h, human; m, murine; SH, Syrian hamster. PE, R-phycoerythrin; FITC, fluorescein isothiocyanate; APC, allophycocyanin; HRP, horse radish peroxidase.

Appendix A4: Bone marrow chimera analysis plots

A



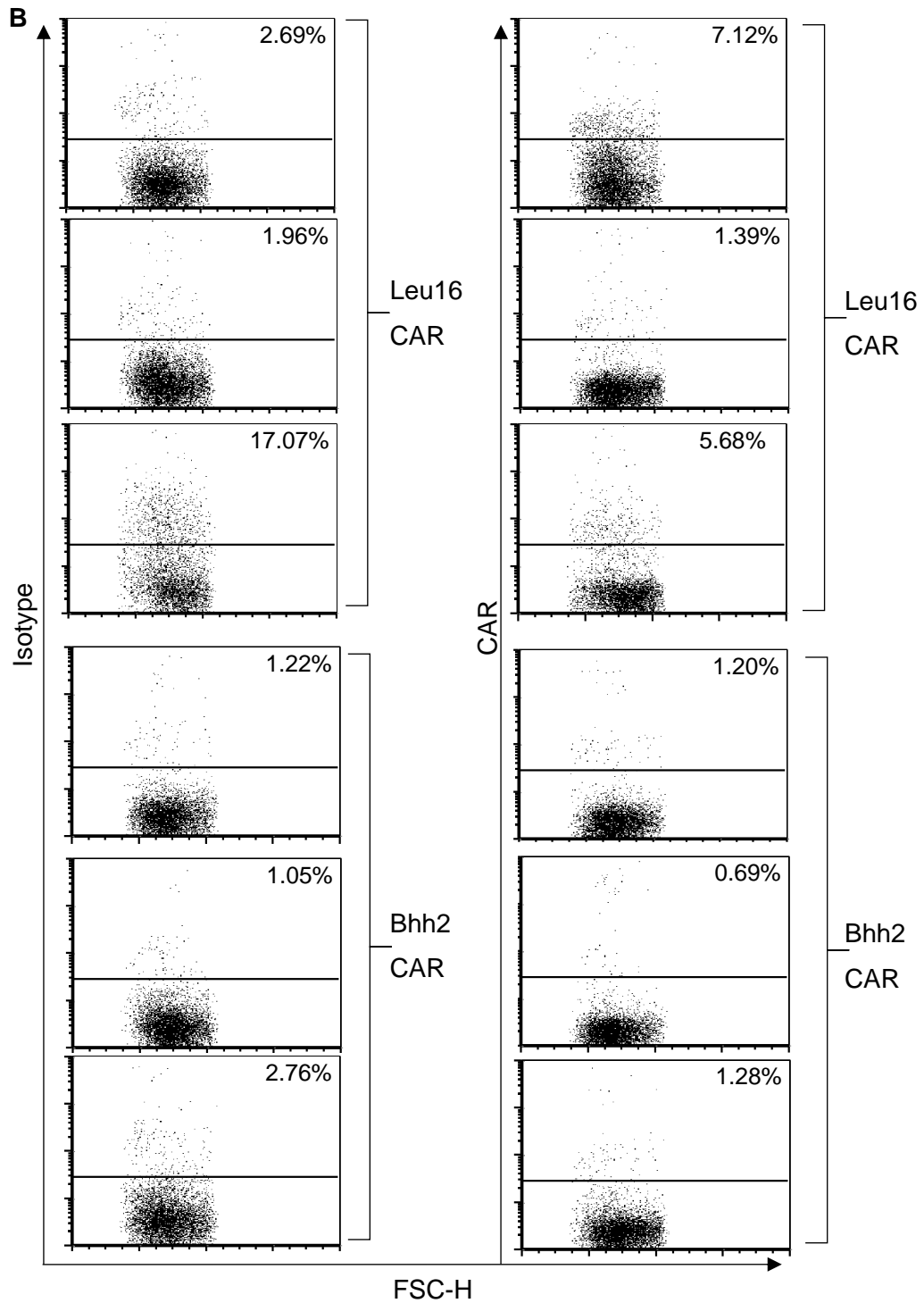
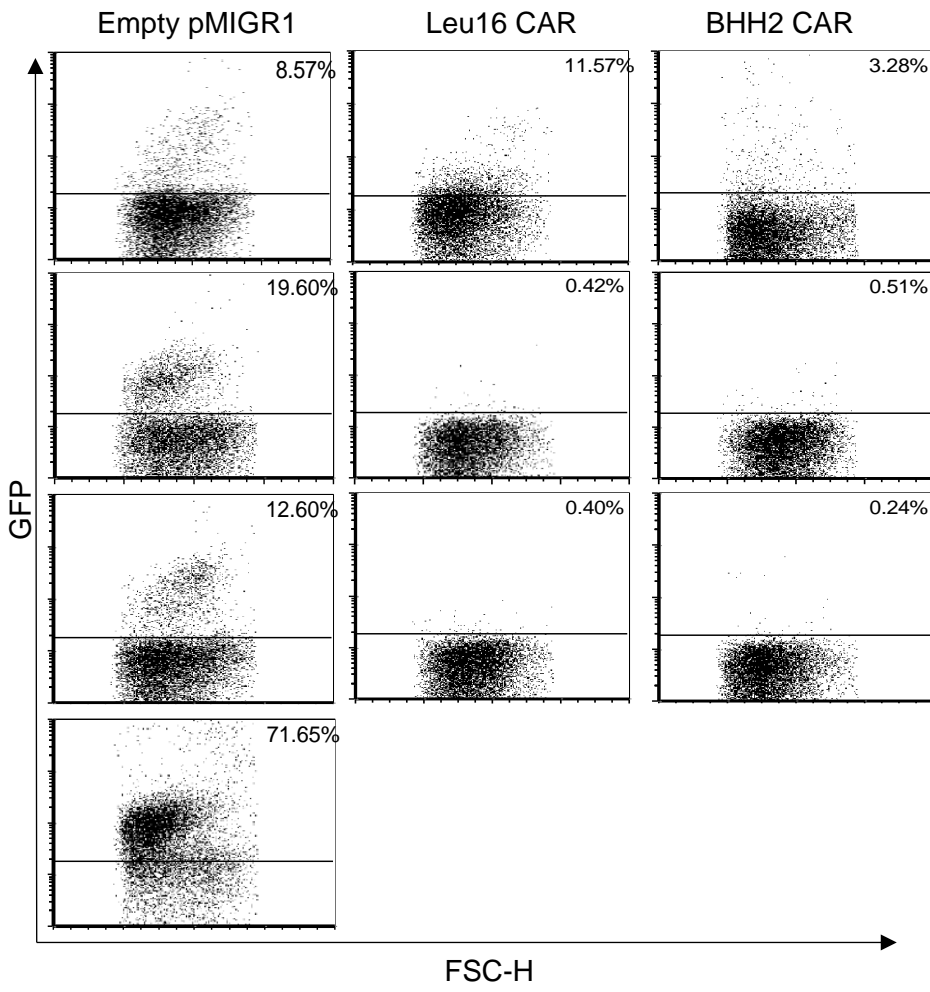
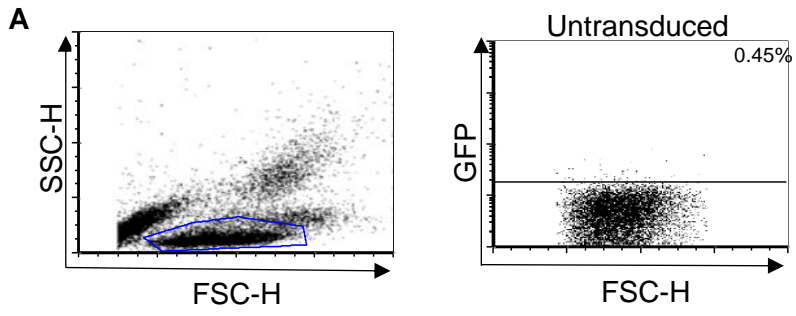


Figure A4.1: Analysis plots of blood samples taken a 6 w post-reconstitution

A: Untransduced cells were gated to generate GFP+ve gate. GFP expression for all individual mice shown.

B: Blood samples of Leu16 and BHH2 CAR-transduced recipients stained with isotype control (PE-anti-SHlgG-Fc; left) and anti-CAR (PE-anti-hlgG-Fc; right) to assess CAR expression in all mice.



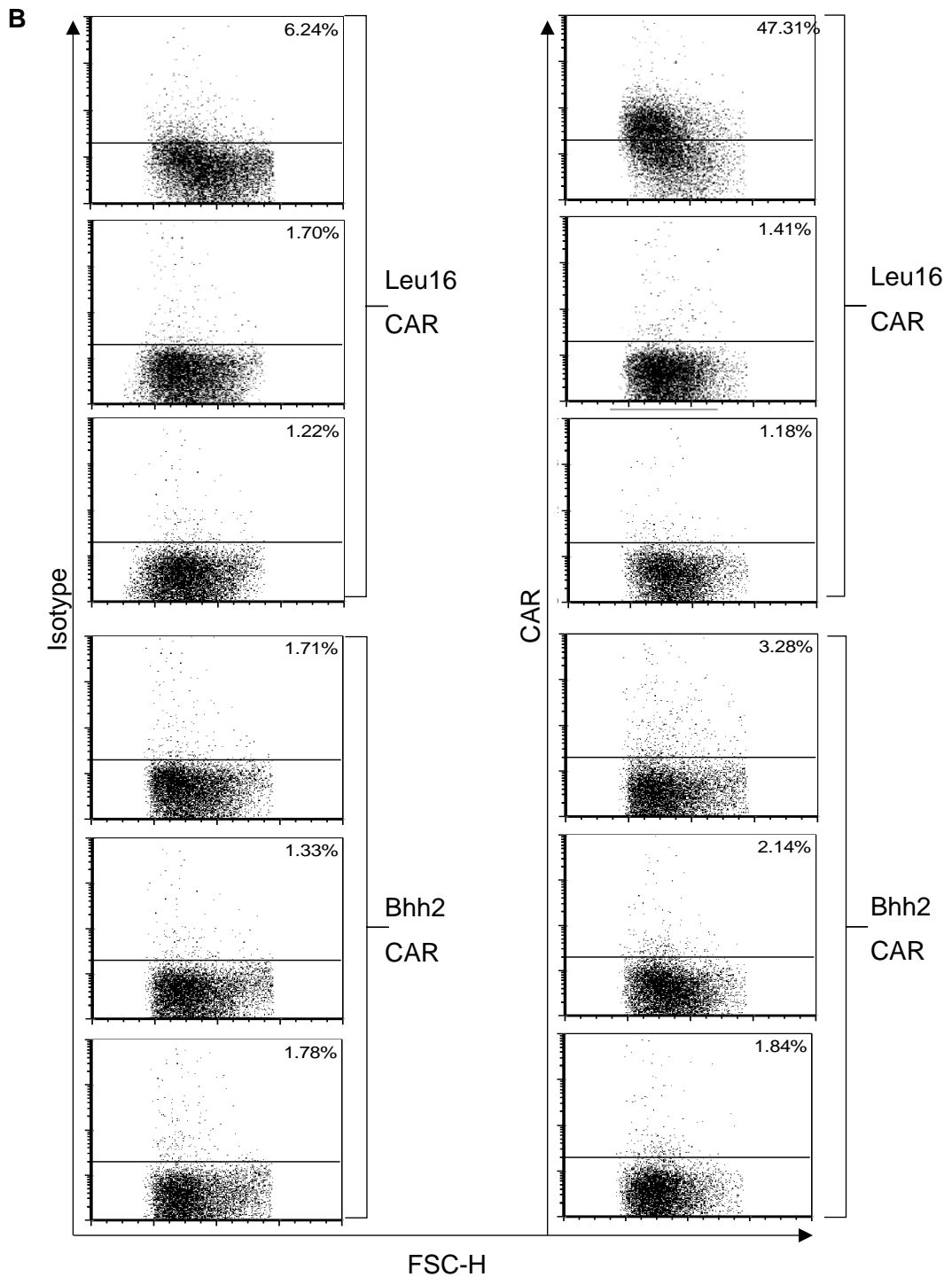


Figure A4.2: Analysis plots of blood samples taken a 10 w post-reconstitution

A: Untransduced cells were gated to generate GFP+ve gate. GFP expression for all individual mice shown.

B: Blood samples of Leu16 and BHH2 CAR-transduced recipients stained with isotype control (PE-anti-SHlgG-Fc; left) and anti-CAR (PE-anti-hlgG-Fc; right) to assess CAR expression in all mice.

Appendix A5: C57/BL6 lymphodepletion

2 C57/BL6 mice were given 5 Gy TBI and serial tail blood samples were taken and analysed by flow cytometry for the presence of different circulating lymphocyte compartments. **Figure A5.1** illustrates the staining profiles performed using anti-murine mAb to identify the cell populations. These were plotted graphically (**Figure A5.2**) to visualise the return of each population post-irradiation.

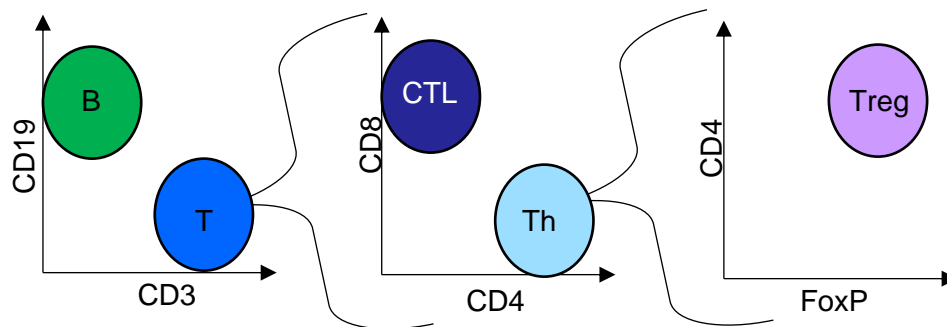


Figure A5.1: Staining profiles for flow cytometric identification of murine lymphocyte compartments in tail blood samples

Anti-CD19-APC, anti-CD3-pacific blue, anti-CD8a-PE-Cy7, anti-CD4-APC-Cy7, anti-FoxP3-APC (all Biolegend) were used to determine cell populations shown prior to irradiation and at d 2, 5, 9, 15, 21 and 42 post-irradiation.

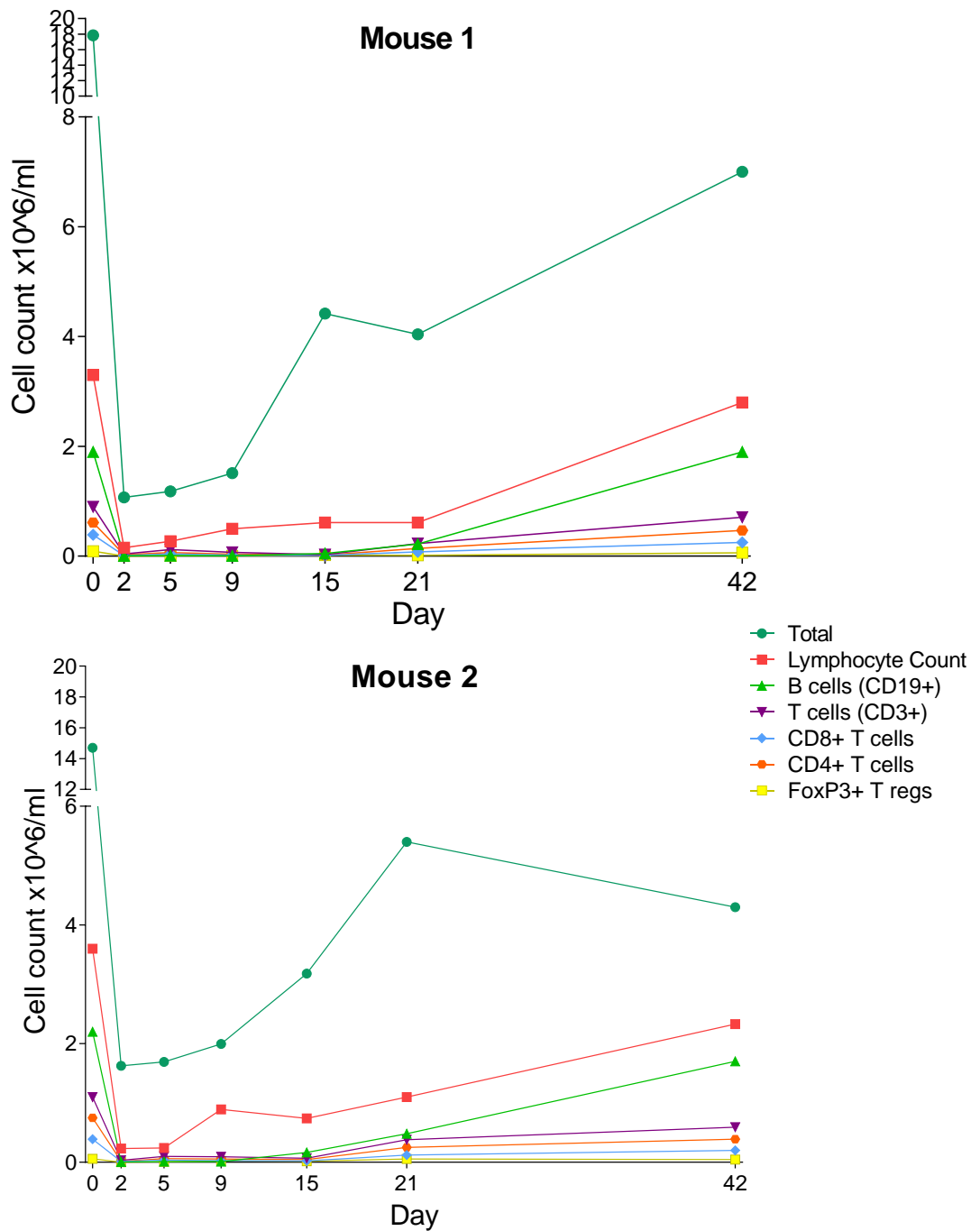


Figure A5.2: Tracking the return of peripheral lymphocyte populations in irradiated C57/BL6 mice

Tail vein blood samples (50 μ l at each time point) were collected (as described in Chapter 2.9.2) and staining was performed as described in Chapters 2.5.1 and 2.5.2 (intracellular FoxP3). Samples were run on a FACSCanto (BD) for analysis and presented graphically.

Appendix A6: Poster presentation abstracts and publication details

2013 BSI Congress:

Immunology. 2013 Dec; 140(Suppl 1): 39–184.

“A comparison of anti-CD20 chimeric antigen receptors in targeting B-cell malignancies R. Britton, R. French & M. Glennie University of Southampton, Southampton, UK Chimeric antigen receptors (CARs) are constructs typically encompassing an antibody single chain variable fragment (scFv) linked via a spacer region to a transmembrane domain allowing surface expression on effector cells. The intracellular region includes activation domains of co-stimulatory molecules to induce effector cell function. Previous studies have shown CARs can elicit potent anti-tumour responses against a variety of B cell malignancies. However, the mechanisms of CAR function and factors determining efficacy remain largely unknown. Anti-human CD20 scFvs were generated by PCR, and purified using an anti-HA column. These comprised heavy and light variable chains derived from the antibodies Leu16, rituximab and B-HH2. CARs were generated using these domains, along with an IgG-Fc spacer and CD4 transmembrane region. Three signalling regions were included in the intracellular region; the CD3f chain and the activation domains of CD28 and 4-1BB. The CARs were expressed transiently on 293F HEK cells and shown to bind CD20 successfully. These interactions have been demonstrated to be specific using a blocking assay. A difference in binding efficiency was observed between the various CARs. Retroviral transduction of the CAR constructs into a T cell reporter line has demonstrated activation upon CD20-CAR interaction in vitro. Activated splenocytes have also been transduced with the CAR constructs and these will be transferred into a humanCD20 transgenic mouse model to investigate their ability to mediate B-cell depletion in vivo and compare the different CARs. CAR-T-cell proliferation and in vivo survival will also be evaluated.”

2014 BSI Congress:

Special Issue: Abstracts of the British Society for Immunology Annual Congress, 1–4 December 2014, Brighton, UK, Volume 143, Issue s2, Pg 129.

A comparison of anti-CD20 chimeric antigen receptors in targeting B-cell malignancies R. Britton, R. French & M. Glennie University of Southampton, Southampton, UK Chimeric antigen receptors (CARs) are constructs typically encompassing an antibody single chain variable fragment (scFv) linked via a spacer region to a transmembrane domain allowing surface expression on effector cells. The intracellular region includes activation domains of co-stimulatory molecules to induce effector cell function. Previous studies have shown CARs can elicit potent anti-tumour responses against a variety of B cell malignancies. However, the mechanisms of CAR function and factors determining efficacy remain largely unknown. Anti-human CD20 scFvs were generated

by PCR, and purified using an anti-HA column. These comprised heavy and light variable chains derived from the antibodies Leu16, rituximab and B-HH2. CARs were generated using these domains, along with an IgG-Fc spacer and CD4 transmembrane region. Three signalling regions were included in the intracellular region; the CD3 ζ chain and the activation domains of CD28 and 4-1BB. The CARs were expressed transiently on 293F HEK cells and shown to bind CD20 successfully. These interactions have been demonstrated to be specific using a blocking assay. A difference in binding efficiency was observed between the various CARs. Retroviral transduction of the CAR constructs into a T cell reporter line has demonstrated activation upon CD20-CAR interaction in vitro. Activated splenocytes have also been transduced with the CAR constructs and these will be transferred into a humanCD20 transgenic mouse model to investigate their ability to mediate B-cell depletion in vivo and compare the different CARs. CAR-T-cell proliferation and in vivo survival will also be evaluated.